LA-12797-T
Thesis

Leaks in Nuclear Grade High Efficiency Aerosol Filters

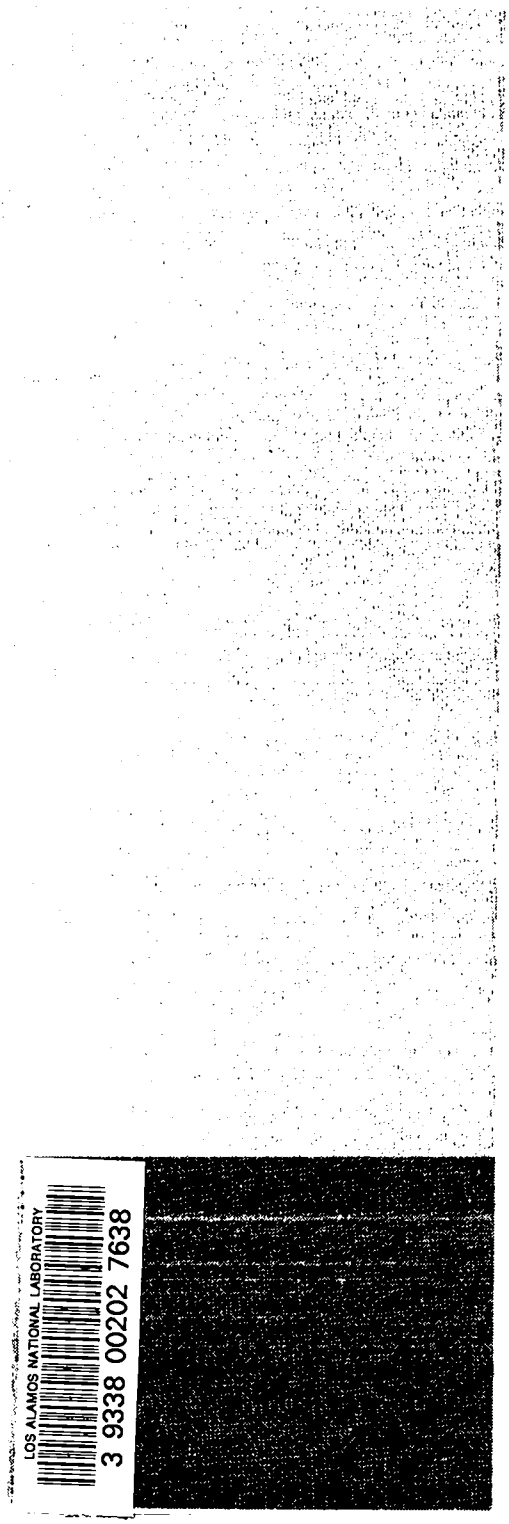

Los Alamos
NATIONAL LABORATORY

Los Alamos National Laboratory is operated by the University of California for the United States Department of Energy under contract W-7405-ENG-36.

This work was supported by the US Department of Energy.

This thesis was accepted by the Department of Environmental Health Sciences, University of California, Los Angeles, Los Angeles, California, in partial fulfillment of the requirements for the degree of Doctor of Philosophy. The text and illustrations are the independent work of the author and only the front matter has been edited by the CIC-1 and ESH-5 staff to conform with Department of Energy and Los Alamos National Laboratory publication policies.

An Affirmative Action/Equal Opportunity Employer

LA-12797-T
Thesis

UC-707, UC-507, UC-907, and UC-607
Issued: July 1994

Leaks in Nuclear Grade High Efficiency Aerosol Filters

Ronald Clyde Scripsick

Los Alamos
NATIONAL LABORATORY
Los Alamos, New Mexico 87545

TABLE OF CONTENTS

LIST OF FIGURES

LIST OF TABLES

LIST OF SYMBOLS

A	Crossectional area of mixer
A_F	Filter media surface area
A_V	Avogadro's number
C_c	Cunningham slip correction factor, $= 1+\frac{\lambda}{d_p}\left(2.514+0.8e^{-0.55d_p/\lambda}\right)$
C_s	True sample concentration
CV_{Dr}	Coefficient of variation for dilution ratio
CV_P	Coefficient of variation for penetration
CV_{ref}	Coefficient of variation of reference point measurements
D	Particle diffusion coefficient
DDr	Downstream dilution ratio
D_m	Actual mixer diameter
D_r	Dilution Ratio
d	Leak diameter
d_c	Equivalent diameter of mixing element channels
d_f	Fiber diameter

d_h Hydraulic diameter

d_m Effective molecular diameter for air

d_p Aerosol particle diameter

f Fanning Friction Factor

g Gravitational Acceleration

H Heterogeneity

H_f Heterogeneity after mixing

H_f^* An upper bound estimate for H_f in air effluent monitoring systems

H_0 Heterogeneity prior to mixing

h Heterogeneity reduction, $= \frac{H_0}{H_f}$

Ku Kuwabara flow hydrodynamic factor, $= -\frac{\ln\alpha}{2} - \frac{3}{4} + \alpha - \frac{\alpha^2}{4}$

k Boltzmann's constant

L Characteristic mixer channel length

L_f Fiber length per unit volume of filter

l Length of capillary

ℓ Leak path length

ℓ_F Filter media thickness

ℓ_e	Entrance length, = C Re d, where C = 0.035 to 0.085
ℓ_{frame}	Frame Leak Path Length
ℓ_{media}	Media Leak Path Length
ℓ_{min}	Minimum Leak Path Length
ℓ_{seal}	Seal Leak Path Length
N	Number of mixing elements
N_c	Coincidence loss counting efficiency
N_d	Downstream particle count
N_{EL}	Number of External Leak Paths
N_{IL}	Number of Internal Leak Paths
N_L	Number of Leak Paths
N_p	Number of plates per mixing element
N_u	Upstream particle count
n_m	Molecular concentration, $= \frac{A_v P_{bar}}{R_g T}$
P	Penetration; Overall Filter Unit Penetration

P_d Frame leak penetration associated with leak paths that exit inside the filter unit downstream of the filter media

Pe Peclet number for flow around a fiber, ratio of convective transport to diffusive transport, $= \frac{U_0 d_f}{D}$

P_{fr} Frame leak penetration

P_{EL} Overall Penetration of External Leaks

P_{ELd} External Leak Penetration Associated with Diffusion Particle Loss

P_{ELs} External Leak Penetration Associated with Sedimentation Particle Loss

P_{IL} Overall Penetration of Internal Leaks

P_{ILd} Internal Leak Penetration Associated with Diffusion Particle Loss

P_{ILs} Internal Leak Penetration Associated with Sedimentation Particle Loss

PL Overall Leak Penetration

P_{LD} Leak Penetration Associated with Diffusion Particle Loss

P_{LR} Leak Penetration Associated with Interception Particle Loss

P_{LS} Leak Penetration Associated with Sedimentation Particle Loss

$P_M(Q)$	Penetration of intact media at flow Q
P(Q)	Overall penetration of filter at flow Q
P_u	Frame leak penetration associated with leak paths that exit inside the filter unit upstream of the filter media
p	Pressure
P_{bar}	Barometric pressure
Q	Volume flow rate
Q_d	Frame leak flow rate from leak paths exiting downstream of media
Q_f	Whole filter unit flow rate
Q_{fr}	Total frame leak flow rate
Q_{de}	Design flow rate
Q_r	Recirculating flow rate
Q_s	Sheath flow rate
Q_u	Frame leak flow rate from leak paths exiting upstream of media
Q_{EL}	Total External Leak flow rate
Q_{ELi}	Flow Rate of External Leak Path i
Q_{ILi}	Total Internal Leak flow rate
Q_{Li}	Flow Rate of Internal Leak Path i

Q_L	Total Leak flow rate
Q_{Lmax}	Maximum Total Leak flow rate
Q_{Li}	Flow Rate of Leak Path i
Q_1	Volume flow rate of stream 1 of two streams to be mixed
Q_2	Volume flow rate of stream 2 of two streams to be mixed
R	Interception parameter
R_c	Interception parameter for channel entry
Re	Flow Reynolds number, $= \frac{\rho U_0 d}{\eta}$
R_{ed}	Interception parameter for plate edge
Re_ℓ	Length Reynolds number, $= \frac{\rho U_0 \ell}{\eta}$
R_g	Gas constant, $= 8.31 \times 10^7 \frac{dyn \bullet cm}{K \bullet mole}$
Ru	Undiluted upstream count rate
r^2	correlation coefficient
r_p	radius of plume
S	Number of spacers
Stk_c	Stokes number for channel entry
Stk_e	Stokes number for plate edges

Stk_m	Stokes number for large particle mixing
s	Standard deviation
T	Absolute temperature
T_c	Plate thickness
t	Time
t_d	Duration of downstream count
t_u	Duration of upstream count
U	Flow velocity toward a single fiber at Kuwabara flow cell vertex
U_0	Free Stream Velocity; Filtration Velocity, face velocity, $= \frac{Q}{A_F}$
u	Particle velocity
V	Electrical potential
Vf	Mixer void fraction
V_{fil}	Filter unit volume
V_o	Free stream air velocity approaching mixing plate edge, $= \frac{4 \bullet Q}{Vf \bullet \pi \bullet D_m^2}$
v_s	Sensitive volume of optical single-particle counter
Vts	Particle Terminal Settling Velocity
W_{IL}	effective air flow resistance of internal leak paths

W_{MP} effective air flow resistance of media pack

X A Kreith and Eisenstadt dimensionless group, $= \frac{\ell}{d} Re^{-1}$

x_c Characteristic dimension describing the change in streamline direction

X_1 Concentration in stream 1 of two streams to be mixed, = 0

X_2 Concentration in streams of two streams to be mixed, = 1

$\bar{x}_b$ Mean concentration with diffusion broadening

$\bar{x}$ Average particle displacement

$\overline{X}$ Mean concentration

Y A Kreith and Eisenstadt dimensionless group, $= \frac{\Delta p}{\frac{1}{2}\rho_f U_0^2}$

Z Gravitational Deposition Parameter

α Volume fraction of fibers, $= \frac{\pi \bullet d_f^2 \bullet L_f}{4}$

Δp Differential pressure

δ_v Flow boundary layer thickness

η Viscosity

η_D Single fiber diffusion collection efficiency

η_{DR} Single fiber collection efficiency in region of maximum penetration

η_R Single fiber interception collection efficiency

λ Gas mean free path

μ Diffusion deposition parameter

μ_m Diffusion deposition parameter for particle losses in static mixing units

ρ_f Fluid mass density

ρ_p Particle mass density

τ Particle relaxation time, $= \frac{\rho_p \bullet d_p^2 \bullet C_c}{18 \bullet \eta}$

ACKNOWLEDGMENTS

I acknowledge the support and guidance of my doctoral committee, William Hinds, Sheldon Friedlander, John Froines, Arthur Winer, Robert Phalen, and James Jackson. I have learned important lessons from each of them. My major advisor and committee chair, Dr. Hinds, is a gifted mentor.

The determining factor in completing this program was my employer, Los Alamos National Laboratory. Without the sustained support of the Laboratory I would not have been successful in the program. Bruce Reinert, my immediate supervisor, supported my efforts over the entire term of the program. James Jackson and Kenneth Hargis took up my cause with Laboratory management. Jess Aragon, John Puckett, Alan McMillan, and Dennis Erickson all supported my work. Mr. Aragon made it possible for me to complete my residency. Mr. Puckett supported my research. Paul Cunningham championed my research topic. With his help funding came from David Post and Cheryl Faust.

A great deal of the credit for the success of the experimental program goes to Thomas Trujillo. Richard Beckman made significant contributions to the analysis of experimental results. Laurie Wiggs provided invaluable advice during each step of the doctoral program. Her wisdom was the most crucial factor in my successful completion of the program.

LEAKS IN NUCLEAR GRADE HIGH EFFICIENCY AEROSOL FILTERS

by

Ronald Clyde Scripsick

ABSTRACT

Nuclear grade high efficiency aerosol filters, also known as high efficiency particulate air (HEPA) filters, are commonly used in air cleaning systems for removal of hazardous aerosols. Performance of the filter units is important in assuring health and environmental protection. The filter units are constructed from pleated packs of fiberglass filter media sealed into rigid frames. Results of previous studies on such filter units indicate that their performance may not be completely predicted by ideal performance of the fibrous filter media. In this study, departure from ideal performance is linked to leaks existing in filter units and overall filter unit performance is derived from independent performance of the individual filter unit components.

The performance of 14 nuclear grade HEPA filter units (size 1, 25 cfm) with plywood frames was evaluated with a test system that permitted independent determination of penetration as a function of particle size for the whole filter unit, the filter unit frame, and the filter media pack. Tests were performed using a polydisperse aerosol of di-2-ethylhexyl phthalate with a count median diameter of 0.2 μm and geometric standard deviation of 1.6. Flow rate and differential pressure were controlled from 1% to 100% of design values. Particle counts were made upstream and downstream of the filter unit with an optical particle counter (OPC). The OPC provided count information in 28 size channels over the particle diameter range from 0.1 to 0.7 μm.

Results provide evidence for a two component leak model of filter unit performance with : 1) external leaks through filter unit frames, and 2) internal leaks through defects in the media and through the seal between the media pack and frame. For the filter units evaluated, these leaks dominate overall filter unit performance over much of the flow rate and particle size ranges tested. Ideal performance was observed only in a narrow range of

particle size near the size of maximum penetration. Internal leaks dominate filter unit leak performance with internal leak penetration as high as 1.5×10^{-4}. Frame leakage contribution to overall filter unit penetration was $\leq 3.6 \times 10^{-5}$.

CHAPTER I. INTRODUCTION

In occupational hygiene there is a hierarchy of hazard control option which proceeds from source to receptor. Control at the source is most effective. This control may involve changes to the process, such as substitution with less hazardous materials or engineering controls to contain or confine hazardous materials. The next level of control is isolation of the source from the receptor through the use of barriers. Administrative controls such as limiting exposure time or modification of work practices may also be used. The final level of control is personal protection such as the use of respirators. This study addresses performance of fibrous filter particulate air-cleaning devices known as high efficiency particulate air (HEPA) filter units. The study relates to the first and last levels of the hazard control hierarchy.

HEPA filter units are commonly used as air cleaners in engineering control applications and they are widely used in air-purifying aerosol respirators. The units are composed of a pleated pack of filter media sealed in a rigid frame (see Figure I-1). The filter media is a fibrous mat made largely from glass fibers.

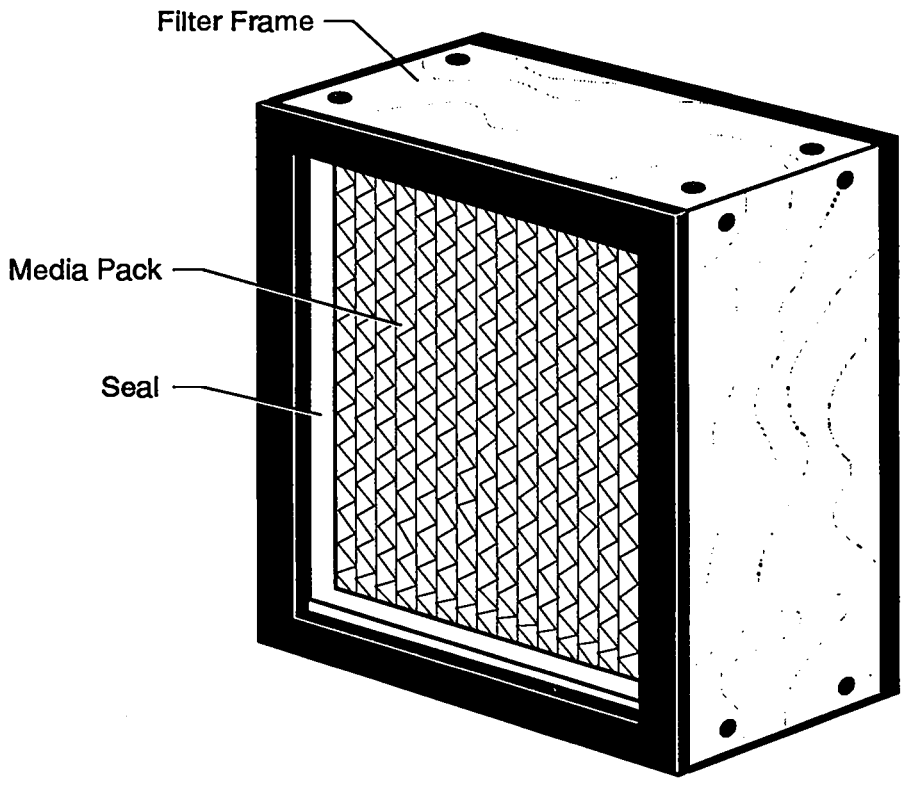

Figure I-1. Nuclear grade HEPA filter unit.

Assuring that HEPA filter units provide adequate protection requires understanding of the mechanisms responsible for their performance. Understanding performance means knowing how and why penetration is affected by such parameters as aerosol size and flow rate. Such understanding helps determine boundaries of operation in which protection can be assured.

Predicting performance of HEPA filter units may come from evaluation of filter unit components, laboratory evaluation of the assembled units, or in situ testing of filter banks. Each of these approaches have their own unique benefits and limitations. This study focuses on laboratory evaluation of the assembled filter units. The evaluation provides information on how performance of assembled units relates to expected performance of individual filter unit components. The evaluation also develops information that can be used to predict how filter units might perform in situ.

Application of control devices such as ventilation air cleaning systems must consider control requirements for non-routine or upset operating conditions as well as routine operating conditions. In this study, performance of HEPA filter units is evaluated under certain routine and non-routine operating conditions. Filter unit performance is evaluated in the flow rate range from design flow rate down to low flow rates. For purposes of this study low flow rates are considered to be flow rates below approximately 20% of design. Low flow rates are encountered in some loss-of-power situations at certain nuclear facilities and at inflections between inhalation and exhalation for air purifying dust respirators.

In this study filter unit performance is examined over a range of aerosol particle sizes. This range extends from ≈0.1 μm diameter to ≈0.7

μm diameter. While a broader challenge aerosol size range is expected in the field, this range is sufficient to examine regions where maximum penetration occurs.

Assuring protection requires knowledge of how filter unit performance is affected by the range of possible operating conditions. Such understanding is needed for design of filter units and design of hazardous material air cleaning systems. Limitations and restrictions imposed by the designs must be heeded in the operation and maintenance of the air cleaning systems. System operators must be aware of the performance characteristics. They need to know, for example, how changes in challenge concentration affect emissions, how changes in challenge particle size affect overall collection efficiency, and how changes in flow rate affect system performance. The operators must be able to balance operation of a facility with protection of health and environment and decide when facility operation may challenge air cleaning systems beyond limits that assure protection.

Filter unit performance characteristics may affect design and operation of air effluent monitors. Some operators (Os92, Dy92, Ni92, and Mc92) of HEPA filter air cleaning systems have proposed relaxing isokinetic requirements for aerosol emissions sampling. Filtration theory predicts almost negligible penetration of particles with aerodynamic

diameters requiring isokinetic sampling. These proposals assumes that performance of the HEPA systems follows theory. Should penetration of these particles be greater than predicted, actual emissions levels could be higher than expected and the increased levels may not be reflected in monitoring results.

Physical characteristics of air emissions directly affect assessment of risk and may be directly affected by filter unit or HEPA system performance. For aerosol emissions, a factor in determining emission rates is the product of the aerosol size dependent filter unit/system penetration and the challenge aerosol size distribution. An increase in challenge aerosol size results in an increase mass emission rates unless the increase is compensated for by a decrease in penetration. Increases in emission rates translate into increased exposure.

Interaction of penetration and size distribution also determines the size distribution of emissions. This size distribution affects respiratory tract deposition which in turn impacts estimated dose.

I.A. Significance

The need for this investigation comes from results of particular studies on filter unit performance (Ko80, Sc86, Hi87a, Sc87a, Sc87b, and Bi88). These studies provide experimental evidence that under some conditions performance of fibrous filter units may differ from predictions of filtration theory. In certain of these studies (Ko80, Sc86, Hi87a, Sc87a, and Sc87b) penetration measurements on assembled filter units were made over a range of flow rates including design flow rate and flow rates at or below 20% of design. At the higher flow rates (>20% of design) a maximum was observed in plots of penetration versus aerosol size in accordance with filtration theory. At the lower rates ($\leq$20% of design) the penetration peak was not observed which is contrary to filtration theory. One of the studies (Bi88) showed at design flow rate a flattening of the penetration plot for aerosol sizes above and below the penetration maximum. This flattening is also not predicted by filtration theory.

These findings suggest at the low flow rates and at aerosol sizes above and below the penetration maximum filter unit performance deviates from filtration theory predictions. Penetration in these flow rate and size regions may be dominated by some aerosol size independent penetration mechanisms such as filter unit leaks.

A leak model for performance of fibrous filters with "pinholes" was described by Thomas and Crane (Th63). In this model penetration

increased as flow rate decreased because of the presumed character of the flow through the installed leaks. Predicted penetration was independent of aerosol size. The models predicted high penetration at low flow rates. If under some conditions assembled filter unit penetration is predicted by a pinhole leak type model, then such models may augment fibrous filtration theory in prediction actual performance. An objective of this study is to examine the applicability of a filter leak model in predicting filter unit performance.

Currently, design of hazardous material handling facility air cleaning systems that use HEPA filter units relies on filtration theory to predict performance. In situations where protection is depended on at low flow rates or at aerosol sizes away from the size of maximum penetration, actual penetration may be higher than the design criteria. Such deviations from the design criteria could impact control of emissions.

I.B. Objectives

The overall objective of this study is to assess and understand mechanisms governing performance of assembled HEPA filter units. As mentioned above, there is experimental evidence suggesting deviation of

filter unit performance from fibrous filtration theory predictions at low flow rates and at particle sizes outside the region of maximum penetration. An initial objective is to develop a preliminary filter leak model that is consistent with data cited in the literature (see Chapter II). In the experimental phase, data is collected that examines and characterizes the potential deviations from fibrous filtration theory (see Chapters III and IV). These data are used to revise the initial filter leak model (see Chapter V). Finally, the revised filter leak model is used to explore potential health and environmental protection implications of the leak performance of HEPA filters (see Chapter VI).

I.C. Previous Research

I.C.1. Fibrous Filtration Theory

Davies (Da73) and Liu (Li85a) have compiled histories on the development fibrous filtration theory. Much of the following review of filtration theory is based on their historical analyses.

Theoretical evaluation of filter media has evolved along two lines:

1) understanding of filtration mechanisms of particle collection and

2) understanding of flow fields in which these mechanisms operate. According to Davies (Da73) results of early German studies (Fr26) first showed a peak in filter penetration as a function of particle size. These results were the first clue that a combination of filtration mechanisms were operating in the performance of a filter. One by one these mechanisms were elucidated. In 1931, impaction was found by Albrecht (Al31) to be an inertial mechanism of collection on fibers for particles on the large size side of the penetration peak. In the same year, Sell (Se31) augmented Albrecht impaction theory to include the interception collection mechanism. Collection of particles on the small size side of the peak was generally believed (Da73) to be associated with particle diffusion which was first theorized by Einstein (Ei05) to be the result thermal-molecular motion. The role of diffusion collection was formalized by Kaufmann in 1936 (Da73) with a model that included diffusion, interception and impaction mechanisms of particle collection for fibrous filters.

To this point filtration theory assumed collection mechanisms were operating in idealized potential flow where the fluid has viscosity, η, equal to 0. The validity of this assumption was questionable near fiber surfaces where viscous effects are of great importance.

In 1942, Langmuir (La42 and La61) reported his filtration theory which accounted for viscous effects in the flow field. However, this model

did not include inertial collection. Langmuir reasoned that because experimental studies available at the time showed penetration increasing with filtration velocity, inertial collection was not important. Consequently, he formulated his theory to include only diffusion and interception mechanisms of particle collection.

Langmuir filtration theory persisted until the middle 1950's when what are referred to as modern filtration theories began to be put forward. These modern theories used updated flow field models (Ku59, Ha59), included diffusion collection formulations that accounted for finite particle size (Fr58), interpreted particle collection in terms of dimensionless groups that describe fibrous filtration (Fr58, Pa60), and acknowledged the role of inertial collection. The modern theories evolved as advances were made in solving viscous flow equations for flow fields around randomly oriented cylinders.

One of the difficulties in modeling the flow field in a fibrous filter was accounting for the effect of neighboring fibers. Modern filter theories all accounted for these neighboring fiber effects in different ways. Independently in 1959, Kuwabara (Ku59) and Happel (Ha59) made major advancements in solving the viscous flow form of the Navier-Stokes equations for flow around one of many randomly-oriented cylinders. Many of the modern filtration theories are based on the Kuwabara flow field. An

experimental study conducted by Lee (Le82a) on penetration of specially prepared filter concluded that of the modern filtration theories which account for the effects of neighboring fibers "those of Spielman and Goren (Sp68), Dawson (Da69), Stechkina et al. (St69), and Yeh and Liu (Ye74) are generally in good agreement with measured data."

Modern experimental and theoretical results for fibrous filter media show that penetration curves have the general appearance as shown in Figure I-2. As the early German studies indicated a penetration maximum exists for every filtration velocity, U_0. For a given media, as U_0 decreases the entire penetration curve lowers as was observed by Langmuir (La42). Modern theories predict this behavior in diffusion dominated regions.

The latest generally accepted formulation comes from Lee and Liu (Le82b). They derived dimensionless groups related to filtration. Coefficients for the groups were estimated from correlation analysis of experimental filtration data in the region of maximum penetration. The study concluded that the dominant filtration mechanisms in this region are diffusion and interception with impaction having a second order effect. Derivations of dimensionless parameters describing diffusion and interception collection combined the boundary layer approach of Friedlander (Fr57, Fr58) and Natanson (Na57) with the Kuwabara flow field (Ku59, Ha59). Single fiber collection efficiency for diffusion, η_D, was

found to be proportional to $\left[\frac{(1-\alpha)}{Ku}\right]^{1/3} \bullet Pe^{-2/3}$, where α = the fiber volume fraction $= \frac{p \bullet d_f^2 \bullet L_f}{4}$, d_f = fiber diameter, L_f = fiber length per unit volume of filter, Ku = the Kuwabara flow factor, Pe = the Peclet number $= \frac{U_0 \bullet d_f}{D}$, D = particle diffusion coefficient in air $= \frac{k \bullet T \bullet C_C}{3 \bullet \pi \bullet \eta \bullet d_p}$, k = Boltzmann's constant, T = absolute temperature, C_C = Cunningham slip correction factor $= 1+\left(\frac{\lambda}{d}\right) \bullet \left(2.514+0.8 \bullet \exp\left(\frac{-0.55 \bullet d_p}{\lambda}\right)\right)$, λ = gas mean free path $= \left(\sqrt{2} \bullet n_m \bullet \pi \bullet d_m^2\right)^{-1}$, n_m = molecular concentration of an ideal gas, d_m = effective molecular diameter of air, and d_p = particle diameter. The proportionality constant was found to be 1.6. Single fiber collection efficiency for interception, η_R, was found to be equal to $\frac{(1-\alpha)}{Ku} \bullet \frac{R^2}{1+R}$ where R = the interception parameter $= \frac{d_p}{d_f}$. Coefficients from correlation analysis were found to be 2.6 for η_D and 0.6 for η_R. The overall penetration in the region of maximum penetration was found to be related to:

$$\eta_{DR} = \eta_D + \eta_R \qquad \text{Equation I-1.}$$

At aerosol particle diameters above 0.5 μm the role of impaction begins to be important. The crossing of penetration curves in Figure I-2 is a result impaction collection. Yeh and Liu (Ye74) derived an expression for the single fiber collection efficiency for impaction. This formulation and the single fiber efficiencies derived by Lee and Liu (Le82b) are used in this study to predict penetration of intact fibrous filter media.

I.C.2. Experimental Fibrous Filter Performance Evaluations

Numerous experimental studies of fibrous filter performance have been conducted throughout the development of filtration theory. Techniques used in these studies progressed with filtration theory and with the development of aerosol measurement and aerosol generation technology. Early filtration studies such as the German study cited by Davies (Da73) were hindered because of poor aerosol size resolution. Generation techniques were not available that could easily produce monodisperse aerosols of preset size. Measurement instruments were not yet available that had the size resolution of modern aerosol spectrometers

and classifiers. Consequently, evaluation of filter performance was relegated to broad bands of aerosol size. The limited resolution of these methods obscured some the finer details of filter performance and complicated interpretation of results.

In 1943, LaMer and Sinclair (La43) reported on a condensation aerosol generator that produced monodisperse aerosols of selected size. Generators of this type were used in the first detailed laboratory studies of filter performance (Ra51) and are still used for quality assurance testing of HEPA filters (DOE90). More recently, filter performance evaluations are being made with modern aerosol spectrometers (Sc72) and classifiers (Li74). These modern aerosol instruments provide aerosol size resolution that permits accurate plotting of penetration values.

I.C.2.a. Fibrous Media Performance

Early penetration measurements on high efficiency glass fiber media were made by Dyment (Dy69). The measurements were made at filtration velocities of ≈13 cm/sec and ≈20 cm/sec. The results show peaks in penetration as predicted by modern filtration theory (Ki75). These data indicate a crossing of the penetration curves at a particle diameter of

≈0.25 μm. These are the first data to exhibit this crossing. Such crossing was long sought as experimental evidence supporting the role of inertial collection in fibrous filters. However, crossing of the curves due to inertial collection effects is expected at larger aerosol sizes than the cross-point in this study (see Figure I-2). A review of these data attributed the crossing to experimental error (Ki75).

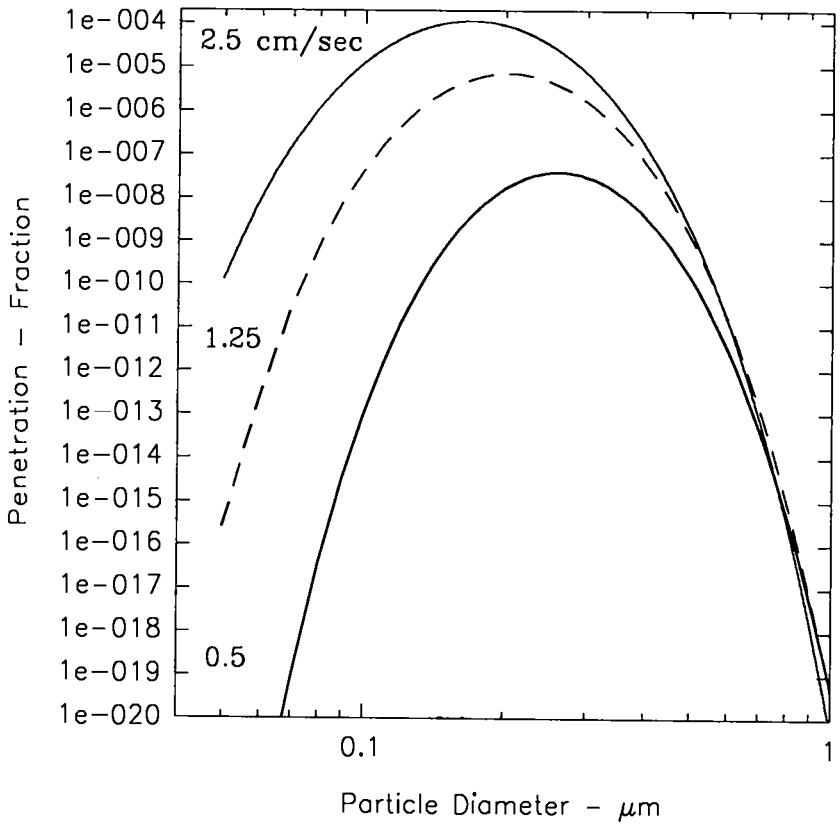

Figure I-2. Performance of HEPA filter media as predicted by fibrous filtration theory.

More recent studies of HEPA filter media were performed by Liu *et al* (Li85b) using an electrostatic classifier. Results showed penetration data similar to predictions of theoretical evaluations (see Figure I-3). The data shows penetration maxima that occur at aerosol sizes predicted by the modern filtration theories. The data showed no crossing of the penetration plots for different filtration velocities.

I.C.2.b. Constructed Filter Performance

Schuster and Osetek were the first to report laser spectrometer penetration measurements on assembled HEPA filter units (Sc77). The measurements were made at the filter design flow rate of 708 Lpm (liters per min, 25 cubic feet per min [cfm]). This flow rate corresponds to a filtration face velocity of roughly 2.5 cm/sec. The penetration measurements show a maximum at ≈0.2 μm diameter which is expected from filtration theory.

Kozuka (Ko80) made penetration measurements on two sizes of HEPA filter units with design flow rates of 708 Lpm and 1420 Lpm (50 cfm). Measurements were made with a laser spectrometer at the design flow rate

and at 20% of the design flow rate. Penetration was observed to decrease steadily with increasing aerosol size. Penetration at 20% design flow rate was distinctly flatter than penetration at the designed flow rate which is contrary to filtration theory predictions and the media evaluation of Liu (Li85b). Review of the published penetration plots showed crossing at a particle diameter of ≈0.6 μm. These are the first data on assembled filter units to exhibit crossing. No mention of the crossing was made in the paper This crossing may be related to impaction collection effects.

Crossing of penetration plots was reported by Scripsick (Sc86) in 1986. Precise penetration measurements were made on several 28.3 M^3/min (1000 cfm) HEPA filter units at design flow rate and at 20% of design flow rate. These flow rates correspond to filtration velocities of ≈2.5 cm/sec and ≈0.5 cm/sec, respectively. An example of the results is plotted with some of Liu's data in Figure I-3. Design flow rate plots show maximum penetration at ≈0.15 μm aerosol diameter. The 20% flow rate measurements were observed to be largely independent of aerosol size which is contrary to theoretical predictions and Liu's(Li85b) measurements on HEPA filter media. The aerosol size of crossover varied for each filter and for the published plots ranged from ≈0.15 μm to >0.4 μm aerosol diameter. This crossing is in the aerosol size range which Lee and Liu

indicated was dominated by diffusion and interception collection and in which inertial collection played a minor role (Le82b).

In 1987 results of a study (Sc87b) of 849 HEPA filters were reported. A laser spectrometer system was used to measure penetration at 15 sizes in the particle diameter range from ≈0.1 μm to ≈0.4 μm. Measurements were made at the design flow rate and at 20% of design. Four sizes of filters were tested with design flow rates from 14.2 M^3/min (500 cfm) to 39.6 M^3/min (1400 cfm). Filters were obtained from a variety of manufacturers and represented a variety of models. Inspection of results showed distinct peaks in penetration at design flow rate. No peak in penetration was observed in the measurements at 20% of design. This result is contrary to filtration theory predictions and the results of experimental media evaluation. Computer analysis of the data showed 90% of the design flow rate measurements had peak penetrations in the 0.14 μm to 0.18 μm diameter range with all design flow rate tests having a maximum at a diameter < 0.22 μm. No such clustering of peak penetration measurements was observed for the 20% of design flow rate measurements. These results are consistent with the conclusion that a large portion of the HEPA filters studied show the deviations from filtration theory that were observed in the detailed HEPA filter measurements reported by Scripsick (Sc86).

Hinds et al (Hi87a, Hi87b) have reported on the performance of "dust, fume, and mist" cartridge filters used on half-mask respirators. Penetration measurements were made using a laser aerosol spectrometer at volume flow rates ranging from 2 Lpm to 150 Lpm. The penetration peak for the highest flow rate is observed to flatten as flow rate is decreased. At the highest flow rates (> 50 Lpm) a penetration maximum is observed at approximately 0.2 μm aerodynamic diameter which is in agreement with filtration theory (Fa88). At lower flow rates the maximum is much less distinct which is contrary to theory. No crossover of the plots for different flow rates was observed.

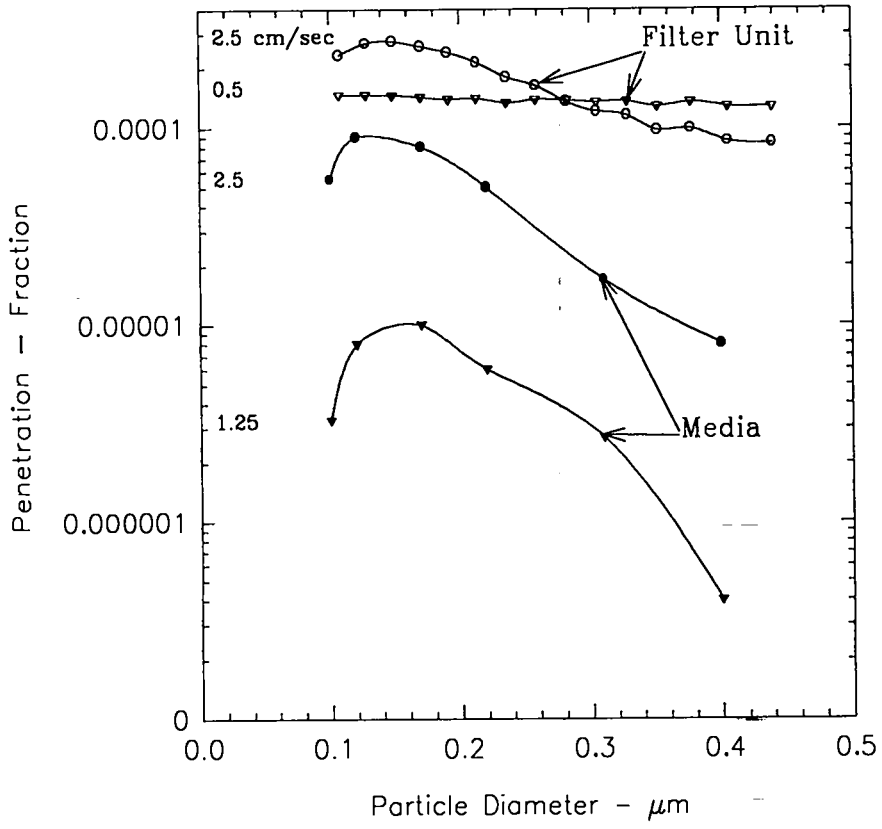

Figure I-3. Penetration data for HEPA media and a HEPA filter unit. The media results display features predicted by fibrous filtration theory. Results for the filter unit show departures from these predictions.

Fardi in 1988 reported on a study similar to Hinds (Fa88). He predicted the size of maximum penetration for "dust, fume, and mist" respirator cartridges to be approximately 0.2 μm particle diameter. His penetration measurements were made with an electrostatic

classifier/condensation nucleus counter system, a laser spectrometer system, and an aerodynamic particle sizing system. He found good agreement among measurements made with the systems. His measurements were made at flow rates of 16 Lpm, 28 Lpm, and 48 Lpm. Distinct penetration maxima were observed at all flows. This result is in agreement with filtration theory but in conflict with the results of Hinds (Hi87a). No crossover was observed.

Biermann and Bergman (Bi88) presented data on HEPA filter unit performance in a paper comparing filter test methods. The data was collected on a 14.2 M^3/min filter operating at the design flow rate. A peak in the penetration data was observed at ≈0.14 μm particle diameter. At particle diameters below ≈0.06 μm and above ≈0.3 μm, penetration is observed to approach a constant non-zero value. This performance in these size ranges is not expected from filtration theory.

I.C.2.c. Filter Performance with Leaks

Evaluation of HEPA filter unit performance must include assessment of leakage in addition to assessment of penetration. That fibrous filters leak is an accepted fact, what is questioned is the degree of leakage. In 1973,

Davies (Da73) wrote "Recent developments in air filtration have been more associated with prevention of edge leakage and mounting than with the intrinsic efficiency of the filter itself, since this is no longer the limiting factor in performance." The Institute of Environmental Sciences (IES) in their standards on HEPA filters (IES86) classifies the filters not only on the degree of penetration but also on their degree of leakage. IES defines pinhole leaks as penetration that "increases with decreasing flows and is relatively independent of particle size."

For this study leaks are defined as unplanned flow-paths in filter units. Leaks in filter units have many potential sources such as defects in media and other filter unit components, damage to media during filter construction, defects in filter construction, and damage to filters during testing, handling ,and transport. Fibrous filter media is fragile and vulnerable to damage (Gi60).

Performance of fibrous filters with leaks was first reported by Knudson and White (Kn45) as part of the development of quality assurance filter test systems. The report is the first to use the term "pinhole effect" to describe the performance of filter units with leaks. An expression for penetration as a function of flow rate was derived in which flow rate through leaks is assumed to have a $\Delta p^{1/2}$ dependence and filter flow rate is assumed to be proportional to Δp, where Δp = filter differential pressure.

In another report, Parrish and Schneider (Pa63) describe the pinhole effect: "The air penetrating the filter medium has laminar or streamline flow characteristics, whereas the air flow through the hole or defect is turbulent. In turbulent flow, pressure drop is proportional to the square of the flow rate, whereas in laminar flow, direct proportionality exists. Since the pressure drop across the hole (defect) must equal the pressure drop across the filter medium, a lesser increase in flow through the hole is required to balance an increase in flow through the filter medium. In other words, proportionately less unfiltered smoke passes through the filter-hole combination with increasing flow in the system, and thus an improvement in the system efficiency is observed." Parrish and Schneider derive an equation that shows leak flow rate proportional to the square root of filter flow rate . Agreement with experimental data is demonstrated using an experimentally determined proportionality constant.

Thomas and Crane (Th63) reported a detailed study of fibrous filter performance with leaks. They derived an equation giving penetration of a filter with holes:

$$P(Q) = P_M(Q) + \left[P(Q_{de}) - P_M(Q_{de})\right]\left[\frac{Q_{de}}{Q}\right]^{1/2} \qquad \text{Equation I-2.}$$

where, P(Q) = overall filter unit penetration at flow rate Q, Q = volume flow rate, $P_M(Q)$ = penetration of intact media at flow rate Q, Q_{de} = design flow rate. The derivation assumes leak flow is in the turbulent region and flow rate is proportional to $\Delta p^{1/2}$. Results of experiments on filters with installed leaks were compared with predictions made using Equation I-2.

Fahrbach (Fa70) described three filter leak regimes. One was the turbulent flow regime of Thomas and Crane (Th63). Another was a laminar flow regime in which leak flow rate was described by the Hagen-Poiseuille equation. The third was transition regime between turbulent and laminar flow.

In 1986, Scripsick reported on studies of filters with installed leaks (Sc86). Penetration measurements were made on a HEPA filter unit with a design flow rate of 28.3 M^3/min using a laser aerosol spectrometer. Measurements were made at the design flow rate and at 20% of the design flow rate on the intact filter and as increasing numbers of leaks were installed. Measurements on the intact filter showed design flow rate penetration greater than penetration at 20% of design, and a penetration maximum in the design flow rate measurements with the 20% flow rate measurements relatively independent of aerosol size. Comparison with measurements on the filter with installed leaks showed 1) the design flow rate penetration peak disappearing as successive leaks were installed, and

2) for the filter with installed leaks, penetration at 20% of the design flow rate was greater than penetration at the design flow rate. These findings are consistent with predictions of pinhole leak performance described by Thomas and Crane (Th63) and leak flow dominating filter unit penetration at lower flow rates.

I.C.3. Leak Flow

Understanding leak flow is important in design and evaluation of several engineering control and personal protection strategies. Early studies of pinhole leaks in filters assumed leak flow rate was proportional to $\Delta p^{1/2}$ (Kn45, Pa63, Th63). Fahrbach (Fa70) described a Poiseuille laminar flow regime and a transition flow regime between laminar and turbulent flows for leaks in filters. In these regimes filter leak flow rate was proportional to Δp raised to powers between 0.5 and 1. A study of respirator facial seal leaks assumed leak flow rate was proportional to $\Delta p^{0.75}$ (Ca88). Studies conducted by Hinds (Hi87a) evaluated installed facial seal leaks with flow rates proportional to Δp raised to powers between 0.5 and 1.

Bird, Stewart, and Lightfoot (Bi60) use a friction factor, f, to predict flow in tubes. Friction factor is proportional to the ratio of Δp and the flow

kinetic energy density, $\frac{1}{2} \bullet \rho_f \bullet U_0^2$, where ρ_f = density of the fluid, U_0 = free stream fluid velocity. This approach allows for determination of flow rate in the Poiseuille laminar flow and turbulent flow regimes but does not predict flow rate in the transition between these regimes.

Leak flow may be affected by developing flow near the entry of a leak. To assess the impact of these entry effects for laminar flow Bird, *et al* (Bi60) introduces an entrance length parameter, ℓ_e, which is an estimate of the travel length for flow to develop a parabolic profile. They give a value of $\ell_e = 0.035 \bullet Re_f \bullet d$, where Re_f is the flow Reynolds number $= \frac{\rho_f \bullet U_0 \bullet d}{\eta}$. The Chemical Engineers' Handbook (Pe50) gives an $\ell_e = 0.065 \bullet Re_f \bullet d$. Friedlander (Fr77) gives an expression for length Reynolds number, $Re_\ell = \frac{\rho_f \bullet U_0 \bullet \ell}{\eta}$ and states that for $Re_\ell < 5 \times 10^5$ the boundary layer for flow along a surface remains laminar. He also defines a flow boundary layer thickness $\delta_V = 1.72 \bullet \ell \bullet Re_\ell^{-1/2}$. A formula for ℓ_e can be derived from these expressions, $\ell_e = 0.085 \bullet Re_f \bullet d$. These formulations provide a method of assessing the portion the leak-path associated with developing flow. Leaks with a large portion of leak-path associated with entry length are less well

described by Poiseuille laminar flow theory than others with only a minor part of the leak-path associated with the entry length.

Kreith and Eisenstadt (Kr57) studied laminar flow in short capillary tubes with length, ℓ, to diameter, d, ratios between 0.45 and 18, and flow $Re_f \leq 1700$. They discovered a correlation between the product of ℓ/d and f, and the product of ℓ/d and Re_f^{-1}. The correlation defines the transition between Poiseuille laminar flow and non-Poiseuille laminar flow that results from entry effects. This correlation was used by Hinds (Hi87a) to explain behavior of installed leaks in respirators that were found to have flow rate proportional to Δp to powers between 0.5 and 1.

I.D. Approach

One assessment that can be made from the cited filter performance data is that filtration theory may not completely explain performance of HEPA filter units. Data supporting deviation from filtration theory exists at low flow rates and in the aerosol size regions outside the region of maximum penetration (Ko80, Sc86, Hi87a, Sc87a, Sc87b, and Bi88). This

assessment is based on the observations that: 1) at low flow rates the penetration maximum predicted by filtration theory disappears and to a first approximation penetration is independent of particle size and 2) at aerosol sizes outside the region of maximum penetration, penetration becomes independent of aerosol size. One potential explanation of these findings is that filter unit performance at these flow rates and in these aerosol size ranges is being dominated by filter unit leaks.

The overall approach for the study is to develop a model predictive of leaky filter performance and to collect experimental data to evaluate the model. Consequently, the study is divided into two phases, a theoretical phase dealing with development of the model and an experimental phase to collect data on filter unit performance.

I.D.1. Theoretical Phase

A comprehensive study of assembled filter unit performance should include an assessment of all filter unit components. Each component should be evaluated for penetration and leakage. Based on this component approach overall filter unit penetration, P, can be written as:

$$P = \left[\sum_i P_i \frac{Q_i}{Q}\right] + \left[\sum_j \frac{Q_j}{Q}\right] \qquad \text{Equation I-3,}$$

where, P_i is penetration through component i, Q_i is flow rate through component i, Q_j is leak flow rate through component j, and Q is total flow rate, $= \sum_i Q_i + \sum_j Q_j$. This equation assumes that penetration through leaks equals 1.

For an intact filter all flow is assumed to go through the media and the media is assumed to be free of leaks. In this case P equals penetration through the media, P_M. In this study the initial filter model will assume that all flow goes through the media and that the media may have leaks. The initial model has the form:

$$P = P_M\left(1 - \frac{Q_L}{Q}\right) + \frac{Q_L}{Q} \qquad \text{Equation I-4,}$$

where, Q_L is leak flow rate.

Equation I-4 can be used to derive Equation I-2 if Q_L is assumed to be proportional to $\Delta p^{1/2}$. Examination of equation I-2 shows that for very low values of Q, penetration values greater than 1 are predicted. This physically impossible result indicates that pinhole leak theory breaks-down

for low values of Q. The reason for the failure is that at low Q values the assumption that leak flow rate, Q_L is proportional to $\Delta p^{1/2}$ is no longer valid. The approach in this study is to assume at low values of Q, the leak flow rate dependence will undergo a transition from an approximately $\Delta p^{1/2}$ at higher Q values to approximately a Δp^1 dependence at lower values of Q. With this approach, at sufficiently low values of Q, predicted penetration approaches a constant.

The initial model formulation of the leak flow rate dependence on Δp comes from the correlation of Kreith and Eisenstadt (Kr57). The correlation defines the relation among Q_L, Δp, ℓ, and d, and for example permits calculation of Q_L given the other parameters. In Chapter II expressions are developed for Q_L and for particle losses in leak flow paths.

I.D.2. Experimental Phase

The overall objective of the experimental phase of the study is to collect data on the performance of fibrous filters that can be used to evaluate deviations from filtration theory. A test aerosol was generated to challenge filter units operating at specific flow rates. At each flow rate measurements of P, Q, and Δp were made.

The test filters were nuclear grade (IES type B, see Chapter III) HEPA filters. They were selected for several reasons:

1) performance of these filter has been observed to deviate from filtration theory,

2) specifications of these filters prohibit patching of pinhole leaks in media and permit such leaks to a specified degree (IES86),

3) rated penetration and expected low flow rate penetration of these filters is in the range of measurement for existing measurement techniques,

4) these filters are the most frequently used in applications for protection of public and worker health, and the environment,

5) these filters are used in many applications where protection is required at low flow rates,

6) there is a large database on performance of these filters and the media used in the filters, and

7) there are many specifications, standards, and regulations pertaining to these filters that may be affected by information developed in this study.

The investigation covers penetration over the 0.1 μm to 0.5 μm aerosol diameter range. This corresponds to the region of maximum penetration at design flow rate for the current generation of type B HEPA filters. Measurement of P in this region offers two advantages: 1) in the rated flow range this is the region of maximum penetration so performance assessment in this size range is conservative for the entire aerosol size spectrum, and 2) in this size range filtration theory predicts penetration quickly dropping below measurable levels as flow decreases so that significant penetration values observed in this region can arguably be attributed to mechanisms other than those considered in filtration theory. Details of the methods used in the experimental phase are given in Chapter III. Experimental results are presented in Chapter IV. In Chapter V, the results are analyzed and interpreted, and conclusions coming from the study are discussed.

CHAPTER II. LEAK FLOW AND LEAK PENETRATION

II.A. Hypothesis

The fundamental hypothesis of this study is that, in certain ranges of flow rate and aerosol size, performance of assembled HEPA filter units can be predicted by a leak flow penetration model. The model assumes that under these conditions filter unit performance is dominated by leak flow and not by mechanisms considered in fibrous filtration theory. Further, the model assumes leak flow rate is completely determined by differential pressure and leak geometry.

A qualitative description of filter unit performance expected from such a model is presented in Figure II-1. Near the design filtration velocity, penetration is characteristic of filtration theory with a distinct maximum observed at the predicted particle diameter. Initially as velocity is reduced, penetration decreases as is predicted by diffusion dominated fibrous filter penetration. Also, the penetration curve begins to flatten in the particle diameter dimension and the penetration maximum disappears. This flattening is not predicted by filtration theory and is the first indication that overall filter unit penetration is being affected by leak flow.

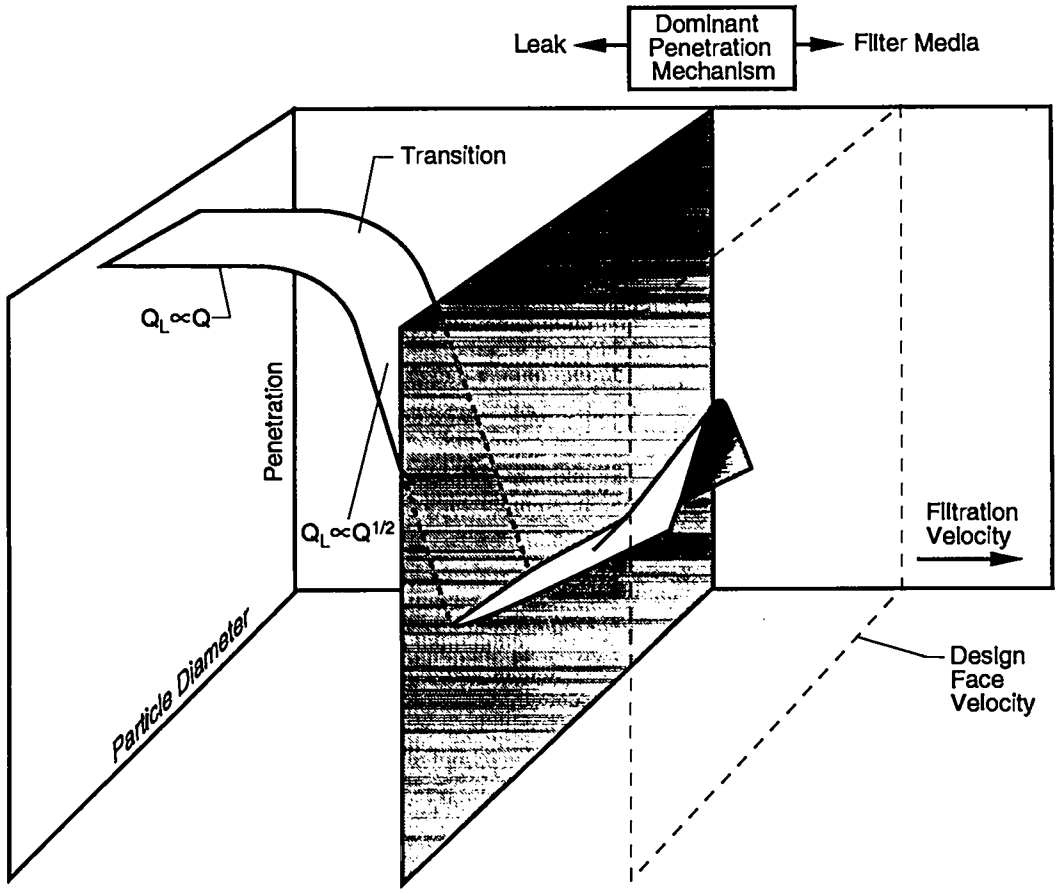

Figure II-1. A qualitative description of filter unit performance predicted by the transition leak flow model.

With further reduction of filtration velocity, penetration becomes largely independent of aerosol size, and a penetration minimum is observed in the penetration/filtration velocity plane. At this minimum, leak flow begins to dominate filter unit penetration. At lower filtration velocities, penetration rises because the proportion of leak flow rate to total flow rate increases.

The increase is the result of the flow character difference between the leak and the filter. Filter flow rate, Q, is proportional to Δp (Fa86) whereas leak flow rate, Q_L, may be proportional to Δp to a power between 0.5 and 1. Thus for $Q_L \propto \Delta p^{1/2}$, $Q_L \propto Q^{1/2}$.

Below a certain filtration velocity, the rise in penetration slows and penetration begins to approach a constant. This transition is a result of leak flow character changing to Poiseuille laminar flow, the same as that in the filter. Further reduction in velocity fails to affect penetration because the proportion of flow rate through leaks relative to that through the filter does not change. In this flow region both filter flow rate and leak flow rate are proportional to Δp and $Q_L \propto Q$.

Performance of individual filter units will vary from this general description. Performance of units with a few small leaks or with no leaks may more closely follow filtration theory. Filter units with small size leaks may not display a penetration minimum because leak flow is in the Poiseuille laminar flow region (see Figure II-2). Depending on the number of small leaks, penetration may not reach a constant value until values much below the design flow rate penetration are reached. Filters with larger leaks will perform more closely to the leak flow prediction shown in Figure II-1.

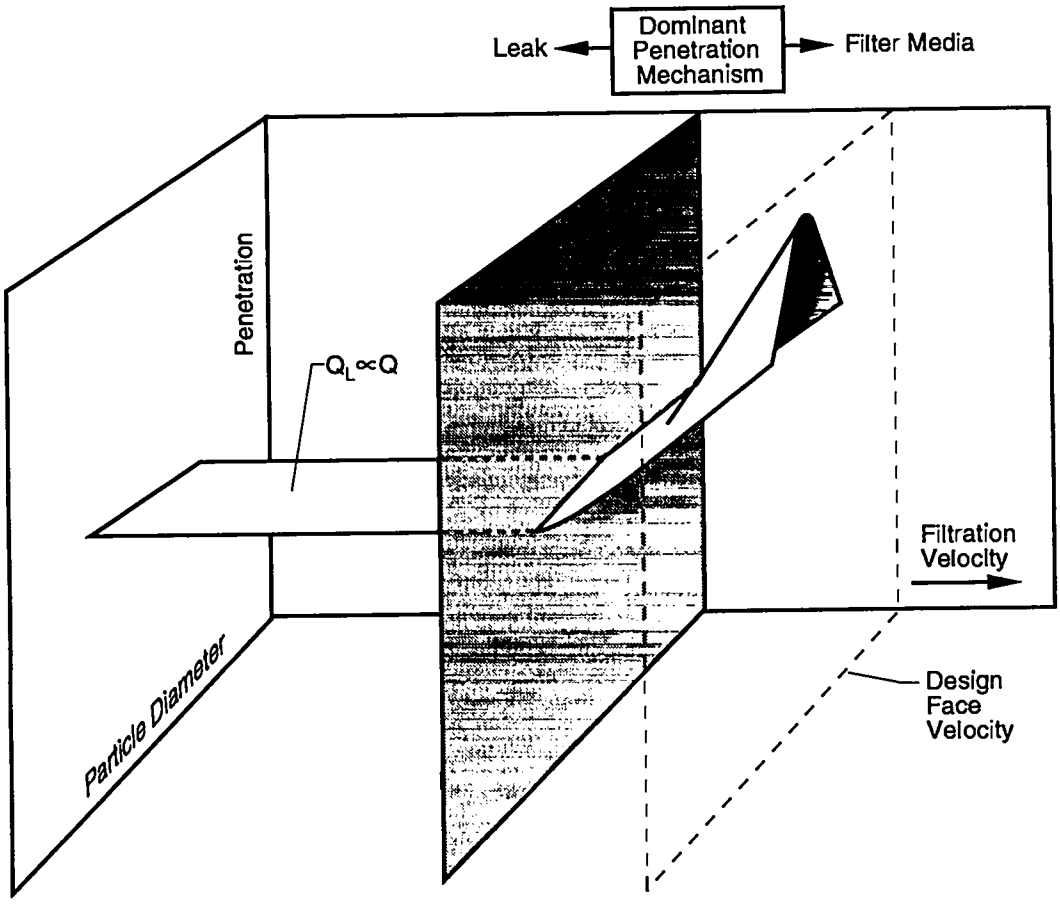

Figure II-2. Performance predicted by transition leak flow model when leak flow character matches that of filter unit.

II.B. Derivation of Transition Leak Flow Model

II.B.1. Leak Flow Character

As mentioned above leak flow rate is assumed to be determined by differential pressure and leak geometry. Its dependence on these parameters varies with leak flow character. The flow rate of viscous flow in a tube is given by the Hagen-Poiseuille equation,

$$Q_L = \frac{\pi \bullet \Delta p \bullet d^4}{128 \bullet \eta \bullet \ell} \qquad \text{Equation II-1,}$$

in which flow rate is proportional to Δp. This flow is refereed to as Poiseuille laminar flow and is characterized by a parabolic flow field when fully developed. According to Fain (Fa86) HEPA filter unit flow rate, Q, is viscous dominated with $Q \propto \Delta p$. Leak flow may deviate from Poiseuille laminar flow in two ways. At flow Reynolds numbers, Re_f, less than approximately 2000, development of Poiseuille laminar flow from inviscid flow at the flow conduit entry creates a region along the conduit in which flow rate is not described by the Hagen-Poiseuille equation. In this region

the viscous sub-layer swells to include the entire conduit cross-section. If this entry length is sufficiently long compared to the conduit length, flow rate over the entire conduit may depart from predictions of the Hagen-Poiseuille equation. This deviation from Poiseuille flow is described by the Kreith and Eisenstadt correlation. At Re_f>2000, the sub-layer can become turbulent and fully developed turbulent flow can result. In this case flow is inertially dominated and flow rate is proportional to Δp to a power <1 but $\geq$ 0.5.

The prediction of a penetration minimum and subsequent rise in penetration with decreasing filtration velocity is predicated on leak flow rate dependence on Δp differing from that of the filter unit. When the two flow rates have the same Δp dependence, fractional leak flow rate becomes independent of flow rate.

To assess leak flow character, the correlation for tube flow in Bird et al (Bi60) was used. The object of this analysis was to determine leak diameters that may have a Δp dependence to a power <1 at Δp values corresponding to Q $\leq$ design flow rate. The nominal design flow rate Δp for type B HEPA filters was estimated as 2230 dyn/cm^2 (0.9" of H_2O). The Bird, et al correlation was used to determine values of f, the Fanning friction factor, corresponding to selected values of flow Reynolds number, Re_f. From the values of Re_f and f, values of the dimensionless group $Re_f(f)^{1/2}$

were calculated. This group depends on Δp, ℓ, and d, and is independent of leak flow rate, Q_L. A plot of $Re_f(f)^{1/2}$ versus Re_f was used to estimate Reynolds number of leak flow over a range of leak diameters. In this analysis a value of 0.0508 cm (0.02") was used for filter thickness, ℓ. This value for ℓ is slightly greater that the minimum thickness of 0.043 cm (0.017") specified for HEPA filters (MS88).

Flow Reynolds numbers >2000 were interpreted as indicating leaks with a Δp dependence to a power <1 and having the potential for non-laminar flow. Flow Reynolds numbers above 2000 were found for leaks with diameters >0.05 cm operating at a Δp of 2230 dyn/cm^2, for leaks with diameters >0.1 cm operating at 250 dyn/cm^2 (0.1" of H_2O), and for leaks with diameters $\geq$1 cm operating at 0.25 dyn/cm^2 (0.0001" of H_2O).

Values of Re_f were also used to evaluate leak entry length, $\ell_e = 0.035 \bullet Re_f \bullet d$ (Bi60). The entry length is used to make corrections to Hagen-Poiseuille flow rate predictions. Leaks with ℓ_e >0.1 ℓ, were interpreted to deviate significantly from Poiseuille laminar flow and have the potential for non-Poiseuille laminar flow. Results showed deviations from Hagen-Poiseuille predictions for leaks operating at a Δp of 2230 dyn/cm^2

with diameters ≥0.01 cm, and for leaks operating at 250 dyn/cm^2 with diameters ≥0.02 cm.

Inspection of HEPA filter frames and media packs revealed no visible leaks. Holes made in the media ≥0.03 cm in diameter were readily visible. No smaller holes were made. Results of this procedure demonstrate that straight-through leaks of the size required to deviate from Poiseuille flow would be visible. Consequently, leak flow behavior of filter units is probably not the result of a small number of straight-through leaks with diameters of few tenths millimeters. The behavior is potentially related to non-straight leak paths with diameters of a few tenths of millimeters and larger, as well as non-straight and straight leak paths with smaller diameters.

These analyses indicate that leak flow character may deviate from Hagen-Poiseuille flow for leak diameters ≥0.01 cm at the type B HEPA filter nominal design Δp of 2230 dyn/cm^2 and a leak path length of 0.2 cm even though Re_f in the leaks is less than 2000. Filters with leaks of this size and greater may display the leak flow performance illustrated in Figure II-1. Filters with no leaks this size or larger are more likely to display performance illustrated in Figure II-2.

II.B.2. Short Capillary Flow Approach

II.B.2.a. Kreith and Eisenstadt Correlation

The work of Kreith and Eisenstadt (Kr57) provides a method for determining Q_L when values for Δp, ℓ, and d are known and Re_f is less than approximately 2000. The values of Q_L are needed to calculate P(Q) in Equation I-4. Kreith and Eisenstadt measured Q_L and Δp for a several combinations of ℓ and d, in the ℓ/d range from 0.45 to 16. These leaks were characterized as short capillaries. They had circular cross-sections and an axis perpendicular to their inlet face.

Data from these measurements were grouped into two dimensionless parameters $X = \frac{\ell}{d} \bullet Re_f^{-1}$ and $Y = \frac{\Delta p}{\frac{1}{2} \bullet \rho_f \bullet U_0^2}$. When plotted against one another these groups form a single curve (see Figure II-3). This curve is referred to as the Kreith and Eisenstadt correlation. The curve permits determining one of the four parameters Q_L, Δp, ℓ, and d, given the other three.

To determine Q_L from Δp, ℓ, and d a plot was made of the dimensionless groups X versus and $XY^{-1/2}$. As can be seen in Figure II-4 when plotted this way, all the Kreith and Eisenstadt (Kr57) data again fall on one curve. The group $XY^{-1/2}$ depends on Δp, ℓ, and d and is independent of Q_L. Consequently, $XY^{-1/2}$ can be calculated given Δp, ℓ, and d. The plot can be used to give a value for X from which Q_L can calculated.

An equation for the curve in Figure II-4 was fit using linear multivariate regression. Values of X and Y were recalculated using the measurement data of Kreith and Eisenstadt (Kr57). The fit had a correlation coefficient, r^2, of >0.99 and a plot of the residuals showed them to be uniformly scattered about 0. Figure II-4 shows the Kreith and Eisenstadt (Kr57) data and the fitted curve. The fit model was:

$$\mathrm{Log}X = \beta_0 + \beta_1 \bullet \mathrm{Log}\left(XY^{-1/2}\right) + \beta_2 \bullet \mathrm{Log}^2\left(XY^{-1/2}\right) \qquad \text{Equation II-2.}$$

The regression analysis gave the following values for the regression constant and coefficients: $\beta_0 = 1.91$, $\beta_1 = 2.33$, and $\beta_2 = 0.22$. Estimates of X from this fit are used to calculate Q_L using the following equation:

$$Q_L = \frac{\pi \bullet \ell \bullet \eta}{4 \bullet \rho_f \bullet X}$$ Equation II-3.

Figure II-4 shows that at high values of $XY^{-1/2}$, X approaches values predicted by the Hagen-Poiseuille equation. Review of X estimates using Equation II-2 indicates that for $XY^{-1/2}$ values >0.083 these estimates begin to deviate from the Hagen-Poiseuille predictions. Consequently, Equation II-3 is used to predict Q_L for values of $XY^{-1/2}$ from approximately 0.001 to 0.083. For values of $XY^{-1/2}>0.083$, the Hagen-Poiseuille equation is used to predict Q_L.

II.B.2.b. Single Leak Model

The first generation single leak model is given in Equation I-4 where intact media penetration, $P_M = \exp\left(-\frac{4 \bullet \alpha \bullet \eta_{DRI} \bullet \ell_F}{\pi \bullet d_f}\right)$, η_{DRI} = single fiber efficiency for diffusion, interception and impaction, ℓ_F = filter media thickness, and Q_L is given by Equation II-3 for $0.001 \leq XY^{-1/2} \leq 0.083$ and by Equation II-1 for $XY^{-1/2}>0.083$. This model is appropriate in situations where filter leak performance is associated with a single leak or multiple

leaks that behave as a single equivalent leak. An example of this performance is shown in Figure II-2. In the region where penetration is constant relative to filtration velocity, leak flow rate is determined by the Hagen-Poiseuille equation. All leaks have the same Δp dependence so that partitioning of leak flow rate is not affected by Δp or Q, and Q_L can be represented by a single equivalent leak.

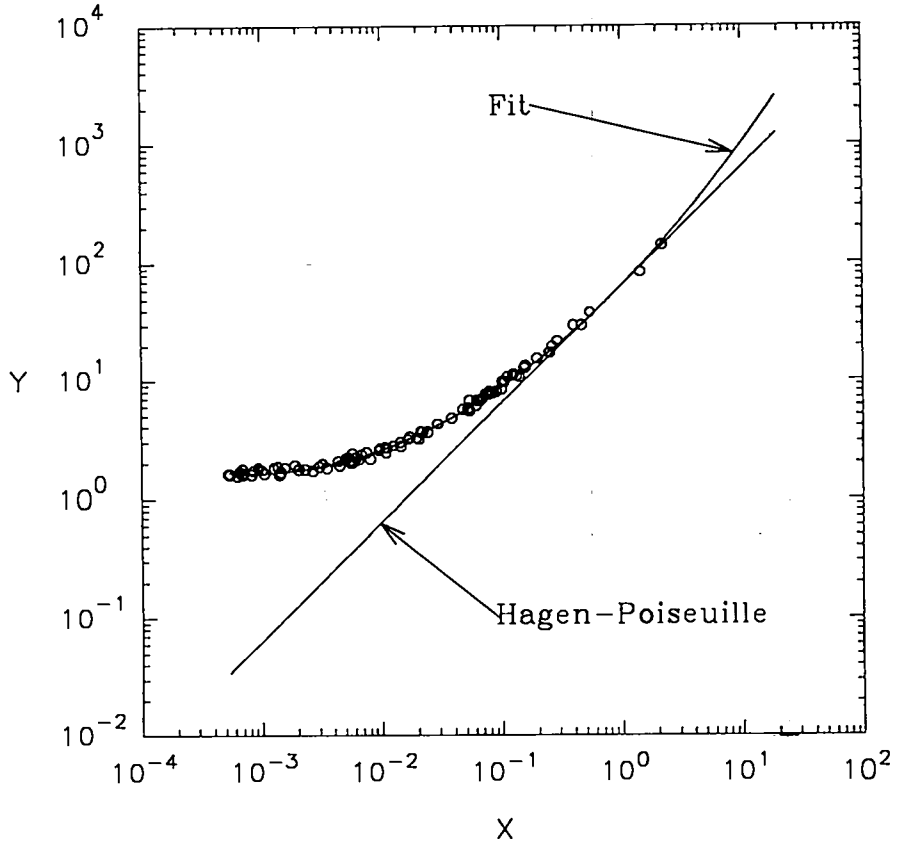

Figure II-3. Kreith and Eisenstadt correlation plot showing experimental data, a fit to the data from regression analysis, and Hagen-Poiseuille predictions.

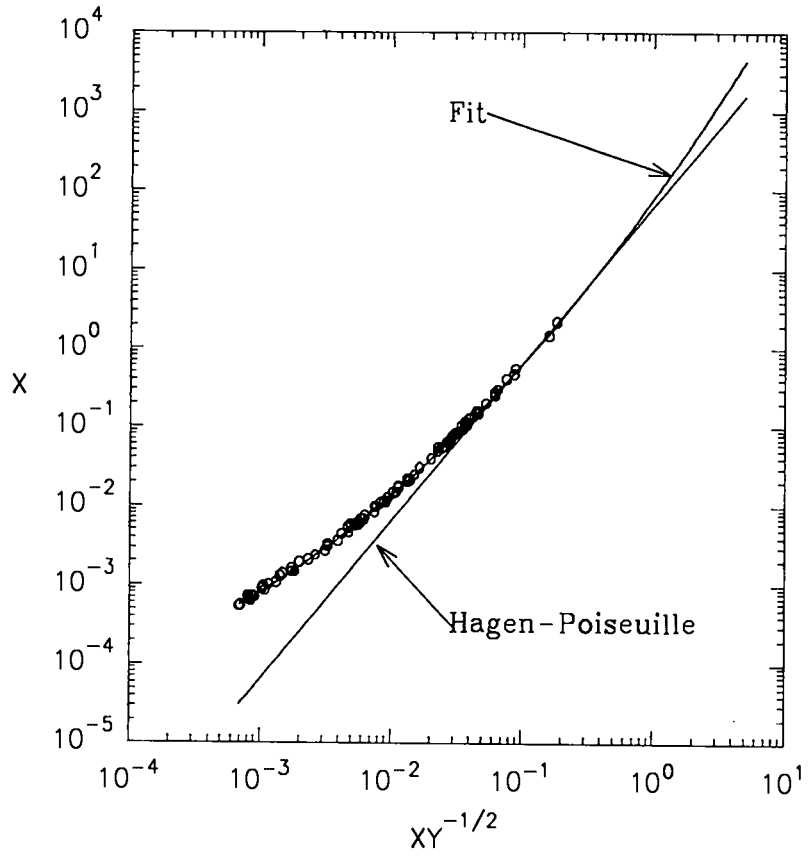

Figure II-4. Graph of X versus $XY^{-1/2}$ showing Kreith and Eisenstadt (Kr57) experimental data, estimates of X from regression analysis, and Hagen-Poiseuille predictions.

Another example where the single leak model may be appropriate is the trivial multiple leak case where all leaks have the same ℓ and d. This performance is a special case of that shown in Figure II-1. In this case filter leak performance is not confined to $XY^{-1/2}>0.083$ and the leak flow rate

dependence on Δp is not fixed. However, because all leaks have the same geometry, at any given $XY^{-1/2}$ the dependence on Δp is the same for each leak. In this situation the overall leak dependence on Δp may change depending on the value of $XY^{-1/2}$ so a penetration minimum and a rise in penetration may be observed. However, the proportioning of leak flow rate among the leaks does not change with $XY^{-1/2}$ and the leak flow rate for each leak is equal to $\sum_{i} \frac{Q_{Li}}{N_L}$, where N_L is the number of leaks.

The Kreith and Eisenstadt correlation was used to examine the trivial multiple leak case. Two identical leaks were modeled with $\ell = 0.0508$ cm and d = 0.0508 cm. The individual leak Q_L was determined over a range of Δp from 2.5×10^{-8} dyn/cm^2 (10^{-11} "of H_2O) to 1.25×10^4 dyn/cm^2 (5" of H_2O) using Equation II-3 for $0.001 \leq XY^{-1/2} \leq 0.083$ and Equation II-1 for $XY^{-1/2} > 0.083$. Flow rate through a single equivalent leak was estimated to be 2 Q_L. The d of the equivalent single leak was determined from the equation,

$$d = \left[\frac{8 \bullet \rho_f \bullet (2 \bullet Q_L)^2 \bullet Y}{\Delta p \bullet \pi^2} \right]^{1/4} \qquad \text{Equation II-4,}$$

which is a restatement of the definition of Y, substituting $\frac{4 \bullet (2 \bullet Q_L)}{\pi \bullet d^2}$ for U_0 and solving for d.

Values of Y were determined from a regression of Y on X (see Figure II-3). Flow rate through the equivalent single leak was set at twice the flow rate of the individual leaks $2 \bullet Q_L$. The length of the single equivalent leak was set at twice the length of the individual leaks or $2 \bullet \ell$. This value of leak length assured that the X values for this leak were the same as those of the individual leaks at any given Δp. This condition is necessary in order for the Δp dependence of the equivalent leak to be the same as that of the individual leaks.

An equation for the data in Figure II-3 was fit using linear multivariate regression. Values of X and Y were recalculated using the measurement data of Kreith and Eisenstadt. The fit had a r^2 of >0.99 and a plot of the residuals showed them to be uniformly scattered about 0. Figure II-3 shows the Kreith and Eisenstadt data and fitted curve. The fit model was:

$$LogY = \beta_0 + \beta_1 \bullet LogX + \beta_2 \bullet Log^2X \qquad \text{Equation II-5.}$$

The regression analysis gave the following values for the regression constant and coefficients: $\beta_0 = 1.83$, $\beta_1 = 1.11$, and $\beta_2 = 0.145$.

Figure II-3 shows for X>0.1, the Y estimates approach values predicted by the Hagen-Poiseuille equation. Review of Y estimates using Equation II-5 indicates that for X >0.45, these estimates begin to deviate from the Hagen-Poiseuille predictions. Consequently, Equation II-4 is used to predict d for values of X from approximately 0.001 to 0.45. For values of X>0.45, the Hagen-Poiseuille equation is used to predict d.

Results of this analysis are shown in Figure II-5. For X>0.45 a constant d of 0.0718 cm was predicted. For $0.001 \leq X \leq 0.45$, the predicted values of d oscillates between 0.067 cm and 0.073 cm. The oscillation may be an artifact of the precision of the fit of the Kreith and Eisenstadt data. Another potential explanation is that the result indicates that no single value of d is sufficient to describe multiple-leak flow behavior in the non-Poiseuille laminar flow region. This ambiguous result may be important to the modeling of multiple flow path systems. A follow-on study to address these issues is described in Section VI.C.1.

II.B.2.c. Multiple Leak Model

The first generation multiple leak model is given in Equation I-4 where $P_M = \exp\left(-\frac{4 \bullet \alpha \bullet \eta_{DRI} \bullet \ell_F}{\pi \bullet d_f}\right)$ and Q_L is the sum of leak flow through

all leaks = $\sum_i Q_{Li}$. The values for the Q_{Li}'s are given by Equation II-3 for $0.001 \leq XY^{-1/2} \leq 0.083$ and by Equation II-1 for $XY^{-1/2} > 0.083$. This model is appropriate in situations where filter leak performance is associated with multiple leaks that behave independently and cannot be represented by a single equivalent leak. An example of this performance is shown in Figure II-1. In the region where penetration is constant relative to filtration velocity, leak flow is determined by the Hagen-Poiseuille equation. All leaks have the same Δp dependence so that partitioning of leak flow is not affected by Δp or Q, and Q_L can be represented by a single equivalent leak. At higher filtration velocities penetration depends on filtration velocity. Leak flow rate dependence on Δp may differ among the individual leaks and partitioning of leak flow will be affected by Δp or Q.

I.C. Filter Unit Boundary Conditions

The performance criteria and dimensions of HEPA filter units constrain the ranges of parameters that determine filter leak flow performance. These parameters include Δp, Q_L, l, and d. Some specifications and dimensions of HEPA filters are listed in Table II-I. Size 1 HEPA filters are evaluated in this study.

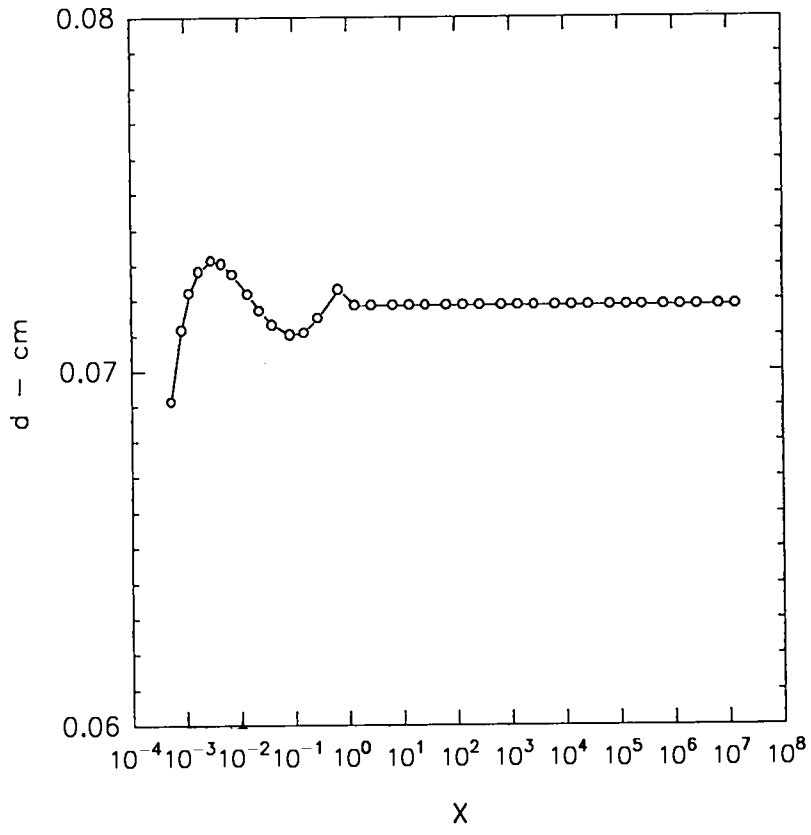

Figure II-5. Prediction of equivalent diameter of a single leak as a function of X.

II.C.1. Differential Pressure

Specifications for HEPA filter units set maximum air flow resistance for the filters at specific flow rates (DOE88). Maximum differential pressures

(Δp) are listed in Table II-I and Figure II-6 shows these Δp values plotted against Q_{de}. Filter units with $Q_{de} \leq 3.5$ M^3/min have a Δp limit of 3238 dyn/cm^2. Units with $Q_{de} \geq 14.2$ M^3/min have a Δp limit of 2491 dyn/cm^2. The size 1 filter units evaluated in this study have a $Q_{de} = 0.708$ M^3/min which means their Δp limit is 3238 dyn/cm^2. Typical, Δp values are found to be approximately 90% of the limit.

Table II-I

Some HEPA Filter Specifications and Dimensions

Size	Nominal Flow Rate - M^3/min	Maximum Δp - dyn/cm^2	Filter Unit Depth - cm
1	0.708	3238	7.78
2	1.42	3238	14.9
3	3.54	3238	14.9
4	14.2	2491	14.9
5	28.3	2491	29.2
6	35.4	2491	29.2
7	42.5	2491	29.2
8	56.6	2491	29.2

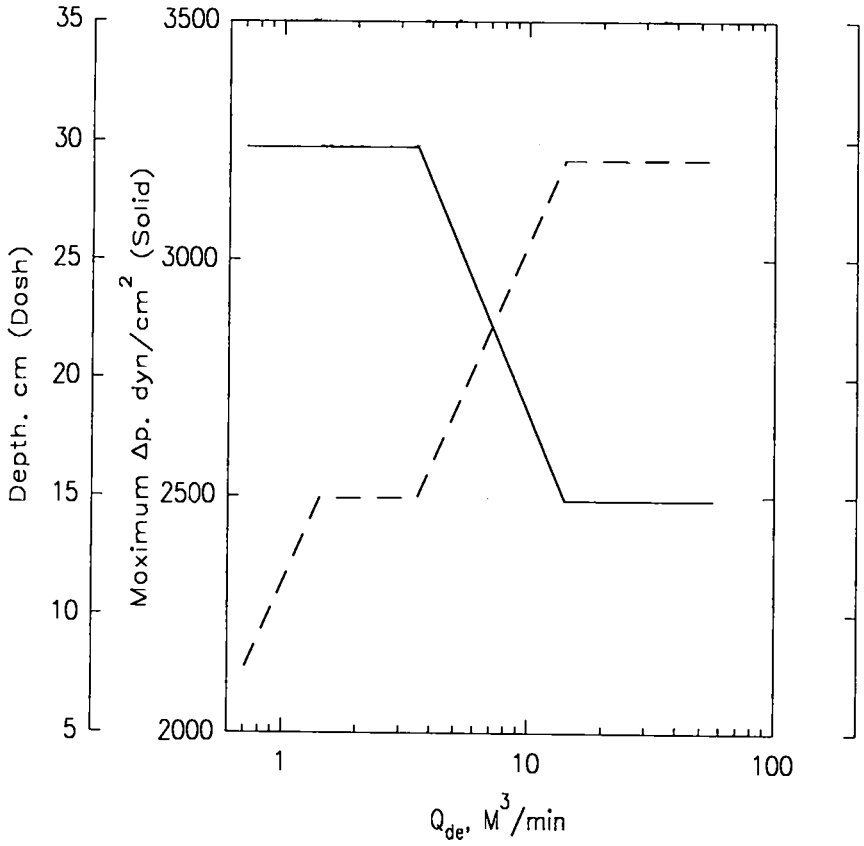

Figure II-6. Plots of filter depth and differential pressure specification versus design flow rate.

II.C.2. Leak Flow Rate

Upper bounds on, the overall filter unit leak flow rate, Q_L, come from quality assurance specifications on filter unit penetration (DOE90). Whole

filter unit penetration is limited to 0.03%. The upper bound of Q_L is estimated from the product of the penetration limit and the total filter unit flow rate. The assumes leaks are the only contributor to overall filter unit penetration and that penetration through leaks, P_L, is 1. For Q_{de} in the range from 0.708 M^3/min to 56.6 M^3/min the maximum Q_L values range from 3.54 cm^3/sec to 283 cm^3/sec. The filters evaluated in this study have a Q_{Lmax} = 3.54 cm^3/sec. Typically, HEPA filter unit penetration is approximately a third of the limit. Consequently, the Q_L at the Δp corresponding to Q_{de} is roughly 1 cm^3/sec.

II.C.3. Leak Path Length and Values of X

Overall filter unit penetration is considered to be the flow-weighted summary of penetration through leaks and intact media. Penetration through leaks depends on leak geometry. Each filter unit component is expected to have distinct leak geometry. Penetration of leaks through filter unit frames and through media packs add to give overall filter unit leak penetration.

Leak path length can be characterized by leak category. Leaks through filter unit frames have a minimum leak path length equal to the

frame thickness. Plywood frame filters are being evaluated in this study. HEPA filter specifications require a minimum thickness of 1.905 cm for these frames (DOE88). Media leaks have a ℓ_{min} equal to the thickness of the media, which is approximately 0.0508 cm. Leaks in the seal between the media pack and the frame may be as short as the media thickness and can be larger that filter unit depth. Filter unit depth varies with Q_{de} from approximately 7.8 cm to 29.2 cm (see Table II-I and Figure II-6). The filter units evaluated in this study have a depth of 7.8 cm. Overall filter unit penetration is thought to be the flow-weighted sum of the penetration for each leak category plus the penetration through intact media.

Using the minimum leak path lengths for the frame and media leaks and the filter unit depth as a characteristic length for seal leaks, values of X were calculated over the range of Q_{de}. Plots of these results are shown in Figure II-7.

Values of X were all below X = 0.45 and Re_f<2000, which indicates these leaks operate in a non-Poiseuille laminar flow regime. These values of X represent minimum values. At lower values of Q_L and larger values of ℓ, values of X increase and leak flow is expected to move closer to the Poiseuille laminar flow region. Typically, Q_L may be no more than a third of Q_{Lmax}. Total filter unit leak flow rate may be associated with a number of

individual leaks, $Q_L = \sum_i Q_{Li}$. The flow rate in each of these leaks, Q_{Li}, would result in reduced values of X for the individual leaks.

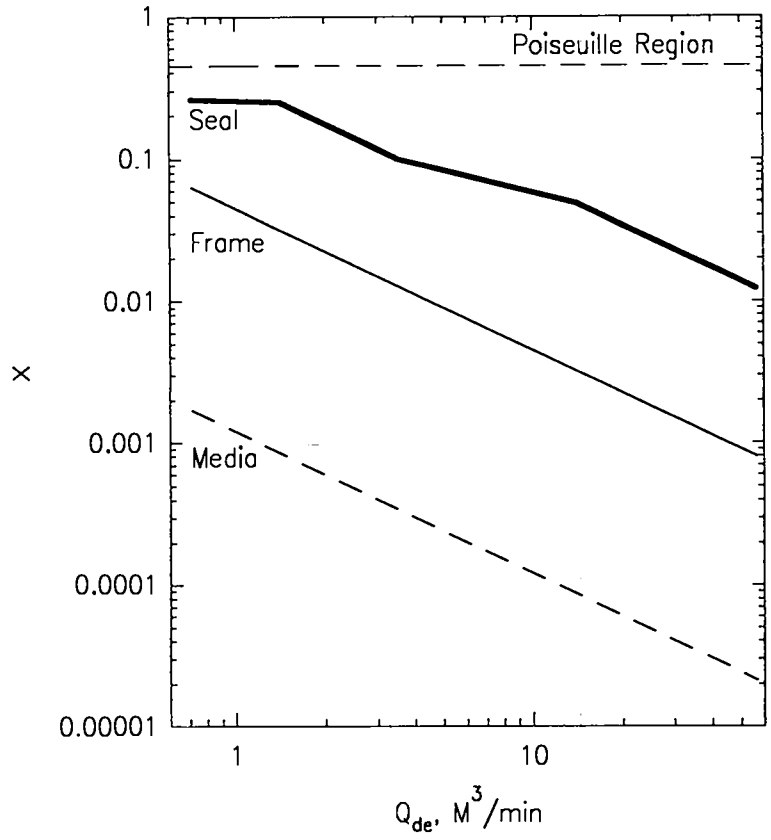

Figure II-7. Values of X for frame, media, and seal leaks plotted against design flow rate.

The frame and media leak path lengths are minimum values representing straight-through paths. Actual flow paths may be indirect. Lengths of these paths are expected to be longer than the minimum values used in the calculations.

Lengths of seal leak paths are unknown. The characteristic length selected for calculation of X represents a straight-through leak in a seal joint extending over the entire depth of the filter frame. Actual seal joint leaks may be indirect. Consequently, longer path lengths than this characteristic length are possible. However, much shorter path lengths are also possible. The length of the seal joints can approach the media width.

Figure II-7 shows the dependence of X on leak type and Q_{de}. The frame leak values of X lie below the Poiseuille region. Values of X for this leak type could be moved into the Poiseuille region by increasing the ℓ/Q_L ratio. This ratio is increased by larger values of ℓ, and by smaller values of Q_L. Indirect leak flow paths through the frame result in larger values of ℓ. Multiple frame leak flow paths result in lower values of Q_L in the individual leaks. Consequently, multiple indirect leaks in the frame move predicted frame leak flow in the direction of the Poiseuille region.

The media leak values of X also lie below the Poiseuille region. This leak type is expected to move toward the Poiseuille region when multiple indirect leaks exist in the media. Relative to the frame leaks, leak length extensions or greater numbers of leaks are required to move the media leaks into the Poiseuille region.

The X values for seal joint leaks can potentially extend from the media leak X values shown Figure II-7 toward the Poiseuille region. As with the other leak types, multiple indirect leaks in the seal joint are associated with higher values of X.

For each leak type, values of X decrease as Q_{de} increases. The highest values of X are associated with the filter units evaluated in this study.

II.C.4. Leak Diameter

The X values can be used to estimate d using the correlation in Figure II-3 to determine Y and Equation II-4 to compute d. Estimates of d are shown for each leak type in Figure II-8. The estimates represent single straight-through leaks with circular cross-sections. For a given Δp and Q_L,

smaller values of d are expected for multiple leaks and larger values of d are expected for indirect leak paths.

The dependence of d on Q_{de} indicates that larger diameter leaks are possible as Q_{de} increases. These larger scale leaks have more potential to have X values below 0.45 and thus to display non-Poiseuille flow. From this analysis these larger filter units are more likely to have performance illustrated in Figure II-1. Conversely, units with lower design flow rates are more likely to have performance shown in Figure II-2. The filter units evaluated in this study have the highest potential for having leak performance in the Poiseuille flow range.

II.D. Leak Penetration

The previous sections described methods of determining filter unit leak character that involved leak flow characteristics. Penetration models derived from this analysis assumed leak penetration, P_L, was unity. Another tool for probing filter leak character is analysis of aerosol penetration through leaks. Penetration behavior over ranges of flow rate and aerosol size may provide information on filter leak geometry that can reaffirm and/or compliment information from leak flow assessments.

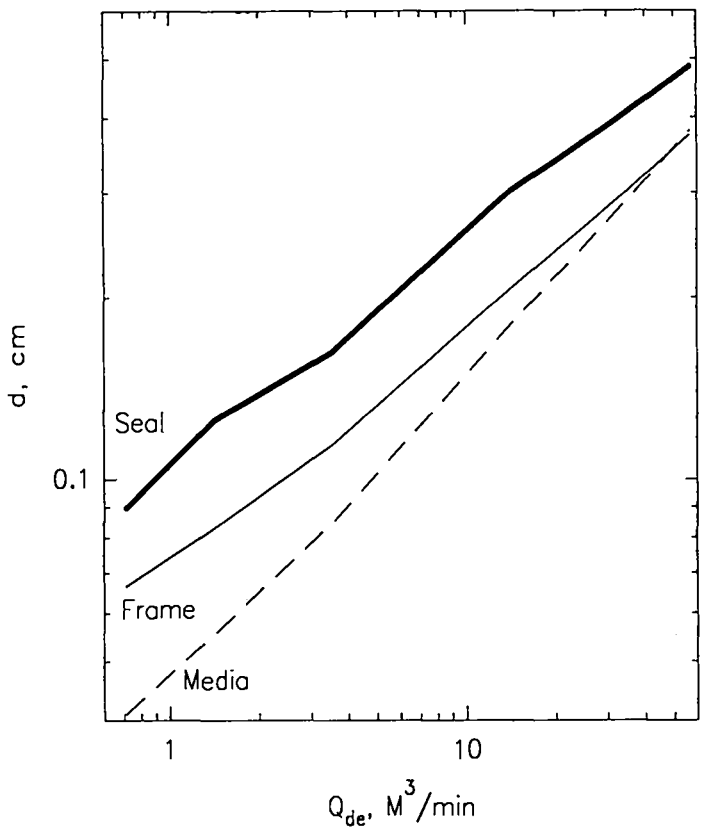

Figure II-8. Estimates of leak diameter for frame, media, and seal leaks plotted against design flow rate. Leaks are assumed to be single, straight-through flow paths with circular cross-sections.

In this section particle collection mechanisms are reviewed that may be important in understanding leak penetration of HEPA filter units. These mechanisms include diffusion, interception, and gravitational sedimentation. Each of these mechanisms depends on leak geometry, and leak flow rate.

The preceding analysis of filter unit leak flow boundary conditions can be used to bound the regions in which individual mechanisms affect leak penetration.

II.D.1. Diffusion Collection

Particles suspended in leak flow can be lost to the sides of the leak when they depart from flow streamlines. One process by which these particles depart from streamlines is particle Brownian motion. For particles on streamlines near sides of leaks these departures can result in deposition on the walls. This loss of aerosol particles is characterized by a diffusion deposition parameter,

$$\mu = \frac{D \bullet \ell}{Q_L} \qquad \text{Equation II-6,}$$

where D = particle diffusion coefficient, ℓ = leak length, and Q_L = leak flow rate. Penetration through right circular leaks in Poiseuille flow is given by,

$$P_{Ld} = 1 - 5.50 \bullet \mu^{2/3} + 3.77 \bullet \mu \qquad \text{Equation II-7,}$$

for $\mu < 0.007$, and

$$P_{Ld} = 0.819 \bullet e^{-11.5 \bullet \mu} + 0.0975 \bullet e^{-70.1 \bullet \mu} + 0.0325 \bullet e^{-179 \bullet \mu} \quad \text{Equation II-8,}$$

for $\mu > 0.007$ (Hi82).

These equations were used to determine ranges of particle size, Q_L, and d, where diffusion losses dominate leak penetration ($P_{Ld} \leq 0.5$). The computer code used in these computations is listed in Appendix A. Results of this analysis are shown in Figure II-9 for frame leaks (ℓ_{frame} = 1.905 cm).

For particle diameters greater than 0.01 μm, losses due to diffusion begin to dominate penetration at $Q_L < 0.03$ cm3/sec. At the specified maximum Δp for size 1 HEPA filters of 3238 dyn/cm^2 (See Section II.C.1), this bound on Q_L corresponds to a leak diameter, d, of ≈0.019 cm. These values are well below the boundary values of Q_L and d for these filters described in Sections II.C.2 and II.C.4. Consequently, diffusion losses are expected to be important in leaks much smaller that the largest leaks expected in the filters.

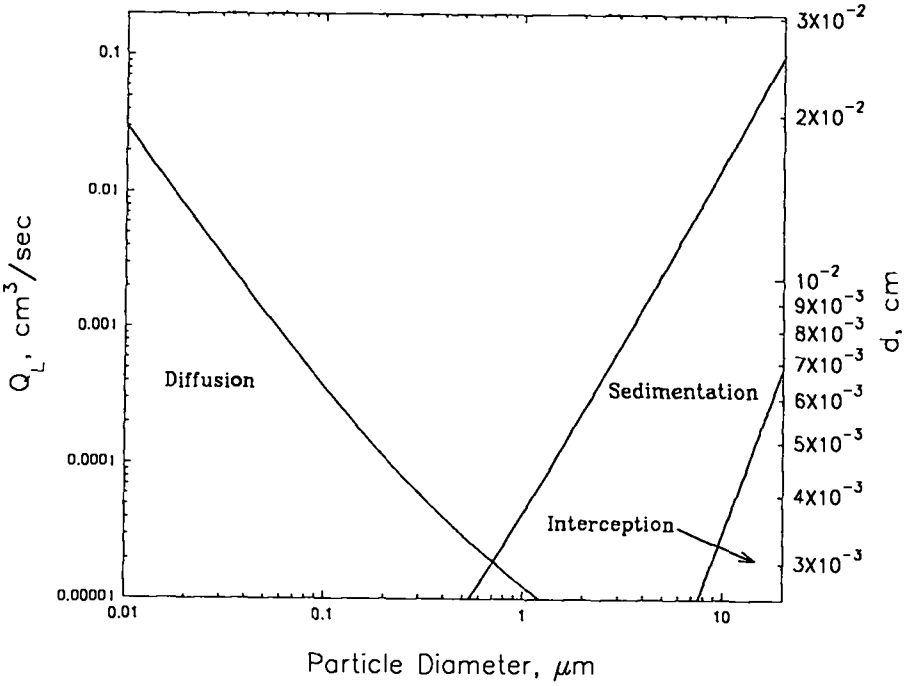

Figure II-9. Plots of frame leak flow rate and leak diameter corresponding to 50% particle loss for diffusion, interception, and gravitational sedimentation collection mechanisms.

II.D.2. Interception Collection

Particles on leak flow streamlines within one particle radius of leak walls can deposit on the wall due to interception. Particle loss by this mechanism is determined by the interception parameter,

$$R = \frac{d_p}{d}$$ Equation II-9,

where, d_p = particle diameter, and d = leak diameter. Penetration through circular leaks is given by,

$$P_{Lr} = 1 - \left(2 \bullet R - R^2\right)$$ Equation II-10.

Penetration for a range of leak geometries was computed using the code listed in Appendix A.

The region where $P_{Lr} \leq 0.5$ is shown in Figure II-9 for frame leaks. Relative to diffusion losses, interception losses are important for larger particles. For particles <20 μm, interception losses begin to dominate at leak diameters <0.007 cm. At a Δp of 3238 dyn/cm^2, this leak diameter corresponds to a leak flow rate of approximately 5 x 10^{-4} cm3/sec.

II.D.3. Gravitational Sedimentation Collection

Particles may deposit in leaks because of gravitational sedimentation. This loss of aerosol particles is determined by the gravitational deposition parameter,

$$Z = \frac{3 \bullet \pi \bullet \ell \bullet d \bullet V_{ts}}{16 \bullet Q_L}$$ Equation II-11,

where, ℓ = leak length, d = leak diameter, V_{ts} = the terminal settling velocity,

$= \frac{\rho_p \bullet d_p^2 \bullet g \bullet C_c}{18 \bullet \eta}$, ρ_p = particle mass density, d_p = particle diameter, g = gravitational acceleration, C_c = Cunningham slip correction factor, η = viscosity of air, and Q_L = leak flow rate.

Penetration through horizontal, circular cross-section leaks operating with Poiseuille flow is given by (Fu89),

$$P_{Ls} = 1 - \frac{2}{\pi}\left[2Z\sqrt{1-Z^{2/3}} - Z^{1/3}\sqrt{1-Z^{2/3}} + \arcsin(Z^{1/3})\right]$$ Equation II-12.

This equation was evaluated to determine the region for frame leaks in which $P_{Ls} \leq 0.5$ using a computer code listed in Appendix A. The region is shown in Figure II-9. For unit density particles with diameters <20 μm, sedimentation losses begin to dominate penetration through leaks operated at a differential pressure of 3238 dyn/cm^2 at leak diameters <0.026 cm and leak flow rates <0.1 cm^3/sec. These leak diameter and leak flow rate

boundaries are again well below the maximum values of these parameters for HEPA filters.

The sedimentation region shown in Figure II-9 includes the interception region. This result suggests that in the interception region, both interception and sedimentation particle losses are important.

II.D.4. Particle Losses in Media and Seal Leaks

Similar particle loss evaluations were performed for media leaks (ℓ_{media} = 0.05 cm) and seal leaks (ℓ_{seal} = 7.78 cm). For media leaks in the same particle size range as shown in Figure II-9, equivalent losses occurred at lower values of Q_L and smaller values of d. At a particle diameter of 0.01 μm and P_{Ld} = 0.5, Q_L for media leaks was ≈0.0008 cm^3/sec and the corresponding value of d was ≈ 0.003 cm. Equivalent losses in seal leaks were at higher values of Q_L and larger values of d. At a particle diameter of 0.01 μm and P_{Ld} = 0.5, Q_L for seal leaks was ≈0.1 cm^3/sec and the corresponding value of d was ≈0.03 cm. The interception region was imbedded in the sedimentation region for all three leak types.

II.D.5. Filter Leak Model with Leak Path Particle Loss

A filter leak model allowing for losses in leak paths is shown in Figure II-10. Leak flow is divided into external and internal paths. An These leak paths are illustrated in Figure II-11. External leak flow paths include those flow streamlines through the filter frame. These streamlines are outside those incident on the filter face. Internal leak flow paths include media and seal leak paths. Streamlines associated with internal leak flow paths are among those incident on the filter face. The remainder of the flow streamlines incident on the filter face are the intact media flow paths.

Total filter unit flow rate, Q, is the sum of the flow rates for each of the flow path categories:

$$Q = Q_{EL} + Q_{IL} + Q_M \qquad \text{Equation II-13,}$$

where Q_{EL} = total external leak flow rate, $= \sum_i Q_{ELi} = \Sigma Q_{ELi}$, Q_{IL} = total internal leak flow rate, $= \sum_i Q_{ILi}$, and Q_M = total intact media flow rate.

Overall filter unit penetration, P, is given by:

$$P = P_{EL}\frac{Q_{EL}}{Q} + P_{IL}\frac{Q_{IL}}{Q} + P_M\frac{Q_M}{Q} \qquad \text{Equation II-14,}$$

where, P_{EL} = penetration in external leak paths, P_{IL} = penetration in internal leak paths, and P_M = penetration of intact media. Equations II-7 and II-8 are used to estimate the contribution of diffusion losses to P_{EL} and P_{IL}. Equation II-12 is used to estimate the contribution of sedimentation losses to P_{EL} and P_{IL}. Losses due to interception are neglected.

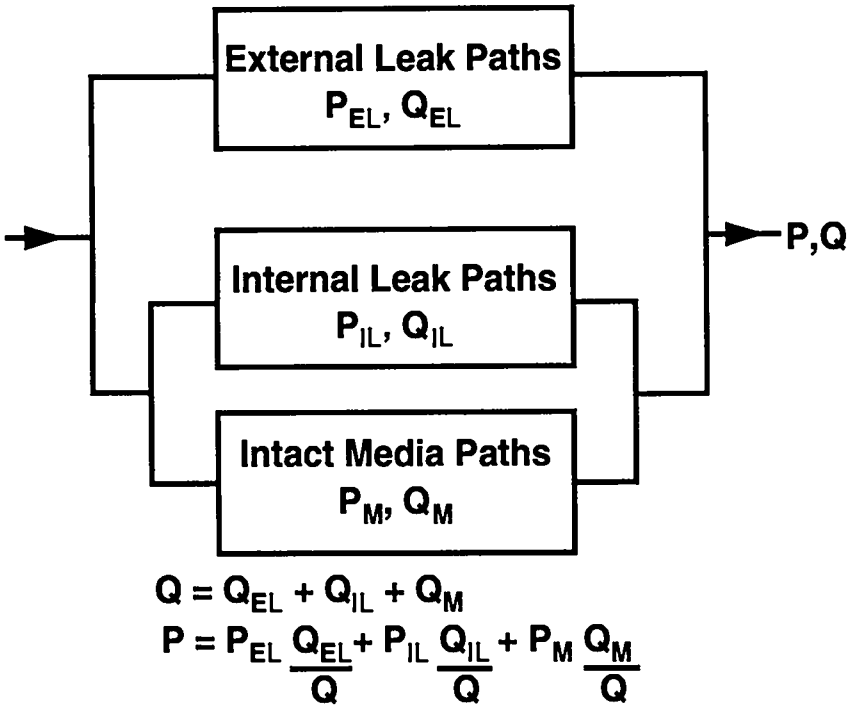

Figure II-10. Filter leak model with particle loss. Model includes external and internal leak paths.

External leak penetration is given by:

$$P_{EL} = P_{ELd} \bullet P_{ELs} \qquad \text{Equation II-15,}$$

where, P_{ELd} = external leak penetration associated with diffusion losses evaluated at $Q_{ELi} = \frac{Q_{EL}}{N_{EL}}$, N_{EL} = the number of external leak paths, P_{ELs} = external leak penetration associated with sedimentation losses evaluated at Q_{ELi}. Similarly, internal leak penetration is given by:

$$P_{IL} = P_{ILd} P_{ILs} \qquad \text{Equation II-16,}$$

where, P_{ILD} = external leak penetration associated with diffusion losses evaluated at $Q_{ELi} = \frac{Q_{EL}}{N_{EL}}$, N_{IL} = number of external leak paths, P_{ILs} = external leak penetration associated with sedimentation losses evaluated at Q_{ILi}.

Example predictions of P_{EL} for frame leaks (ℓ_{frame} = 1.905 cm) are shown in Figure II-12. The predictions are made over the Δp range from 1% to 100% of the nominal filter unit Δp of 2491 dyn/cm^2 when operating at Q_{de}. For this example $Q_L = Q_{EL} + Q_{IL} = 10^{-5}$ Q, $Q_{EL} = 0.2\ Q_L$, $N_{EL} = 10$,

and $\rho_p = 1$ g/cm^3. The computer code used to make these predictions is listed in Appendix A.

The effect of diffusion losses on P_{EL} is observed with the decrease in P_{EL} at the smaller particle sizes. For the highest differential pressure (Δp = 2491 dyn/cm^2) P_{EL} approaches the upper limit of 0.2 $Q_L/Q = 2 \times 10^{-6}$ at the largest particle sizes. At lower values of Δp, the effect of sedimentation particle losses is observed with P_{EL} decreasing at the larger particle sizes.

This example is extended to predict total filter unit penetration, P, at Δp = 2491 dyn/cm^3 and $P_M = 0$ (see Figure II-13). Whole filter unit penetration is determined by adding frame penetration, P_{EL}, to media pack penetration, P_{IL} (labeled "Media"). In this example, P_{IL} is determined with $Q_{IL} = 0.8\ Q_L = 8 \times 10^{-5}$, and $N_{IL} = 1$.

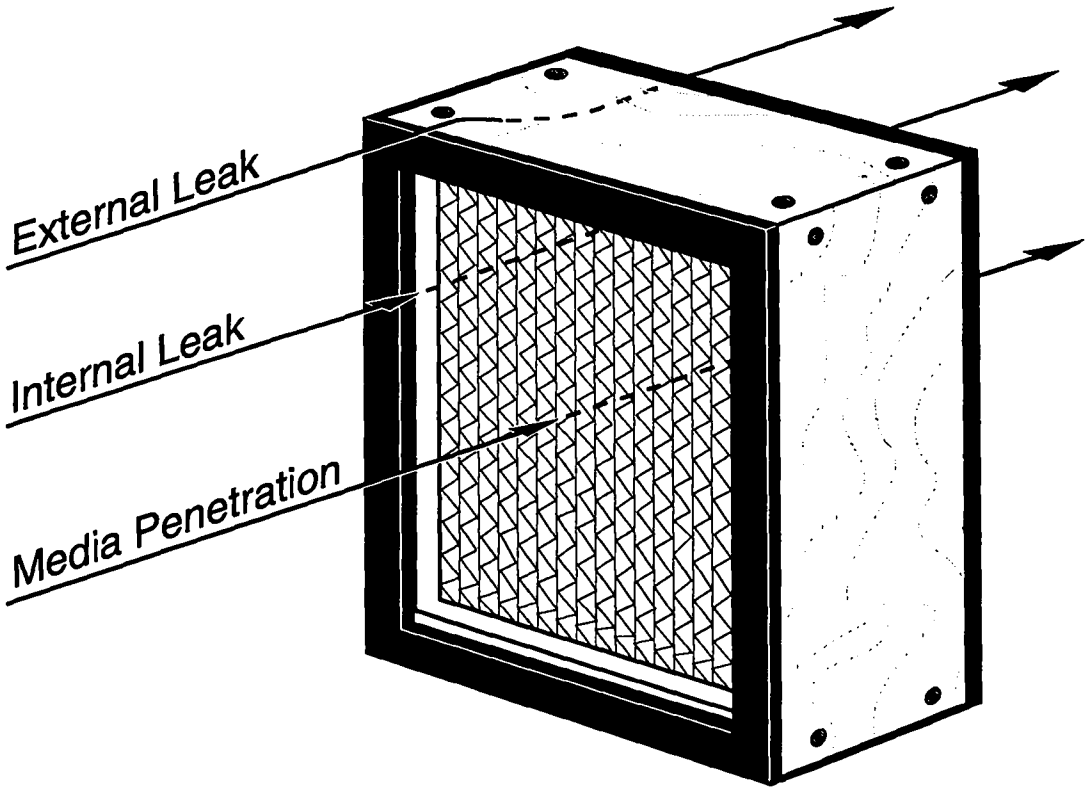

Figure II-11. External and internal leak flow paths.

Diffusion losses are apparent at the small particle sizes. No sedimentation losses are evident even at the largest particle sizes. At the larger particle sizes, P_{IL} approaches the upper limit of 8×10^{-6} and P approaches the upper limit of 10^{-5}.

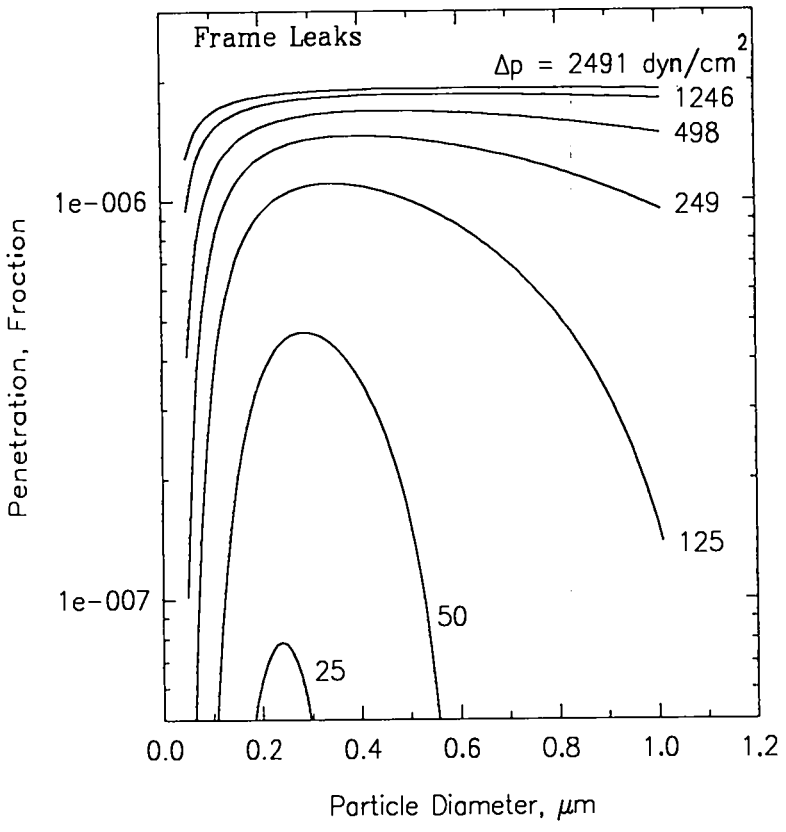

Figure II-12. Frame penetration predictions over the Δp range from 25 dyn/cm^2 to 2491 dyn/cm^2. Predictions consider particle collection by diffusion and sedimentation.

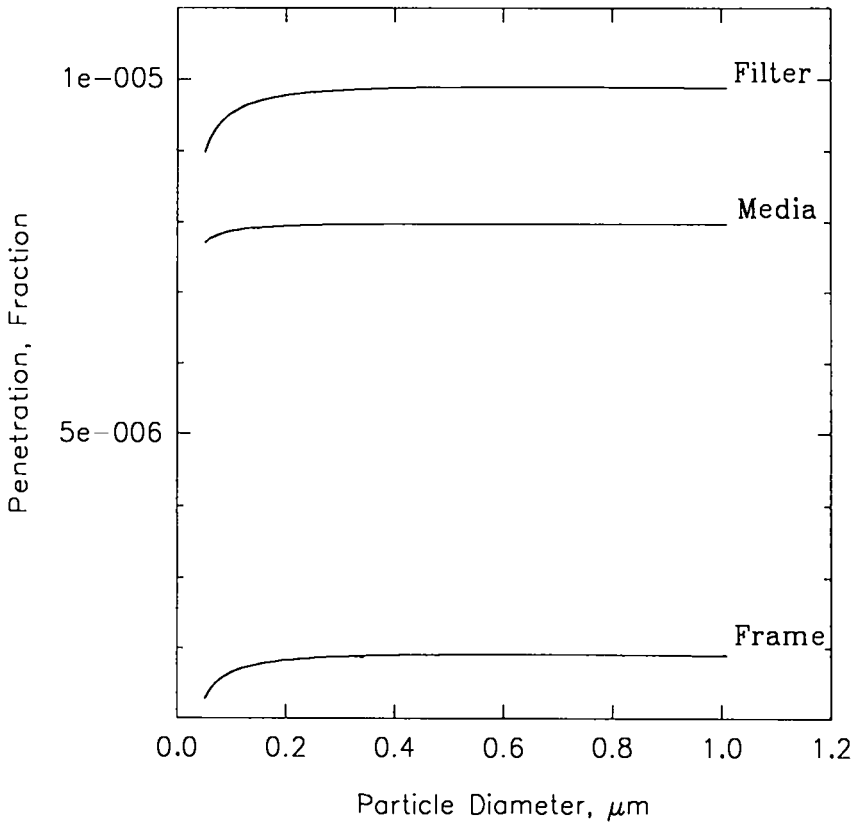

Figure II-13. Predictions of frame, media pack (media and seal), and whole filter leak penetration at $\Delta p = 2491$ dyn/cm^2. Intact media penetration (P_M) set to 0.

CHAPTER III. TECHNIQUES FOR EVALUATING PERFORMANCE OF HIGH EFFICIENCY FILTER UNITS

III.A. Introduction

Collection of airborne particles by fibrous filter mats is commonly used in 1) air cleaning/filtration applications to remove particles suspended in process air, in hospitals and clean rooms, 2) respiratory protection applications where hazardous particles are removed from breathing air, and 3) sampling of airborne particles. Air filtration aspects of dust respirators has been reviewed by Brown (Br89). Lippmann has described the use and evaluation of fibrous filters for air sampling (Li78).

In this chapter I describe techniques developed to evaluate performance of fibrous filter units commonly used to control air emissions of hazardous particulate materials. These units are referred to as nuclear grade high efficiency particulate air (HEPA) filters. The filters consist of a pleated media pack sealed into a rigid frame. An exploded view of one of these filters is shown in Figure III-1. The media pack includes a folded sheet of media with corrugated separators placed in the folds. The filter frame is made of frame boards with gaskets sealed to the edges of the

boards. Adhesive is used to seal frame joints, and gaskets, and to seal the media pack to the frame.

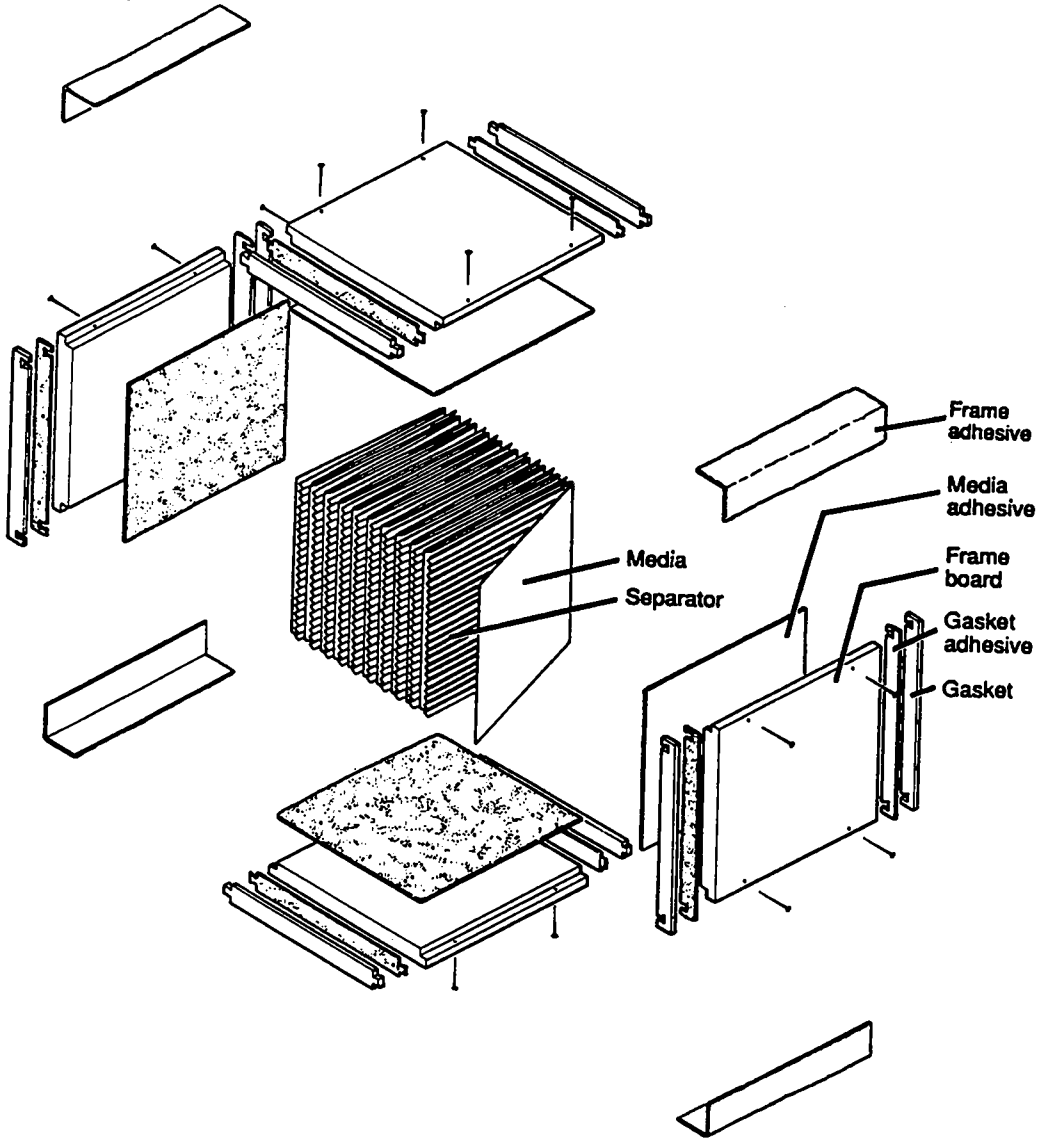

Figure III-1. An exploded view of a HEPA filter unit showing the individual filter components. The media pack consists of a folded sheet of media with separators placed in the folds. The frame is made from frame boards with gaskets sealed to the edges of the boards.

The filters are used in critical applications to protect health and the environment. Consequently, techniques used to evaluate filter performance are important in assuring this protection. Understanding of the performance of the entire filter requires overall filter unit evaluation as well as evaluation of the performance of the components that make up the filter unit. The techniques described in this chapter allow for independent evaluation of the filter frame and media pack as well as evaluation of the entire filter. Assessing independent contributions of the frame and media pack to overall filter unit performance provides a detailed understanding of mechanisms governing filter unit performance. This understanding is important in predicting operation limits for the filter units and planning improvements in filter unit design.

The development of filter evaluation techniques evolved with development of fibrous filter media. The first concerted efforts to develop these techniques coincide with the push to develop respiratory protection against chemical warfare agents in the first half of the 20th century (Da73). In this era techniques were developed to 1) provide data to improve media performance, and 2) understand gaps in protection. A filter study approach developed in this period involved generation of aerosols with narrow and adjustable size distributions (Fr26, La43). In these studies

penetration measurements could be made using instruments that measured aerosol concentration integrated over particle size, such as photometers. The responsibility for size-selection in the studies was placed on the generation system and not on the detection method. Data from these studies provided information on penetration as a function of aerosol size in the range of maximum penetration. This information was needed to evaluate and adjust hypotheses on mechanisms governing fibrous filter performance. Experimental aerosol filtration research programs used this approach into the 1950's (Ra51). In the mid-50's the monodisperse challenge approach formed the basis for standards on quality assurance (QA) testing of nuclear grade HEPA filters (MS56). These test procedures are still used for QA filter testing (DOE90).

By the beginning of the 1960's techniques became available that used polydisperse test aerosols with aerosol size-selective techniques to measure aerosol concentration such as electron microscopy (Fi56). With the advent of various aerosol spectrometers aerosol filtration researchers began to use them to measure filter penetration. Dyment (Dy70) used the Goetz aerosol spectrometer to measure penetration as a function of particle size in the diameter range from 0.03 μm to approximately 1 μm. In the mid-1970's the first measurements of filter penetration were being made with optical particle counters such as laser aerosol spectrometers

(LASs) (Sc72, Sc76, Sc77). These spectrometers extended the particle diameter range of optical particle counters to less than 0.1 μm, below the size of maximum penetration for nuclear grade HEPA filter media.

Scripsick has evaluated a LAS system for QA testing of nuclear grade HEPA filters (Sc84, Sc86, Sc87a, and Sc87b). The system uses a polydisperse challenge aerosol. The high flow rate version of this system has been adopted by the US Department of Energy as an approved QA test method and is being certified by the US Army as their QA test method.

In 1985 Liu reported on measurements of filter media penetration with an electrostatic classifier (EC) system (Li85b). The classifier system allows for penetration measurements down to particle diameters <0.05 μm and does not require calibration for aerosol size as do laser spectrometers. The classifier is a differential electric mobility analyzer that can produce monodisperse aerosols whose size is adjusted by the voltage applied on a center electrode. Penetration is determined from the ratio of monodisperse aerosol concentration measurements made upstream and downstream of the test media. The measurements Liu reported were made with a condensation nucleus counter (CNC).

Recently, Fardi (Fa88) measured penetration of respirator filters using monodisperse aerosols in the diameter range from approximately 0.01 μm to approximately 1 μm. Concentration measurements upstream

and downstream of the test filters were made with a CNC, and a LAS. Review of these data indicate agreement in penetrations determined from the two measurement methods.

The filter test system described in this paper is based on the LAS system developed by Scripsick (Sc87a). A diagram of the test system is shown in Figure III-2. A polydisperse challenge aerosol is produced by compressed-air operated jets submerged in the liquid aerosol material. The aerosol is diluted and carried to the test filter with filter air flow from blower. Air flow through the test filter is drawn from this flow stream. Mixers are used upstream and downstream of the test filter to assure uniform mixing. Aerosol concentration measurements upstream and downstream of the test filter unit are made with a LAS. Upstream aerosol samples are diluted using a variable, capillary diluter. An inclined gage and micromanometer are used to make differential pressure measurements. Volume flow rate measurements are made with a laminar flow element (LFE) system.

The test system is used to evaluate performance of filter unit components as well as overall filter unit performance. Techniques have been developed to independently assess frame leakage and media pack leakage as well as overall filter unit penetration. In this chapter results of

test system component evaluations are presented and techniques developed to evaluate filter unit performance are described.

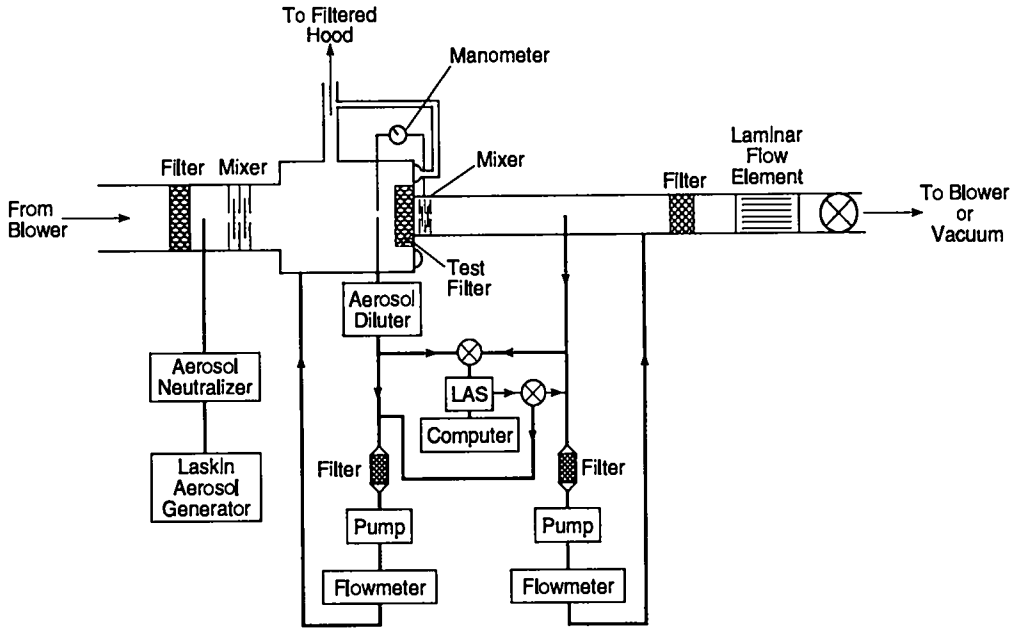

Figure III-2. Diagram of the test system used to evaluate filter performance.

III.B. Test Filter Units

III.B.1. Introduction

The primary objective of this study is to evaluate the performance of fibrous filter units used in hazardous material handling facilities. The units

are made of a pack of pleated fibrous media sealed in a rigid frame (see Figure III-1). The formulation of the media has been developed over several decades and has been the object of extensive theoretical and experimental investigation. Performance of the units has been assumed to be completely determined by the performance of the media. One of the objectives of the present study is to evaluate this assumption.

The filter units evaluated in this study are nuclear grade high efficiency particulate air (HEPA) filters. The Institute of Environmental Sciences designates these filters as "type B" HEPA filters (IES86). Specifications and standards for design, materials, construction, and performance of these filter units come from a variety of federal and national-consensus organizations. The specific units evaluated in this study were procured under the specifications of US Department of Energy (DOE) nuclear standard NE-F-3-45 (DOE88).

Nuclear grade HEPA filters are frequently used in air cleaning applications to remove highly hazardous particles in air effluent. This type filter is used in nuclear power plants in many countries of the world including the United States. The US DOE uses these filters in nuclear and hazardous material handling facilities. The US military uses these filters for protection against nuclear, chemical, biological threats. The filters are used in hospitals to control air emissions of chemical and biological

aerosols and to assure air quality in operating rooms and medical laboratories. Pharmaceutical companies use these filters to remove biologically active compounds from air streams.

In the United States there are four major manufacturers of nuclear grade HEPA filters. Filter units were obtained from each of these manufacturers.

The filters obtained for the study were size 1 (DOE88) units which typically have outside dimensions of 20 cm x 20 cm x 8 cm (8" x 8" x 3 1/16") and a nominal design air flow rate of 708 Lpm (25 CFM). The specified maximum differential pressure at this air flow rate is 3.25×10^3 dynes/cm^2 (1.3" of H_2O). Filter frames were made of plywood. The DOE specifications call for exterior plywood, grade A-A, A-B, or A-C with a minimum thickness of 1.9 cm (3/4"). Filter media is a paper mat made of glass fibers.

An exploded view of a filter unit is shown in Figure III-1. The pleated media pack consists of a sheet of media folded like a hand-held paper fan. The pleating allows for a media area much greater than the open cross-sectional area of the upstream face of the filter frame. The pleated media pack is sealed into the rigid frame. The frame gives strength to the filter unit and allows for sealing of the filter unit to the plenum mounting plate.

The filter units are mounted in plenums typically with the downstream filter gaskets sealed to the plenum mounting plate. The frame and upstream filter face are exposed to the challenge. Flow is pulled through the filters with ventilation system fans located downstream of the filter sections. The filter sections are operated at pressures negative relative to atmospheric pressure.

III.B.2. Description of Units Evaluated in the Study

A total of 14 filter units were evaluated in the study. Samples from each of the four major US manufacturers were evaluated. Table III-I lists the manufacturers, the number of filters tested from each manufacturer, and the nominal design flow rate. Each of the filter units were inspected and measured. Data for each filter unit are presented in Appendix B. The effective media area was estimated as part of these filter inspections. Estimates of effective area averaged over all filters of a given manufacturer are listed in Table III-I. The effective media area is used to determine filtration velocity from the filter volume flow rate. Values for filtration velocity at design flow rate are listed in Table III-I.

Table III-I

Filter Unit Specifications

Company	Number of Filters	Design Flow Rate, Lpm	Effective Media Area, cm^2	Filtration Velocity, cm/sec
Donaldson Company Inc.[a]	5	708	3012	3.9
Flanders Filters Inc.	3	920	7739	2.0
American Air Filter [b]	3	708	3646	3.2
Cambridge Filter Corporation[c]	3	708	3556	3.3

[a] - Formerly Mine Safety Appliances, Inc.

[b] - An Allis-Chambers Company

[c] - Now Farr Company

Filter units supplied Flanders Filters Inc. (Washington, NC) had more than twice the media area of the other filter units. The design volume flow rate for these filters in this study was approximately 30% higher than the flow rate used for the other filters.

III.C. Test System Evaluation

III.C.1. Aerosol Generation

The compressed-air operated jets used in the aerosol generator (see Figure III-3) are Laskin nozzles (Ec63). Aerosol production by these nozzles has been attributed to 1) shearing of liquid by the jet and 2) bursting of bubbles produced by the jet in the liquid (Hi83).

The aerosol generator has four independently operated nozzles and four single-jet impactors. The impactors limit the large particle concentration in the exiting aerosol. At an operating pressure of 138 kPa (20 PSIG) on the nozzles, the impactors have a cutoff diameter of approximately 1 μm.

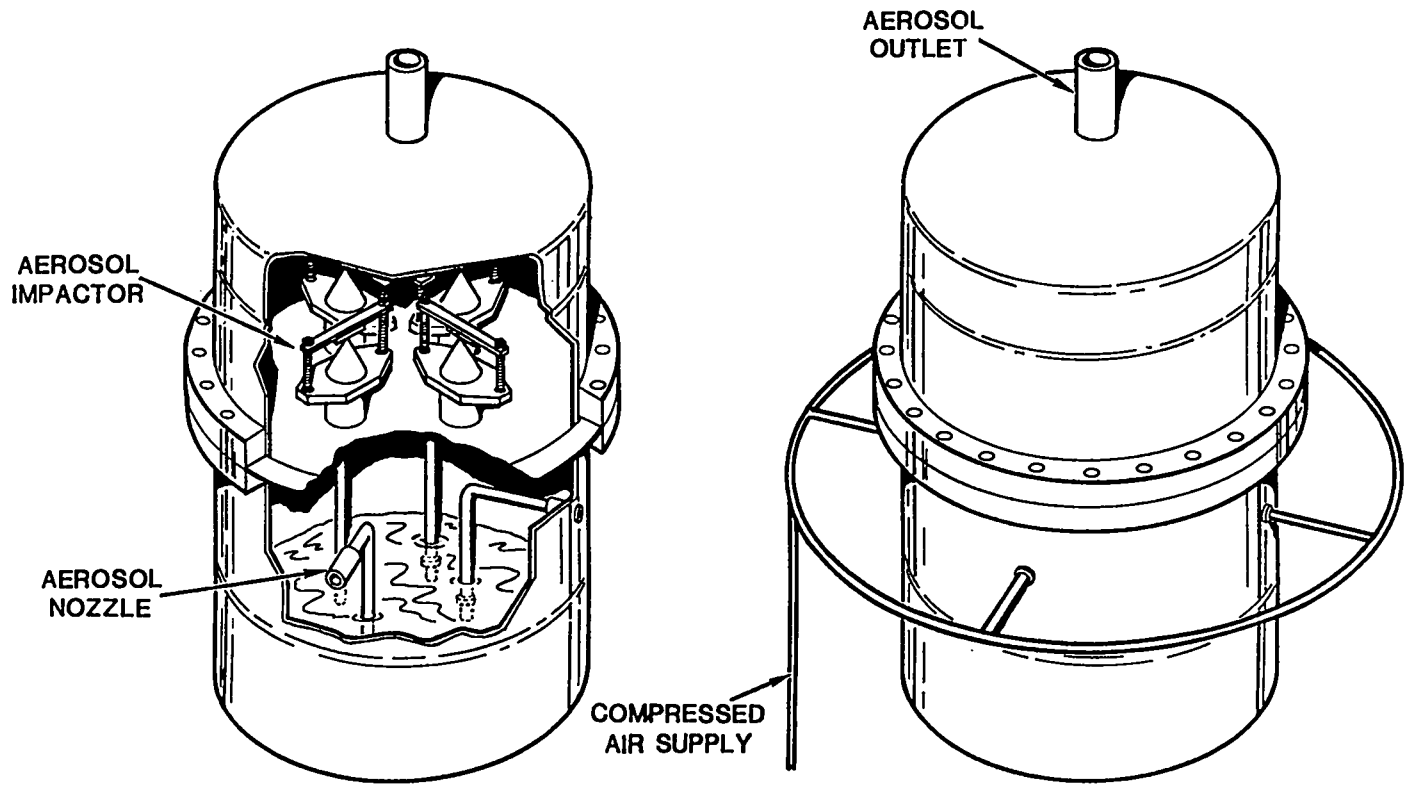

Figure III-3. Aerosol generation system.

The liquid aerosol material is di(2-ethylhexyl) phthalate (DEHP, CAS# 117-81-7). Physical properties of DEHP pertinent to the filter evaluations are listed in Table III-II. The primary reason for choosing DEHP was its low vapor pressure. The low vapor pressure reduces aerosol evaporation effects during long residence time measurements.

DEHP was found to be a carcinogen in laboratory animals (NTP82). The current TLV-TWA for DEHP of 5 mg/m^3 does not consider the carcinogenic potential of the compound (ACGIH91). To control inhalation exposures aerosol size is limited to particles with diameters less than approximately 1 μm and challenging of test filters is conducted in a plenum vented to a filtered hood (See Figure III-2). Personal and area air samples collected within the laboratory indicated DEHP concentrations in the range from approximately 0.025 mg/m^3 to just under 0.05 mg/m^3. Since the time these samples were collected hood performance has been improved and leaks in the plenum have been sealed.

The aerosol generator is normally operated with pressure of 138 kPa on the nozzles. At this operating pressure measurements of aerosol size with a LAS system show the challenge aerosol to have a count median diameter of approximately 0.2 μm and a geometric standard deviation of approximately 1.6. The maximum challenge concentration is 3 x 10^6 $particle/cm^3$.

Table III-II

Pertinent Physical Properties of DEHP
(at 20°C unless noted otherwise)

Property, Units	Value	Reference
Mass Density, g/cm^3	0.985	Fl93
	0.9843	Be83
Refractive Index	1.486[a]	Fl93
	1.487[b]	Be83
Vapor Pressure, kPa	9.44×10^{-9}	Lo81
	6.92×10^{-8}[c]	Fr70

---

a - Wavelength not reported.

b - Measured at a wavelength of 0.589 μm.

c - Extrapolated from Frostling's data (Fr70).

The stability of the challenge aerosol has been evaluated as a function of particle size and time. The coefficient of variation for concentration over a 16 hr period is plotted against particle diameter in Figure III-4. Coefficient of variation is <0.05 for particle diameters <0.4 μm. For particle diameters >0.4 μm the coefficient of variation is <0.1.

The steady output of the generator is achieved after the generating liquid is saturated with bubbles. These bubbles are produced by operating the generator for a period to allow bubble build-up. The duration of the stabilization period is related to the volume of generating liquid, and the

number of nozzles. The generator used in this study required approximately 4 hr to reach a steady output.

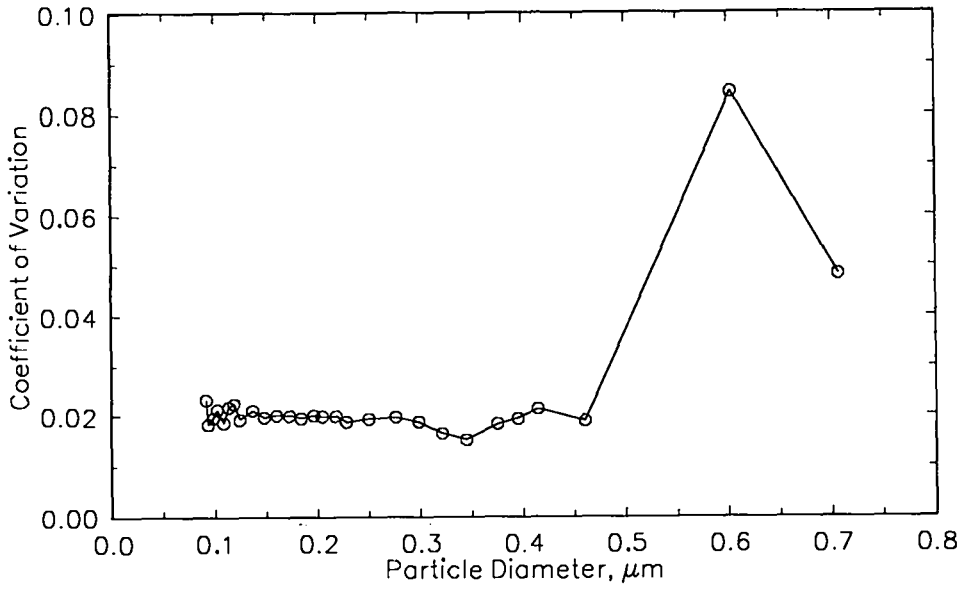

Figure III-4. Coefficient of variation for concentration measurements made over a 16 hr period plotted against particle size.

III.C.2. Aerosol Mixing

III.C.2.a. Introduction

Assurance of spatially uniform aerosol concentration is a common requirement in aerosol evaluations. In studies that use test aerosols, aerosols are often required to be uniformly mixed in the test system flow. A uniform concentration is fundamental to obtaining representative aerosol samples.

Some examples of procedures that require uniform aerosol concentrations are 1) filter evaluations, 2) aerosol dilution, and 3) aerosol emissions monitoring. Filter evaluations require that the test aerosol challenge be uniform over the entire filter face and that the penetrating aerosol be uniformly mixed in the flow exiting the filter. In situations where aerosol dilution is used accurate knowledge of the degree of dilution often depends on aerosol being uniformly mixed after exiting the dilution device. The accuracy of emissions monitoring frequently relies on the assumption that the aerosol is uniformly mixed in the effluent flow at the sampling point. In this section considerations for applying principles of gas mixing

to the mixing of aerosols are outlined and results of an evaluation of a commercial mixer are presented.

III.C.2.a.i. Mixing Theory

A measure of the non-uniformity of aerosol or gas concentration is the concentration heterogeneity (H) which is defined as the standard deviation of concentration (s) over a region divided by the mean concentration ($\overline{X}$) in that region. Mixing can be described as the combination of two streams, 1 and 2, of uniform concentration (H=0), X_1=0 and X_2=1 (Ta79). In this description $\overline{X}$ can be defined as:

$$\overline{X} = \frac{Q_2}{Q_1 + Q_2} \qquad \text{Equation III-1}$$

where Q_1 and Q_2 are the volume flow rates for streams 1 and 2. Equation III-1 assumes the number of sample points in each stream is proportional to the stream-to-total flow rate ratio, $\frac{Q_i}{\sum_i Q_i}$. Likewise, s can be written as:

$$s = \sqrt{\bar{X} \bullet \left(1 - \bar{X}\right)}$$ Equation III-2,

and H as:

$$H = \sqrt{\frac{1}{\bar{X}} - 1}$$ Equation III-3.

III.C.2.a.ii. Mixing Devices and Mechanisms

III.C.2.a.ii.a. Turbulent Diffusion

Procedures to mix either aerosols or gases serve to reduce H from some initial value H_0 to final value H_f. Turbulent or eddy diffusion is a commonly used method for mixing both gases and aerosols. Aerosol systems are often found in the literature that depend on this mechanism for achieving uniform mixing. The method takes advantage of the mixing action of eddies generated in turbulent flow. The degree of mixing depends on residence time which is often interpreted in terms of duct

lengths. Hampl et al (Ha86) studied mixing of gases in a duct. Results were stated in terms of duct diameters to achieve a specified value of H_f. They found that >50 duct diameters were needed to achieve $H_f = 0.05$ for smooth, straight duct. The initial conditions of the study (H_0) where only specified qualitatively so that estimates of reduction in H, $h = \frac{H_0}{H_f}$, were not possible.

III.C.2.a.ii.b. Passive Mixing Devices

Other mixing methods involve placement of passive devices in the flow path. An example of these passive devices is the Stairmand disk which is an annular orifice placed perpendicular to the flow direction. The flow disturbance caused by the orifice promotes mixing. These devices are used to mix aerosols. Silverman et al (Si71) indicates that a "uniform" concentration profile is achieved 4 to 6 duct diameters downstream from the disk.

Another passive mixing device is the static mixing unit or Sulzer gas mixer (Ta79). These units were designed for mixing gases and are produced by Koch Engineering Inc. of Wichita, Kansas. The units are composed of mixing elements separated by lengths of empty tubing (see

Figure III-5). The greater the number of elements the greater the degree of mixing. Each element is composed of a stack of corrugated metal plates welded with corrugations perpendicular to one another. Elements are arranged in a mixing unit with the plates stacked alternately horizontal and vertical.

According to Koch Inc. (Is91) three mechanisms account for the mixing these units provide: 1) cut mixing, 2) shear mixing and 3) turbulent mixing. As flow enters a mixing element it is "cut" into several streams by the entries to the corrugated channels (see Figure III-6). These channels serve to transport the streams transverse to the incident flow direction. In the illustration, streams are shifted horizontally so that a stream initially on the far left side of the tube is channeled to the right and vice versa. This channeling results in a horizontal rearrangement of the streams as they exit the first element. An analogous shifting of the streams occurs vertically in the next element.

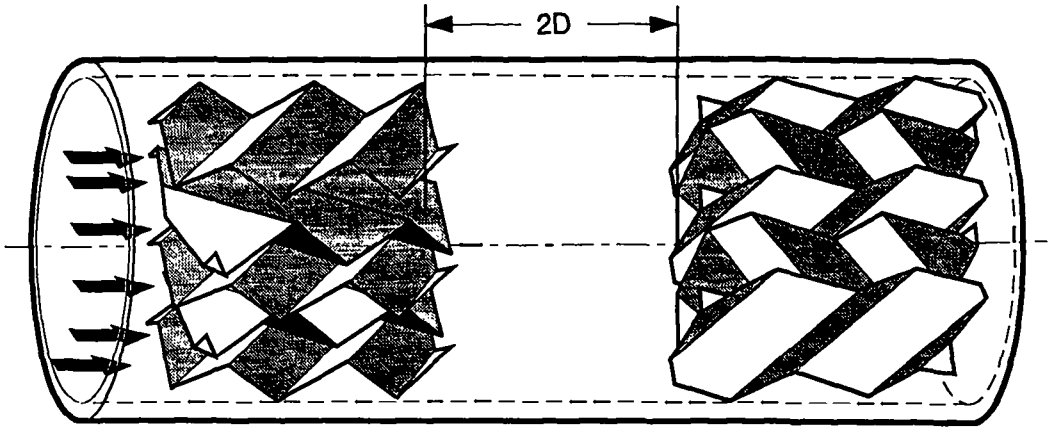

Figure III-5. A drawing of a static mixing unit showing the corrugated plates that make up a mixing element and the separation between adjacent elements.

While individual streams negotiate the corrugation channels, mixing occurs where adjacent streams cross one another (see Figure III-7). The crossing of the peak of one corrugation with the trough of another creates a region of shear. In the region, momenta from the streams are exchanged causing mixing transverse to the individual channel directions.

Mixing units are operated in the range with channel flow well in the turbulent region down to flow Reynolds numbers (Re) below 350. Turbulent mixing occurs within the channels when the units are operated in the turbulent region. As described above, the eddys generated in turbulent flow result in a mixing action.

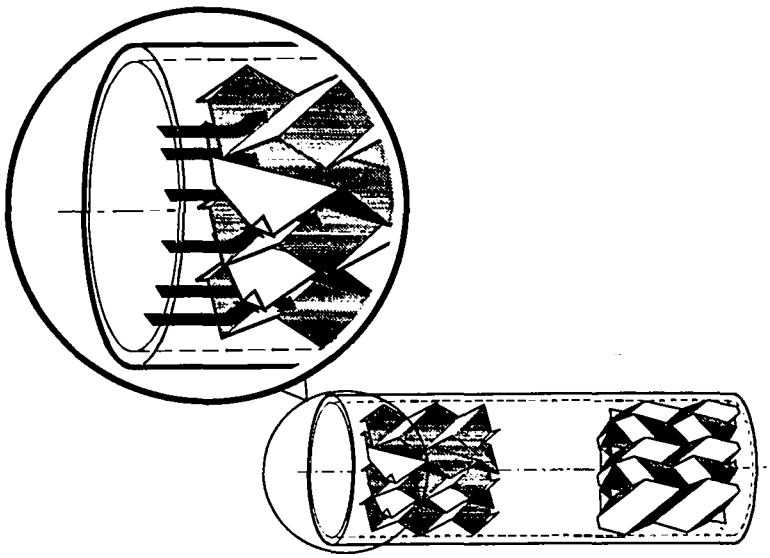

Figure III-6. A drawing showing how flow entering a mixing unit is cut into streams that are diverted orthongonally to the incident flow direction.

The mixing of gases by static mixing units has been evaluated by Tasucher and Streiff (Ta79). They found that the mixing action of the

elements persisted in the tube at the exit of the element for approximately two tube diameters. In order to take full advantage of the mixing capacity of the elements, mixing units are fit with spacers two tube diameters long between each element. For SMV type mixing units (Koch Engineering Inc., Wichita, KA) correlation (ls91) of Tasucher and Streiff's data shows:

$$h = 0.43^{-N} \bullet 0.51^{-2S} \qquad \text{Equation III-4}$$

where N = the number of mixing elements and S = the number of spacers $\leq$N.

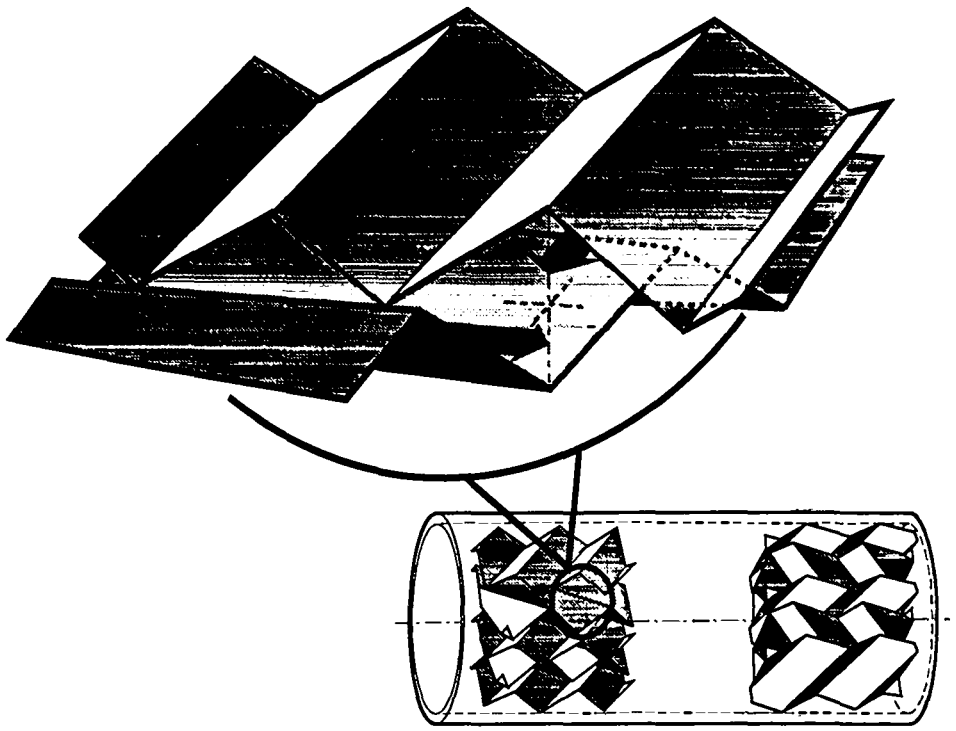

Figure III-7. A drawing showing a region inside a mixing element where adjacent streams cross one another. Within regions such as these the streams exchange momentum.

III.C.2.a.iii. Application of Mixing Theory to Aerosol Evaluations

In Equation III-3, $\overline{X}$ can be interpreted in terms of specific parameters characteristic of the example aerosol evaluation procedures mentioned above. For filter evaluations, $\overline{X}$ may be set equal to P, the overall filter penetration. The worst-case mixing condition downstream of

a filter occurs when all penetrating aerosol is associated with a single leak point. Less localized penetration results in a lower value of H_0. In this worst-case P can be written as:

$$P = \frac{Q_2}{Q_1 + Q_2} = \overline{X} \qquad \text{Equation III-5}$$

where Q_1 is the volume flow rate through the intact portion of the filter and Q_2 is the volume flow rate through the leak point.

Substituting P for $\overline{X}$ in Equation III-3 we see that, for $P \leq 1$, H_0 increases as P decreases. This result means that as filter penetration decreases the aerosol penetrating the filter becomes less well-mixed. Filter evaluations frequently require representative samples of the aerosol leaving filter. If this aerosol becomes less well-mixed as P decreases, the sampling error associated with concentration heterogeneity will increase as P decreases.

The derivation above points out a general limitation of mixing procedures. Because mixing procedures serve to reduce H_0 by some factor, h, values of heterogeneity (H_f) at the exit of a mixer placed downstream of a test filter will also increase as P decreases. So, for a

given mixer, values of H_f may rise above acceptable limits as values of P drop below a particular value.

The above analysis assumes no mixing between the downstream filter face and mixer inlet. At a minimum, particle thermal diffusion can be expected to broaden the penetrating aerosol plume by the time it encounters the mixer inlet. This broadening would result in a reduced H_0.

The extent of plume broadening by particle diffusion can be estimated by determining the average particle displacement,

$$\bar{x} = \sqrt{2 \bullet D \bullet t}, \qquad \text{Equation III-6,}$$

where, D = the particle diffusion coefficient in air, t = travel time from filter to mixer $= \frac{V_{fil}}{2 \bullet Q}$, V_{fil} = filter unit volume, and Q = the volume air flow rate through the filter. This displacement can then be used to calculate the mean concentration at the mixer inlet after broadening,

$$\overline{x_b} = P + \frac{2 \bullet \pi \bullet \bar{x} \bullet \left(r_p + \frac{\bar{x}}{2} \right)}{A} \qquad \text{Equation III-7,}$$

where, r_p = radius of plume at filter $= \sqrt{\frac{P \bullet A}{\pi}}$, and A = cross-sectional area of mixer.

An example of the predicted effect of diffusion on H_f is shown in Figure III-8. As predicted by Equation III-3, H_f increases as P decreases. When the contribution of diffusion mixing is considered, an upper limit of H_f is observed and H_f becomes independent of P below a certain value of P (e.g. $P \approx 1 \times 10^{-8}$). Below this value of P, the diffusion effect on mixing become important in estimating the final heterogeneity.

An example filter penetration plot is shown in Figure III-9. Also on this plot are predicted values of P that correspond to $H_f = 0.05$,$P_{H_f=0.05}$. At a given particle size, data above the $P_{H_f=0.05}$ values have $H_f<0.05$ and those below have $H_f>0.05$. In this example we see that over half the P measurements have $H_f<0.05$. The maximum value of H_f associated with the P measurements was <12.5%. Plotting penetration measurements in this manner assists in identifying regions where mixing may contribute significantly to sampling error.

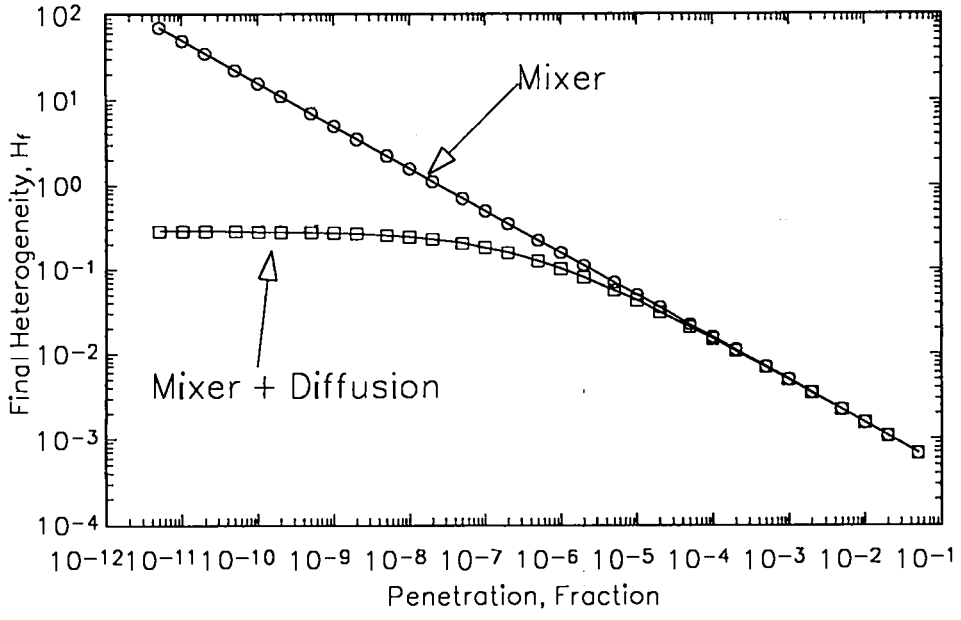

Figure III-8. A plot showing the effect of diffusion mixing on predicted heterogeneity for filter penetration measurements. Predictions of H_f for the mixer are based on h = 0.000156, with N = 4 and S = 4. The estimated diffusion contribution is for 0.1 μm diameter particles.

Dilution ratio, Dr, is a characteristic parameter of dilution procedures that can be related to $\overline{X}$. Dilution procedures often involve combining two streams, a dilution stream, and a stream to be diluted. An example of an aerosol diluter is shown in Figure III-10. Aerosol flowing through the capillary at a known volume flow rate, Q_2 is combined with gas that has passed a high efficiency filter at volume flow rate Q_1. When

the two streams are completely mixed, the resulting dilution ratio is related to $\overline{X}$ as follows:

$$Dr = \frac{Q_1 + Q_2}{Q_2} = \overline{X}^{-1}$$ Equation III-8.

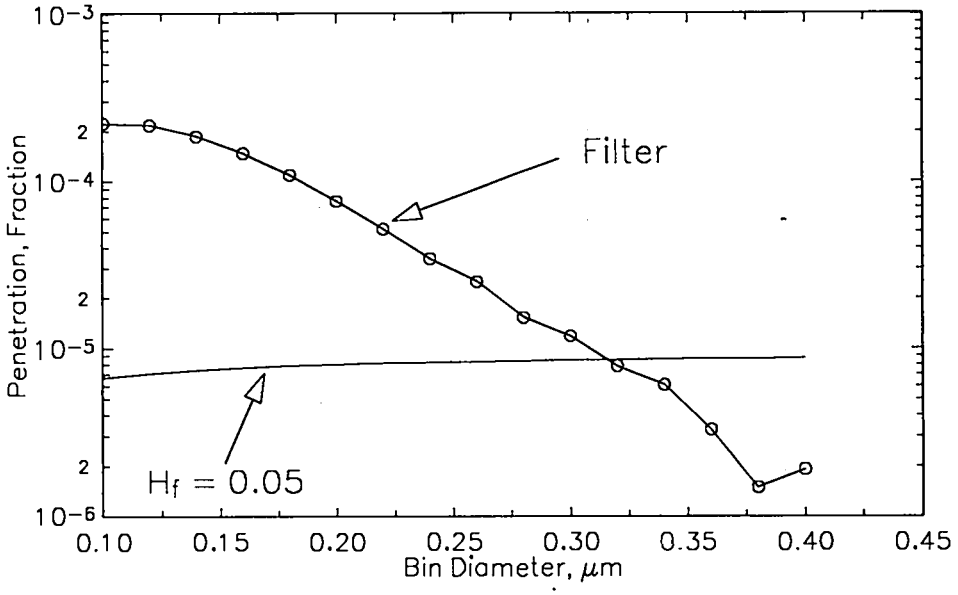

Figure III-9. A plot showing typical penetration values and penetration values corresponding to $H_f = 0.05$, $P_{hf=0.05}$. Penetration values greater than the $P_{hf=0.05}$ estimates are associated with H_f values below 0.05. Penetration values lower than the $P_{hf=0.05}$ estimates are associated with H_f values above 0.05.

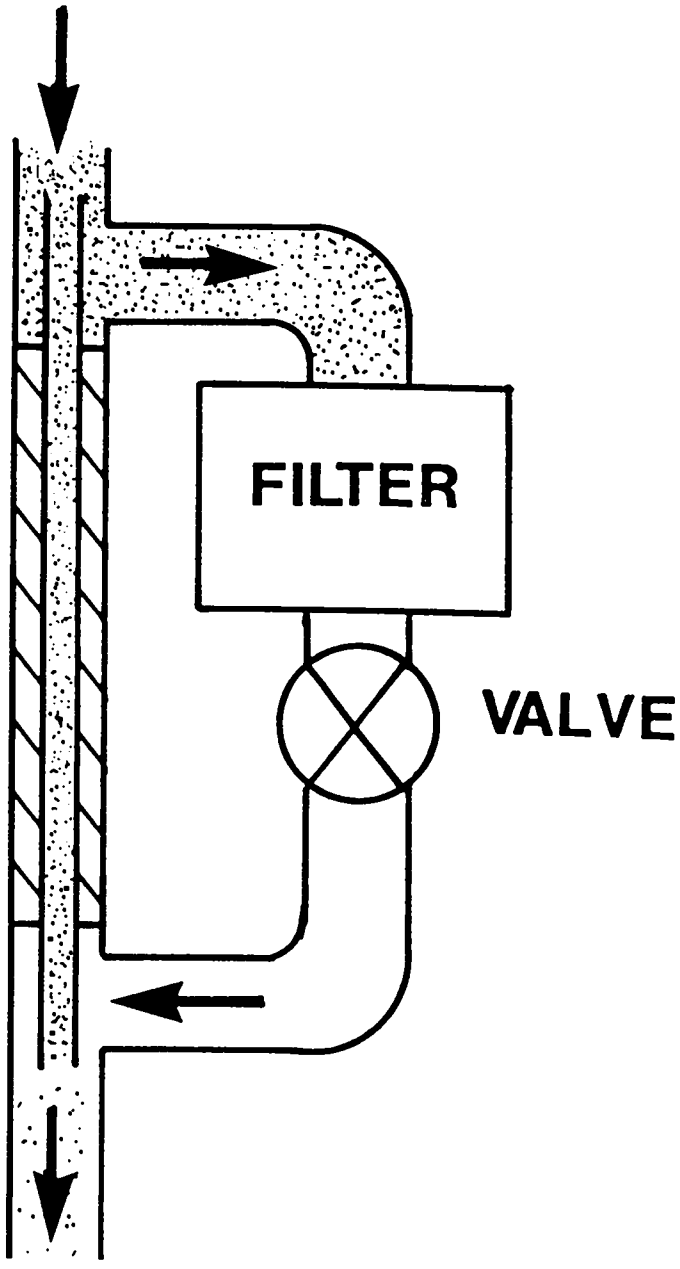

Figure III-10. A schematic of a capillary aerosol diluter.

From Equation III-3 as Dr increases, H also increases. This result indicates that aerosol exiting a dilution section of an aerosol evaluation system becomes less well-mixed as Dr increases. Often in aerosol evaluations, system sections downstream of a dilution section require uniform concentration profiles. Some examples of such sections include exposure chambers, sampling sections, and reaction chambers. In these situations the assumption of uniform concentration becomes less valid as the value of Dr increases. Mixing devices placed between the sections will serve to reduce H. System design should include estimates of H_0, the heterogeneity at the exit of the dilution section and H_f, the heterogeneity required at the downstream section.

Dilution in aerosol evaluation systems rarely exceeds a Dr = 10000. Errors in measurement of Q_1 and Q_2 at values of Dr>10000 result in significant errors in estimating Dr. Using Equations III-3 and III-8, a Dr = 10000 corresponds to a H_0 of approximately 99.99. To obtain an H_f of 0.05 under these conditions requires an approximate 2000-fold reduction in H_0. For values of Dr<10000 lower values of h would be required to obtain an $H_f \leq 0.05$

For aerosol emissions monitoring, $\overline{X}$ can be interpreted as the concentration used to determine the quantity of material released. Errors made in estimating $\overline{X}$ result in errors in determining emission level. A

component of the error in estimating $\overline{X}$ is the sampling error associated with H_f at the sampling point. This heterogeneity is a complex function of the volume flow rates of the air effluent system entries, Q_i, and the heterogeneity reductions between the entry points and the sampling point, h_i. An upper bound estimate of H_f is:

$$H_f^* = \frac{\sqrt{\frac{\sum_i Q_i}{Q_{imin}} - 1}}{h_{imin}} \qquad \text{Equation III-9}$$

where, Q_{imin} = the lowest Q_i, and h_{imin} = the smallest h_i. Typically, h_{imin} will be associated with the upstream entry nearest the sampling point, whereas Q_{imin} could be associated with any entry. The higher the values of Q_{imin} or h_{imin}, the lower the values of H_f^*. In air effluent systems, rarely would Q_i values be below 0.2 m^3/min and typically $\Sigma Q_i < 2000$ m^3/min. Under these conditions, an $h_{imin} \approx 2000$ would be required to achieve an $H_f^* = 0.05$. At this same value of H_f^*, smaller values of h_{imin} would be required for greater values of Q_{imin} and/or lower values of ΣQ_i. This analysis predicts that most air effluent systems require an h no greater than 2000 between the last entry and the sampling point to achieve an H_f at the sampling point of 0.05 or less.

III.C.2.a.iv. Air Flow Resistance of Passive Mixers

In certain of the situations described above additional mixing may be required beyond the turbulent mixing inherent in the system. In these cases the application of passive mixing devices may be appropriate. One of the considerations in using these devices is their energy requirements. Because these devices use the kinetic energy of the stream flow to achieve mixing they put extra demands on system air movers. Tasucher and Streiff (Ta79) compared air flow resistance of some passive mixing devices. The static mixing units achieved the greatest degree of mixing with the lowest flow resistance. Various configurations of empty pipe (turbulent mixing) had slightly lower resistance's but required more than a factor of ten greater mixing lengths to achieve the same degree of mixing. An orifice device had more than a factor of ten greater resistance than static mixing units and a slightly greater mixing length. From this analysis, the static mixing units appear to be beneficial when large reductions in mixing lengths are required and a small increase in resistance can be accommodated.

III.C.2.a.v. Application of Static Mixing Units To Aerosol Evaluations

III.C.2.a.v.a. Mixing of Aerosols

Static mixing units have been developed and evaluated for the mixing of gases. In certain situations the mixing of aerosols may differ from that of gases. For example when inertial mechanisms such as turbulent or shear mixing are employed, mixing of aerosol particles with large aerodynamic diameters may differ from the mixing of gases. Consequently, application of the units to the mixing of aerosols requires an understanding of how the performance of the units for gases relates to the performance with aerosols. There are few references in the literature addressing the use of the units for the mixing of aerosols. Gogins et al (Go87) evaluated certain static mixing units for use in a filter evaluation system. They found $H_f<0.04$ downstream of a type "AX" mixing units (Koch Engineering Inc.). No specification of H_0 was given. Results of evaluations on mixers used in the present study are given in Section III.C.2.c.

III.C.2.a.v.b. Aerosol Loss In Static Mixing Units

In certain applications of the mixers in aerosol studies, aerosol loss in the mixers is important. These applications generally involve situations where the mixer is placed in between the point where information on aerosol properties is required and the point where the properties are determined. Some examples of these applications include 1) filter evaluations where the penetrating aerosol is mixed prior to obtaining a downstream sample, and 2) aerosol dilution, where samples downstream of the diluter and mixer are used to determine properties upstream of the diluter.

Gogins et al (Go87) measured aerosol loss in the type AX mixers. Losses were <2 % in the 0.1 μm to 0.4 μm particle diameter range and <10% in the 0.4 μm to 1 μm diameter range.

Aerosol loss mechanisms can be divided into four categories: 1) diffusion, 2) interception, 3) sedimentation, and 4) inertia. For the static mixing units the effectiveness of diffusion as a loss mechanism will be related to a diffusion deposition parameter:

$$\mu_m = \frac{D \bullet L}{Q}$$ Equation III-10,

where, D = particle diffusion coefficient, L is a characteristic mixer channel length, and Q is mixer volume flow rate. This form of the deposition parameter was chosen because channel width and height are approximately equal for the mixers. The characteristic channel length is taken to be the length of the mixer. This length is proportional to the true total channel length for each mixer size because of the scaling of the various mixer sizes. This formulation of μ_m does not allow for accurate prediction of the magnitude of diffusional losses but does permit extrapolation of losses measured for one size mixer to mixers of other sizes.

The relative likelihood for interception losses in the mixers is determined by an interception parameter, R. For interception losses at the mixing plate edges:

$$R_{ed} = \frac{d_p}{T_c} \qquad \text{Equation III-11,}$$

where d_p = particle diameter and T_c = the plate thickness. For interception losses within the corrugation channels:

$$R_c = 2 \bullet \frac{d_p}{d_c} - \left(\frac{d_p}{d_c}\right)^2 \qquad \text{Equation III-12,}$$

where d_C = the equivalent diameter of a channel. Again, these formulations of R allow for extrapolation to other size mixers.

Sedimentation losses are not expected to contribute significantly to overall losses in the mixers. Aerosol losses by sedimentation depend on particle settling velocity and residence times in the mixer. Sub-micrometer aerosol particles have settling velocities less than 35 μm/sec and design of the mixers necessitates operation with low residence times. Sedimentation losses would be larger for particles micrometer size and larger.

Inertial loss mechanisms include impaction and turbulent deposition. The mixers are operated at flow Reynolds numbers below 6000. At these Reynolds number turbulent deposition is expected to be negligible for sub-micrometer aerosol (Fr77).

Particle losses by impaction will predominantly occur at plate edges and at the beginning of channels. These losses will be dependent on the local Stokes number for each site. The Stokes number for plate edge losses is given by:

$$Stk_e = \frac{\tau \bullet V_0}{T_c}$$ Equation III-13,

where τ = particle relaxation time $= \frac{\rho_p \bullet d_p^2 \bullet C_c}{18 \bullet \eta}$, ρ_p = particle mass density, C_c = Cunningham slip factor, η = viscosity of air, V_0 = the maximum mixer air velocity $= \frac{4 \bullet Q}{Vf \bullet \pi \bullet D_m^2}$, Vf = void fraction, D_m = actual mixer diameter, and T_c = plate thickness. The formulation for V_0 gives maximum values for the air stream velocity approaching the plate edge and thus results is upperbound estimates of Stk_e.

Stokes number for losses at the channel entry is given by:

$$Stk_c = \frac{\tau \bullet V_0}{d_h}$$ Equation III-14,

where τ = particle relaxation time, V_0 = the free stream air velocity approaching the channel entry, and d_h = the hydraulic diameter for the mixer.

III.C.2.b. Experimental Methods

In this evaluation, performance of static mixing units used in the filter evaluation system shown in Figure III-2 is investigated. The mixing unit upstream of the test filter is used to assure test aerosol challenge concentration is uniform over the upstream filter face. The degree of mixing provided by this unit is determined from concentration measurements over the filter face.

Mixing units downstream of the test filter are used to assure the downstream aerosol is uniformly mixed prior to sampling. The mixing performance of these units for aerosols is evaluated against predictions made from gas mixing measurements. Aerosol losses in the units are measured and interpreted in terms of an analysis of potential loss mechanisms.

III.C.2.b.i. Mixer Performance

III.C.2.b.i.a. Upstream Mixer

The upstream mixer is an SMV type mixer (Koch Engineering, Inc.) with N = 4 and S = 1. Using Equation III-4, the expected value of h for the mixer is approximately 112. The mixer is used to mix the aerosol from the

aerosol generator with filtered test system air from a blower. Aerosol is injected into the system air flow immediately upstream of the mixer. For the mixer evaluation, the volume flow rate of the aerosol stream, Q_2, was set to approximately 30 Lpm. The total volume flow rate through the upstream mixer, $Q_1 + Q_2$, was set to approximately 3600 Lpm, where Q_1 is the volume flow rate supplied by the blower. Using Equations III-1 and III-3, these values of Q_1 and Q_2 indicate a value of $H_0 \approx 10.9$. The aerosol stream is a DEHP aerosol with a count median diameter of approximately 0.2 μm and a geometric standard deviation of approximately 1.6. The expected heterogeneity downstream of the mixer under these conditions is $H_f = 0.097$, based on Equation III-4.

The concentration profile downstream of the mixer was measured over the cross section of the 36 cm x 36 cm rectangular plenum at the upstream face of the test filter. Figure III-11 shows the grid of sample points over this cross section. Between measurements at grid points, measurements were made at a reference point located at 0 cm, 1.27 cm Concentration measurements were made at 15 aerosol sizes in the diameter range from 0.1 μm to 0.4 μm using a LAS (Particle Measuring Systems, Inc. Model LAS-X-M, see Section III.C.4.). Measurements were made with a volume flow rate of approximately 0.6 Lpm pulled through the

test filter. The measurements were repeated with a test filter volume flow rate of approximately 17 Lpm.

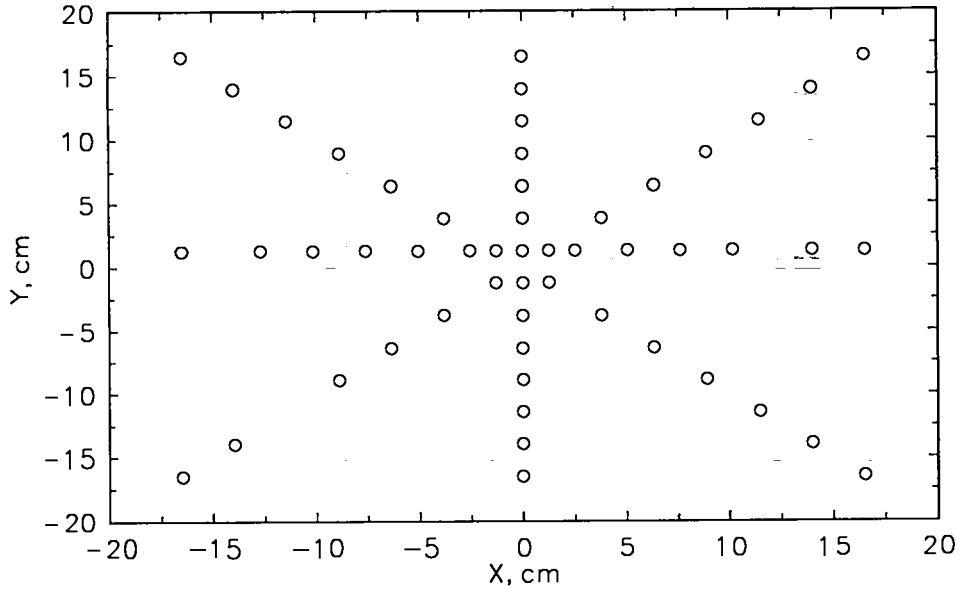

Figure III-11. Sampling point locations for the upstream mixer evaluations.

III.C.2.b.i.b. Downstream Mixers

There is a downstream mixer for every decade of test filter flow rate. Table III-III lists pertinent mixing unit specifications such as test air flow rate range. The 1" and 2" mixers have S = 4, whereas the other mixers have S = 1. All mixers have N = 4.

Table III-III

Downstream Mixer Specifications

Model	Nominal Diam., inches	Actual Diam., cm	Q Range [a], Lpm	S[b]	N_p[c]	Re[d]
SMV-DY	1/4	0.914[e]	0.708 - 7.08	1	5	350
SMV-CY	3/4	2.08	7.08 - 70.8	1	6	1170
SMV-CY	1	2.08	7.08 - 70.8	4	6	1170
SMV-BY	1 1/2	4.06	70.8 - 708	1	6	5320
SMV-BY	2	4.75	70.8 - 708	4	6	3890

[a] - Volume flow rate (Q) range.

[b] - S = number of spacers.

[c] - N_p = number of plates per element.

[d] - Flow Reynolds number at maximum Q.

[e] - Mixer lengths equal actual mixer diameter except for the 1/4" mixer which has a length of 1.27 cm.

Experimental evaluation of downstream mixer performance entailed challenging a mixer with aerosol penetrating a test filter. A hole approximately 3 mm in diameter was installed in the center of the filter. Operating the filter at 7.08 LPM, aerosol concentration measurements were made in the plane of the sampling probe with the downstream mixer replaced with an empty pipe. The LAS-X-M described in Section III.C.4 was used to make the measurements. Grid point measurements were taken along a horizontal traverse (Y = 0) of the test flow duct (see Figure III-12). Reference point measurements were taken at the center of the duct before and after each grid point measurement. These data provide information on the heterogeneity challenging the mixer (H_0).

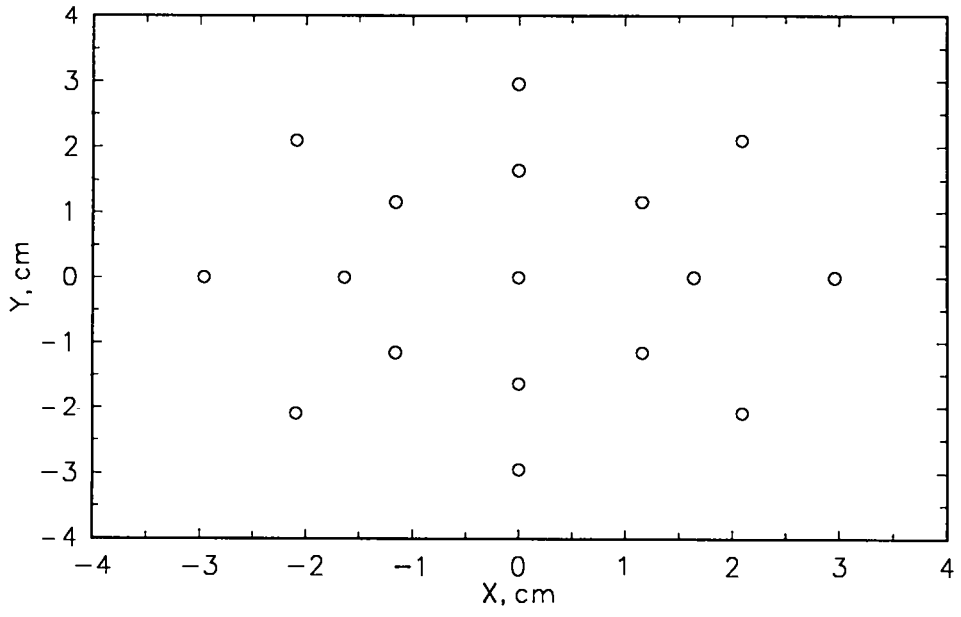

Figure III-12. Sampling point locations for the downstream mixer evaluations.

To evaluate mixer performance the empty pipe was replaced with the 3/4" mixer. The concentration profile downstream of the mixer was measured over the cross section of a 7.62 cm circular duct in the plane of the sampling probe. Figure III-12 shows the grid of sample points over this cross section. Before and after grid point measurements, measurements were made at a reference point located at 0, 0. Concentration measurements were made at 15 aerosol sizes in the diameter range from 0.1 μm to 0.4 μm using the LAS. Profile

measurements were made with the mixer operating at 7.08 Lpm and 70.8 Lpm.

Another set of measurements were made after the center hole in the filter unit was sealed and another hole was installed in the corner of the filter unit. Profile measurements were made with the mixer operating at 7.08 Lpm and at 70.8 Lpm.

III.C.2.b.ii. Aerosol Loss Evaluation

To measure losses in the downstream mixers a test manifold was constructed as in Figure III-13. In the test leg of the manifold an empty pipe and a mixer were interchanged. The reference leg of the mixer consisted of an empty pipe.

Challenge aerosol mixed with the upstream mixer was directed to the test and reference legs alternately with a the three-way valve located upstream of the manifold legs. Aerosol samples were collected downstream of the manifold with the LAS-X-M. Particle counts in the 15 LAS aerosol size bins were recorded. Alternating measurements between the reference and test legs were repeated between 6 and 12 times. These measurement sets were made with a mixer in the test leg and repeated

with empty pipe in the test leg. Losses in the 1/4" and 3/4" mixers were evaluated in this manner at both extremes of their flow rate ranges.

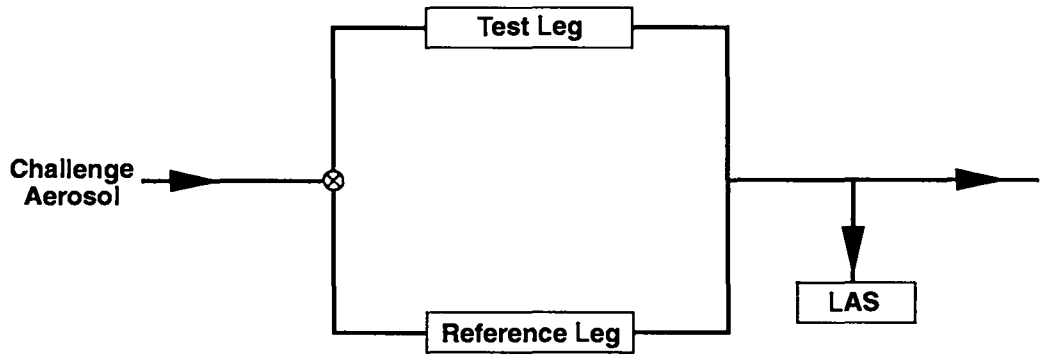

Figure III-13. A schematic of the test manifold used in the aerosol loss evaluations of the downstream mixers.

III.C.2.c. Results and Analysis

III.C.2.c.i. Mixer Performance

III.C.2.c.i.a. Upstream Mixer

Heterogeneity downstream of the upstream mixer (H_f) was calculated from the standard deviation and average of the concentration measurements made on the 36 cm x 36 cm grid using Equation III-3. The coefficient of variation for the reference point measurements (CV_{ref}) was

calculated from the standard deviation and average of these measurements. The reference point measurements are an indication of the generation/sampling system stability during the period in which the grid point measurements were made. Figure III-14 shows results of these calculations for a test flow rate of approximately 0.6 Lpm. Values of H_f ranged from above 2.7% to almost 4.9%. The values of CV_{ref} ranged from just over 2.4% to almost 4.4%.

The observed values of H_f were very close to the observed values of CV_{ref}. This result indicates that the variability observed in the grid measurements was dominated by variations in the generation/sampling system and that variation associated solely with location was below limits of detection. Consequently, the observed H_f associated strictly with sample point location was much less than the H_f predicted using Equation III-4. This finding may at least be partially explained by mixing mechanisms not accounted for in Equation III-4. An example of these additional mixing mechanisms is turbulent mixing that takes place downstream of the mixer in the pipe leading to the test filter plenum, at the transition from the pipe to the plenum, and at the flow-straightening screen hung transverse to flow over the entire plenum cross section.

Figure III-14 shows the heterogeneity calculation results plotted against aerosol particle size. The dependence of H_f on particle size

appears to be fully accounted for by the CV_{ref} particle size dependence. These results give no insight as to the dependence of the portion of H_f solely related to sample point location on particle size.

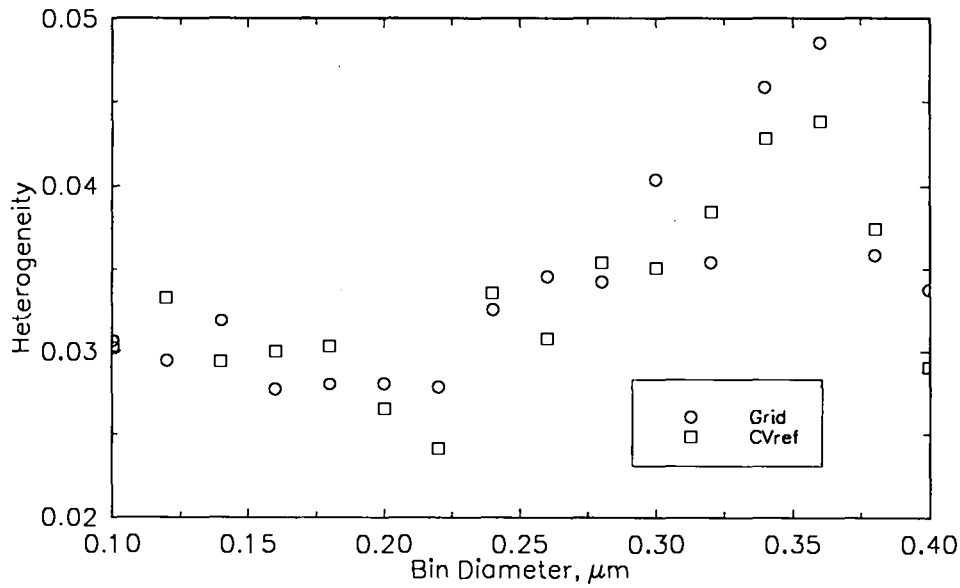

Figure III-14. Results of the upstream mixer evaluation showing heterogeneity for the grid points and the coefficient of variation for the reference point measurements.

Similar measurements were made at a test flow of approximately 17 Lpm. The results of these measurements did not differ from those made at approximately 0.6 Lpm. This finding indicates that mixing of the challenge aerosol is not affected by changes in test flow rate in this range.

During penetration measurements generator flow rate, Q_2, is normally increased by more than a factor of four over the Q_2 used in this evaluation. At the same time total flow rate, $Q_1 + Q_2$, will remain approximately constant. The increase in Q_2 will result in a greater value of $\overline{X}$. Examination of Equation III-3 shows that under these conditions H_f is expected to decrease and better mixing results than were observed in this evaluation can be expected.

III.C.2.c.i.b. Downstream Mixers

Values of H_0 for the downstream mixer evaluations were calculated from the average and standard deviation of the grid concentration measurements made with empty pipe in the downstream mixer location. Values of concentration coefficient of variation at the reference point (CV_{ref}) were calculated from the average and standard deviation of the reference point measurements. Values of H_0 and CV_{ref} are compared in Figure III-15. Heterogeneity of the grid point measurements (H_0) ranged from just above 21% to just below 26%. Whereas, CV_{ref} values ranged from just below 3% to just over 11%. Estimates of H_0 solely related to grid point location were determined by subtracting the standard deviation of the

reference point measurements from the standard deviation of the grid point measurements and dividing difference by the average of the grid point measurements. These H_0 estimates ranged from just below 15% to almost 22%. These results show that the variation in concentration along the traverse was greater than the time variation in concentration at the reference point. The results indicate non-uniform mixing in the sampling probe plane.

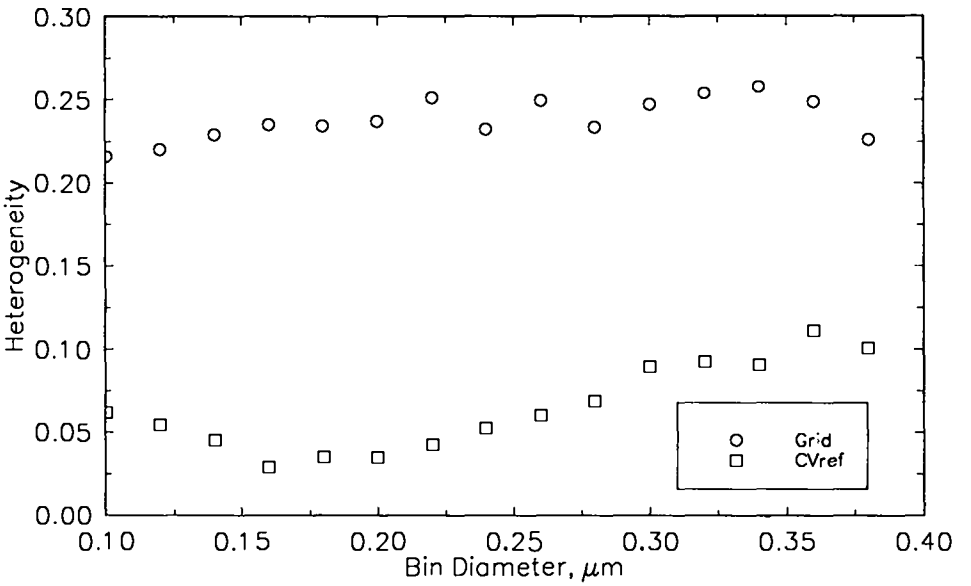

Figure III-15. Results of challenge aerosol measurements for downstream mixer evaluations. The test filter with an installed center hole was operated at a flow rate of 7.08 Lpm.

The estimates of H_0 solely related to grid point location can be used with Equation III-4 to predict H_f. For the 3/4" mixer, the predicted H_f values lie between 0.1% and 0.2%.

Estimates of P can be made using Equation III-3 with P substituted for $\overline{X}$ and , these estimates of H_0 indicate a P between 0.95 and 0.98. These values of P are much greater than expected for the filter even with the installed leak. A possible explanation for the observed values of H_0 is that mixing between the filter and the sampling probe plane reduced the heterogeneity of the aerosol exiting the filter.

The standard deviation and average of grid point measurements made after the 3/4" downstream mixer was re-installed were used to determine H_f. CV_{ref} for the downstream mixer was calculated from the standard deviation and average of the associated reference point measurements. Figure III-16 shows results of these calculations with the mixer operating at approximately 7.08 Lpm and the hole in the center of the filter. Values of H_f ranged from just over 2% to just over 3.5%. CV_{ref} values ranged from just over 1.5% to just under 3.25%.

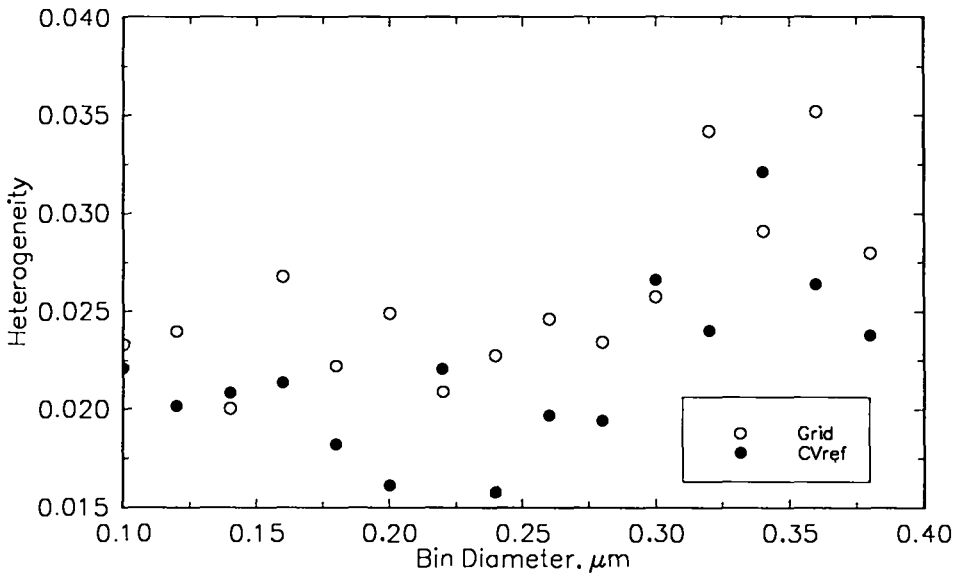

Figure III-16. Evaluation results for the 3/4" downstream mixer operated at 7.08 Lpm. A hole was installed in the center of the test filter.

The observed values of H_f were very close to the observed values of CV_{ref}. This indicates that the variability observed in the grid measurements was dominated by variations in the generation/sampling system and that variation associated solely with grid point location was below limits of detection.

The observed values of H_f were more than an order of magnitude greater than the value of H_f predicted by Equation III-4. This result is expected given the variations in the generation/sampling system. Values

of H_f equal to the predictions of Equation III-4 would not be discernible amid the generator/sampling system variations.

The grid and reference measurements made at a test flow of 70.8 Lpm were used to determine corresponding values of H_f and CV_{ref}. Results of these determinations are shown in Figure III-17. These results did not differ from those made at 0.25 CFM. The H_f values were not discernible from the CV_{ref} values, again indicating variation associated solely with grid point location was below limits of detection.

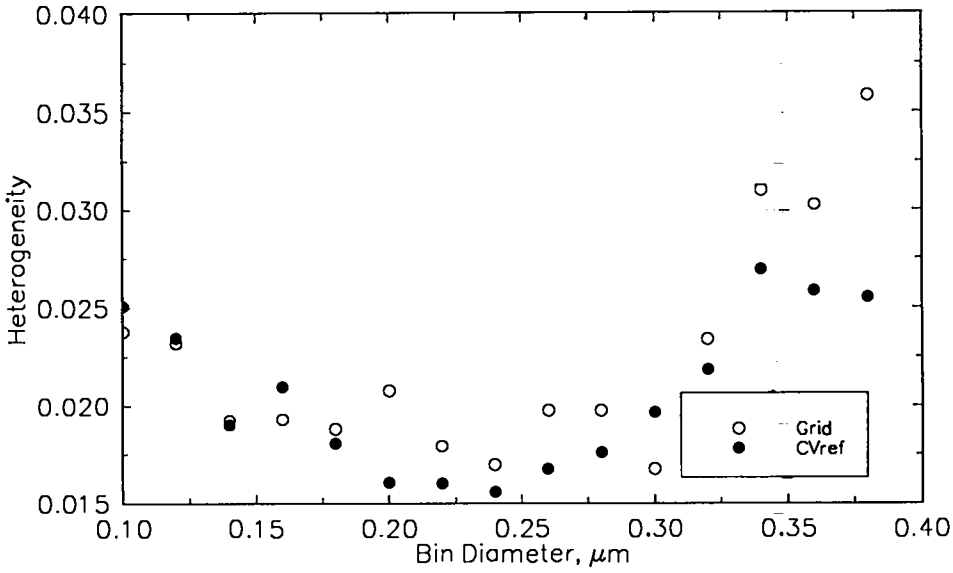

Figure III-17. Evaluation results for the 3/4" downstream mixer operated at 70.8 Lpm. A hole was installed in the center of the test filter.

Operating at a flow rate of 70.8 Lpm, pin-hole leak theory (Th63) predicts filter penetration to drop to approximately 30% of the penetration

at 7.08 Lpm. The penetration decrease translates into a more than 7-fold increase in H_0. Operating at 70.8 Lpm, the H_0 estimates, solely related to grid point location, range from approximately 1.49 to approximately 1.52. Using Equation III-4 and these values of H_0 predicts $H_f \approx 1.3\%$. The observed values of H_f were all greater than the predicted H_f. Values of H_f equal to the prediction are potentially discernible amid the generator/sampling system variations. The apparent domination of observed H_f values by CV_{ref} suggests that the method used to predict H_f may overestimate actual H_f values.

Another set of measurements were made after the center hole in the test filter was sealed and another hole placed in a corner of the filter. Measurements were taken at operating flows of 7.08 Lpm and 70.8 Lpm. Averages and standard deviations were used to calculate values of H_f and CV_{ref}. These values are plotted against aerosol size in Figures III-18 and III-19. For the measurements at 7.08 Lpm, H_f estimates varied from over 5% to approximately 13%. The corresponding CV_{ref} estimates ranged from over 4% to less than 14%. At 70.8 Lpm, the estimates of H_f and CV_{ref} varied from just over 2% to almost 10% and from over 2% to under 11%, respectively.

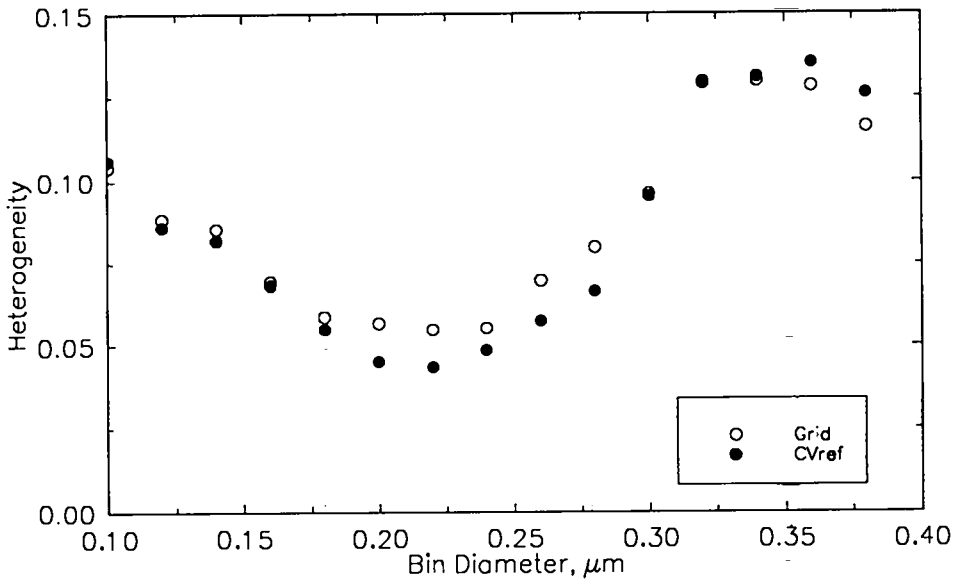

Figure III-18. Evaluation results for the 3/4" downstream mixer operated at 7.08 Lpm. A hole was installed in a corner of the test filter.

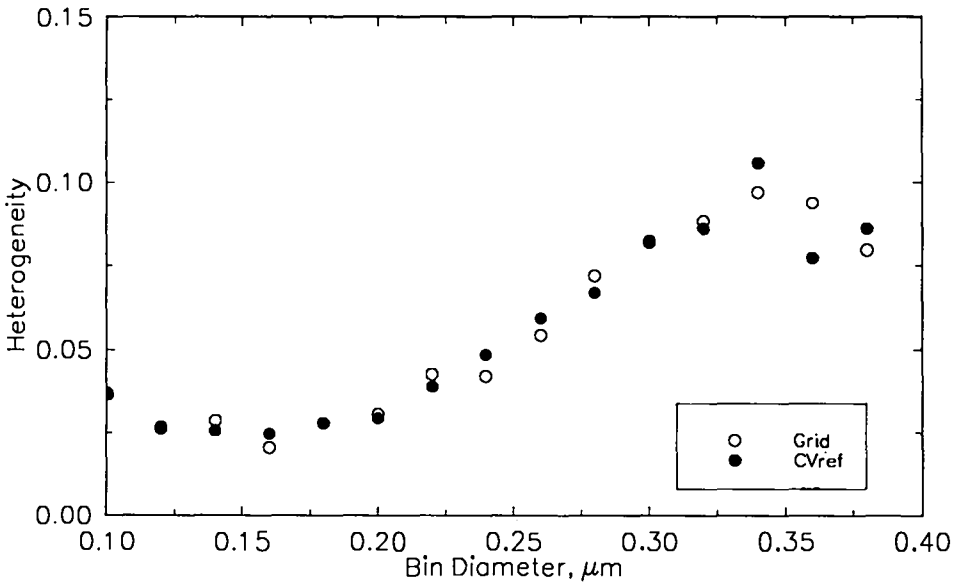

Figure III-19. Evaluation results for the 3/4" downstream mixer operated at 70.8 Lpm. A hole was installed in a corner of the test filter.

At both flows the observed values of H_f were very close to the CV_{ref} values. This result again indicates that concentration variation with location was dominated by changes in the generation/sampling system.

Values of H_f had a larger range for the corner-hole measurements than the center hole measurements. Because the H_f values were so closely tied to generation/sampling variations, the range increase is thought to be related to these variations rather than to concentration variations solely associated with grid location.

Variation of H_f values with aerosol size appears to be tied to variations in the generation/sampling system. In the evaluations of both the upstream and downstream mixers observed changes in H_f are followed by similar changes in CV_{ref}. Values of both parameters are at the upper end of their range at the largest aerosol sizes. This variation may be related to lower aerosol concentrations at these sizes. Poisson statistics predicts that the coefficient of variation varies as the inverse square-root of particle count.

In the filter evaluation system, the 1" and 2" mixers are used as downstream mixers for the whole filter and media pack tests (see Section III.D.3.). Frame penetration measurements are made with a 1/4" mixer used as the downstream mixer. A 1/4" mixer is also used downstream of the diluter.

The predicted performance of these mixers is shown in Figure III-8. Experimental results suggest actual performance is better, with actual heterogeneity being more than an order of magnitude lower than predicted. At a particle diameter of 0.1 μm, predicted mixer performance depends on penetration down to $P \approx 10^{-8}$. For lower penetration values heterogeneity remains constant at just less than 30%. Given the experimental results, actual heterogeneity, for this size particle could be on the order of 3%. The error in penetration estimates that results from

this level of heterogeneity is small compared to counting errors predicted from Poisson distribution statistics (See Section IV.D). Consequently, errors from aerosol concentration heterogeneity were neglected in assessment of penetration uncertainty.

III.C.2.c.ii. Aerosol Loss Evaluation

Aerosol loss was calculated by dividing the difference in the test leg and reference leg particle counts by the reference leg particle count. Tests were performed to determine statistical significance of differences in loss estimates in empty pipe and in the mixers. An F-test was used to determine if sample variance estimates were statistically different. In situations where no statistical difference was found in the variance estimates a t-test for the equality of two means from populations with equal but unknown variances was used. When a statistical difference in the variances was found a t-test for equality of two means for populations with unequal and unknown variances was used.(Di57)

Results of the aerosol loss measurements are shown in Figures III-20 - III-23. Average mixer aerosol loss was <2% relative to losses in the

reference leg. This result is comparable with the loss value reported by Gogins (Go87) in the 0.1 μm to 0.4 μm particle diameter range.

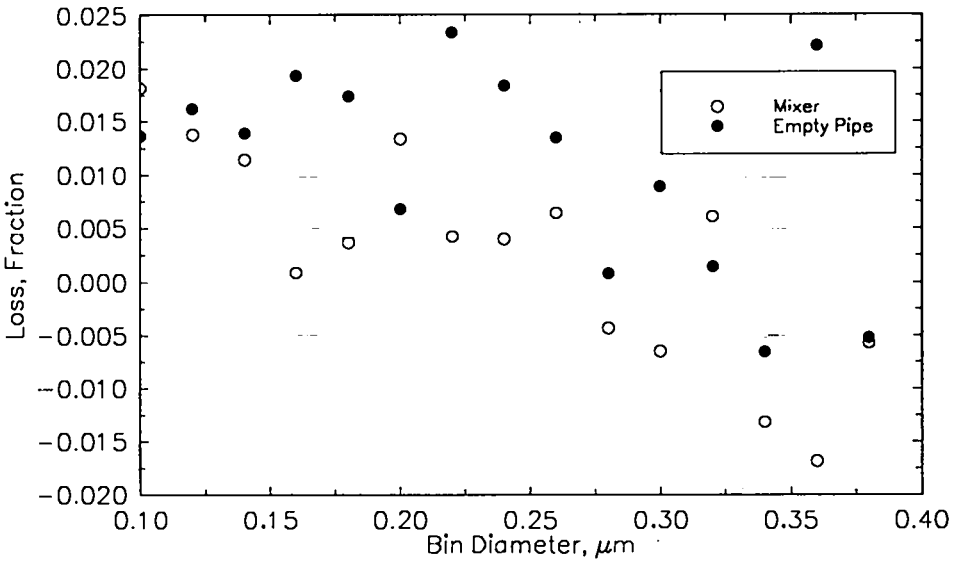

Figure III-20. Results of aerosol loss measurements on 1/4" mixer and empty at a flow rate of 0.708 Lpm.

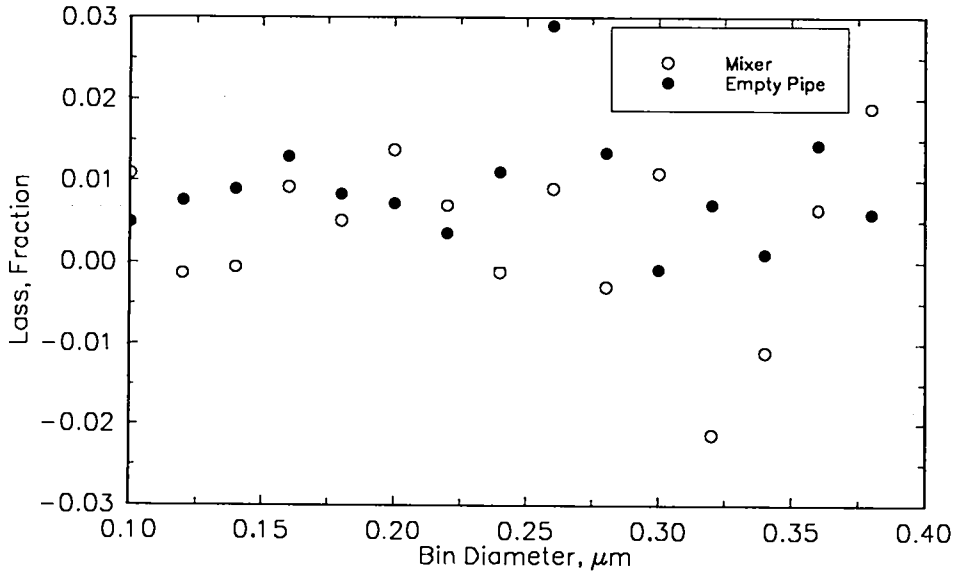

Figure III-21. Results of aerosol loss measurements on 1/4" mixer and empty at a flow rate of 7.08 Lpm.

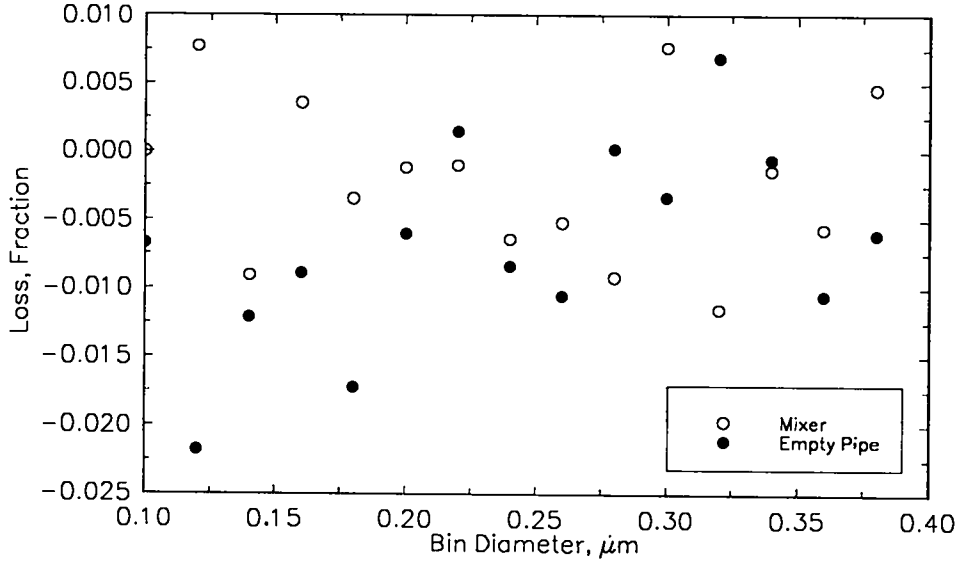

Figure III-22. Results of aerosol loss measurements on 3/4" mixer and empty at a flow rate of 7.08 Lpm.

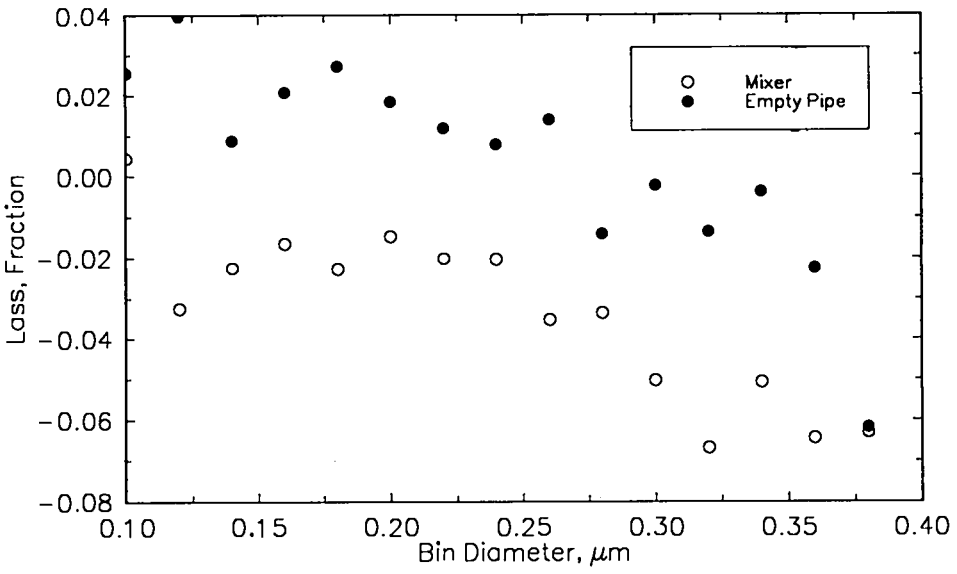

Figure III-23. Results of aerosol loss measurements on 3/4" mixer and empty at a flow rate of 70.8 Lpm.

Average empty pipe losses were as high as 4%. Comparing mixer losses with those in empty pipe showed only one case where the mixer losses were greater and where the difference was statistically significant. In this case mixer losses were <1%. In all other cases where the mixer loss point estimate was greater than the empty pipe estimate, the difference was not found to be statistically significant at the 95% confidence level.

A negative loss indicates greater loss in the reference leg than in the test leg. Negative losses were observed for both empty pipe and

mixers. The reason for negative losses is not known. Some negative losses would be expected if actual losses were of the same magnitude or lower than the detection limit for the test system. Negative losses would also be expected if losses were directly related to residence time such as are diffusion losses. Empty pipe residence time is between 19% and 43% greater than mixer residence time.

III.C.2.c.iii. Assessment of Aerosol Loss in Static Mixers

Mixer evaluations discussed above were completed on the 1/4" and 3/4" mixers. Results of these tests have been extrapolated to the 1", 1 1/2", and 2" mixers.

Losses in the 1", 1 1/2", and 2" mixers were predicted from the measurements on the 1/4" and 3/4" mixers using the analysis of potential loss mechanisms above and specifications of the mixing elements. Specifications of the mixing elements are listed in Table III-IV.

Table III-IV

Mixing Element Specifications

Nominal Diam., inches	T_c[a], cm	d_h[b], cm	Vf[c]
1/4	0.030	0.244	0.84
3/4	0.091	0.356	0.70
1	0.091	0.356	0.70
1 1/2	0.091	0.635	0.72
2	0.091	0.635	0.72

a - plate thickness

b - d_h = hydraulic diameter

c - Vf = void fraction

To assess the contribution of diffusion losses for the various mixers sizes, values of diffusion deposition parameter μ_m, were calculated using Equation III-10. Values of μ_m were determined at the minimum flow for each mixer which corresponds to the condition for the greatest diffusion losses. The value of D in Equation III-10 was determined using the nominal value of mean free path for Los Alamos, $\lambda = 0.086$ µm. Figure III-24 shows results of these calculations for $d_p = 0.065$ µm and $d_p = 0.1$ µm. Values of μ_m were all found to be less than 2×10^{-6}. These values of μ_m indicate extremely low losses. Values of µ for the 1", 1 1/2", and 2" mixers

were less than or equal to the values for the 1/4" and 3/4" mixers. Consequently, diffusion losses in the large mixers are not expected to contribute any more to overall losses than do diffusion losses in the small mixers.

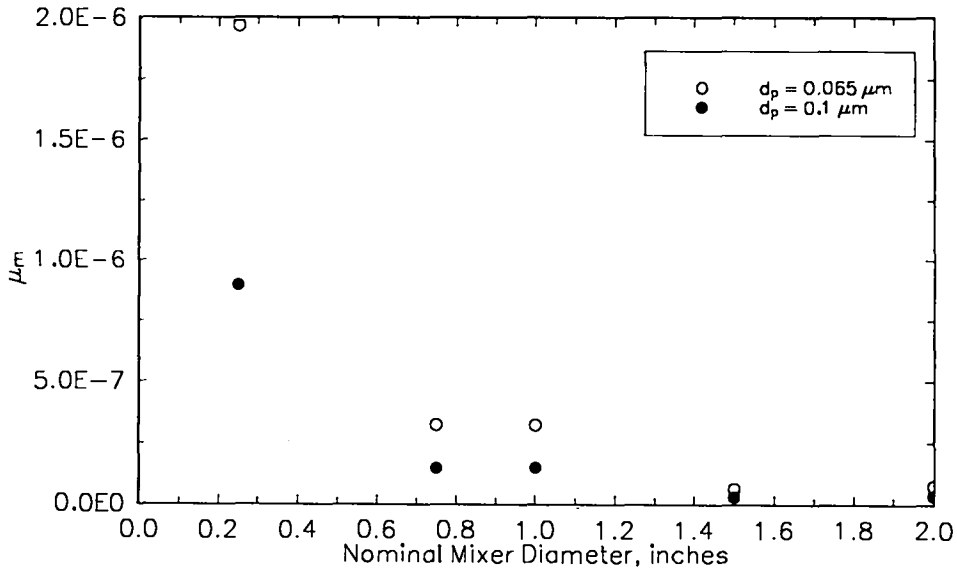

Figure III-24. Results of diffusion loss analysis showing values of μ_m for d_p = 0.065 μm and 0.1 μm.

Interception losses in the mixers were investigated by computing values of R_{ed} and R_c for the various mixer sizes using Equations III-11 and III-12, respectively. Results of the computations are shown in Figures III-25 and III-26 for d_p = 0.4 μm, 0.5 μm, and 1 μm. Values of R_{ed} and R_c were all found to be less than 0.0035. Again, values of R_{ed} and R_c for the large mixers were below or equal to R_{ed} and R_c values for the small

mixers. Consequently, interception losses in the large mixers are not expected to contribute any more to overall losses than do interception losses in the small mixers.

Stokes numbers were calculated to evaluate losses due to impaction at mixing plate edges and entries. Equations III-13 and III-14 were used in these calculations. The velocity V_0 used in the calculations corresponded to the maximum mixer Q. Losses are expected to decrease at lower values of Q. The value of C_c used in the calculation of τ was based on $\lambda = 0.086$ µm. Results of these calculations are shown in Figures III-27 and III-28 for $d_p = 0.4$ µm, 0.5 µm, and 1 µm.

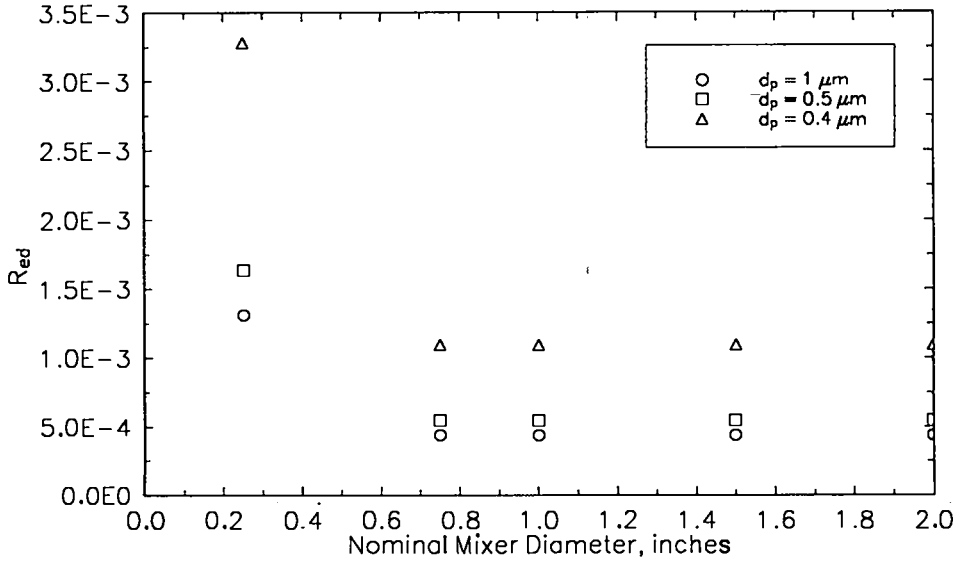

Figure III-25. Results of interception loss analysis showing values of R_{ed} for $d_p = 0.4$ µm, 0.5 µm, and 1 µm.

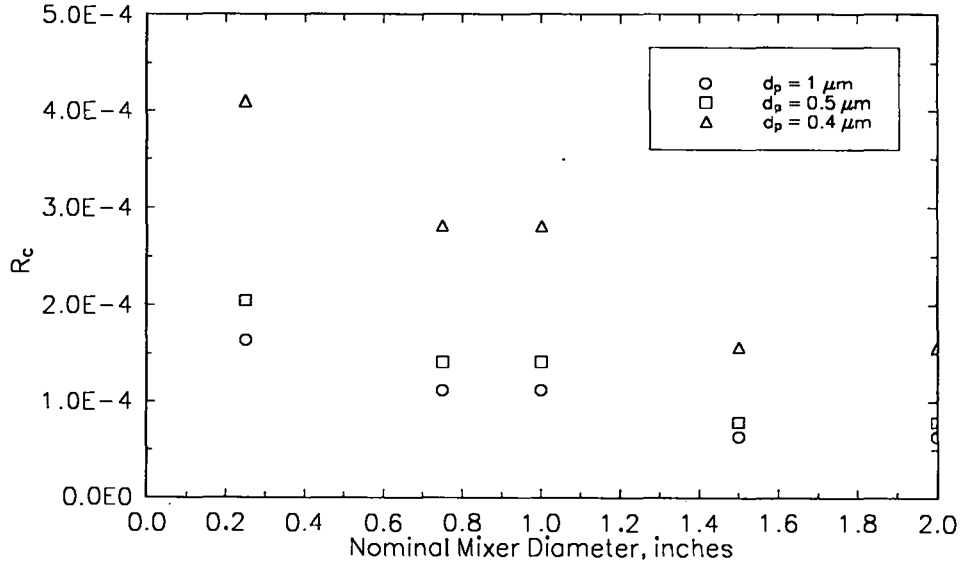

Figure III-26. Results of interception loss analysis showing values of R_c for d_p = 0.4 μm, 0.5 μm, and 1 μm.

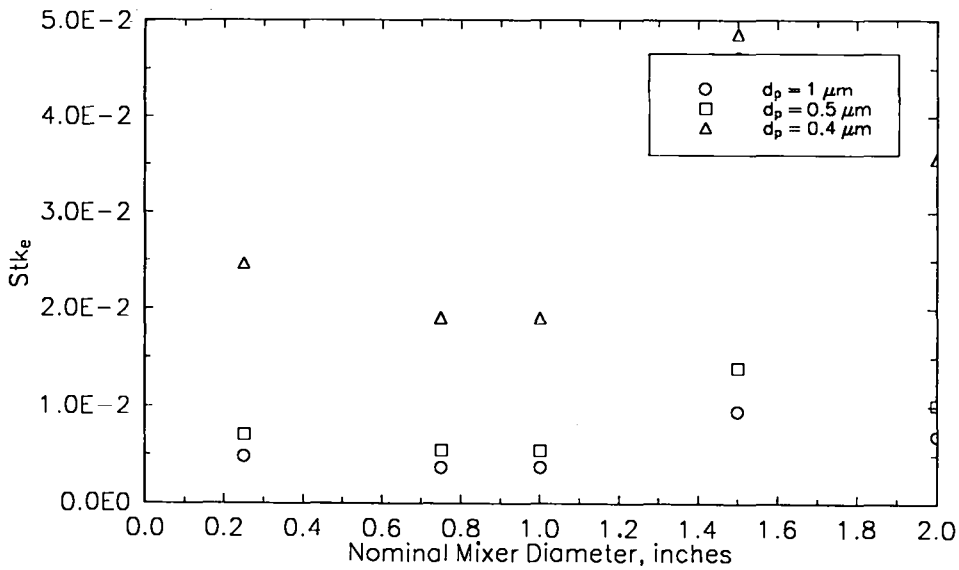

Figure III-27. Results of impaction edge loss analysis showing values of Stk_e for d_p = 0.4 μm, 0.5 μm, and 1 μm.

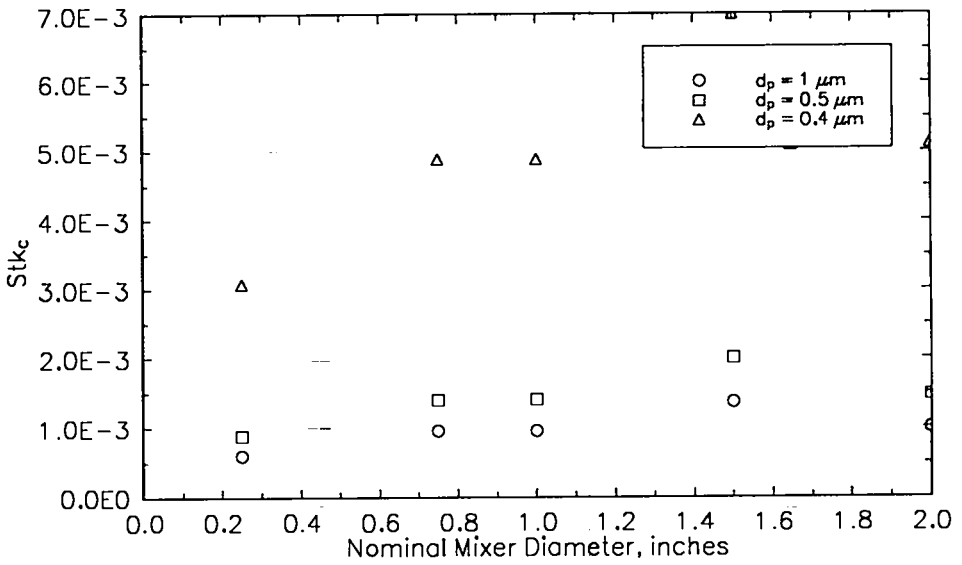

Figure III-28. Results of impaction entry loss analysis showing values of Stk_c for d_p = 0.4 μm, 0.5 μm, and 1 μm.

Edge losses were found to have Stk_e less than 0.05. This value of Stk_e indicates that impaction losses at plate edges are extremely small. Values of Stk_e for the 1" mixer were less than or equal to the values for the 1/4" and 3/4" mixers. Consequently, the contribution of impaction edge losses to overall losses in the 1" mixer is expected to be no greater than the contribution of these losses to the overall losses in the 1/4" and 3/4" mixers.

The values of Stk_e for the 1 1/2" and 2" mixers were greater than the corresponding values for the 1/4" and 3/4" mixers. This result

indicates that impaction edge losses in the 1 1/2" and 2" mixers are expected to exceed losses of this type in the 1/4" and 3/4" mixers. However, the magnitude of loss in these larger mixers is expected to be negligible because of the low values of the Stokes number for these losses.

Impaction entry losses were found to have Stk_c <0.007. This value of Stk_c indicates that impaction losses at channel entries are extremely small. Values of Stk_c for the 1" mixer were no greater than these values for the 1/4" and 3/4" mixers. Consequently, the contribution of impaction entry losses to overall losses in the 1" mixer is expected to be no greater than the contribution of these losses to the overall losses in the 1/4" and 3/4" mixers.

The values of Stk_c for the 1 1/2" and 2" mixers were greater than the corresponding values for the 1/4" and 3/4" mixers. This result indicates that impaction entry losses in the 1 1/2" and 2" mixers are expected to exceed losses of this type in the 1/4" and 3/4" mixers. However, the magnitude of loss in the larger mixers is expected to be negligible because of the low values of the Stokes number for these losses.

The analysis of loss mechanisms indicates that losses should be low. This conclusion is in agreement with measurements made on the 1/4" and 3/4" mixers.

Analysis of losses in the 1" mixer shows that for every loss mechanism expected losses are no greater than expected losses in the smaller mixers. Consequently, the overall losses in the 1" mixer are not expected to be greater than the losses observed in the smaller mixers.

For the 1 1/2" and 2" mixers, diffusion and interception losses are expected to be no greater than those losses in the 1/4" and 3/4" mixers. However, impaction losses in the large mixers are predicted to be higher than those losses in the small mixers. Nonetheless, overall losses in these large mixers are expected to be negligible. This conclusion follows from the expectation that losses by diffusion, interception, and impaction are low. Diffusion and interception losses are expected to be low because observed losses in the small mixers were low. Impaction losses are expected to be low because values of the parameters that predict these losses indicate losses to be negligible. From the analysis and experimental results, losses in the mixers for DEHP particles with diameters in the range from 0.1 μm to 0.4 μm are expected to be <10%.

III.C.2.d. Discussion and Conclusion

III.C.2.d.i. Mixer Performance

The evaluation of mixer performance provided no evidence that aerosol mixing performance was any poorer than predictions based on gas mixing results. Even in evaluations where expected values of H_f were greater than or equal to the nominal values of CV_{ref}, the observed values of H_f were not distinguishable from the CV_{ref} values. If anything, these evaluations suggest the gas mixing results predict poorer mixing than observed for the aerosols in this study.

In these mixer performance evaluations, measurements were limited to particles in the diameter range from ≈0.1 μm to ≈0.4 μm. Mixing of aerosols in this size range is expected to mimic mixing of gases because convection dominates their transport. Particles of this size are expected follow flow streamlines. Deviations from streamlines because of particle inertia are expected to be negligible. Deviation from streamlines because of particle Brownian motion is expected to be less than these deviations for gases due molecular diffusion.

III.C.2.d.ii. Aerosol Loss

Estimates of aerosol loss in mixers was not distinguishable from loss in empty pipe. Given this finding and results from the analysis of loss mechanisms, losses in mixers are expected to be negligible under operational conditions of the filter evaluation system.

The evaluation of losses was limited to particle diameters $\geq$0.065 µm but $\leq$1 µm. Diffusion losses for particle sizes below this range may be greater than these results indicate and interception and inertial losses for particle sizes above this range may be greater than these results indicate. Aerosol losses of particles outside this size range may not be negligible and should be evaluated.

III.C.3. Aerosol Dilution

The aerosol diluter used in the filter evaluation system is a variable, capillary diluter as shown in Figure III-10. Design of this diluter is patterned after a diluter made by ATEC Inc., Calabasas, CA. The dilution ratio for this diluter is given in Equation III-8. The value of Q_2 is determined by the differential pressure across the capillary. The relation between Q_2 and the differential pressure is given by the Hagen-Poiseuille equation:

$$Q_2 = \frac{\pi \bullet \Delta p \bullet d^4}{128 \bullet \eta \bullet l} \qquad \text{Equation III-16}$$

where, Δp = differential pressure, d = inside diameter of capillary, η = viscosity of gas flowing through capillary, and l = the length of the capillary. Substituting Equation III-16 for Q_2 into Equation III-10 we find:

$$Dr = 40.74 \frac{(Q_1 + Q_2) \bullet \eta \bullet l}{\Delta p \bullet d^4} \qquad \text{Equation III-17}$$

For the diluter used in the filter evaluation system d = 0.053 cm, and l = 15 cm. The total flow through the diluter, $Q_1 + Q_2$, is 5 Lpm. Predicted values of Dr are shown in Figure III-29 for the Δp = 100 Pa, 200 Pa, 500 Pa, and 2.5 KPa. This range of Δp settings was used during test system component evaluation, filter test procedure development, and filter evaluations.

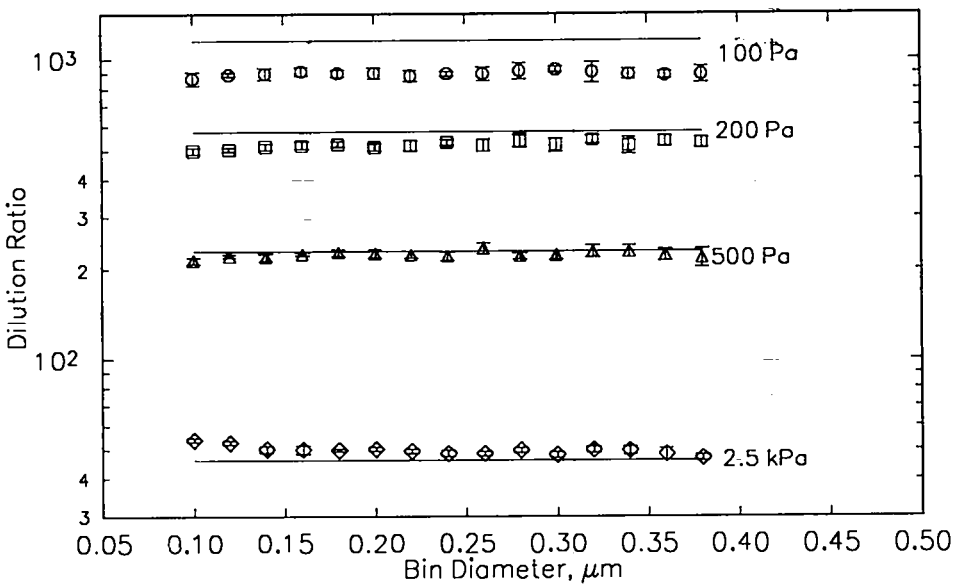

Figure III-29. A plot of predicted values of Dr and values of Dr determined from aerosol measurements made with the LAS-X-M. Parameter is capillary differential pressure.

Measurements of Dr were made over this same range of Δp using the LAS-X-M LAS (see Section III.C.4). Results of these measurements are shown in Figure III-29. These data show measured Dr being largely independent of aerosol size as are the predicted Dr values. The measured Dr values fall below predictions at Δp settings of 100 Pa and 200 Pa by as much as 26%.

Measurements of Dr at 100 Pa and 200 Pa were repeated using the HSLAS (see Section III.C.4). These results are plotted with the LAS measurements in Figure III-30. The HSLAS measurements (solid circles and solid squares) are closer to the predicted values than the LAS-X-M values. An increase in Dr with particle size is observed in the HSLAS data.

Typically penetration measurements were made with the diluter operating at 100 Pa. A pilot study was carried out in which penetration measurements were made with the LAS-X-M. The Dr values measured with the LAS-X-M were used to determine upstream concentration in these pilot study measurements. Penetration values determined using the LAS-X-M measured Dr's would overestimate penetration by as much as 35% relative to penetration values determined using theoretical values of Dr.

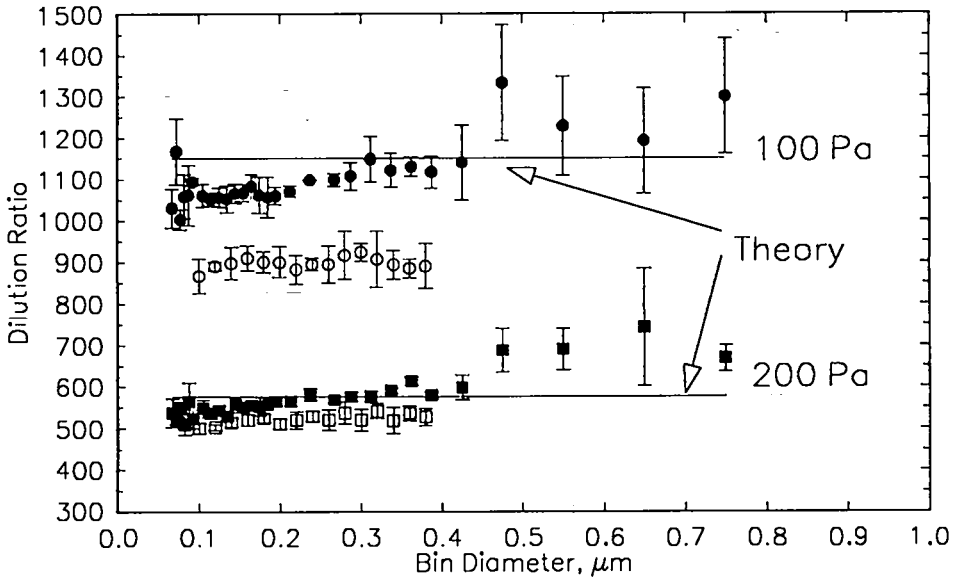

Figure III-30. A plot of predicted values of Dr and values of Dr determined from aerosol measurements made with the HSLAS. Parameter is capillary differential pressure.

Penetration measurements in the formal study were made using the HSLAS. The Dr values determined with the HSLAS were used to determine upstream concentration in these formal study measurements.

III.C.4. Aerosol Size and Concentration Measurements

III.C.4.a. Laser Aerosol Spectrometers: Specifications And Principles of Operation

The laser aerosol spectrometers used in the filter evaluation system are models LAS-X-M and HSLAS made by Particle Measuring Systems, Inc. Boulder, CO. The spectrometers are optical single-particle counters that use a laser as the illumination source. The LAS-X-M is a model LAS-X with the particle size range reduced to 0.09 μm to 0.4 μm diameter for polystyrene latex particles. Particle counts are classified by size into 15 bins and an overcount bin with a built-in multi-channel pulse height analyzer. The HSLAS has a particle size range from 0.065 μm to 1 μm according to the manufacturer's calibration for polystyrene latex particles. The HSLAS classifies particles into 32 size bins. The spectrometers were operated at a sample flow rate of ≈1 cm^3/sec.

A diagram of the scattering chamber for the spectrometers is shown in Figure III-31. Scattering takes place within the laser cavity. Light scattered from a particle traversing the laser beam is collected and focused onto a photodetector. The intensity of the scattered light is an

index of particle size and the number of scattering events is interpreted in terms of particle concentration.

The spectrometers use helium-neon lasers which produce nearly monochromatic light at a wavelength of 0.6328 μm. The laser tube is sealed at one end with a window set at Brewster's angle relative to the axis of the tube. The window allows light polarized parallel to the incident plane to be transmitted with minimal loss. Operation of the laser requires the establishment of a standing wave in the optical cavity (Kl70). The intensity of light incident on a particle at a point in this standing wave is described by the superposition of two plane wave fronts traveling in opposite directions (Pi79 and So84). Light intensity incident on a particle traversing the center of the laser beam perpendicular to the beam axis follows a radial Gaussian distribution (Kn79). The mean incident intensity on the particle depends on the location of the particle path relative to the nodes and anti-nodes of the standing wave.

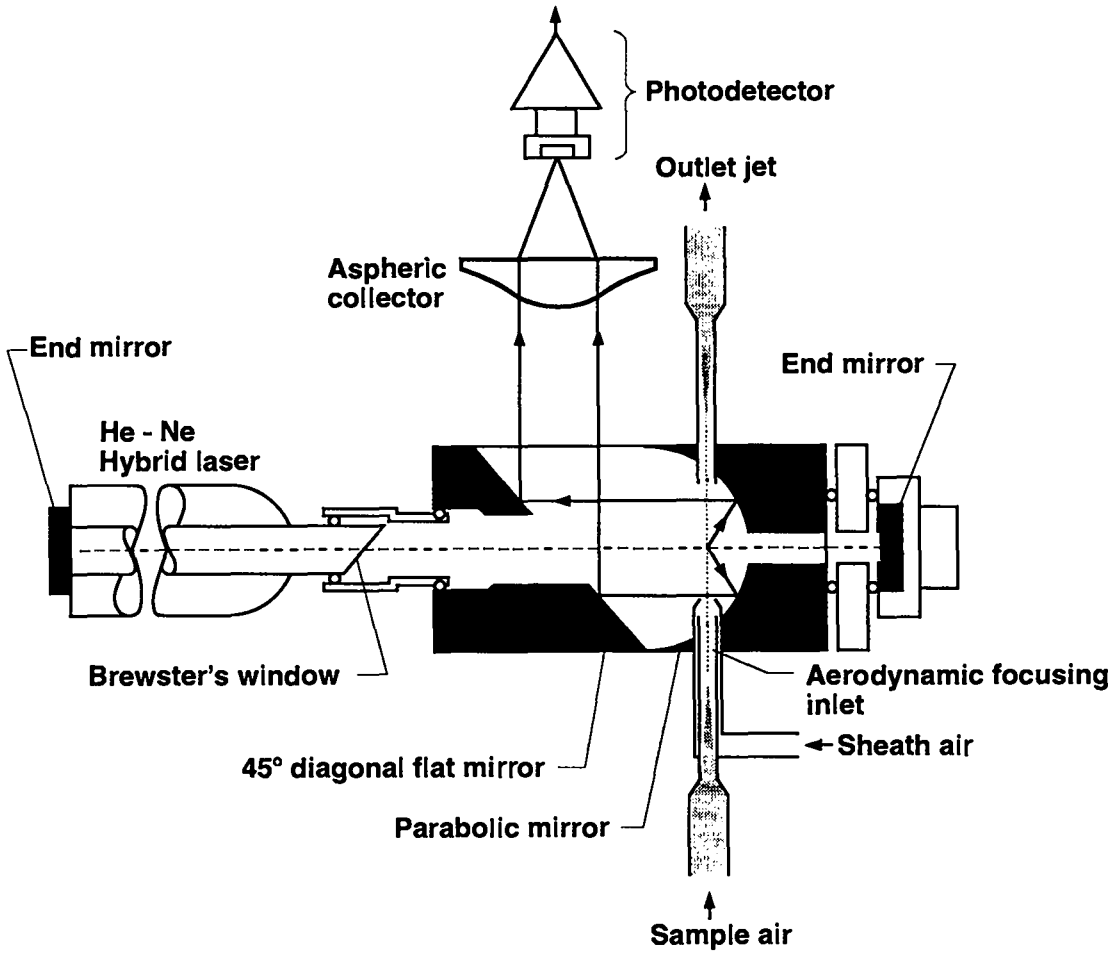

Figure III-31. A diagram of the scattering chamber for the laser aerosol spectrometers.

The point at which the particle stream intersects the laser beam is at the focal point of the parabolic mirror. At this point, according to the manufacturer, the LAS-X-M laser beam is ≈600 μm in diameter and the HSLAS beam is ≈1000 μm in diameter. The width of the sample stream at this point is reported to be ≈200 μm (PMSLASX, PMSHSLAS).

Light scattered by aerosol particles from the laser beam is collected with the parabolic mirror. The mirror collects light over angles in the scattering plane from ≈35° to ≈120° and over azimuthal angles of 2π radians. The collected light is focused on a photodectector.

III.C.4.b. Aerosol Sizing

Scattered light intensity is related to particle size according to Mie theory. Soderholm and Salzman (So84) used Mie theory to describe the dependence of scattered light intensity on particle diameter, particle refractive index and location of the particle path relative to the nodes of the laser beam standing wave for the LAS-X. They suggested that the best approximation of the mean scattered light intensity from an individual particle might come from averaging the Mie theory predictions over all possible particle trajectories relative to the nodes/antinodes of the standing wave.

Liu and Szymanski (Li86) found good agreement between calculations using the Soderholm-Salzman method and spectrometer response to monodisperse aerosols of known size and refractive index. Measurements on a LAS-X model with a lower particle size limit of 0.12

μm diameter showed a lower response value for DEHP aerosols than indicated by the manufacturer's calibration with polystyrene particles. Scripsick and Soderholm (Sc87a) reported similar results for DEHP aerosols using a 0.09 μm LAS-X. These results showed the underestimation of DEHP particle size increased as particle size decreased. A <10% difference was observed in the particle diameter range from ≈0.15 μm to ≈0.4 μm. At a particle diameter of 0.12 μm the underestimation was ≈20%.

In this study the sizing accuracy of the HSLAS was evaluated using monodisperse DEHP aerosols produced by a model 3071 electrostatic classifier (EC). A diagram of the experimental apparatus is shown in Figure III-32. The classifier was adjusted to give a particle count peak at the edges and center of individual bins of the spectrometer. Aerosol size was determined from the classifier voltage settings using:

$$d_p = \frac{3.86 \bullet 10^{-6} \bullet C_c \bullet V}{\eta \bullet Q_s} \qquad \text{Equation III-18}$$

where d_p is particle diameter in μm, C_c = Cunningham slip factor, V is electric potential in volts, η is viscosity of air in poise, and Q_s is the sheath volume flow rate in Lpm. This equation is an implicit function in d_p,

because C_c depends on d_p. A computer program was written to solve for d_p. A listing of the program is found in Appendix A.

The effects of temperature, T, and barometric pressure, P_{bar}, were taken into account in these calculations. Values of λ used to calculate C_c were adjusted for T and P_{bar} according to this equation:

$$\lambda = \frac{R_g \bullet T}{\sqrt{2} \bullet \pi \bullet Av \bullet P_{bar} \bullet d_m^2} \qquad \text{Equation III-19}$$

where, R_g is the ideal gas constant, Av is Avogadro's number, and d_m is the effective molecular diameter for air.

Values of η were adjusted for temperature using a linear fit to cited values of η over the temperature range from 0°C to 40°C. A plot of the cited values and the fit is shown in Figure III-33. The EC measurements were made over a temperature range from 19°C to 29°C.

Results of the EC measurements are plotted in Figure III-34. The measurements show an upward shift in the particle size associated with the spectrometer bins relative to the PSL calibration. Liu and Szymanski (Li86) found a shift in the same direction when comparing LAS-X response for DEHP aerosols and PSL aerosols.

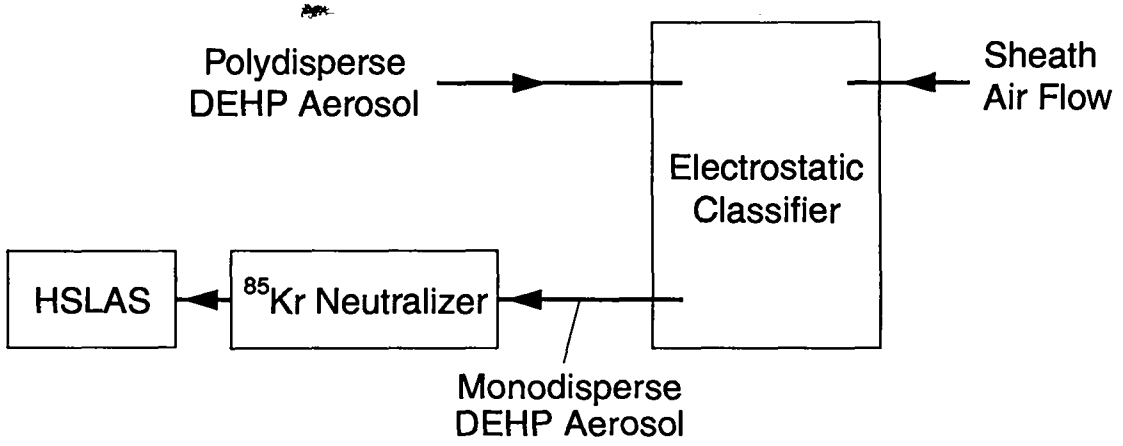

Figure III-32. A schematic of the experimental apparatus used to determine aerosol size of HSLAS bin centers and edges.

Estimates of particle diameter for the HSLAS bin centers are listed in Table III-V. For DEHP, these diameter estimates range from 0.0916 μm for bin 1 to 0.707 μm for bin 28. The fractional difference between PSL diameters and DEHP diameters ranged from just over 0.07 to just under 0.36. The highest fractional differences occurred at both ends of the particle diameter range. The DEHP diameter estimates were used in this study. Measurements made with the HSLAS were limited to this range of particle diameters.

Table III-V

Aerosol Size Calibration of HSLAS

Bin	Particle Diameter - μm PSL	DEHP	Fractional Difference
1	0.0675	0.0916	0.357
2	0.0725	0.0938	0.294
3	0.0775	0.0988	0.275
4	0.0825	0.103	0.248
5	0.0875	0.109	0.246
6	0.0925	0.113	0.222
7	0.0975	0.119	0.221
8	0.105	0.125	0.190
9	0.115	0.137	0.191
10	0.125	0.148	0.184
11	0.135	0.16	0.185
12	0.145	0.173	0.193
13	0.155	0.184	0.187
14	0.165	0.196	0.188
15	0.175	0.205	0.171
16	0.185	0.218	0.178
17	0.195	0.228	0.169
18	0.2125	0.25	0.176
19	0.2375	0.276	0.162
20	0.2625	0.299	0.139
21	0.2875	0.322	0.12
22	0.3125	0.345	0.104
23	0.3375	0.376	0.114
24	0.3625	0.395	0.09
25	0.3875	0.415	0.071
26	0.425	0.461	0.085
27	0.475	0.603	0.269
28	0.55	0.707	0.285

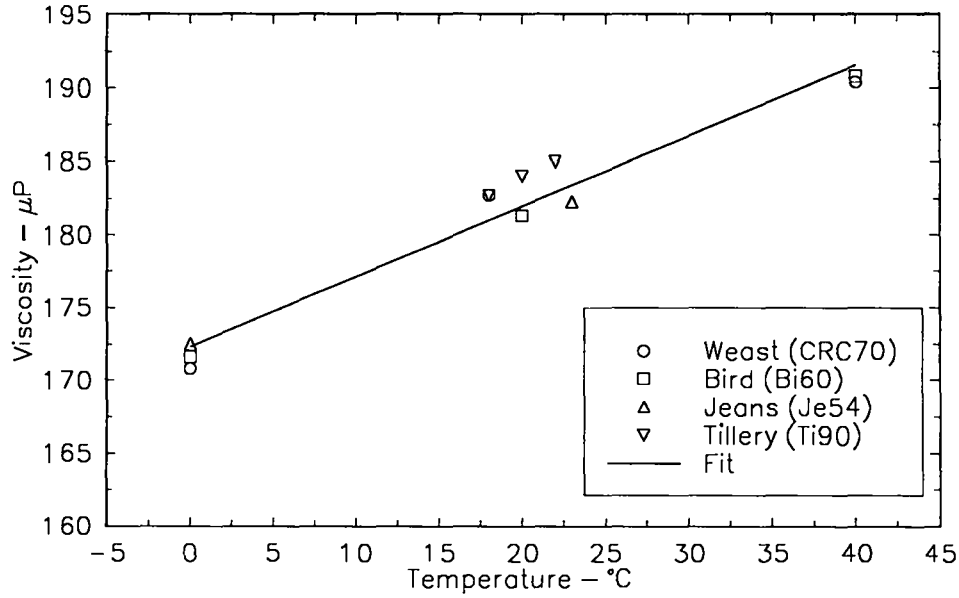

Figure III-33. A plot of air viscosity measurements in the temperature range from 0° C to 40° C and a linear fit of these data.

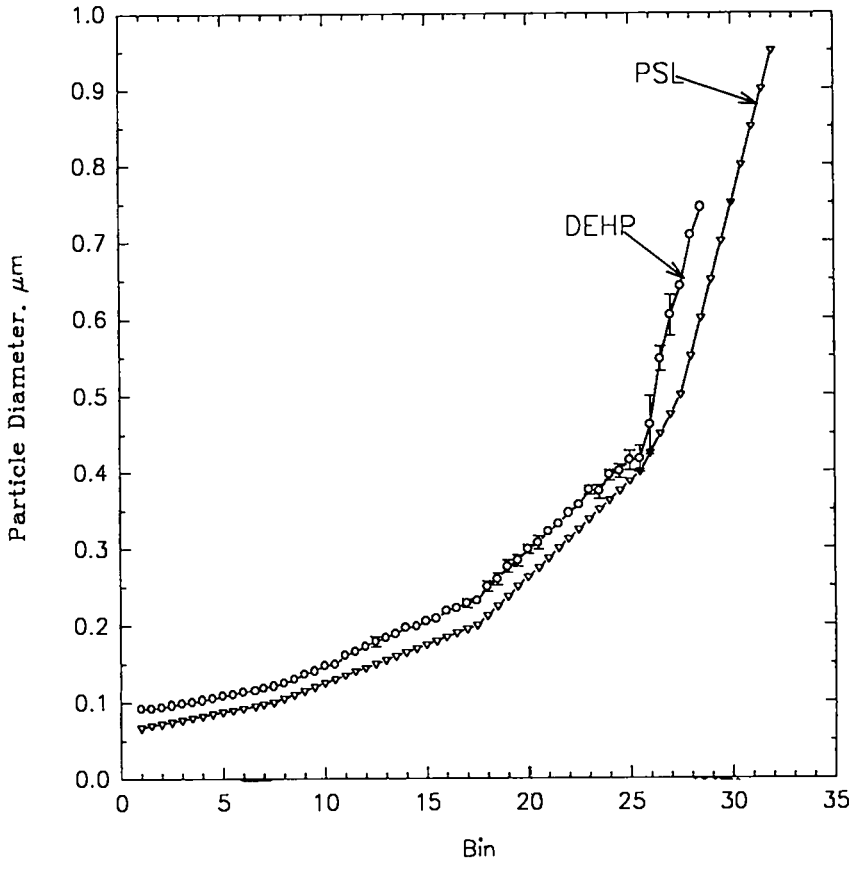

Figure III-34. Particle diameter assignments of HSLAS bins for PSL and DEHP particles. The PSL values come from the manufacturer. DEHP values come from EC measurements at bin centers and edges.

III.C.4.c. Aerosol Concentration Measurement

For optical single-particle counters the accuracy of aerosol concentration measurements depends on instrument counting efficiency.

Efficiencies below 100% result from particle losses which include aerodynamic losses between the point of sampling and the point of detection and coincidence losses that occur when more than one particle occupies the sensitive volume (v_s). Efficiencies greater than 100% result from background counts due to electrical noise.

Aerodynamic losses are a strong function of particle size. Dominant mechanisms for these losses are sedimentation and inertial deposition (We86). Consequently these losses increase with increasing particle size.

A number of investigators have evaluated these losses in the 0.12 μm version of the LAS-X (Hi84, Hi86, Ge86, Li86, and We86). Data of Hinds and Kraske (Hi84, Hi86) show a decrease in counting efficiency with particle diameter above 2 μm. No aerodynamic loss data has been reported for the 0.09 μm version of the LAS-X-M or the HSLAS. Sample inlets for these LAS's are similar to that of the 0.12 μm LAS-X.

The concentration measurements made in this study are referenced to a challenge concentration measurement at the same particle size. The counting efficiency related solely to aerodynamic losses should be the same for the measurement and its reference. Consequently, the ratio of these measurements is independent of the aerodynamic loss counting efficiency.

Liu and Szymanski (Li86) have describe particle losses observed at particle sizes approaching the lower size limit of detection for the 0.12 μm LAS-X. They state that the counting efficiency at the limit of detection is zero. Gebhart and Roth report a significant particle loss at 0.167 μm diameter for the 0.12 μm LAS-X. Liu and Szymanski indicate these small particle losses are related to instrument design and alignment of optics. As with the aerodynamic losses, the relative concentration measurements made in this study should be independent of these losses.

Coincidence losses are solely related to the true sample concentration, C_S, and v_S. Counting efficiency for coincidence loss is given by Hinds (Hi82) as:

$$N_c = \exp-(C_s \bullet v_s)N_C = e^{-Cs\ vs} \qquad \text{Equation III-20}$$

For the LAS's used in this study the v_S is defined by the intersection of the particle stream with the laser beam. Using the manufacturer's specifications and approximating the shape of intersection as that of a right-circular cylinder, the values of v_S are calculated to be $\approx 1.88 \times 10^{-5}$ cm^3 for the LAS-X-M and $\approx 3.14 \times 10^{-5}$ cm^3 for the HSLAS. Using Equation III-20 and $C_S = 3 \times 10^3$ particles/cm^3 gives calcuated values of N_C for the LAS-X-M of ≈95% and for the HSLAS of ≈91%. Scripsick (Sc84,

Sc87) found good agreement between concentration measurements of the 0.09 μm version of the LAS-X and a condensation nucleus counter (model 3030, TSI Inc., Minneapolis, MN) for concentrations up to 5000 particles/cm^3. No studies on the coincidence counting efficiency of the HSLAS have been reported in the literature.

Background counts are prevalent at the smallest sizes detected by the instrument where pulse-height discrimator levels are closest to the electrical noise band. Voltage excursions can result in false small diameter particle counts by the pulse height analyzer. Specifications for the spectrometers call for these counts to be limited to 12 counts per hr integrated over all bins. Laboratory background measurements verified operation within these specifications for both spectrometer units.

The impact of background counts is most apparent at low aerosol concentrations and long count times. An example HSLAS background count is shown in Figure III-35. This count was taken with the filter evaluation system operating normally except for the aerosol generator being off. The count was taken for 15 hr. The integrated count rate was 12 counts/hr. Count rate was observed to decrease with increasing bin number. The maximum number of counts observed in the 15 hr period was 37 in bin 2. Bin counts dropped to 0 at bin 10 with one count being observed in bin 16.

Low aerosol concentrations requiring long count times are usually encountered downstream of test filters operating at <20 % of design flow rate. An example of a low concentration sample is shown in Figure III-35. This sample was collected over a 6.5 hr period with the evaluation system operating normally, the generator on, and the test filter operating at 10% of the design flow rate. Count rates up to bin 10 matched the background count rates. At bins above bin 10 the count rates were greater than the background counts. Counts in these bins are assumed to be associated with particles that penetrated the test filter.

III.C.5. Measurement of Differential Pressure

The difference in static pressure between across a filter provides the force that moves air through the filter. The magnitude of the pressure difference determines the rate of air flow through the filter and through any leaks in the filter. Measurements of pressure differential are made across test filters as part of the filter evaluations performed in this study. Static pressure taps are located in the center of flow stream immediately upstream and downstream of the filter. The taps are connected to a manifold of differential pressure instruments. The primary measurement

instrument is a micromanometer (model M-1430, Dwyer Instruments Inc., Michigan City, IN 46360) . An inclined gage (model 100.5, Dwyer Instruments Inc.) and differential pressure gages (model 2004, 0-4" of H_2O; model 2001, 0-1" of H_2O, and model 2301, -0.5-0-+0.5" of H_2O Dwyer Instruments Inc.) are used to check the micromanometer readings and to monitor differential pressure during tests. These instruments were read to the nearest half scale division.

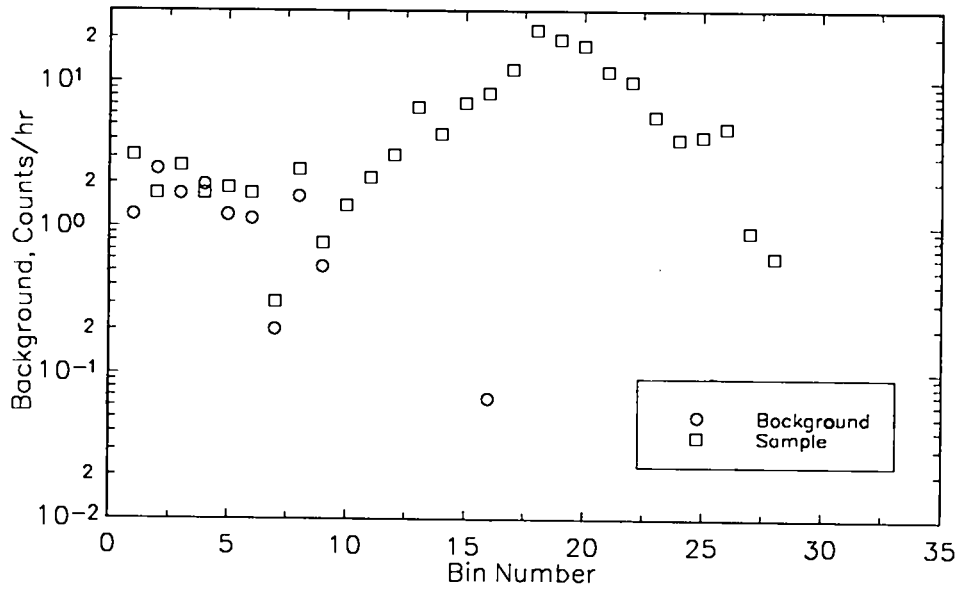

Figure III-35. Particle count data from background and test filter measurements. Test filter particle counts exceed background counts for bins above bin 10.

The micromanometer uses an electrical conductivity level indicator. The manometer fluid is water with a sodium fluoroscein dye (CAS#518-47-8). A fixed electrode is submerged in the manometer fluid. The other electrode is a needle probe attached to a micrometer movement. An electrical circuit is completed when the probe contacts the manometer fluid. A bridge circuit with a microammeter is used to detect electrical current flow. The probe is lowered towards the manometer fluid until a deflection of the ammeter needle is observed. Fluid level relative to a zero differential pressure level is read from the micrometer. Differential pressure is equal to twice the measured fluid level in units of mm of H_2O.

The micromanometer is attached to a heavy steel base that is leveled to maintain vertical alignment of the manometer. The micromanometer measures differential pressures in increments of approximately 10 dyn/cm^2 (approximately 0.005 " H_2O) from approximately 10 dyn/cm^2 to approximately 5000 dyn/cm^2. Micromanometer measurements are compared with those of the other differential pressure instruments in Figure III-36. These measurements rarely differ by more than 20 dyn/cm^2. The spread of x-axis values at discreet y-axis values at the lowest differential pressures is at least partially related to reading the y-axis values from at scale and the x-axis values from a vernier. Linear regression correlation coefficients (r^2) for

these data are all greater than 0.99. Constants for linear fit models range from just over -13 dyn/cm^2 to approximately -2.6 dyn/cm^2. Coefficients for the fit ranged between 0.995 and 1.04.

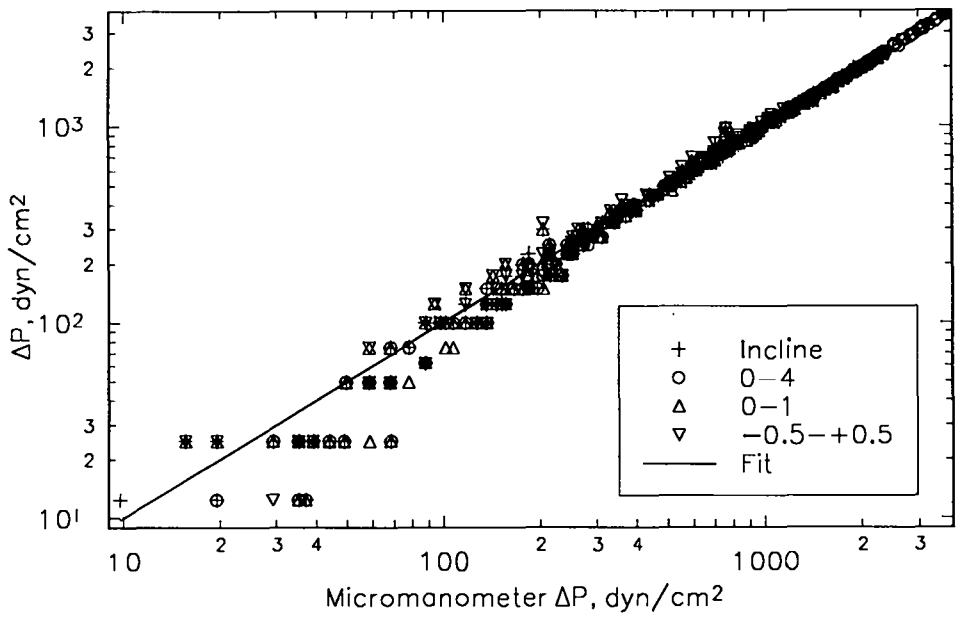

Figure III-36. Comparison of differential pressure measurements by various instruments with measurements of a micromanometer.

III.C.6. Flow Rate Measurements

Test filter flow rate was measured using a laminar flow element (LFE) system (model LFS-2, Meriam Instrument, Cleveland, OH). The

LFE system consists of a set of laminar flow elements and a differential pressure measurement device. Laminar flow elements are devices constructed such that volume flow rate through the device is directly proportional to the differential pressure across the device. The element has a core made of a sheet of corrugated metal wound around a central wire. The core is sealed into a length of tubing. Static pressure taps are located in the tubing at the entrance and exit of the core. The taps are connected to the pneumatic side of a pressure transducer. The electrical output of the transducer is input to an analog to digital converter and a microprocessor. The microprocessor uses this input, constants from flow element calibration, and data from a temperature sensor to compute volume flow rate. Input from the temperature sensor is used to compensate for temperature effects on viscosity.

Each LFE spans a decade in flow rate. The LFE set consists of six elements capable of measuring volume flow rates from 7.08×10^{-4} Lpm (2.5×10^{-5} CFM) to 708 Lpm (25 CFM). Each element is calibrated by the manufacturer using procedures and standards traceable to the National Institute of Standards and Technology (NIST). The manufacturer certifies an accuracy for the LFS-2 better than ± 1.0 % of the indicated flow rate.

Measurements of frame leak flow rate, sample flow rate and LAS flow rate were made with an electronic bubble flow meter (BFM, model D-

800275, Gilian Instrument Corp., West Caldwell, NJ 07006). The BFM measures the travel time of bubble film as it sweeps out a known volume in flow cell. Infrared photodetectors are used to determine the travel time of the film as it traverses a length of the cell. A microprocessor computes volume flow rate from the measured time and the volume associated with the flow cell length. A digital readout presents the flow rate in units of cm^3/min or Lpm depending on the flow cell size.

The BFM uses three sizes of flow cells to measure flow rates from approximately 2 cm^3/min to over 20 Lpm. Each cell is calibrated by the manufacturer in accordance with procedures and standards traceable to NIST. The manufacturer certifies an accuracy of $\pm$ 0.5%.

Measurements of frame leak flow rates below approximately 2 cm^3/min were made with the LFE system. A comparison of LFE and BFM measurements is shown in Figure III-37. On average, the LFE measurements underestimate the BFM measurements by 7% of the BFM measurements. The reason for this underestimation is not understood. A possible factor in the measurement difference is the error in BFM measurements associated with of the volume occupied by water vapor introduced in the flow as it passes through the BFM.

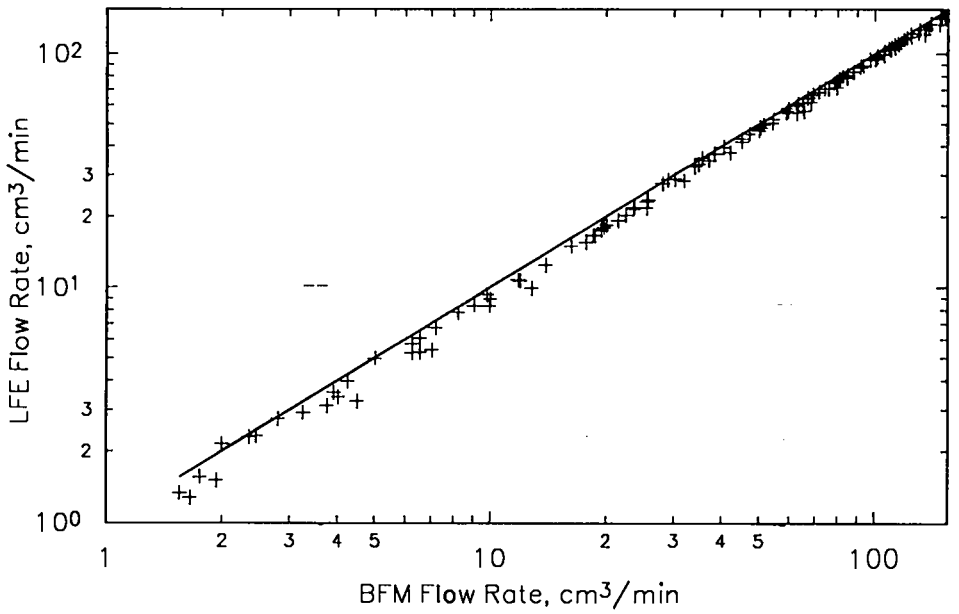

Figure III-37. A comparison of flow rate measurements of the LFE and the BFM.

III.C.7. Nominal Conditions of Measurements

Experimental measurements were made in the Occupational Health Laboratory (OHL) of Los Alamos National Laboratory at Los Alamos, New Mexico. Air for the experimental test system was drawn from within OHL. Air temperature within OHL is thermostatically controlled. The building ventilation system has no provisions for controlling moisture content of building air.

Temperature of test system air flow was monitored just upstream of the LFE system (see Figure III-2). Nominal air flow temperature was 20°C with a range from ≈18°C to ≈25°C. OHL is at an altitude above sea level of 2250 m (Bo90). Mean barometric pressure at OHL is 585 mm Hg (Bo90). Standard conditions for this study were 20°C and 585 mm Hg.

Seasonal variations in relative humidity are observed within OHL. Typically relative humidity varies from ≈10% in the winter to ≈50% in the summer. Excursions in relative humidity up to 70% occur in association with summer precipitation events. The lowest measured relative humidity during the experimental phase of the study was 10%. Relative humidity within OHL as low as 4% is expected during the coldest periods of outdoor temperature based on outdoor dew point and outdoor to indoor temperature differential.

III.D. Filter Unit Evaluation Protocol

Filter unit evaluations were divided into two phases, a pilot study phase and a formal study phase. The pilot study was used to determine ranges of measured parameters and finalize development of measurement

techniques, of test system configuration, and of evaluation protocol. The resulting filter unit evaluation regimen was employed in the formal study.

III.D.1. Pilot Study

Five filter units from a single manufacturer were evaluated in the pilot study. Typically, measurements of penetration, differential pressure, and flow rate were made with the filter frame unsealed and sealed. Normally, measurements were at 1%, 2%, 5%, 10%, 20%, 50%, and 100% of filter unit design flow rate (see Section III.B.2.). Table III-VI gives the evaluation schedule for each filter unit.

Table III-VI

Pilot Study Evaluation Schedule

Filter Unit ID	Frame Unsealed	Frame Sealed
5-2C		X
7-2C	X	X
2-2C	X	
4-2C	X	X
8-2C	X	X

Measurements of penetration, differential pressure, and flow rate were made with the test system shown in Figure III-2. Penetration was determined from aerosol concentration measurements made upstream and downstream of test filter units. Upstream and downstream aerosol samples were collected at a flow rate of 5 Lpm. Upstream samples were diluted using the aerosol diluter described in Section III.C.3. Aerosol concentration in upstream and downstream samples was measured with a the LAS-X-M (see Section III.C.4). Penetration values for each spectrometer bin were calculated using the following equation:

$$P = (N_d/t_d)/((N_u/t_u)\ Dr) \qquad \text{Equation III-2}$$

where, P = filter unit penetration, N_d = downstream particle count, t_d = duration of downstream count, N_u = upstream particle count, t_u = duration of upstream count, and Dr = dilution ratio. In the pilot study typically, six replicates of penetration determinations were. Differential pressure and filter unit flow rate measurements were made using the techniques described in Sections III.C.5 and III.C.6.

Measurements on whole filter units represented integrated performance of all the filter components. These whole filter tests indicate

performance of the filter units expected when installed in an air cleaning system.

The mounting of filter units for whole filter tests is illustrated in Figure III-38a. Filters units were placed on a back-plate with the downstream gasket contacting a polished metal area in the center of the plate. In the pilot study a solid back-plate was used. In the formal study a slotted back-plate such as illustrated in Figure III-38a was used to allow challenge aerosol to pass by the filter frame. A compression plate held in place by four threaded metal rods was placed over the upstream face of the filter unit. The upstream gasket contacted a polished metal area on the downstream side of the compression plate. The compression plate was carefully moved to press against the upstream gasket using four nuts on the threaded rods. The nuts were tightened until a 50% compression of the gaskets was achieved (ASME89a).

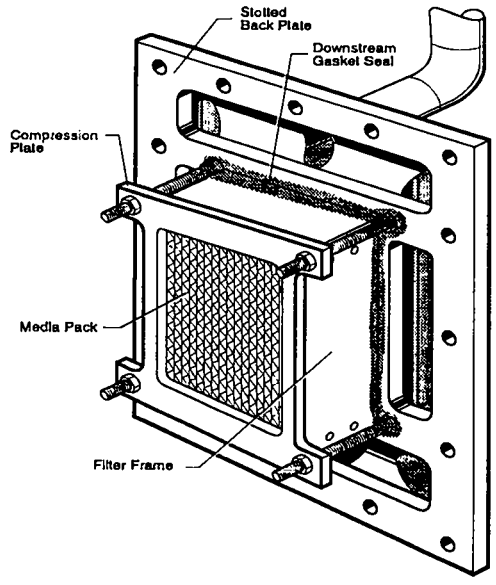

(a)

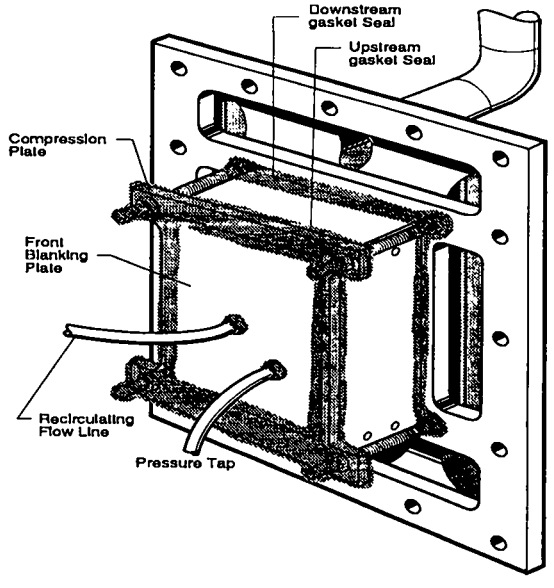

(b)

Figure III-38. Test configurations used for (a) whole filter tests, (b) frame tests,

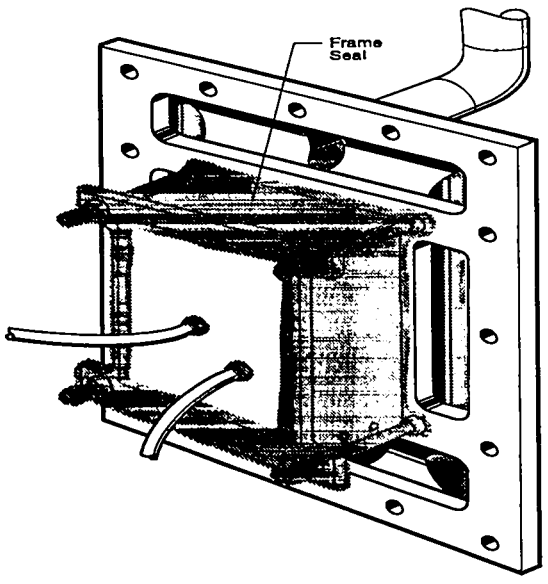

(c)

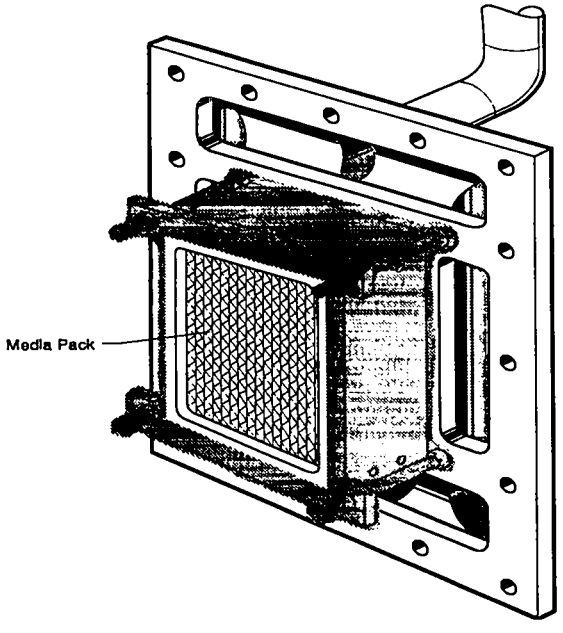

(d)

Figure III-38 (cont.). (c) sealed frame tests, and (d) media pack test.

Gasket leakage is considered to be a result of installation not filter unit performance. To eliminate effects of gasket leakage the unsealed frame measurements were made with the downstream gaskets sealed with a sealant. The seal extended from the wood frame just upstream the wood/gasket joint to the surface of the back-plate (see Figure III-39b). A wax and a variety of silicone rubber products were tested as sealant. The sealant ultimately selected was 3145 RTV (Dow Corning Corporation, Midland, MI 48640).

Measurement of filter unit performance with sealed frames serves to isolate performance of the media pack and the sealant joint from that of the whole filter unit (see Figure III-1). The contrast between the sealed frame or media pack measurements and the unsealed frame or whole filter measurements on the same filter unit partitions performance between filter unit components.

Sealed frame measurements were made with the upstream gasket sealed to the compression plate, the downstream gasket sealed to the back-plate, and a sealant applied to the flat surfaces of the frame (see Figure III-38d). In the pilot study, the flat surfaces of the frame were sealed with either wax or a silicone rubber sealant. The 3145 RTV sealant was used in the formal study.

The following procedure was used to assure sealing of the frame. Blanking plates were sealed to both sides of a compression plate (See Figure III-40). Sealing of these blanking plates was assured with pressure decay tests. The back blanking plate was removed and the front blanking plate/compression plate assembly was mounted on the upstream filter face and the gaskets were compressed as described above. The compressed upstream gasket was sealed to the compression plate with the silicon rubber sealant. A negative pressure was then pulled on the downstream side of the filter unit/blanking plate assembly with a valve/vacuum system operating under critical flow conditions. The negative pressure was monitored as the frame was sealed. As the pressure approached -15" of H_2O relative to ambient, the valve was closed and pressure decay was used to assess the frame seal. Sealing continued until pressure decay from -15" of H_2O to -14.5" of H_2O took more than ten minutes. Once the frame seal was assured the front blanking plate was removed and the sealed-frame filter performance measurements were made.

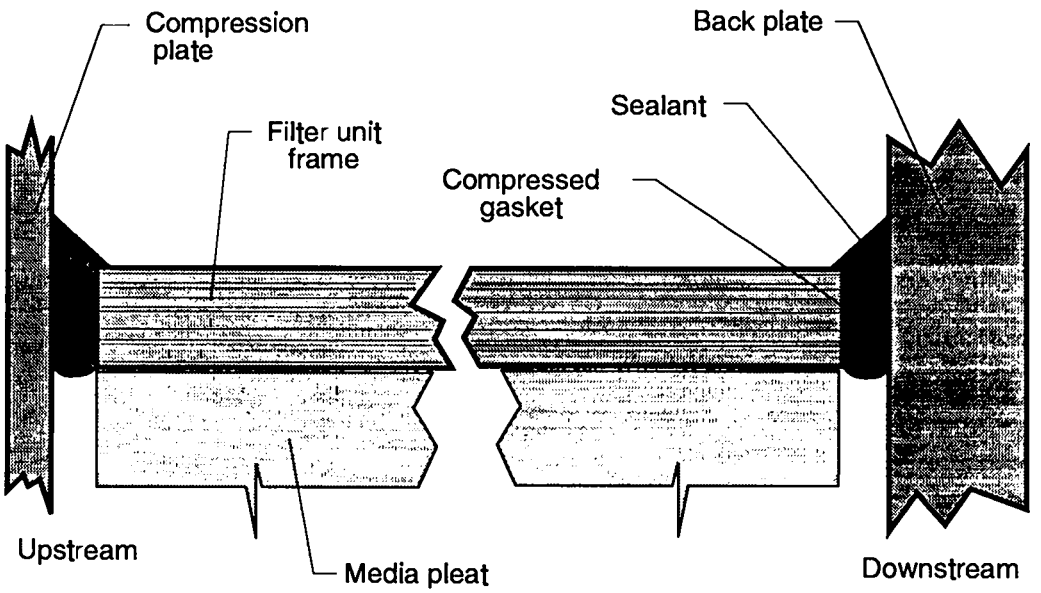

Figure III-39. Detail of upstream and downstream gasket seals.

III.D.2. Frame Leak Evaluation Technique

Frame leakage can only be assessed indirectly from the unsealed and sealed frame evaluations. Penetration in unsealed units that was not accounted for in measurements on the units after frame sealing was attributed to frame leakage. To supplement the filter unit evaluation, methods to directly assess frame leak penetration and frame leak flow rate were developed.

Frame leak evaluations were made on filter units with the upstream filter face blanked-off and the upstream and downstream gaskets sealed.

This test configuration is illustrated in Figure III-38b. The configuration permitted isolation of frame leakage by blocking all other potential flow paths. To blank-off the upstream filter face the front blanking plate was sealed to the compression plate. This seal was assured using the compression plate sandwich technique described above and illustrated in Figure III-40. Sealing of the gaskets was accomplished through compression and use of the silicone rubber sealant (see Figure III-39).

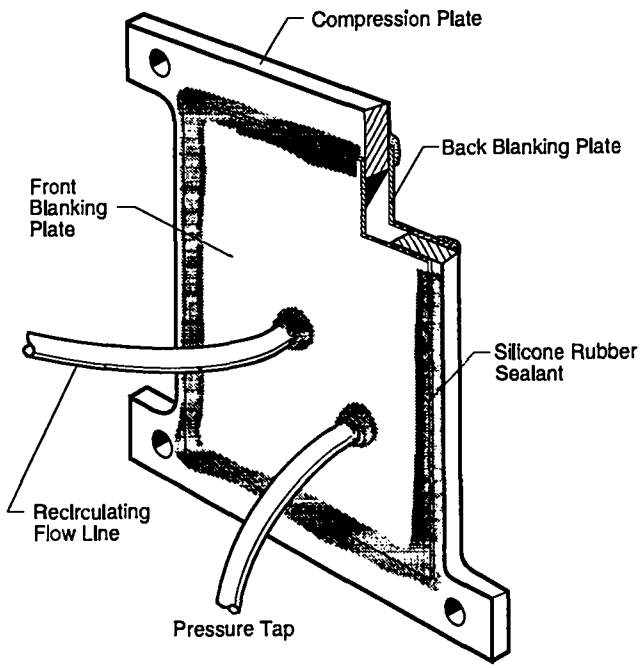

Figure III-40. Cut-away drawing of compression plate sandwich used to assure seal of the front blanking plate to the compression plate.

Frame leak penetration measurements were made using the test system illustrated in Figure III-41. The filter unit was challenged and upstream samples were collected in the same manner as described for the unsealed frame and sealed frame measurements.

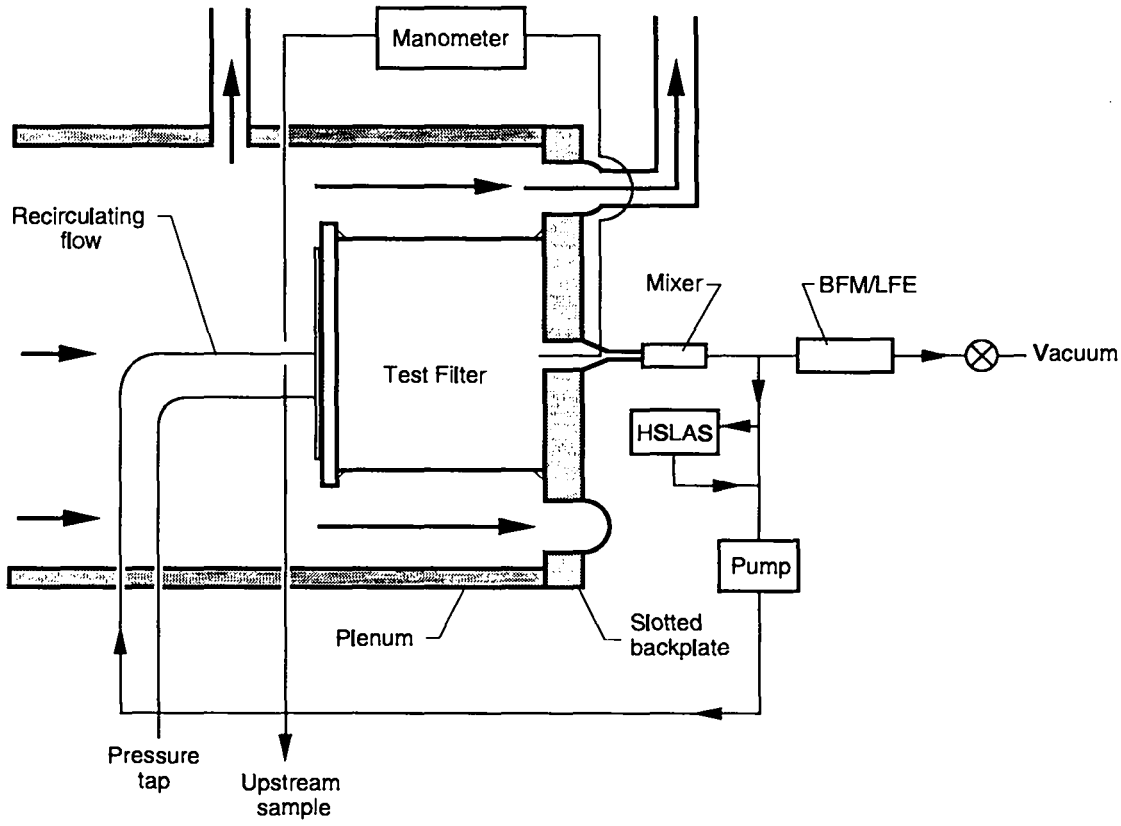

Figure III-41. Frame leak measurement system showing recirculating flow line.

Downstream samples were collected from a recirculating flow. This flow was returned through a high efficiency filter to the center of the front

blanking plate. At this point the flow served as a carrier for aerosol penetrating the filter frame. Laser spectrometer measurements of the downstream aerosol without the recirculating flow indicated the aerosol was possibly being affected by evaporation during its transit to the sample point. Estimates of the aerosol residence time without recirculating flow were found to be of the same magnitude or greater than particle life-time estimates based on evaporation. The downstream recirculating flow rate was adjusted to lower residence times to less than 10% of the estimated particle life-time and effects attributed to evaporation subsided.

Frame leak flow is pulled with a vacuum system connected to the recirculating flow loop downstream of the mixer (see Figure III-41). Flow rate is controlled with a valve that is operated at critical flow conditions.

Tests performed with this system and filter unit configuration are sensitive to frame leaks that exit inside the filter unit upstream as well as downstream of the media (see Figure III-42). Frame leak flow rate can be expressed as:

$$Q_{fr} = Q_u + Q_d, \qquad \text{Equation III-22}$$

where, Q_{fr} = total frame leak flow rate, Q_u = frame leak flow rate from leak paths exiting upstream of media, and Q_d = frame leak flow rate from leak

paths exiting downstream of media. In the field filter units are operated without blanking plates. Under this condition $Q_u = 0$ because almost no pressure difference exists between upstream of the filter unit and inside the filter unit upstream of the media. With the blanking plate on, Q_u can be reduced to zero by adjusting the recirculating flow rate until the differential pressure across the media equals the differential pressure across the frame.

Aerosol penetration through filter unit frames can be written as:

$$P_{fr} = P_u \bullet \frac{Q_u}{Q_{fr}} + P_d \bullet \frac{Q_d}{Q_{fr}} \qquad \text{Equation III-23}$$

where, P_{fr} = frame leak penetration, P_u = frame leak penetration associated with leak paths that exit inside the filter unit upstream of the filter media, P_d = frame leak penetration associated with leak paths that exit inside the filter unit downstream of the filter media. In the field, leak paths exiting upstream of the media do not contribute to frame penetration because $Q_u = 0$. In this situation, $P_{fr} = P_d$. With the blanking plate on, these paths would not contribute particles to frame penetration because particles exiting upstream of the media would be collected very efficiently

as they traverse the media on their way to the downstream side of the filter unit. In this situation,

$$P_{fr} = P_d \bullet \frac{Q_d}{Q_{fr}}, \qquad \text{Equation III-24.}$$

Consequently, frame penetration measured in this configuration would underestimate P_d by the ratio of Q_{fr}/Q_d.

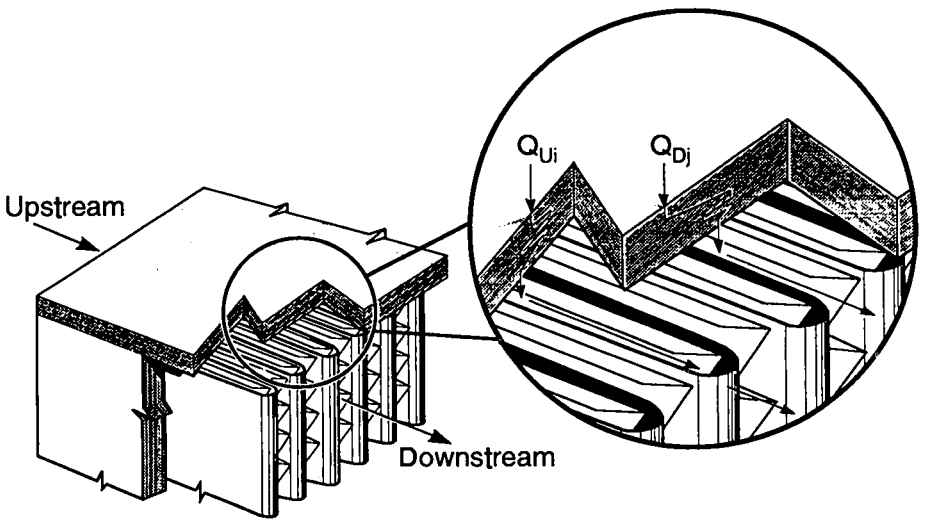

Figure III-42. Drawing illustrating frame leak flow paths that exit inside the filter unit upstream (Q_{Ui}) and downstream (Q_{Di}) of the folded media sheet.

Estimates of frame leak penetration were determined from LAS measurements using the following equation:

$$P_{fr} = \frac{\frac{N_d}{t_d} \bullet DDr}{\frac{N_d}{t_d} \bullet Dr}$$ Equation III-25

where, N_d = downstream particle count, t_d = duration of downstream count, DDr = downstream dilution ratio = $(Q_r + Q_{fr})/Q_{fr}$, Q_r = recirculating flow rate, N_u = upstream particle count, t_u = duration of upstream count, and Dr = upstream dilution ratio. These calculated values of P_{fr} underestimate Pd by a factor of 2 - Q_r/Q_f, where Q_f = the whole filter unit flow rate . This factor assumes that the effective frame flow resistance is the same for paths exiting upstream and downstream of the media and that $Q_d << Q_f$. Frame penetration measurements were made with Qr ranging from 5 Lpm to 13 Lpm.

Frame leak flow rate measurements were made with the flow measurement devices described in Section III.C.6. The BFM was used for flow rates down to 2 cm^3/min. The LFE system was used at flow rates below 2 cm^3/min. The measurements of Q_{fr} are related to estimates of Q_d according to Equation III-22. The measured Q_{fr} values overestimate Q_d by a factor of 2 - Q_r/Q_f, again assuming the effective frame flow resistance is the same for flow paths exiting upstream and downstream of the media and that $Q_d << Q_f$.

Frame leak flow rate measurements were made over a range of differential pressures that included the range of pressures in which the unsealed frame and sealed frame measurements were made. Frame leak penetration measurements were made at the same differential pressures as were the whole filter tests. The differential pressure measurements were made with the pressure measurement instruments described in Section III.C.5.

III.D.3. Formal Study

Nine filter units were evaluated in the formal study. Filter units were selected randomly from filter shipments from three manufacturers. Three filters were selected from each manufacturer.

Protocol for the evaluations is outlined in Table III-VII. Typically, measurements of penetration, differential pressure, and flow rate were made on 1) the whole filter unit with the frame unsealed, the filter face unblanked, and the downstream gasket sealed, 2) on the filter frame with the face blanked and the upstream and downstream gaskets sealed, and 3) on the media pack with the frame sealed and the face unblanked. Normally, measurements were made at differential pressures

corresponding to 1%, 2%, 5%, 10%, 20%, 50%, and 100% of filter unit design flow rate (see Section III.B.2.). Single penetration measurements were made at each flow rate for all but one of the filter units in the formal study. Penetration determinations on filter unit 9351 were made in triplicate.

Table III-VII

Formal Study Protocol

I. Sealing of Downstream Gasket
II. Whole Filter Unit Tests
A. Whole Filter Flow Rate and Differential Pressure Measurements
B. Whole Filter Penetration Determinations
III. Sealing of Blanking Plate and Upstream Gasket
IV. Frame Tests
A. Frame Leak Flow Rate and Differential Pressure Measurements
B. Frame Leak Penetration Determinations
V. Sealing of Filter Frame
VI. Media Pack Tests
A. Media Pack Flow Rate and Differential Pressure Measurements
B. Media Pack Penetration Determinations

III.D.3.a. Sealing of Downstream Gasket

Filter units were carefully removed from their shipping cartons. Labels on filter frame surfaces that could be readily removed were removed carefully and glued in a laboratory notebook. Labels not easily removed were left on the frame so as to not in any way disturb the frame surface.

Filter units were then centered on the slotted back-plate so that the downstream gasket was flush against the polished metal surface of the back-plate. The compression plate was lowered onto the upstream gasket along four threaded rods. The gaskets were compressed against their respective sealing surfaces by tightening nuts on the threaded rods against the compression plate until a 50% compression of the gaskets was achieved.

After compressing the gaskets, the silicone rubber sealant was used to seal the downstream gasket to the slotted back-plate (see Figure III-39b). Seals extended from the wooden frame just upstream of the downstream gasket to the back-plate. The sealant was applied in multiple coats.

Complete sealing of this gasket is critical to eliminate effects of gasket leaks. Leaks in this gasket could interfere with evaluation of leaks in other filter components. Assurance of downstream gasket sealing comes when the filter frame is sealed. The frame sealing is subsequent to whole filter tests and frame tests. Gasket leaks that could affect the outcome of these tests would not be discovered until after the tests were conducted. Because frame sealing is not reversible, the tests could not be repeated. Discovery of significant gasket leakage during frame sealing requires discarding of data collected to that point. No gasket leaks were found in these studies.

III.D.3.b. Whole Filter Unit Tests

Whole filter tests were performed on filters units with the frame unsealed and the downstream gaskets sealed (see Figure III-38a). The tests consisted of measurement of flow rate and differential pressure and determination of whole filter penetration.

III.D.3.b.i. Whole Filter Flow Rate and Differential Pressure Measurements

After sealing the downstream gasket, initial whole filter flow rate and differential pressure measurements were made. Flow rate measurements were made with the LFE system described in Section III.C.6. Differential pressure measurements were made with instruments described in Section III.C.5. Differential pressure measurements were made at 1%, 2%, 5%, 10%, 20%, 50%, and 100% of the design flow rate. Measurements of flow rate and differential pressure were made prior to whole filter penetration measurements. Flow rate and differential pressure measurements were repeated during and after whole filter penetration determinations to evaluate filter unit loading.

III.D.3.b.ii. Whole Filter Penetration Determinations

Whole filter penetration determinations were made with the test system shown in Figure III-2. Penetration was determined from aerosol concentration measurements made upstream and downstream of test filter units. Upstream and downstream aerosol samples were

collected at a flow rate of 5 Lpm. Upstream samples were diluted using the aerosol diluter described in Section III.C.3. Aerosol concentration in upstream and downstream samples was measured with a HSLAS (see Section III.C.4). Penetration values for each spectrometer bin were calculated using Equation III-21. Typically, penetration measurements were made at 1%, 2%, 5%, 10%, 20%, 50%, and 100% of design flow rate.

III.D.3.c. Sealing of Blanking Plate and Upstream Gasket

After the whole filter tests, the compression plate was replaced with another compression plate. The new compression plate had a blanking plate sealed to its upstream side. This seal was assured using the compression plate sandwich technique described in above (see Figure III-40). The new compression plate assembly was tightened onto the filter unit until 50% compression of the gaskets was reestablished.

Once the compression plate assembly was tightened into place the upstream gasket was sealed with the silicone rubber sealant. Seals extended from the wooden frame just downstream of the upstream gasket to the compression plate (see Figure III-39a). The sealant was applied in multiple coats.

Complete sealing of this gasket is critical to eliminate effects of gasket leaks. Leaks in this gasket could interfere with evaluation of leaks in filter frames. Assurance of upstream gasket sealing comes when the filter frame is sealed. The frame sealing is done after the frame tests. Gasket leaks that could affect the outcome of these tests would not be discovered until after the tests were conducted. Because frame sealing is not reversible the tests could not be repeated. Discovery of significant upstream gasket leakage during frame sealing requires discarding of frame test data. No gasket leaks were found in these studies.

III.D.3.d. Frame Tests

Frame tests were performed on filter units with the frame unsealed, the upstream and downstream gaskets sealed, and the filter face blanked-off (see Figure III-38b). In this configuration measurements of frame leak flow rate, differential pressure were made, and determinations of frame leak penetration were made.

III.D.3.d.i. Frame Leak Flow Rate and Differential Pressure Measurements

Once the gaskets were sealed and the filter face was blanked-off, measurements of frame leak flow rate and differential pressure were made. The test configuration used in these measurements is shown in Figure III-38b.

Frame leak flow is pulled with a vacuum system connected to the recirculating flow loop downstream of the mixer (see Figure III-41). Net flow rate through the frame was controlled with a valve that is operated at critical flow conditions.

Frame leak flow rate measurements were made with the flow measurement devices described in Section III.C.6. The BFM was used for flow rate down to 2 cm^3/min. The LFE system was used at flow rates below 2 cm^3/min.

Frame leak flow rate measurements were made over a range of differential pressures that included the range of pressures in which the whole filter tests were made. The differential pressure measurements were made with the pressure measurement instruments described in Section III.C.5.

III.D.3.d.ii. Frame Leak Penetration Determinations

Frame leak penetration determinations were made using the test system illustrated in Figure III-41. The filter unit was challenged and upstream samples were collected in the same manner as described for the whole filter tests.

Downstream samples were collected from a recirculating flow. This flow was returned through a high efficiency filter to the center of the front blanking plate. At this point the flow served as a carrier for aerosol penetrating the filter frame.

Estimates of frame leak penetration were determined from HSLAS measurements using Equation III-25. These calculated values of P_{fr} underestimate P_d by a factor of $2 - Q_r/Q_f$, where Q_f = the whole filter unit flow rate . This factor assumes that the effective frame flow resistance is the same for paths exiting upstream and downstream of the media and that $Q_d << Q_f$. Frame penetration measurements were made with Qr ranging from 5 Lpm to 13 Lpm.

III.D.3.e. Sealing of Filter Frame

After completing the frame tests the filter unit frame was sealed with the silicone rubber sealant (see Figure III-38c). Initially during the sealing process, a negative pressure is pulled on the filter unit with a valve/vacuum system operated at critical flow conditions (see Figure III-41). Differential pressure across the frame was monitored as the frame was sealed. Increases in differential pressure associated with sealing of a portion of the filter frame were recorded in a laboratory notebook. As the differential pressure approached -15" of H_2O relative to ambient, the valve was closed and pressure decay was used to assess the sealing of the frame. Sealing continued until pressure decay from -15" of H_2O to -14.5" of H_2O took more than ten minutes.

A procedure was used to systematically seal filter frames. First, each of the nails and/or staples used to fasten the frame joints were sealed. Next the seams at each joint were sealed. Then the area between the fasteners and the seams were sealed so that the sealed area extended in approximately 3 cm on either side of each frame corner. Finally, the area between the sealed corners was sealed. Additional sealant coats were applied as required to seal the filter unit.

Leaks remaining after this sealing procedure were attributed to leaks in the front blanking plate, the upstream gasket, and/or the downstream gasket. The magnitude of these leaks was quantified using the pressure decay technique. Attempts were made to locate and seal these leaks prior to going on to the media pack tests.

III.D.3.f. Media Pack Tests

After the frame sealing procedure was completed the front blanking plate was removed. Media pack tests were performed on filters units in this configuration (see Figure III-38d). These tests consisted of measurement of media pack flow rate and differential pressure and determination of media pack penetration.

III.D.3.f.i. Media Pack Flow Rate and Differential Pressure Measurements

Flow rate measurements were made with the LFE system described in Section III.C.6. Differential pressure measurements were made with instruments described in Section III.C.5. Differential pressure

measurements were made 1%, 2%, 5%, 10%, 20%, 50%, and 100% of the design flow rate. Measurements of flow rate and differential pressure were made prior to media pack penetration determinations. Flow rate and differential pressure measurements were repeated during and after the penetration determinations to evaluate the effect of filter unit loading.

III.D.3.f.ii. Media Pack Penetration Determinations

Media pack determinations were made with the test system shown in Figure III-2. Penetration was determined from aerosol concentration measurements made upstream and downstream of test filter units. Upstream and downstream aerosol samples were collected at a flow rate of 5 Lpm. Upstream samples were diluted using the aerosol diluter described in Section III.C.3. Aerosol concentration in upstream and downstream samples was measured with the HSLAS (see Section III.C.4). Penetration values for each spectrometer bin were calculated using Equation III-21. Typically, penetration determinations were made at 1%, 2%, 5%, 10%, 20%, 50%, and 100% of design flow rate.

CHAPTER IV. EXPERIMENTAL RESULTS

In this chapter a summary of the experimental results is presented for the whole filter tests, frame tests, and media pack tests described in Section III.D.3. For each test, flow rate, differential pressure, and penetration results are described. Data plots are used to depict the range of observed values, to illustrate particular features of the results, and to show typical performance. In some cases descriptive statistics are tabulated for each filter unit. A more detailed presentation of test results for each filter unit is given in Appendix B.

IV.A. Whole Filter Unit Tests

Whole filter tests were performed on filters units with the frame unsealed and the downstream gaskets sealed (see Figure III-38a). This installation configuration mimics the typical field installation of the filter units. The tests consisted of measurement of flow rate (Q) and differential pressure (Δp), and determination of whole filter penetration at 28 particle sizes. These results are considered to be representative of filter unit field

performance. Whole filter tests were conducted in both the pilot study and the formal study.

IV.A.1. Whole Filter Flow Rate and Differential Pressure Measurements

After sealing the downstream gasket, initial whole filter flow rate and differential pressure measurements were made. Flow rate measurements were made with the Laminar Flow Element system described in Section III.C.6. Differential pressure measurements were made with instruments described in Section III.C.5. Differential pressure measurements were typically made at 1%, 2%, 5%, 10%, 20%, 50%, and 100% of the design flow rate (Q_{de}). These flow rate and differential pressure measurements were made prior to whole filter penetration determinations. The measurements were repeated during and after the penetration determinations to evaluate effect of filter unit loading on flow rate and differential pressure.

Examples of initial flow rate measurement results from the formal study are plotted against differential pressure in Figure IV-1. In both the

pilot and formal study, the differential pressure required to initially achieve the Q_{de} was below 4000 dyn/cm^2 (<1.61 "H_2O).

Flow rate was observed to increase linearly with differential pressure. The solid lines in Figure IV-1 are linear regression fits to the data. Table IV-I lists linear regression correlation coefficients (r^2) for each filter unit. All values of r^2 were $\geq$0.99.

The plots in Figure IV-1 show data from the highest and lowest resistance filters in the formal study. In both the pilot and formal studies, the initial air flow resistance ranged from 0.083 $\frac{\text{dyn}}{\text{cm}^2}\frac{\text{sec}}{\text{cm}^3}$ to 0.219 $\frac{\text{dyn}}{\text{cm}^2}\frac{\text{sec}}{\text{cm}^3}$ (see Table IV-I). Air flow resistance is the ratio differential pressure to air flow rate.

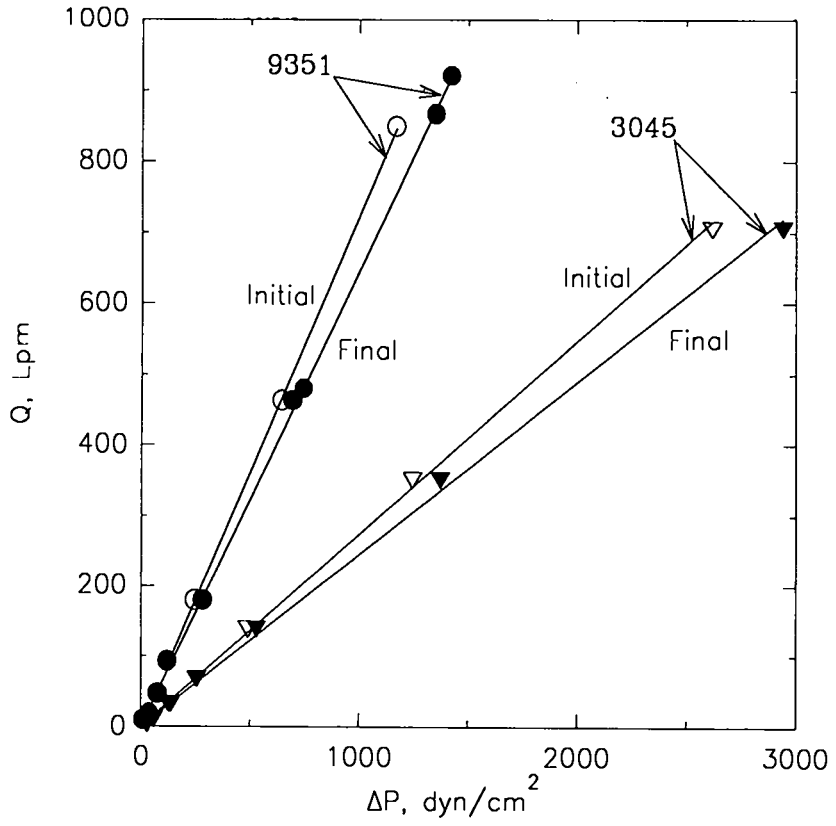

Figure IV-1. Plot of whole filter flow rate versus differential pressure for filter units 9351 and 3045. Initial measurements were made prior to whole filter penetration determinations, final measurements were made after the determinations.

Table IV-I
Correlation Coefficients and Air Flow Resistances from Whole Filter Tests

		INITIAL		FINAL		
STUDY	FILTER ID	r^2	RESISTANCE dyn sec cm^2 cm^3	r^2	RESISTANCE dyn sec cm^2 cm^3	%CHANGE[a]
PILOT	7-2C	1.00	0.165	—	—	—
	2-2C	1.00	0.201	0.99	0.760	278
	4-2C	0.99	0.145	1.00	0.209	44
	8-2C	1.00	0.181	1.00	0.216	16
FORMAL	9351	1.00	0.083	1.00	0.092	12
	9346	1.00	0.101	1.00	0.106	4
	9343	1.00	0.097	1.00	0.107	11
	3037	1.00	0.215	1.00	0.244	13
	3045	1.00	0.219	1.00	0.245	12
	3041	1.00	0.218	1.00	0.232	6.8
	3597	1.00	0.181	1.00	0.182	0.95
	3598	1.00	0.178	1.00	0.184	3.4
	3591	1.00	0.186	1.00	0.193	4.1

[a] $\%\text{change} = \left(\frac{\text{FINAL RESISTANCE} - \text{INITIAL RESISTANCE}}{\text{INITIAL RESISTANCE}} \right) X\ 100$

During testing, aerosol particles collected by test filters would increase filter unit air flow resistance. The increased resistance required subsequent tests to be conducted at differential pressures greater than would be required for unloaded filters. The increased differential pressure potentially affected penetration though filter unit leak flow paths and could confound evaluation of the leak flow performance of the filters. Some filter loading was unavoidable given the nature of penetration tests. Steps were taken to minimize the degree of loading during tests.

The effect of loading was assessed by repeating measurements of flow rate and different pressure during and at the end of whole filter penetration determinations. Examples of the final flow rate measurements are plotted against differential pressure in Figure IV-1.

As with the initial measurements, the final flow rate measurements were observed to increase linearly with differential pressure. Linear fits to these data are shown as solid lines in Figure IV-1. Table IV-I lists r^2 for the final measurements. All values of r^2 were ≥ 0.99.

Table IV-I list the per cent increase in resistance over the course of whole filter penetration tests. The largest increase was over 278%. In the formal study increases ranged from slightly below 1% to 13%.

IV.A.2. Whole Filter Penetration Determinations

Whole filter penetration determinations were made with the test system shown in Figure III-2. Penetration was determined from aerosol concentration measurements made upstream and downstream of test filter units using a laser aerosol spectrometer. In the pilot study, concentration measurements were made with the LAS-X-M laser spectrometer. In the formal study, the measurements were made with the HSLAS spectrometer (see Section III.C.4). Penetration values for each spectrometer bin were calculated using Equation III-21. Typically, penetration determinations were made at 1%, 2%, 5%, 10%, 20%, 50%, and 100% of Q_{de}.

Examples of penetration results from the formal study are plotted against aerosol particle diameter in Figures IV-2 and IV-3. Penetration generally decreased with filter unit flow rate, Q. At the highest values of Q, a peak in the penetration versus particle size plots was observed. In general, the peak penetration value decreased as Q was lowered (See Figure IV-3). The particle diameter at which the penetration maximum occurred increased as Q was lowered. At the lowest values of Q, penetration generally increased with aerosol size. Exceptions to this trend

seen in Figure III-3 are associated with background counts (see Section III.C.4.c).

Whole filter penetration ranged from $\approx 10^{-10}$ to a maximum of just under 0.03%. The data plotted in Figure IV-2 includes the highest observed penetration values. Figure IV-3 includes some the lowest observed penetration values.

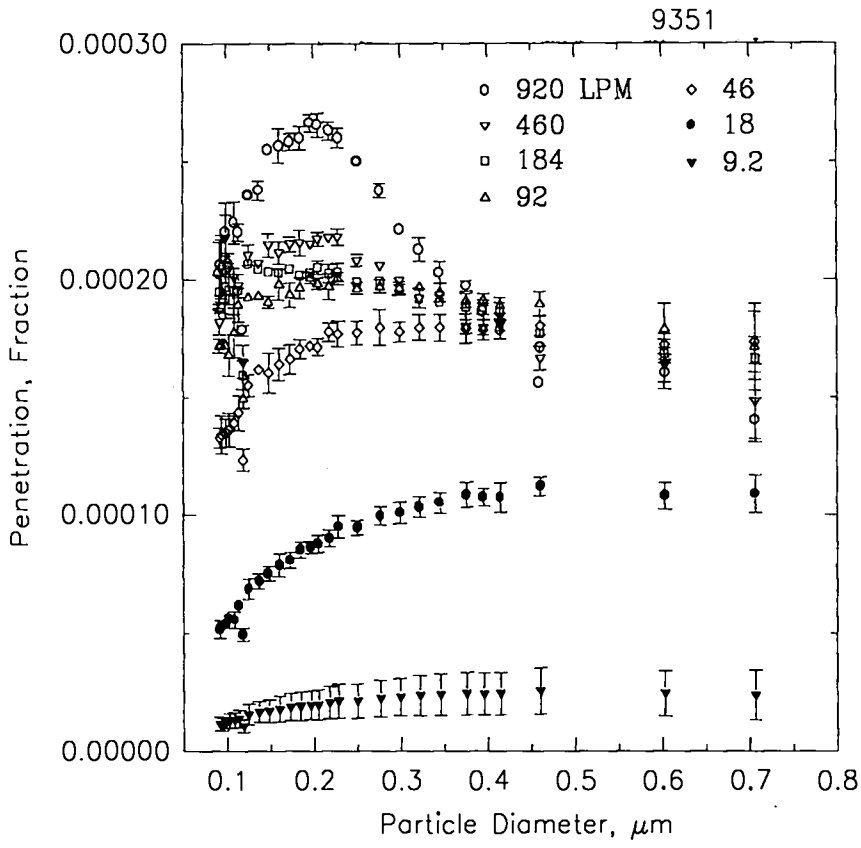

Figure IV-2. Whole filter penetration data for filter 9351.

Maximum penetration and the aerosol size at which the maximum was observed are listed in Table IV-II for each filter unit. In the formal study, maximum penetration values varied from 6.45×10^{-5} to 2.66×10^{-4}. The diameter of maximum penetration varied from 0.148 μm to 0.218 μm. The filtration velocity for these measurements ranged from just under 2 cm/sec to 3.18 cm/sec.

In the pilot study, maximum penetration values were observed within the range of those in the formal study. Maximum penetrations occurred in the smallest spectrometer bin. Filtration velocity for these measurements ranged from just over 2.5 cm/sec to just over 5 cm/sec.

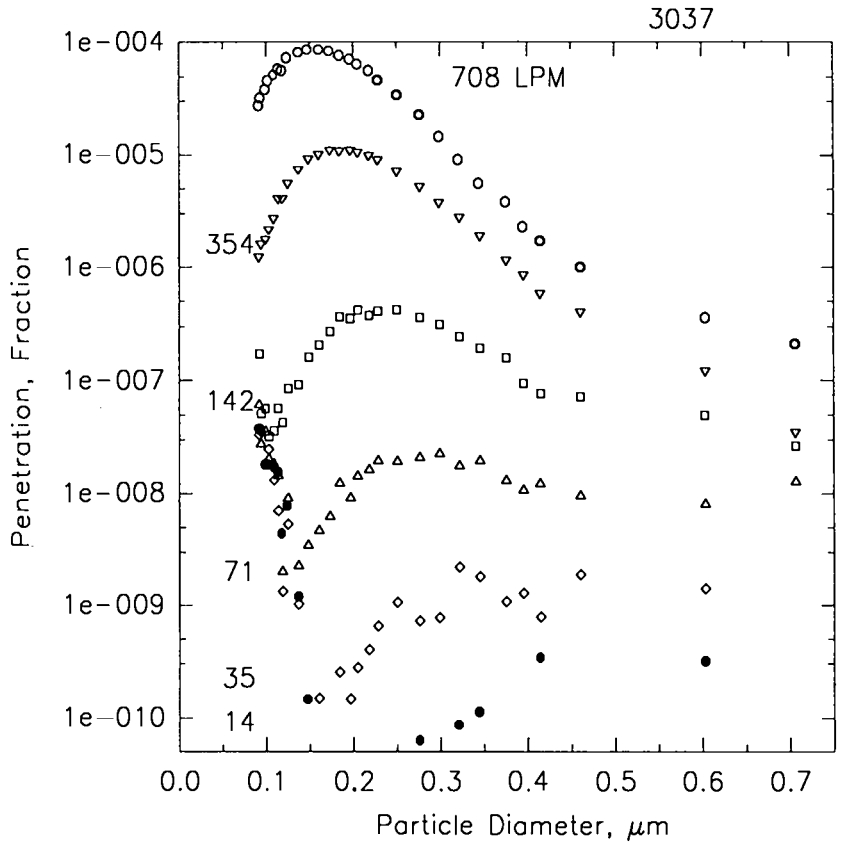

Figure IV-3. Whole filter penetration data for filter 3037.

IV.B. Frame Tests

Frame tests were performed on filters units with the frame unsealed, the upstream and the downstream gaskets sealed, and the filter face blanked-off (see Figure III-38b). This installation configuration

isolates the frame from the other filter unit components and permits independent evaluation frame leak flow rate and frame leak penetration. The tests consisted of measurement of frame leak flow rate (Q_{fr}) and differential pressure (Δp), and determination of frame leak penetration (P_{fr}). These results are considered to be representative of the frame contribution to filter unit field performance. Frame tests were conducted only in the formal study.

IV.B.1. Frame Leak Flow Rate Evaluation

Frame leak flow rate measurements were made with the bubble flow meter and the Laminar Flow Element systems described in Section III.C.6. Differential pressure measurements were made with instruments described in Section III.C.5. The flow rate and differential pressure measurements were typically made over a range of differential pressures corresponding to filter flow rates of <1% to >100% of the Q_{de}. These flow rate and differential pressure measurements were made prior to frame leak penetration determinations. No loading effects were observed on frame leak flow resistance.

Table IV-II

Maximum Penetration for Whole Filter Tests

STUDY	FILTER ID	Q_{de}, Lpm	U_o, cm/sec	P_{max}, Fraction	d_p at P_{max}, µm
PILOT	7-2C	920	5.06	0.000166	0.1
	2-2C	920	5.10	0.000217	0.1
	4-2C	920	5.10	0.000151	0.1
	8-2C	920	5.10	0.000161	0.1
FORMAL	9351	920	1.97	0.000266	0.196
	9346	920	2.01	6.45E-05	0.218
	9343	920	1.96	7.77E-05	0.196
	3037	708	3.24	8.56E-05	0.148
	3045	708	3.24	0.000112	0.160
	3041	708	3.24	9.5E-05	0.173
	3597	708	3.37	0.000158	0.173
	3598	708	3.22	0.000145	0.184
	3591	708	3.37	0.000181	0.173

Examples of frame leak flow rate measurement results are plotted against differential pressure in Figure IV-4. Flow rate was observed to

increase linearly with differential pressure. The solid lines in Figure IV-4 are linear regression fits to the data. Table IV-III lists linear regression correlation coefficients (r^2) for each filter unit. All values of r^2 were >0.98.

The plots in Figure IV-4 show data from the filter unit frames with the highest and lowest leak flow resistance. Air flow resistance ranged from 800 $\frac{dyn}{cm^2}\frac{sec}{cm^3}$ to just over 5500 $\frac{dyn}{cm^2}\frac{sec}{cm^3}$ (see Table IV-III). The lowest resistance was associated with a frame in which a hairline crack was found in the sealant of a frame corner joint. The leak flow resistance increased as the crack was sealed during the frame sealing process.

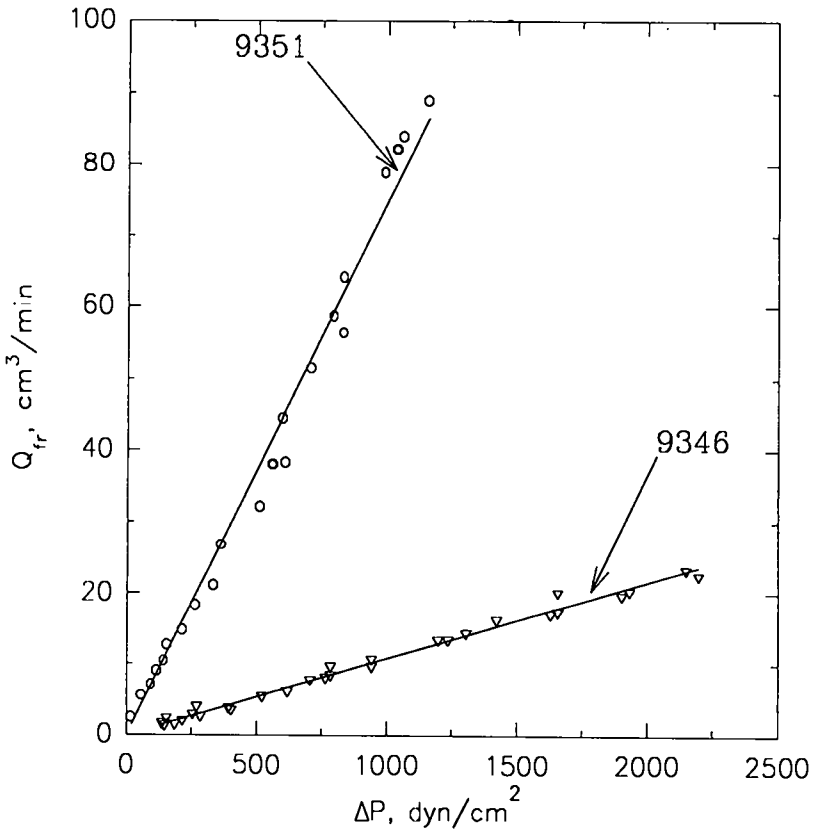

Figure IV-4. Plot of frame leak flow rate versus differential pressure for filter units 9351 and 9346.

Table IV-III

Correlation Coefficients and Leak Flow Resistance from Frame Tests

FILTER ID	r^2	RESISTANCE $\frac{dyn\ sec}{cm^2\ cm^3}$
9351	0.99	800
9346	0.99	5550
9343	1.00	3430
3037	1.00	1490
3045	1.00	1630
3041	1.00	1510
3597	1.00	1020
3598	1.00	4020
3591	1.00	2160

IV.B.2. Frame Penetration Determinations

Frame penetration determinations were made with the test system shown in Figure III-41. Penetration was determined from aerosol

concentration measurements made upstream and downstream of sealed-frame filter units using the HSLAS (see Section III.C.4). Penetration values for each spectrometer bin were calculated using Equation III-25. Typically, penetration was determined at differential pressures corresponding to filter flow rates of 1%, 2%, 5%, 10%, 20%, 50%, and 100% of Q_{de}.

Examples of penetration results are plotted against aerosol particle diameter in Figures IV-5 and IV-6. Frame penetration (P_{fr})generally decreased with whole filter unit flow rate, Q. For a given Q, frame penetration in the smallest particle size range increased with particle diameter. This penetration increase diminished at larger sizes the penetration increase diminished. In some cases, at the largest aerosol sizes slight decreases in frame penetration were observed. The high penetration values at the lowest particle sizes in Figure IV-6 were associated with background counts (see Section III.C.4.c).

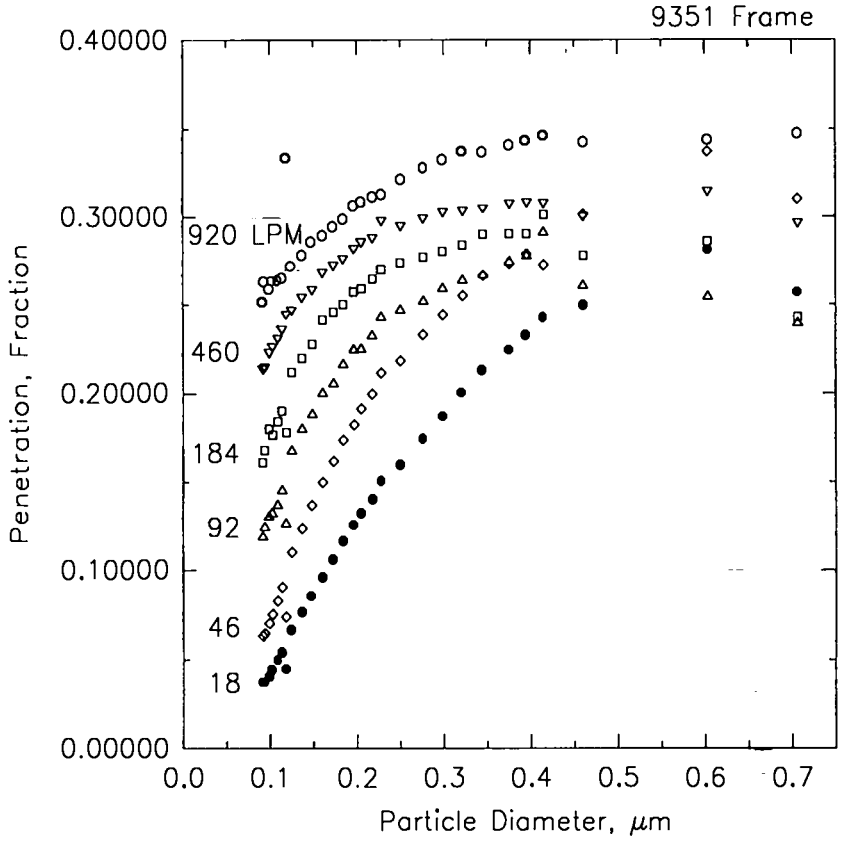

Figure IV-5. Frame penetration data for filter 9351.

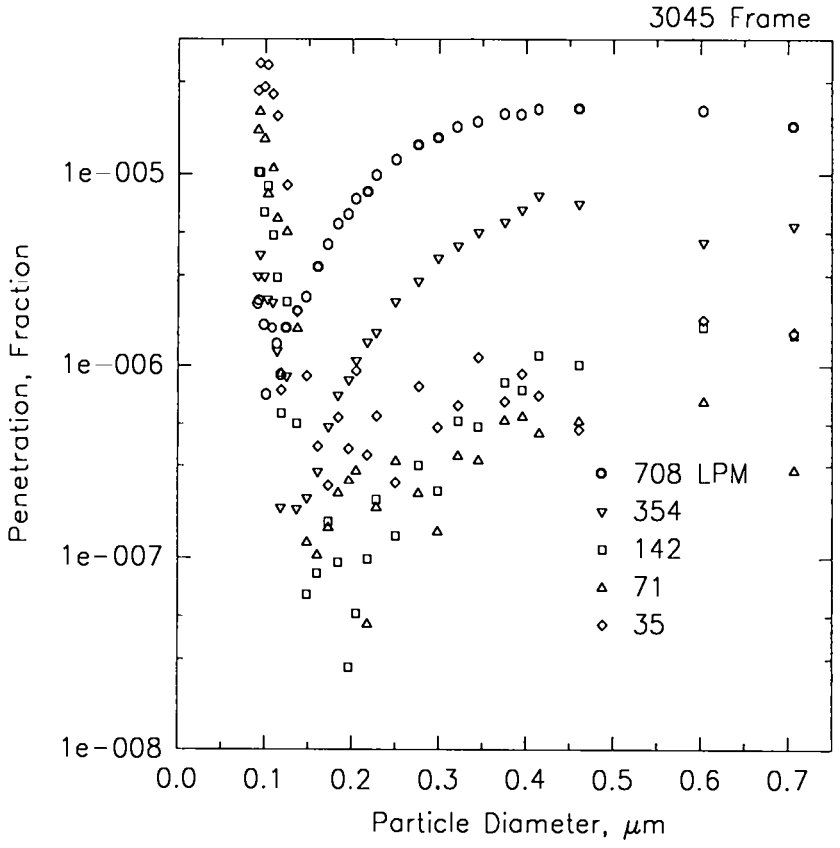

Figure IV-6. Frame penetration data for filter 3045.

Frame penetration ranged from $\approx 10^{-7}$ to ≈0.35. The data plotted in Figure IV-5 includes the highest observed frame penetration values. These values were associated with the frame in which the hairline crack was discovered. Figure IV-6 includes some of the lowest observed frame penetration values.

Maximum penetration and the aerosol size at which the maximum was observed are listed in Table IV-IV for each filter unit. Maximum penetration values varied from 2.17×10^{-5} to 0.35. The diameter of maximum penetration ranged from 0.376 μm to 0.707 μm.

Table IV-IV

Maximum Penetration for Frame Tests

FILTER ID	Q_{de}, Lpm	P_{max}, Fraction	d_p at P_{max}, µm
9351	920	0.347	0.707
9346	920	0.0507	0.461
9343	920	0.000203	0.707
3037	708	0.00206	0.461
3045	708	2.17E-05	0.461
3041	708	0.0133	0.396
3597	708	0.00123	0.376
3598	708	0.00262	0.603
3591	708	9.71E-05	0.603

IV.C. Media Pack Tests

After completing frame tests on a filter, the frame was sealed with silicone rubber sealant (see Figure III-38c). Tests were conducted to assure completeness of sealing. The procedure used to assure the seal

is described in section III.D.3.e. After the frame sealing procedure, the front blanking plate was removed. Media pack tests were performed on filters units in this configuration (see Figure III-38d). These tests consisted of measurement of media pack flow rate and differential pressure, and determination of media pack penetration.

Measurements on filter units with sealed frames isolate filter performance related solely to the media pack and the sealant joint between the frame and media pack (see Figure III-1). The contrast between these measurements and the other tests partitions performance amongst filter unit components.

IV.C.1. Media Pack Flow Rate and Differential Pressure Measurements

After sealing the downstream gasket, initial media pack filter flow rate and differential pressure measurements were made. Flow rate measurements were made with the Laminar Flow Element system described in Section III.C.6. Differential pressure measurements were made with instruments described in Section III.C.5. Differential pressure measurements were typically made at 1%, 2%, 5%, 10%, 20%, 50%, and

100% of the design flow rate (Q_{de}). These flow rate and differential pressure measurements were made prior to media pack penetration determinations. The measurements were typically repeated during and after the penetration determinations to evaluate effect of filter unit loading on flow rate and differential pressure.

Examples results of initial flow rate measurement from the formal study are plotted against differential pressure in Figure IV-7. In both the pilot and formal study, the differential pressure required to initially achieve the Q_{de} was below 4000 dyn/cm^2 (<1.61 "H_2O).

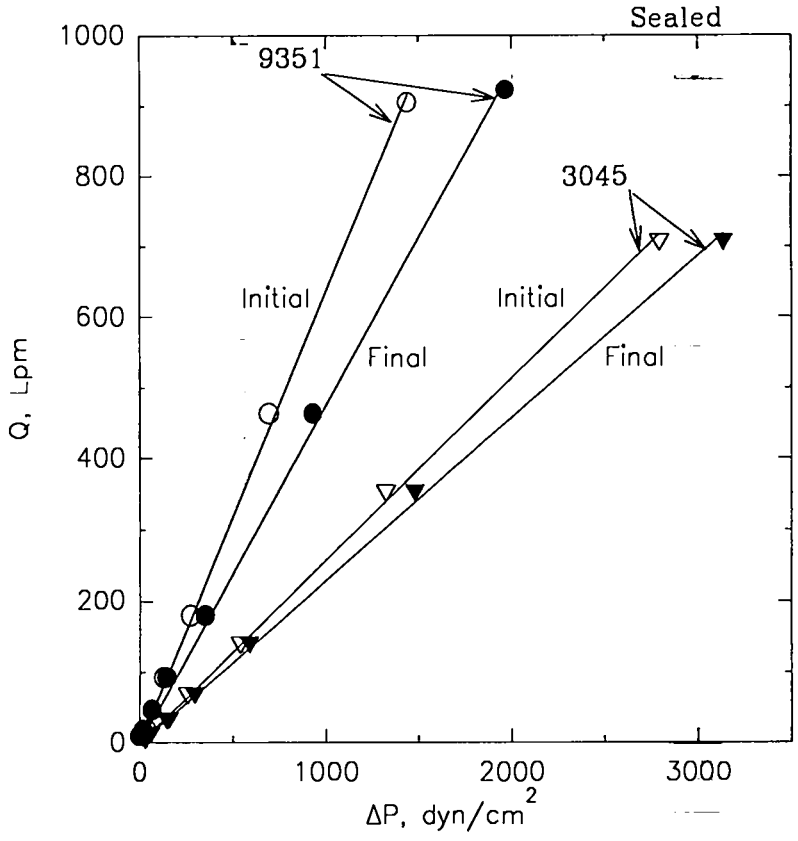

Figure IV-7. Plot of media pack flow rate versus differential pressure for filter units 9351 and 3045. Initial measurements were made prior to media pack penetration determinations, final measurements were made after the determinations.

Flow rate was observed to increase linearly with differential pressure. The solid lines in Figure IV-7 are linear regression fits to the

data. Table IV-V lists linear regression correlation coefficients (r^2) for each filter unit. All values of r^2 were ≥ 0.97.

The plots in Figure IV-7 show data from the formal study for the highest and lowest resistance filters. In both the pilot and formal studies, the initial air flow resistance ranged from 0.094 $\frac{dyn}{cm^2}\frac{sec}{cm^3}$ to 0.239 $\frac{dyn}{cm^2}\frac{sec}{cm^3}$ (see Table IV-I).

During testing, aerosol particles collected by the media pack increased pack air flow resistance. The increase resistance required subsequent tests to be conducted at differential pressures greater than would be required for unloaded packs. The increased differential pressure potentially affected penetration though media pack leak flow paths and could confound evaluation of the leak flow performance of the filters. Some filter loading was unavoidable given the nature of penetration tests. Steps were taken to minimize the degree of loading during tests.

The effect of loading was assessed by repeating measurements of flow rate and differential pressure during and at the end of media pack penetration determinations. Examples of the final flow rate measurements are plotted against differential pressure in Figure IV-7.

Table IV-V

Correlation Coefficients and Air Flow Resistances from Media Pack Tests

STUDY	FILTER ID	r^2	INITIAL RESISTANCE $\frac{dyn\ sec}{cm^2\ cm^3}$	r^2	FINAL RESISTANCE $\frac{dyn\ sec}{cm^2\ cm^3}$	%CHANGE[a]
PILOT	5-2C	0.99	0.239	—	—	—
	7-2C	0.97	0.200	—	—	—
	4-2C	1.00	0.180	1.00	0.258	43
	8-2C	1.00	0.206	1.00	0.232	13
FORMAL	9351	1.00	0.094	1.00	0.126	34
	9346	1.00	0.108	1.00	0.109	1.1
	9343	1.00	0.105	1.00	0.108	2.9
	3037	1.00	0.234	1.00	0.273	17
	3045	1.00	0.234	1.00	0.263	12
	3041	1.00	0.231	1.00	0.246	6.7
	3597	1.00	0.182	1.00	0.185	1.2
	3598	1.00	0.184	1.00	0.185	0.28
	3591	1.00	0.193	1.00	0.206	6.4

[a] $\%change = \left(\frac{\text{FINAL RESISTANCE - INITIAL RESISTANCE}}{\text{INITIAL RESISTANCE}}\right) X\ 100$

As with the initial measurements, the final flow rate measurements were observed to increase linearly with differential pressure. Linear fits to these data are shown as solid lines in Figure IV-7. Table IV-V lists r^2 for the final measurements. All values of r^2 were >0.99.

Table IV-V list the per cent increase in resistance over the course of media pack penetration tests. The largest increase was over 43%. In the formal study increases ranged from slightly below 0.3% to 34%.

IV.C.2. Media Pack Penetration Determinations

Media pack penetration determinations were made with the test system shown in Figure III-2. Penetration was determined from aerosol concentration measurements made upstream and downstream of test filter units using a laser aerosol spectrometer. In the pilot study, concentration measurements were made with the LAS-X-M laser spectrometer. In the formal study, the measurements were made with the HSLAS spectrometer (see Section III.C.4). Penetration values for each spectrometer bin were calculated using Equation III-21. Typically, penetration determinations were made at 1%, 2%, 5%, 10%, 20%, 50%, and 100% of Q_{de}.

Examples of penetration results from the formal study are plotted against aerosol particle diameter in Figures IV-8 and IV-9. Penetration generally decreased with filter unit flow rate, Q. At the highest values of Q, a peak in the penetration plots was observed. In general, the peak penetration value decreased as Q was lowered (See Figure IV-8). The particle diameter of maximum penetration increased as Q was lowered. At the lowest values of Q, penetration generally increased with aerosol size. Media pack penetration ranged from $\approx 10^{-10}$ to a maximum of just under 0.03%. The data plotted in Figure IV-8 includes the highest observed penetration values. Figure IV-9 includes some of the lowest observed penetration values.

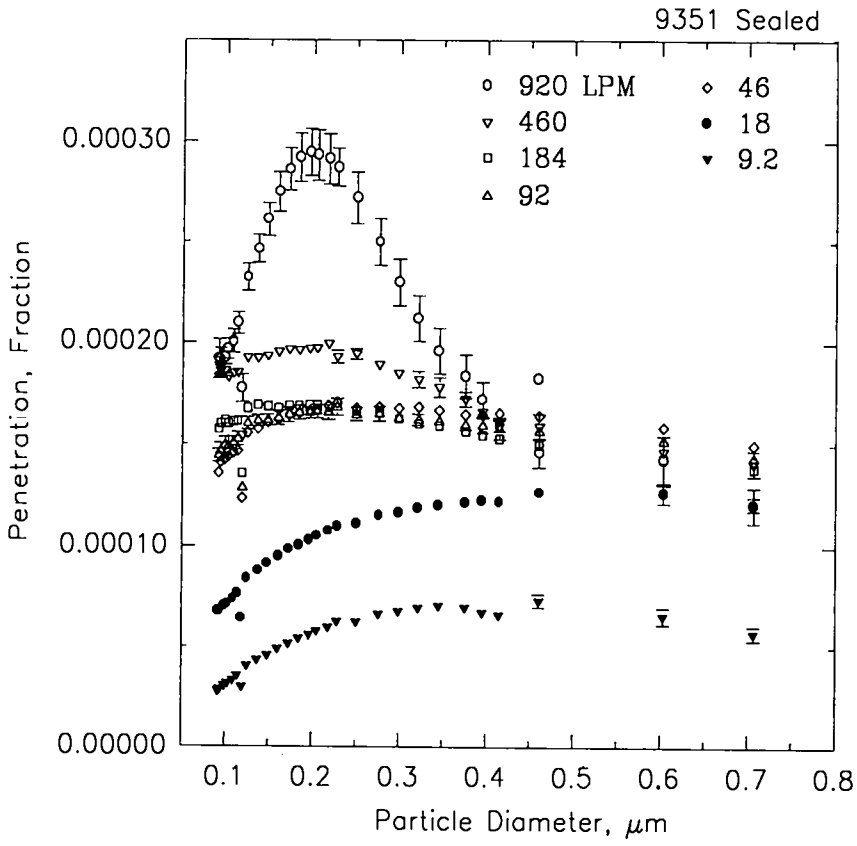

Figure IV-8. Media pack penetration data for filter 9351.

Maximum penetration and the aerosol size at which the maximum was observed are listed in Table IV-VI for each filter unit. In the formal study, maximum penetration values varied from 6.38×10^{-5} to 2.95×10^{-4}. The diameter of maximum penetration varied from 0.148 μm to 0.196 μm.

The filtration velocity for these measurements ranged from just under 2 cm/sec to 3.18 cm/sec.

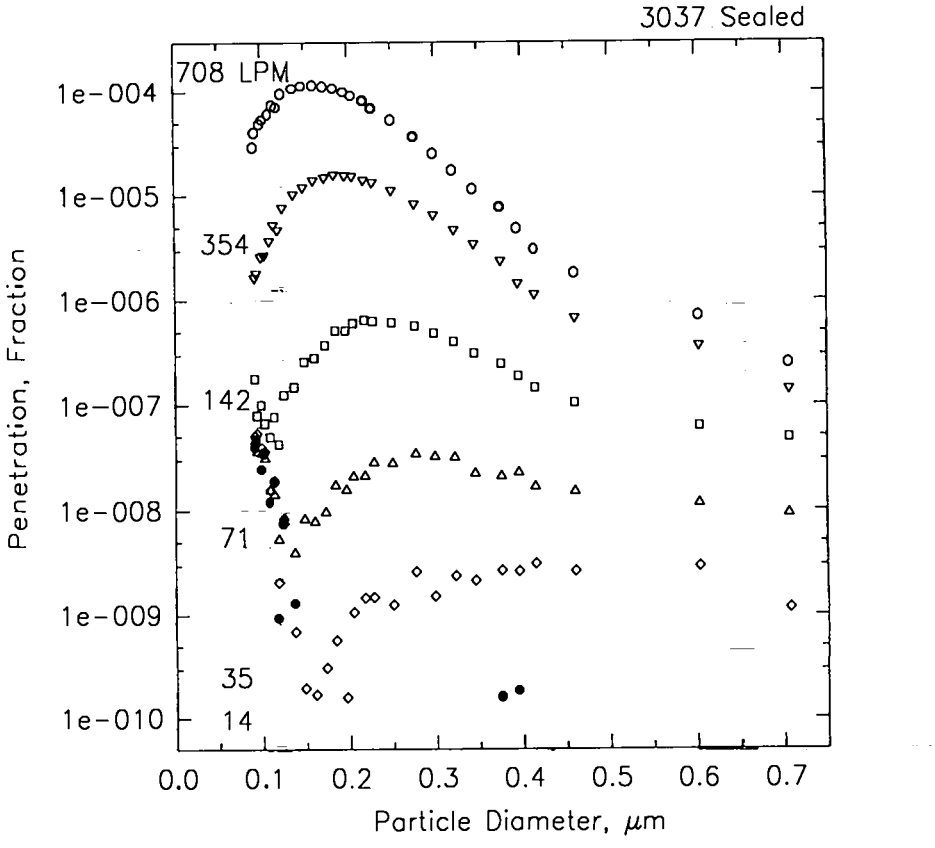

Figure IV-9. Media pack penetration data for filter 3037.

In the pilot study, maximum penetration values were observed in the range from 2.08 x 10-5 to 0.000231. Filtration velocity for these measurements ranged from just over 2.5 cm/sec to just over 5 cm/sec. At the velocities over 5 cm/sec, the maximum penetration occurred in the

spectrometer bin of the smallest particle size. A penetration maximum was observed at a bin diameter of 0.12 μm for the measurements made at 2.56 cm/sec.

Table IV-VI
Maximum Penetration for Media Pack Tests

STUDY	FILTER ID	Q_{de}, Lpm	U_o, cm/sec	P_{max}, Fraction	d_p at P_{max}, μm
PILOT	5-2C	460	2.55	2.08E-05	0.14
	7-2C	920	5.06	0.000193	0.10
	4-2C	920	5.10	0.000203	0.10
	8-2C	920	5.10	0.000231	0.10
FORMAL	9351	920	1.97	0.000295	0.196
	9346	920	2.01	7.83E-05	0.196
	9343	920	1.96	6.38E-05	0.196
	3037	708	3.24	0.000114	0.160
	3045	708	3.24	0.000145	0.160
	3041	708	3.24	0.000121	0.148
	3597	708	3.37	0.000173	0.173
	3598	708	3.22	0.000180	0.173
	3591	708	3.37	0.000254	0.173

IV.D. Uncertainty in Penetration Determinations

The overall uncertainty in penetration determinations was evaluated by repeat measurements of upstream and downstream particle counts. The standard deviation and average of the determinations was used to calculate point estimates of the coefficient of variation for penetration (CV_P). A sample of the calculated CV_P values are plotted against penetration in Figure IV-10. In these data CV_P generally increases as penetration decreases. Values of CV_P are all below 0.8.

An important factor in the overall uncertainty of the penetration determinations is the error associated with particle count measurements. Estimates of CV_P were made using a Poisson error model for penetration determinations described by Scripsick (Sc86, Sc87a):

$$CV_P = \left[(PR_u t_d)^{-1} + \frac{Dr}{R_u t_u} + CV_{Dr}^2 \right]^{1/2} \qquad \text{Equation IV-1,}$$

where, P = fractional penetration, R_U = undiluted upstream count rate, t_d = duration of downstream counting period, Dr = dilution ratio, t_U = duration

of upstream counting period, CV_{Dr} = coefficient of variation for dilution ratio. The first term in Equation IV-1 is the downstream Poisson error contribution to CV_P. The second term is the upstream Poisson error contribution. The last term is the contribution from the error in dilution ratio. Errors associated with aerosol mixing were found to be small compared to the Poisson counting errors (see Section III.C.2.c.i.b) and were neglected in predicting CV_P.

Estimates of CV_P as a function of P are plotted in Figure IV-10 for $R_u = 10^5$ particles/sec, $t_d = 6 \times 10^4$ sec, Dr = 1093, t_u = 60 sec, CV_{Dr} = 0.03. The values of R_u, Dr, CV_{Dr} came from averages of the values in the formal study. The value of t_d is at the high end of the range of downstream counting periods used in both the pilot and formal studies. The t_u value is the lowest value used in the studies.

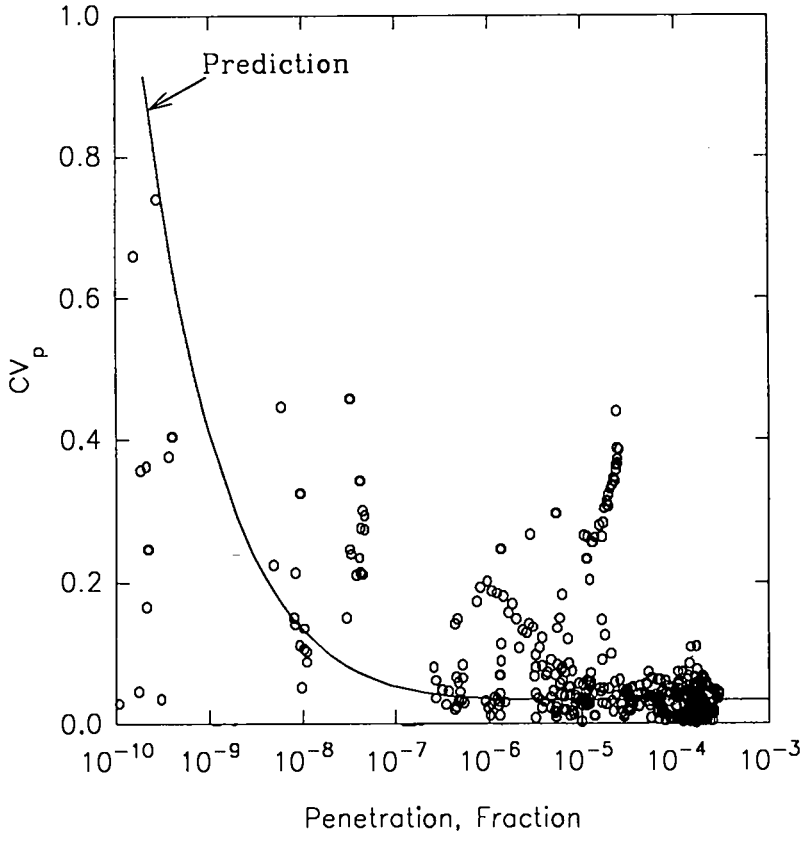

Figure IV-10. Coefficient of variation for penetration determinations (CV_P) plotted against penetration. Data points come from repeated penetration determinations. Prediction calculated using Equation IV-1.

At penetrations above 10^{-6}, CV_P is dominated by the last two terms in Equation IV-1. In this region CV_P is just over 0.03. At lower values of

P, the first term in Equation IV-1 begins to dominate and CV_P increases as P decreases.

The point estimates of CV_P from repeated P determinations follow the general trend of the predicted CV_P values. However in a number of cases the point estimates are much greater than the prediction. Review of the data indicates that some of these high estimates are related to such factors as 1) t_d for the point estimates being $<6 \times 10^4$ sec, and 2) challenge particle count rate being $<10^5$. In these cases the CV_P may still be largely dependent on the Poisson error and Equation IV-1 could be used by adjusting the values of the parameters. Some of the other high point estimates were found to be associated with aerosol loading affects on penetration which is not accounted for in the Poisson model.

CHAPTER V. ANALYSIS, INTERPRETATION, AND CONCLUSIONS

A general conclusion of this study is that the performance of HEPA filter units evaluated here can be explained by a leak flow model such as that shown in Figure II-10. In this chapter, evidence for this conclusion is presented. Results from frame tests are analyzed to show how they pertain to the external leak path part of the model. Results from the media pack tests are interpreted in terms of the internal leak path portion of the model. The summation of the frame and media pack tests results are compared to results of the whole filter tests. Test results are examined for the effect of loading on filter unit performance. Finally, data is presented that indicates non-Poiseuille leak flow performance observed in one of the filter units.

V.A. Evidence for External Leak Paths

Three types of evidence was observed that supports the existence of the external leak path in the wood frame HEPA filter units evaluated in this study. These include 1) comparison of whole filter and media pack

test results, 2) measurements of frame leak flow rate, and 3) results from the frame penetration determinations. The frame penetration results are fit with the leak penetration model for frame leaks described in Section II.D..

V.A.1. Comparison of Whole Filter and Media Pack Test Results

The first indication that leaks in filter unit frames contributed to overall filter penetration came in the pilot study. Whole filter and media pack tests were conducted on certain of the filters evaluated in that study (See Table III-VI). In one case a decrease in penetration was observed when the filter unit frame was sealed. This decrease is shown in Figure V-1 for penetration determinations made at Q = 920 Lpm. For both the unsealed and sealed cases penetration is observed to decrease as particle size (bin diameter) increases. At bin diameters less than ≈0.3 μm penetration is thought to be determined by intact media penetration. The penetration differences between unsealed and sealed cases in this particle size region may be the result of filter media loading. At bin diameters greater than ≈0.3 μm penetration values for the unsealed and sealed frame begin to diverge. The divergence increases as particle size increases with the penetration values associated with the unsealed frame

being greater than the sealed frame values. The penetration difference in this particle size region is thought to be the result sealing of leaks in the filter frame. These data suggest that the frame leaks account for a whole filter penetration of approximately 10^{-5}. When the frame is sealed penetration in this particle size region decreases to below 10^{-5}.

A plot of penetration for the unsealed and sealed cases is shown in Figure V-2 for the filter operating at Q = 46 Lpm. The difference in penetration in this plot is more dramatic than the data shown in Figure V-1. In this plot the penetration differs by more than an order of magnitude over the entire particle size range. Penetration in the unsealed case is thought to be dominated by leaks in the frame. A likely explanation for the increase in penetration with particle is diffusion losses in the frame leaks. Penetration approaches 10^{-5} at the largest particle sizes. The residual penetration after sealing the frame appears to be associated with intact media penetration. Media penetration is expected to drop-off sharply with decreasing filtration velocity whereas leak penetration can be independent of whole filter flow rate.

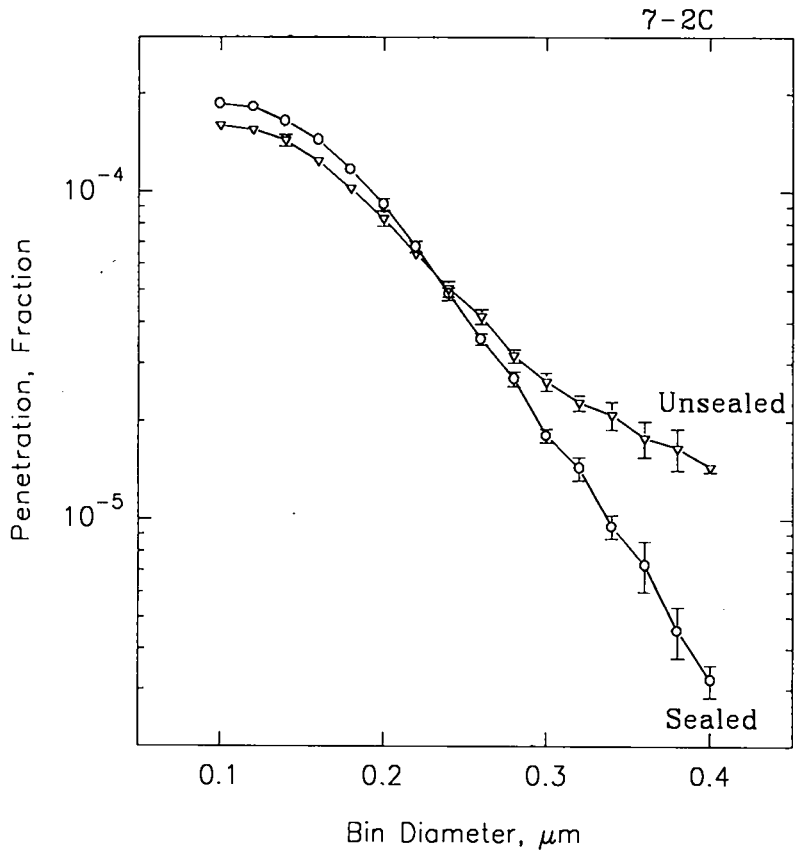

Figure V-1. Penetration data showing a reduction in penetration at bin diameters greater than ≈0.3 μm when the filter unit frame is sealed. Filter unit operating at Q_{de}.

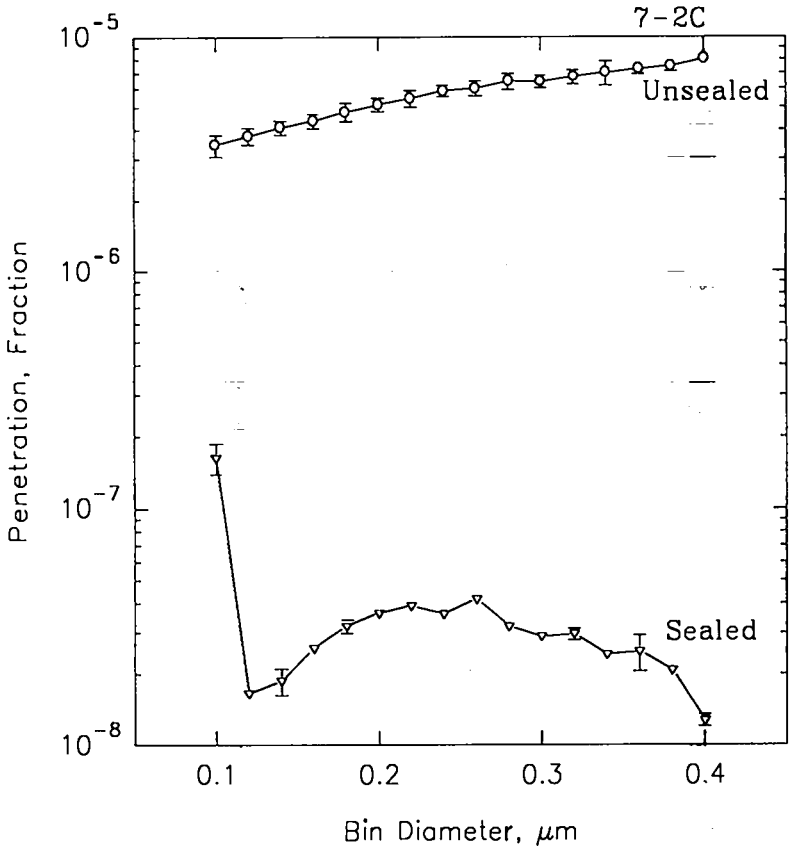

Figure V-2. Penetration data showing a reduction in penetration at all bin diameters when the filter unit frame is sealed. Filter unit operating at 5% of Q_{de}.

These data represent the most dramatic drop in penetration observed in both the pilot and formal studies. Typically frame penetration was ≤20% of the total observed leak penetration.

V.A.2. Frame Leak Flow Rate Evaluation

In the formal study, differential pressures corresponding to whole filter unit flow rates in the range from <1% to >100% of Q_{de} were applied across filter unit frames to determine if the differential pressures induced leak flow through the frames. Frame leak flows were detected in every filter unit evaluated in the formal study.

Frame leak flow rates as a fraction of whole filter flow rates (f_{fr}) were found in the range from 1.82×10^{-5} to 1.77×10^{-4} (see Table V-I). These flow rate fractions translate directly to an upper bound estimate of the frame leak contribution to overall filter unit penetration. The fractions represent the total frame leak flow rate and not that portion of the flow rate that exits the frame downstream of filter media (f_{ELD}). The f_{ELD} portion of frame leak flow rate is the only portion that contributes particles to frame penetration. All particles in the portion that exits upstream of the media (f_{ELU}) are collected by the media prior to exiting the filter unit. The f_{fr} fractions also overestimate the frame contribution to filter unit penetration because these fractions do not account for particle losses in frame leak flow paths.

Table V-I

Upper Bounds on Frame Penetration

Filter ID	f_{fr}	$\hat{P}_{frwf}$*
9351	1.04E-4	3.61E-5
9346	1.82E-5	9.23E-7
9343	2.83E-5	5.74E-9
3037	1.44E-4	2.97E-7
3045	1.34E-4	2.91E-9
3041	1.44E-4	1.91E-6
3597	1.77E-4	2.18E-7
3598	4.43E-5	1.16E-7
3591	8.61E-5	8.36E-9

*- Maximum frame contribution to whole filter penetration

In the formal study direct measurements of frame leak flow rate (Q_{fr}) were made with the filter unit in the test configuration shown in Figure III-38b. All measured Q_{fr} values were less than the Q_{Lmax} for size 1 filter units (See Section II.C.2.). Results from linear regression analysis shows

frame leak flow rate to be proportional to Δp to the first power (See Table IV-III). This finding indicates that frame leak flow observed in this study is in the Poiseuille laminar flow region (X>0.45). Frame flow rate dependence on Δp is the same as that observed for whole filter flow rate (See Table IV-I). Consequently, the contribution of frame penetration to whole filter penetration should be independent of whole filter flow rate (Q), if leak path particle loss is neglected. The whole filter and media pack penetration data in Figures V-1 and V-2 displays this independence.

The results from the frame sealing procedure indicate that the flat plywood surfaces are the primary source of leak flow. Very little blocking of frame leak flow was accomplished by sealing frame corners. In every filter unit, the most dramatic rise in air flow resistance occurred during sealing of the surfaces.

These results indicate that the primary source of the frame leak flow is directly through the flat surfaces of the plywood boards used to construct the frame. Another research group has observed air flow through wood bodies. Koponen (Ko91) has reported "air permeation" through certain wood species and a plywood when a differential pressure was applied.

V.A.3. Frame Penetration Evaluation

After it was established that a leak flow could be induced across filter unit frames, tests were conducted to determine if this flow could carry aerosol particles. Again, in every filter evaluated, particles were found to penetrate the wood frame to the downstream side of the filter. This was considered proof of the existence of an external leak path.

Upper bound estimates on frame leak contribution to whole filter penetration ($\hat{P}_{frwf}$) ranged from 2.91×10^{-9} to 3.61×10^{-5} (See Table V-I). These estimates are based on the highest measured frame penetration diluted in the total filter unit flow rate contrasted with f_{fr} with is based on the frame leak flow rate. The estimates of $\hat{P}_{frwf}$ account for particle losses at the maximum frame penetration. In every case $\hat{P}_{frwf}$ was less than the corresponding value of f_{fr}. This difference is thought to be a result of particle losses in frame leak flow paths and the fact that only a fraction of the measured frame leak flow rate carried particles to the downstream side of the filter unit.

Considering only leak flow character, frame penetration should be independent of particle size and whole filter flow rate. In this case leakage would be dominated by forced convection alone and leak path penetration would be 1. Frame penetration observed in this study was found to vary

with both of these parameters (See Figures IV-5 and IV-6). These variations are thought to be solely a result of particle losses in frame leak flow paths. Consequently, both convection and leak path particle loss determine frame penetration.

As described in Section II.D. the penetration model for frame leaks considers only convection and leak path particle loss and does not account for f_{ELD}. To account for f_{ELD} two categories of external leak paths are considered:

1) leak paths that exit the frame upstream of the filter media, and thus contributes flow but no particles to the overall external leak path flow, and

2) leak paths that exit the frame downstream of the filter media and thus potentially contribute both flow and particles to the overall external leak path flow. A diagram of this model is shown in Figure V-3. The total flow rate through this flow system is:

$$Q_{EL} = Q_{ELD} + Q_{ELU} \qquad \text{Equation V-1,}$$

where, Q_{EL} = the overall external leak flow rate, Q_{ELD} = the total external leak flow rate that exits downstream of the filter media, and Q_{ELU} = the total external leak flow rate that exits upstream of the filter media. The

frame leak penetration based on the way measurements were made in these experiments is then given by:

$$P_{EL} = P_{ELD}\frac{Q_{ELD}}{Q_{EL}} + P_{ELU}\frac{Q_{ELU}}{Q_{EL}} \qquad \text{Equation V-2,}$$

where P_{EL} = the overall external leak penetration, P_{ELD} = effective penetration of the external leak flow paths that exit the frame downstream of the filter media, and P_{ELU} = effective penetration of the external leak flow paths that exit the frame upstream of the filter media. Particles in the flow that exits upstream of the media are all assumed to be collected in the media as the flow exits the filter unit, so $P_{ELU} = 0$ and Equation V-2 becomes:

$$P_{EL} = P_{ELD}\frac{Q_{ELD}}{Q_{EL}} = P_{ELD}f_{ELD} \qquad \text{Equation V-3,}$$

where, f_{ELD} = the fraction of Q_{EL} that exits downstream of the filter media = Q_{ELD}/Q_{EL}.

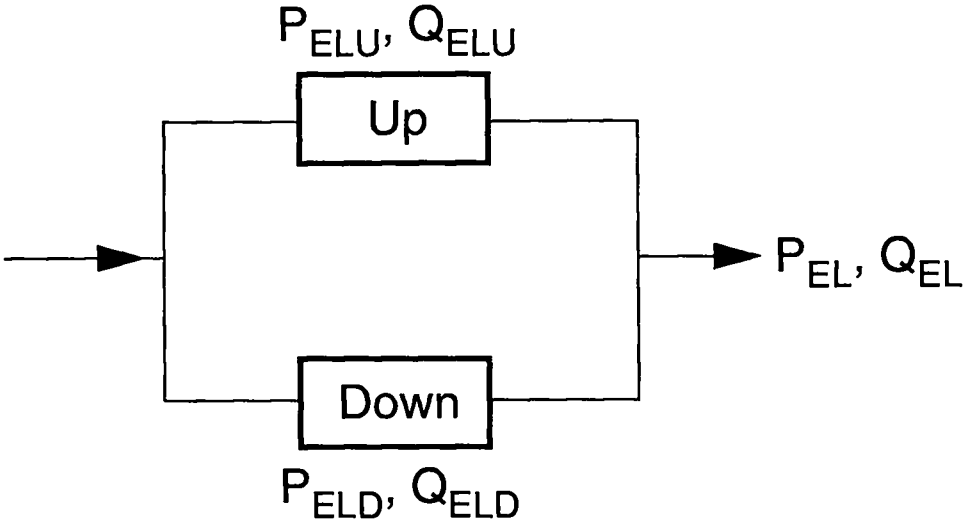

$$Q_{EL} = Q_{ELD} + Q_{ELU}$$

$$P_{EL} = P_{ELD} \frac{Q_{ELD}}{Q_{EL}} = P_{ELD} f_{ELD}$$

Figure V-3. Flow diagram of external leak model showing flow paths that exit upstream of filter media and downstream of filter media.

When $P_{ELD} = 1$, forced convection is assumed to dominate frame penetration. In this case frame penetration is independent of particle size. For values of $P_{ELD} < 1$ both convection and leak path particle loss determines frame penetration. As in Section II.D.5, P_{ELD} is assumed to be determined by diffusion and sedimentation particle collection

mechanisms. Losses due to interception are neglected. An expression for P_{ELD} analogous to Equation II-15 in Section II.D.5 is:

$$P_{ELD} = P_{ELDd} P_{ELDs} \qquad \text{Equation V-4,}$$

where, P_{ELDd} = the contribution of diffusion collection to P_{ELD}, and P_{ELDs} = the contribution of sedimentation collection to P_{ELD}. P_{ELDd} is assumed to be a function of the diffusion deposition parameter μ:

$$\mu = \frac{D\ell_{ELD}}{Q_{ELDi}} = \frac{D\ell_{ELD} N_{ELD}}{Q_{EL} f_{ELD}}$$

Equation V-5,

where, D = the particle diffusion coefficient, ℓ_{ELD} = the effective length of the downstream external leak paths for diffusion losses, Q_{ELDi} = the effective flow rate through individual downstream external leak paths for diffusion losses = $Q_{EL}\, f_{ELD}/N_{ELD}$, and N_{ELD} = the effective number of external leak paths exiting downstream of the filter media for diffusion losses. P_{ELDd} is determined by using this definition of μ in the equations

for diffusion losses in tubes given in Section II.D.1 as equations II-7 and II-8.

P_{ELDs} is assumed to be a function of:

$$Z = \frac{3\pi}{16}\frac{\ell_{ELDs} d_{ELDs} V_{ts}}{Q_{ELDsi}} = 0.631\frac{\pi^{3/4}\eta^{1/4}V_{ts}}{\Delta p^{1/4}Q_{EL}^{3/4}}\frac{\ell_{ELDs}^{5/4}N_{ELDs}^{3/4}}{f_{ELDs}^{3/4}} \qquad \text{Equation V-6,}$$

where, Z = the gravitational deposition parameter, ℓ_{ELDs} = the effective length of the downstream external leak paths for sedimentation losses = $\ell_{ELD} - \left[(\ell_{ELD} - \ell_{EL\,min})\left(\frac{1-e^{-Z}}{1-e^{-1}}\right)\right]$, ℓ_{ELmin} = minimum leak path length for external leaks, for the wood frames evaluated in this study ℓ_{ELmin} = 1.905 cm, d_{ELDs} = the effective diameter of the downstream external leak paths for sedimentation losses, which from the Hagen-Poiseuille equation = $\left[\frac{Q_{ELDsi}128\eta\ell_{ELDs}}{\pi\Delta p}\right]^{1/4}$, V_{ts} = the particle terminal settling velocity, Q_{ELDsi} = the effective flow rate through individual downstream external leak paths for sedimentation losses = $\frac{Q_{EL}f_{ELDs}}{N_{ELDs}}$, f_{ELDs} = the effective fraction of Q_{EL} that exits downstream of the filter media for sedimentation losses =

$f_{ELD} - \left[f_{ELD} \left(\frac{1 - e^{-Z}}{1 - e^{-1}} \right) \right]$, and N_{ELDs} = the effective number of external leak paths exiting downstream of the filter media for sedimentation losses = $N_{ELD} - \left[(N_{ELD} - 1) \left(\frac{1 - e^{-Z}}{1 - e^{-1}} \right) \right]$. Equation V-6 is a re-statement of Equation II-11 in Section II.D.3. P_{ELDs} is determined by using this definition of Z in the equation for sedimentation losses in tubes given in Section II.D.3 as equation II-12.

The sedimentation collection mechanism gives P_{ELDs} identically equal to 0 for sufficiently low values of Q_{ELDsi} at a given particle size, and for sufficiently large values of d_p at a given Q_{ELDsi}. Consequently, as Q_{EL} decreases and as d_p increases, certain of the individual downstream leak flow paths cease to contribute particles to the overall external leak flow. For purposes of the model, these downstream flow paths become equivalent to upstream flow paths in that they continue to contribute flow but cease contributing particles. This contribution change begins with the longest of the downstream paths and progresses to successively shorter paths. The progression results in shortening of the effective leak path length, reduction in the effective number of downstream leak paths, and lowering of the fraction of external leak flow rate that carries particles.

The decrease in the values of these parameters depends on Z. This model assumes that for Z = 0, the parameters ℓ_{ELDs}, N_{ELDs}, and f_{ELDs} take on the values of ℓ_{ELD}, N_{ELD}, and f_{ELD}, respectively. At higher values of Z, the model assumes the values decrease according to the exponential functions shown above. At Z = 1, these parameters take on their minimum values which are ℓ_{ELmin} = 1.905 cm for ℓ_{ELDs}, 1 for N_{ELDs}, and 0 for f_{ELDs}.

The decrease in the values of these parameters depends on Z. This model assumes that for Z = 0, the parameters ℓ_{ELDs}, N_{ELDs}, and f_{ELDs} take on the values of ℓ_{ELD}, N_{ELD}, and f_{ELD}, respectively. When Z=0 there are no predicted sedimentation losses so the distribution of leaks considered for diffusion losses and sedimentation losses are identical. At higher values of Z, the model assumes the values decrease according to the exponential functions shown above. In this range of Z values the longest leak paths cease contributing particles so different leak distributions are considered for the two loss mechanisms. At Z = 1, these parameters take on their minimum values which are ℓ_{ELmin} = 1.905 cm for

ℓ_{ELDs}, 1 for N_{ELDs}, and 0 for f_{ELDs}. For this value of Z, all leak paths have ceased contributing particles and the greatest difference between leak distributions exists.

In these equations for P_{EL}, the parameters Q_{EL}, and Δp are measured quantities, and D and V_{ts} are calculated from the particle diameter. Fits of the frame penetration to this model were made setting P_{EL} equal to the measured frame penetration P_{fr} and Q_{EL} equal to the measured frame leak flow rate Q_{fr}. The fit parameters were ℓ_{ELD}, N_{ELD}, and f_{ELD}. An example of the fit results is shown in Figure V-4. Values of these fit parameters for each filter unit are listed in Table V-II.

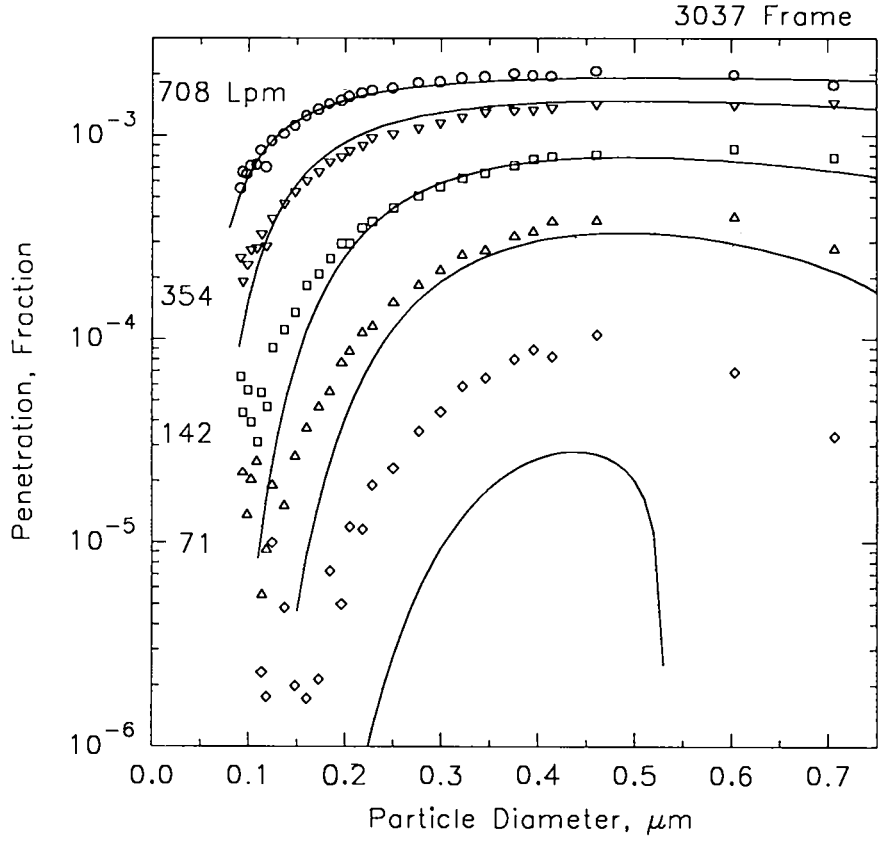

Figure V-4. External leak model fit to frame leak penetration data.

The physical interpretation of the individual fit parameters denotes limits on their possible values. Values of ℓ_{ELD} should not be less than the thickness of the filter frame which is 1.905 cm. Values of N_{ELD} should not be less than 1 and values of f_{ELD} should be between 0 and 1. The fits were constrained to these limits, so that the values listed in Table V-II

represent the best fit within the boundaries of these limits. In some cases better fits to the data could be obtained outside these boundaries. For example, better fits to data from filter unit 9351 were obtained when values of ℓ_{ELD} were not constrained to be >1.905 cm.

The tendency for fits to improve when constraints on the fit parameters were removed raises questions about the appropriateness of the model to represent the data. The model is based on the external leak flow rate and particle loss being represented by N_{ELD} straight circular cross-section leaks each with length ℓ_{ELD} and diameter d_{ELD}. In fact the leak paths are almost certainty not straight, they are not likely to be circular or even uniform in cross-section along their length, and they are probably not all the same length or diameter. What is expected is a variety of branched leak paths with a distribution of shapes, lengths, and cross-sections. The flow and particle loss characteristics for such complex flow path geometries has not been solved. The tendency for fits to improve when fit parameter constraints are removed may be an indicator of the limitations of this simplified model for predicting performance for the more complex flow path geometries.

Table V-II

Fit Parameters for External Leak Paths

Filter ID	ℓ_{ELD}, cm	N_{ELD}	f_{ELD}
9351	1.91	115	0.3893
9346	22.2	16.8	0.0750
9343	11.9	19.4	0.00250
3037	4.81	14.0	0.00268
3045	2.12	4.51	7.28E-5
3041	4.08	71.0	0.0159
3597	21.8	3.81	0.00198
3598	3.79	71.8	0.00689
3591	2.97	3.68	2.13E-3

Two other modeling approaches were evaluated. One approach entailed fixing $\ell_{ELDs} = \ell_{ELD}$, $N_{ELDs} = N_{ELD}$, and $f_{ELDs} = f_{ELD}$. In this approach changes in particle contribution of downstream leak paths were not linked to values of Q_{ELDsi} and d_p. In the other approach f_{ELD} in Equation V-3 was replaced with f_{ELDs}, and ℓ_{ELD}, N_{ELD}, and f_{ELD} in

Equation V-5 were replaced with ℓ_{ELDs}, N_{ELDs}, and f_{ELDs}, respectively.

With this approach particle contribution changes were considered in estimating P_{ELDd} as well as P_{ELDs}. Fits of the data with these alternative models were not as good as those that considered particle contribution changes only when estimating P_{ELDs}.

V.A.4. Summary and Conclusions from External Leak Path Evaluations

The experimental evidence gathered in the frame penetration evaluations supports the existence of an external leak path component to the model of filter unit performance. A decrease in penetration was observed after sealing of a filter unit frame. Air flow through plywood filter unit frames was detected when a differential pressure was applied. The air flow was found to carry particles from the upstream side of the filter unit to the downstream side.

Frame penetration determinations suggest that some portion of the aerosol particles traveling along the frame leak paths may deposit within the leaks. Analysis of potential loss mechanisms indicates that diffusional and gravitational sedimentation collections processes dominate these

losses. Fits to the data were achieved using a model that considered these mechanisms.

V.B. Evidence for Internal Leak Paths

Evidence supporting the existence of internal leak paths comes exclusively from penetration determinations of media packs. Internal leaks are the result of incomplete sealing of the media pack to the interior of the filter unit frame and defects in the filter media. Internal leak flow streamlines are intermingled with those incident on the filter face. These streamlines cannot be physically isolated from those that are incident on the intact portions of the media pack. Consequently, only indirect assessments of internal leak flow rate and internal leak penetration are possible. These assessments come from review of the data and from fitting the data to internal leak models.

V.B.1 Review of Media Pack Penetration Results

The internal leak contribution to overall media pack performance for some of the filter units was obvious from review of the data. An example

of such data is shown in Figure IV-8. At aerosol diameters >0.4 μm, data at all flow rates except the lowest (9.2 Lpm) collapse on one another. This collapse is not expected from filtration theory. The media pack penetration in this size range is thought to be dominated by internal leaks. The reduced penetration at the lowest flow rate is possibly the result of particle losses in internal leak paths.

At aerosol diameters <0.4 μm media pack penetration is determined by a combination of penetration mechanisms depending on flow rate. At the highest flow rate (920 Lpm) the peak in the penetration data is a hallmark characteristic of intact media penetration predicted by filtration theory. At the lower flow rates this peak disappears and internal leak penetration is thought to be dominating media pack penetration.

At the intermediate flow rates of 46 Lpm to 184 Lpm, the penetration data collapses. In this region penetration is largely independent of particle size as well as flow rate. This independence indicates 1) internal leaks are dominating media pack penetration in this region, 2) particle loss in these leak paths is minimal under these conditions, and 3) leak flow rate dependence on Δp is the same as that for the entire media pack. Media pack flow rate was found to be proportional to Δp to the first power (See Table IV-V). This suggests that the internal leak flow is in the Poiseuille laminar flow region (X>0.45).

At the smallest particle diameters at these intermediate flows and over the entire range of particle diameters at the lowest flow rates (18 Lpm and 9.2 Lpm) the effect of leak path particle loss is evident. For a given particle size, penetration decreases with flow rate. At the lowest flow rates, penetration increases with particle size up to a particle diameters of $\approx$0.4 μm. At larger particle diameters a slight decrease in penetration is observed. This penetration behavior suggests these internal leak particle losses may be dependent on diffusional and gravitational sedimentation mechanisms.

For some of the filter units, interpretation of the role of internal leaks in media pack penetration was not obvious. An example where interpretation was difficult is filter unit 3037 (See Figure IV-9). For this filter unit, the penetration peak, indicative of intact filter media penetration persists to flow rates as low as 71 Lpm. At Q = 35 Lpm, penetration could either be related to intact media penetration or to internal leak penetration with diffusional/sedimentation losses in the leak paths. The contribution of internal leaks is not obvious from review of the data. The contribution of leaks down to a penetration of $\approx 10^{-8}$ appears minimal. At lower penetrations the contribution is not clear. There are no obvious features of internal leak penetration. Features of media penetration and those suggesting leak path particle loss run together. Information that lies

outside the range of measurement is needed to ascertain the leak contribution.

Filter units 9351 and 3037 define the range of ease/difficulty in interpreting the role of internal leaks in media pack performance. Other filter units where the internal leak role was as obvious as for filter unit 9351 include 9343,3041, and 3597. Except for filter unit 3597, the data from these filter units indicate that the internal leak flow is in the Poiseuille laminar flow region ($X>0.45$). The data from filter unit 3597 suggests the internal leak flow is in the non-Poiseuille laminar flow region ($X<0.45$). This finding is explored in Section V.D..

Other filter units where the leak contribution was as difficult to define as for filter unit 3037 include 9346, and 3045. The two remaining filter units in the formal study (3598 and 3591) fall in between these extremes.

V.B.2 Internal Leak Penetration Model

One method to objectively assess the leak contribution in these filter units is fitting the data to an internal leak model. As described in Section II.D. the portion of the penetration model for media pack leaks

considers both intact media penetration and internal leak penetration. This portion of the overall filter unit penetration model is shown in Figure II-10. Total media pack flow rate, Q_{MP}, is given by:

$$Q_{MP} = Q_M + Q_{IL} \qquad \text{Equation V-7,}$$

where, Q_M = the flow rate through the intact portion of the media, and Q_{IL} = the internal leak flow rate. Media pack penetration is then given by:

$$P_{MP} = P_M \frac{Q_M}{Q_{MP}} + P_{IL} \frac{Q_{IL}}{Q_{MP}} = P_M(1 - f_{IL}) + P_{IL} f_{IL}$$

Equation V-8,

where P_{MP} = overall media pack penetration, P_M = penetration through the intact portion of the media, P_{IL} = penetration through internal leak paths, and f_{IL} = the fraction of the media pack flow rate through internal leak paths.

An expression for P_M come from fibrous filtration theory:

$$P_M = \exp\left(\frac{-4\alpha\eta_{DR}\ell_F}{l_H \pi d_f}\right) \qquad \text{Equation V-9,}$$

where, α = the fiber volume fraction, η_{DR} = the effective single fiber collection efficiency for diffusion and interception (See Equation I-1), ℓ_F = filter media thickness, I_H = filter media inhomogeneity factor (Ru86, He90), and d_f = effective fiber diameter.

When $P_{IL} = 1$, forced convection is assumed to dominate media pack leak penetration. In this case the leak portion of the media pack penetration is independent of particle size. For values of $P_{IL} < 1$ both convection and leak path particle loss determines media pack leak penetration. As in Section II.D.5, P_{IL} is assumed to be determined by diffusion and sedimentation particle collection mechanisms. Losses due to interception are neglected. An expression for P_{IL} is Equation II-16 in Section II.D.5.. P_{ILd} is assumed to be a function of:

$$\mu = \frac{D\ell_{IL}}{Q_{ILi}} = \frac{D\ell_{IL}N_{IL}}{Q_{IL}f_{IL}} \qquad \text{Equation V-10,}$$

where, μ = the diffusion deposition parameter, D = the particle diffusion coefficient, ℓ_{IL} = the effective length of the internal leak paths for diffusion losses, Q_{ILi} = the effective flow rate through individual internal leak paths for diffusion losses = $Q_{MP}\, f_{IL}/N_{IL}$, and N_{IL} = the effective number of

internal leak paths for diffusion losses. P_{ILd} is determined by using this definition of μ in Equations II-7 and II-8.

P_{ILs} is assumed to be a function of:

$$Z = \frac{3\pi}{16}\frac{\ell_{ILs} d_{ILs} V_{ts}}{Q_{ILsi}} = 0.631\frac{\pi^{3/4}\eta^{1/4}V_{ts}}{\Delta p^{1/4} Q_{MP}^{3/4}}\frac{\ell_{ILs}^{5/4} N_{ILs}^{3/4}}{f_{ILs}^{3/4}} \qquad \text{Equation V-11,}$$

where, Z = the gravitational deposition parameter, ℓ_{ILs} = the effective length of the downstream external leak paths for sedimentation losses = $\ell_{IL} - \left[(\ell_{IL} - \ell_{ILmin})\left(\frac{1-e^{-Z}}{1-e^{-1}}\right)\right]$, ℓ_{ILmin} = minimum leak path length for internal leaks, for the media packs evaluated in this study ℓ_{ILmin} = 0.0508 cm, d_{ILs} = the effective diameter of internal leak paths for sedimentation losses, which from the Hagen-Poiseuille equation = $\left[\frac{Q_{ILsi}128\eta\ell_{ILs}}{\pi\Delta p}\right]^{1/4}$, V_{ts} = the particle terminal settling velocity, Q_{ILsi} = the effective flow rate through individual internal leak paths for sedimentation losses = $\frac{Q_{MP} f_{ILs}}{N_{ILs}}$, f_{ILs} = the effective fraction of Q_{MP} that passes through internal leak paths for

sedimentation losses = $f_{iL} - \left[f_{iL} \left(\frac{1 - e^{-Z}}{1 - e^{-1}} \right) \right]$, and N_{ILS} = the effective number of internal leak paths for sedimentation losses = $N_{iL} - \left[(N_{iL} - 1) \left(\frac{1 - e^{-Z}}{1 - e^{-1}} \right) \right]$.

Using the Hagen-Poiseuille equation to interpret d_{ILS} in terms of ℓ_{ILS}, Q_{ILSi}, and Δp assumes internal leak flow is in the Poiseuille laminar flow region. P_{ILS} is determined by using this definition of Z in the equation for sedimentation losses in tubes given in Section II.D.3 as Equation II-12.

The sedimentation collection mechanism gives P_{ILS} identically equal to 0 for sufficiently low values of Q_{ILSi} at a given particle size, and for sufficiently large values of d_p at a given Q_{ILSi}. Consequently, as Q_{IL} decreases and as d_p increases, certain of the individual internal leak flow paths cease to contribute particles to the overall media pack flow. For purposes of the model, these flow paths become equivalent to intact media flow paths in that they continue to contribute flow but cease contributing particles. This contribution change begins with the longest of the internal leak paths and progresses to successively shorter paths. The progression results in shortening of the effective length of internal leak paths, reduction in the effective number of internal leak paths, and lowering of the fraction of media pack leak flow rate that carries particles.

The decrease in the values of these parameters depends on Z. This model assumes that for Z = 0, the parameters ℓ_{ILs}, N_{ILs}, and f_{ILs} take on the values of ℓ_{IL}, N_{IL}, and f_{IL}, respectively. When Z=0 there are no predicted sedimentation losses so the distribution of leaks considered for diffusion losses and sedimentation losses are identical. At higher values of Z, the model assumes the values decrease according to the exponential functions shown above. In this range of Z values the longest leak paths cease contributing particles so different leak distributions are considered for the two loss mechanisms. At Z = 1, the parameters take on their minimum values which are ℓ_{ILmin} = 0.0508 cm for ℓ_{ILs}, 1 for N_{ILs}, and 0 for f_{ELDs}. For this value of Z, all leak paths have ceased contributing particles and the greatest difference between leak distributions exists.

In these equations for P_{MP}, the parameters Q_{MP}, and Δp are measured quantities, and D and V_{ts} are calculated from the particle diameter. Values of α, $\ell_{F/H}$, d_f were estimated as 0.0445, 0.043 cm, and 2.6×10^{-5} cm, respectively. Fits of the media pack penetration data were

made using the following fit parameters: ℓ_{IL}, N_{IL}, and f_{IL}. An example of the fit results is shown in Figure V-5.

The best fits were obtained with data at a given media pack flow rate. Fits of data at more than one flow rate were not as good. This result indicates that the flow rate dependency was not adequately accounted for in the model. A number of potential reasons exist for this inadequacy. One reason may related to loading effects on media pack penetration. These effects are described in Section V.D.. The effects could result in changes in the effective leak geometry so that a fixed set of fit parameters may not adequately predict penetration over a range of flow rates.

Another potential reason for the inadequacy may be related to non-Poiseuille leak flow effects on penetration. These effects are described in Section V.E.. The non-Poiseuille effects could mitigate some of the leak path particle loss effects on penetration and result in observed leak penetration being higher than that predicted by the particle loss model.

Parameter values obtained from fits to filter unit 3041 data are listed in Table V-III. The range of these values is indicative of that obtained from fits to data of other filter units. Values of ℓ_{IL} were frequently $>10^5$ cm. Values of N_{IL} were typically <20. Values of f_{IL} ranged from 10^{-7} to 1.

The physical interpretation of the individual fit parameters denotes limits on their possible values. Values of ℓ_{IL} should not be less than the minimum thickness of the filter media which is 0.0508 cm. Values of N_{IL} should not be less than 1 and values of f_{IL} should be between 0 and 1.

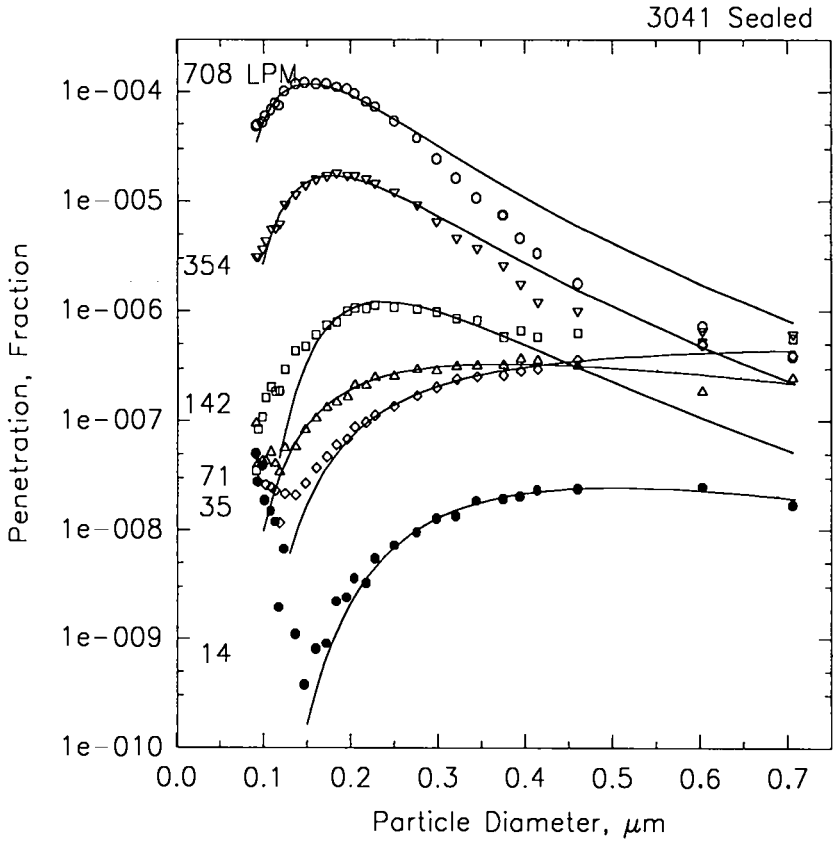

Figure V-5. Internal leak model fits to media pack penetration data.

Table V-III

Fit Parameters for Internal Leak Paths - Filter Unit 3041

Flow Rate -Lpm	ℓ_{IL} -cm	N_{IL}	f_{IL}
708	6.37E6	8.94	0.125
354	7.30E5	5.99	0.0138
142	450	1.34	6.82E-6
71	31.8	2.52	1.28E-6
35	0.0508	870	9.38E-7
14	4.89	2.48	3.40E-7

The fit parameter values respected these limits. However, many of these values indicate leak geometries clearly outside the region of geometries that are physically reasonable or are expected given the penetration data. An upper bound on the values of ℓ_{IL} should be on the order of ten times the media pack pleat depth. The nominal pleat depth for the size 1 filter units that were evaluated is ≈5.2 cm. So that, an upper bound on ℓ_{IL} could be expected to be ≈52 cm. Using filter unit 3041 as an example (See Table V-III), fit estimates of ℓ_{IL} at the two highest flow rates

are orders of magnitude larger than this upper bound. These large fit estimates are clearly outside a region of physically probable leak lengths.

Review of penetration data for filter unit 3041 indicates a value of f_{IL} on the order of 10^{-6} (See Figure V-5). This indication comes from the observed values of P_{MP} at particle diameters >0.4 μm and at all but the lowest flow rate. Fit estimates of f_{IL} at media pack flow rates from 14 Lpm to 142 Lpm are of this magnitude (See Table V-III). At the higher media pack flow rates, fit values of this parameter are several orders of magnitude greater than 10^{-6}. The larger fit values of f_{IL} are clearly outside the range of f_{IL} expected from review of penetration data.

Reasons for the internal leak model fitting data with these large fit parameter values are not known. Certainly, all shortcomings described for the external leak model in approximating the complexities of actual leak geometries have some application to the internal leak model. One additional feature associated with the internal leak model is that at the smaller particle sizes and higher flow rates media penetration masks diffusional leak path particle losses. These are the conditions under which the model predicts unrealistic values of the fit parameters. Inspection of the data shows under these conditions very few data points lie in leak dominated regions. Examination of the fit parameters for sedimentation losses under these conditions revealed that the parameters were scaled to

values in the expected ranges. Consequently, the fit parameter values under these conditions are greatly dependent on the scaling functions (See Equation V-11).

V.B.3. Summary and Conclusions of Media Pack Penetration Evaluations

The experimental evidence gathered in the media pack penetration evaluations supports the existence of an internal leak path component to the model of filter unit performance. Review of the media pack penetration results revealed operating regions where obvious departures from filtration theory performance were observed. In these regions media pack performance was possibly explained by a model that included internal leak paths. In all but one case internal leak flow appeared to be in the Poiseuille laminar flow regime.

A variety of media pack leak performance was observed from filter unit to filter unit. Observed leakage was controlled to the level that all filter units met limits on penetration. The variety suggests that the observed leakage was below quality control limits of filter unit manufacturing.

The media pack penetration determinations suggest that some portion of the aerosol particles traveling along the internal leak paths may deposit within the leaks. Analysis of potential loss mechanisms indicates that diffusional and gravitational sedimentation collections processes dominate these losses. Fits to the data were achieved using a model that considered these mechanisms.

V.C. Whole Filter Unit Performance

Combining frame test results with those from the media pack tests should approximate the results obtained in the whole filter tests if all filter unit flow paths were accounted for in the evaluations. The whole filter penetration, P, is estimated as:

$$P = P_{MP}\frac{Q_{MP}}{Q} + P_{EL}\frac{Q_{EL}}{Q} \qquad \text{Equation V-12.}$$

Estimates of P were determined from frame test and media pack test results. An example of these estimates is plotted in Figure V-6. The estimates approximate the whole filter penetration data quite well. This result indicates that the overall filter unit penetration is fully accounted for by the frame and media pack measurements.

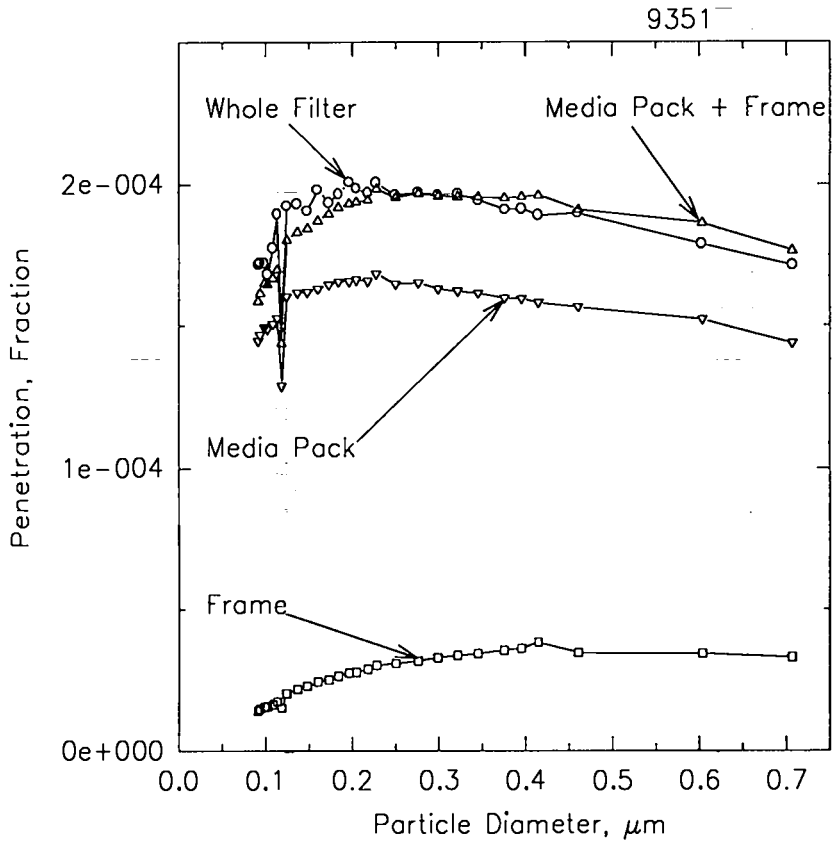

Figure V-6. Whole filter penetration data plotted with the summation media pack and frame penetration data.

In Figure V-6, frame test penetration accounts for approximately 20% of the overall penetration. Typically, media pack leak penetration was the dominant contributor to overall leak penetration. This example shows the greatest observed frame penetration contribution.

V.D. Effects of Loading on Filter Unit Performance

As testing of a filter unit progressed, collected aerosol material accumulated in the unit. This loading of the unit was linked to certain effects on filter unit performance. Effects were observed in whole filter tests and media pack tests only. No loading effects were observed in the frame tests. The effects of loading were associated with collection of aerosol material by the filter media.

V.D.1. Loading Effects on Air Flow Resistance

One of the observed effects was the increase in air flow resistance described in Chapter IV (See Figures IV-1 and IV-7 and Tables IV-I and IV-V). Air flow resistance was observed to increase as testing progressed for both the whole filter tests and the media pack tests. Resistance increases were directly related to air flow rate and duration of test.

An increase in fibrous filter air flow resistance with accumulation of aerosol material is expected both from theory and from previous experimental work. A number of studies have focused on loading of HEPA filters. Letourneau, et al (Le89) investigated loading of HEPA filter media

with solid aerosol particles. Media air flow resistance was found to increase with mass loading. They found modest agreement between experimental results and theoretical predictions.

Smith et al (Sm91) reported experimental results on size 5 nuclear grade HEPA filter units loaded with a salt aerosol. Air flow resistance increased with filter unit weight gain.

Novick, et al (No92) studied loading of HEPA filter media with solid aerosol particles. Increases in air flow resistance were correlated with mass loading.

V.D.2. Loading Effects on Penetration

The other loading effect observed in the present study was increased penetration with filter unit loading. Examples of this finding are shown in Figures V-7 and V-8.

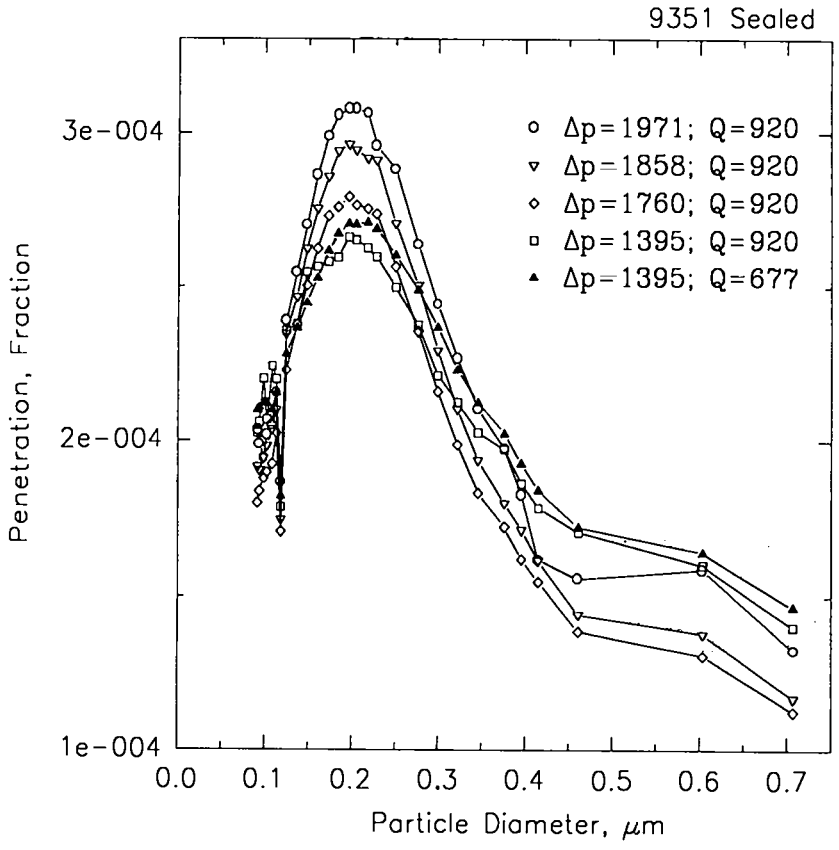

Figure V-7. Increase in peak penetration with liquid aerosol particle loading of filter unit.

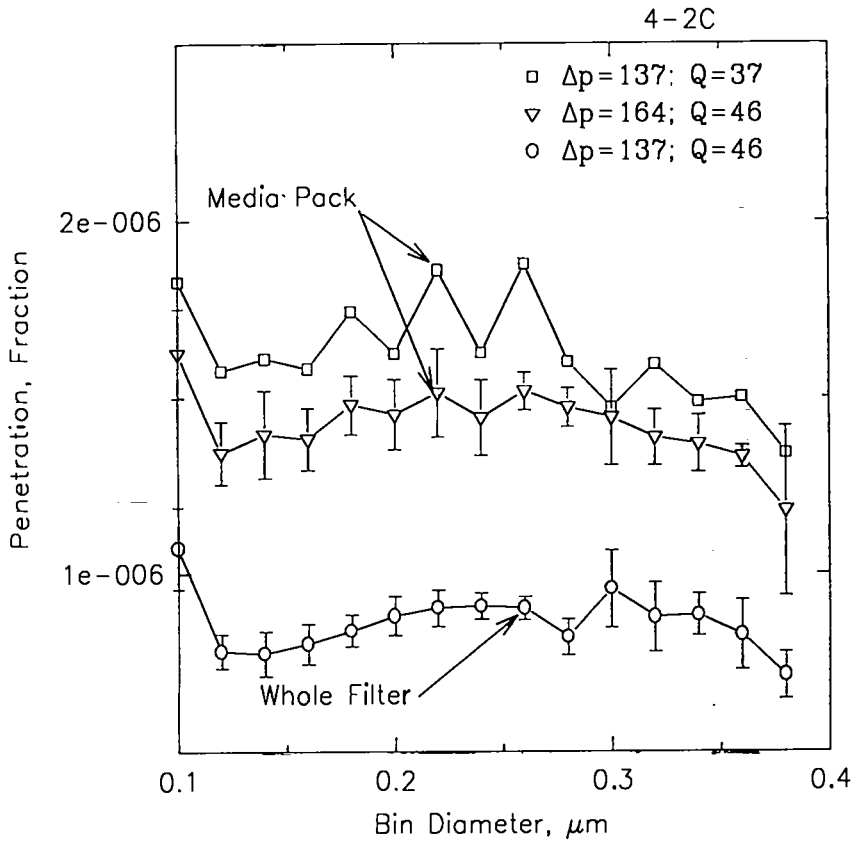

Figure V-8. Increase in leak penetration with liquid aerosol particle loading of a filter unit.

V.D.2.a. Penetration Effects in the Intact Media Region

Figure V-7 shows results of successive penetration determinations on a single filter unit operating in a region where intact media is thought to

dominate filter unit penetration. Differential pressure measurements made with the filter operating at Q_{de} = 920 Lpm are an indicator of degree of loading. The increase in Δp is a result of the filter unit air flow resistance increasing as aerosol particles accumulate.

The peaks in the penetration plots are predicted by fibrous filtration theory and indicate that the intact media is dominating overall penetration. Peak penetration is observed to increase as the filter unit loads while flow rate is maintained at 920 Lpm. This increase is thought to be the result of loading effects of liquid particles on the intact media. Payet, et al (Pa92) reported increases in peak penetration for HEPA filter media loaded with liquid aerosol particles. Loading with solid aerosol particle can act to decrease penetration the solid particle serve as additional collection sites.

The penetration increase is reversed when the loaded filter is operated at the initial Δp = 1395 dyn/cm^2. The increase in peak penetration and the reversal are performance effects expected when flow through a portion of the media is blocked. This behavior reversal indicates the dominant loading effect on the media is restriction or blocking of flow paths within the media. When the filter unit is operated at a constant flow rate the filtration velocity, U_0, increases as the filter loads. The greater U_0 results in penetration increasing in the peak penetration region where diffusion collection dominates. When the loaded filter unit is operated at a

lower flow rate, U_0 returns to some previous value and a reduction in peak penetration is observed.

The fidelity of the penetration reversal suggests that blocking is the dominant effect for the degree of loading observed in this study (less than a 50% increase in Δp). The reversal indicates that a portion of filter media remains unaffected by collected aerosol material. When U_0 is returned to some previous value the penetration effects due to loading disappear. The loaded filter operates as would a smaller portion of the unloaded filter. This return would not be expected if liquid aerosol particles were affecting fiber diameter or if solid particles were serving as additional collection sites. Therefore, at this degree of loading, other loading effects on HEPA media, such as those on fiber diameter, d_f, and solidity, α, described by Payet, et al (Pa92), appear to be at least secondary.

Testing for reversal of penetration increase may be an important tool for examining loading effects. In the loading range where blocking dominates the effect on penetration the fidelity of reversal should be quite good. Degradation of the reversal fidelity could be used as an indicator of the boundary between the loading region where the blocking effect dominates and the region where other effects begin to be important.

V.D.2.b. Penetration Effects in the Internal Leak Region

Figure V-8 shows results of successive penetration determinations on a single filter unit operating in a region where internal leaks are thought to dominate filter unit penetration. Differential pressure measurements made with the filter operating at Q = 46 Lpm are an indicator of degree of loading. The increase in Δp is a result of the filter unit air flow resistance increasing as aerosol particles accumulate.

Penetration independence of particle size is an indication leaks in the media pack are dominating overall penetration. Penetration is observed to increase as the filter unit loads and flow rate is maintained at 46 Lpm. This increase is thought to be the result of loading effects of liquid particles on the intact media. Leak flow path particle loss calculations indicate that particles collect preferentially in intact media. Consequently, air flow resistance through the media pack is expected to increase faster than the resistance of the leak flow paths. The fraction of media pack flow rate that passes through internal leaks, f_{IL}, is assumed to depend on these resistances as follows:

$$f_{IL} = \frac{Q_{IL}}{Q_{MP}} = \frac{\Delta p_{IL}}{W_{IL}} \frac{W_{MP}}{\Delta p_{MP}} \qquad \text{Equation V-13,}$$

where, Δp_{IL} = differential pressure across internal leaks, W_{IL} = effective air flow resistance of internal leak paths, W_{MP} = effective air flow resistance of media pack, Δp_{MP} = differential pressure across media pack. For $\Delta p_{IL} = \Delta p_{MP}$,

$$f_{IL} = \frac{W_{MP}}{W_{IL}} \qquad \text{Equation V-14.}$$

Consequently, as W_{MP} increases relative to W_{IL}, f_{IL} increases. and because P_{IL} increases with f_{IL}, P_{IL} also increases. So, in a region where the product of P_{IL} and f_{IL} dominates P_{MP} (see Equation V-8 with $P_M = 0$), P_{MP} is expected to increase as the filter unit loads.

Media pack penetration was observed to be greater than whole filter penetration in certain filter units. An example of this observation is shown in Figure V-8. The incremental penetration increase is thought to be the result of the intervening loading. In many cases the penetration increase attributed to loading was greater than the contribution of external leaks. In these situations media pack penetration was greater than whole filter penetration.

The increased penetration is maintained even when the filter unit is operated at the unloaded differential pressure (Δp = 137 dyn/cm^2; Q = 37 Lpm). This result is expected when the filter unit is operated in a region where media pack flow rate and internal leak path flow rate have the same dependence on differential pressure. Media pack flow rate was determined to be proportional to differential pressure to the first power (See Section IV.C.1). Consequently, these results are evidence that internal leak flow rate is also proportional to differential pressure to the first power.

Penetration determinations made on filter units at various degrees of loading with liquid aerosols may be a useful tool for detecting and evaluating internal leaks in media packs. Internal leaks are indicated when penetration reversal is observed in certain filter unit operating regions and not in others. In regions where reversal is not observed, operation of the filter unit at the unloaded differential pressure can reveal certain characteristics of internal leaks. Loaded filter penetration being largely independent of differential pressure and particle size indicates that leak flow character is similar to that of the media pack and that leak path particle loss is minimal. An increase in penetration may indicate non-Poiseuille leak flow. A decrease in penetration suggests enhanced leak path particle loss.

V.E. Evidence for Non-Poiseuille Laminar Leak Flow

The boundaries of leak geometry and leak flow imposed by design requirements on HEPA filter units are discussed in Section II.C. These boundary conditions indicate that the largest allowable leaks in HEPA filter units may be in the non-Poiseuille laminar flow region as defined in Section II.B.2. From the analysis of the boundary conditions, size 1 HEPA filters appear to have the least likelihood of displaying non-Poiseuille leak flow behavior as illustrated in Figure II-1. This behavior appears to be more likely in larger size filters.

The bulk of results from the experimental studies demonstrate that leak flow in size 1 HEPA filter is in the Poiseuille laminar flow regime. All data collected on external leaks indicates external leak flow is in this flow regime. All but one of the internal leak data sets supports this conclusion.

Data collected in whole filter and media pack tests on filter unit 3597 are the only results in these studies that display non-Poiseuille laminar flow behavior. An example of these results is presented in Figure V-9. Penetration is observed to decrease as flow rate is reduced from 708 Lpm to 142 Lpm. Over this same flow rate range, peaks in the penetration

plots disappear. This performance is indicative of penetration undergoing a transition from an operating region in which intact media dominates penetration into a region where internal leaks dominate penetration. At flow rates below 142 Lpm a gradual increase in penetration is observed. For leaks operating in the Poiseuille flow regime, penetration is expected to either remain constant or to decrease when there is particle loss in leak paths. The gradual penetration increase suggests that leak flow character differs from that of the intact media. Flow rate and differential pressure measurements on the media pack indicate flow rate is proportional to differential pressure to the first power. Under these conditions media pack penetration would be expected to increase if internal leak flow rate was proportional to differential pressure to a power less than one (See Sections I.C.2.c.,I.D.1, II.A. and II.B.). Leak flow rate is proportional to differential pressure raised to a power between 0.5 and 1 in the non-Poiseuille laminar flow region.

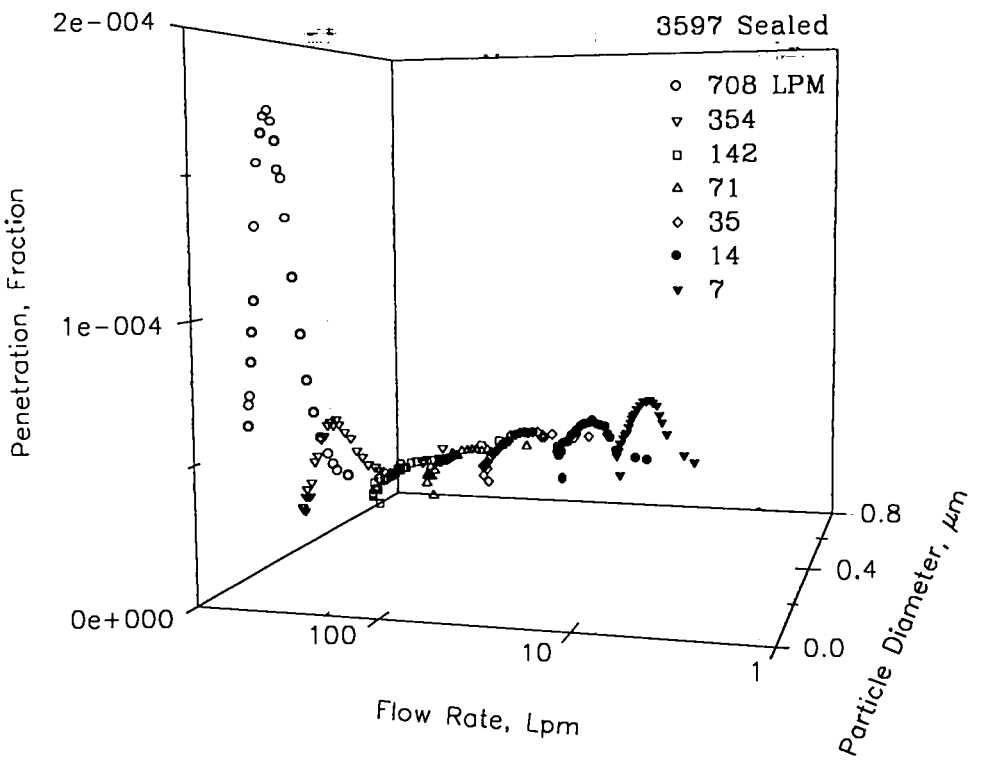

Figure V-9. Media pack penetration data demonstrating non-Poiseuille laminar leak flow behavior.

There is limited data in the literature showing increases in filter unit penetration as flow rate is reduced. Data of Kozuka et al (Ko80) shows such increases for size 1 and size 2 (Q_{de} = 1420 Lpm) HEPA filter units at particle diameters above 0.6 µm. Scripsick (Sc86) reports increased penetration at low flow rates for size 5 (Q_{de} = 28.3 M3/min) HEPA filter units. Results of the present study links these obsevered increases in

penetration to filter unit leaks operating in the non-Poiseuille laminar flow region.

V.F. Conclusions on Leak Performance of Small HEPA Filter Units

Leaks were found in every filter unit examined in this study. These leaks are described as flow paths that bypass the intact media portion of the filter units. Evaluation of the performance of the entire filter unit and its individual components show that leak penetration is an important feature of the overall performance. The data suggest that intact media penetration may only be important in the limited range of particle size and filter unit flow rate where fibrous filtration theory predicts maximum penetration. In other parts of the filter unit operating domain leaks existing in the filter unit may dominate overall filter unit performance. A mapping of dominant penetration mechanisms for one filter unit is shown in Figure V-10. In this figure intact media dominates penetration at fractional flow rates above 0.3 and at particle diameters below approximately 0.3 μm diameter. At the lowest flow rates and the smallest particle diameters penetration is dominated by diffusion losses in leak flow paths. For larger particle diameters, sedimentation losses in leak flow paths dominate

penetration at the lowest flow rates. At higher flow rates penetration of the large particles is determined by forced convection.

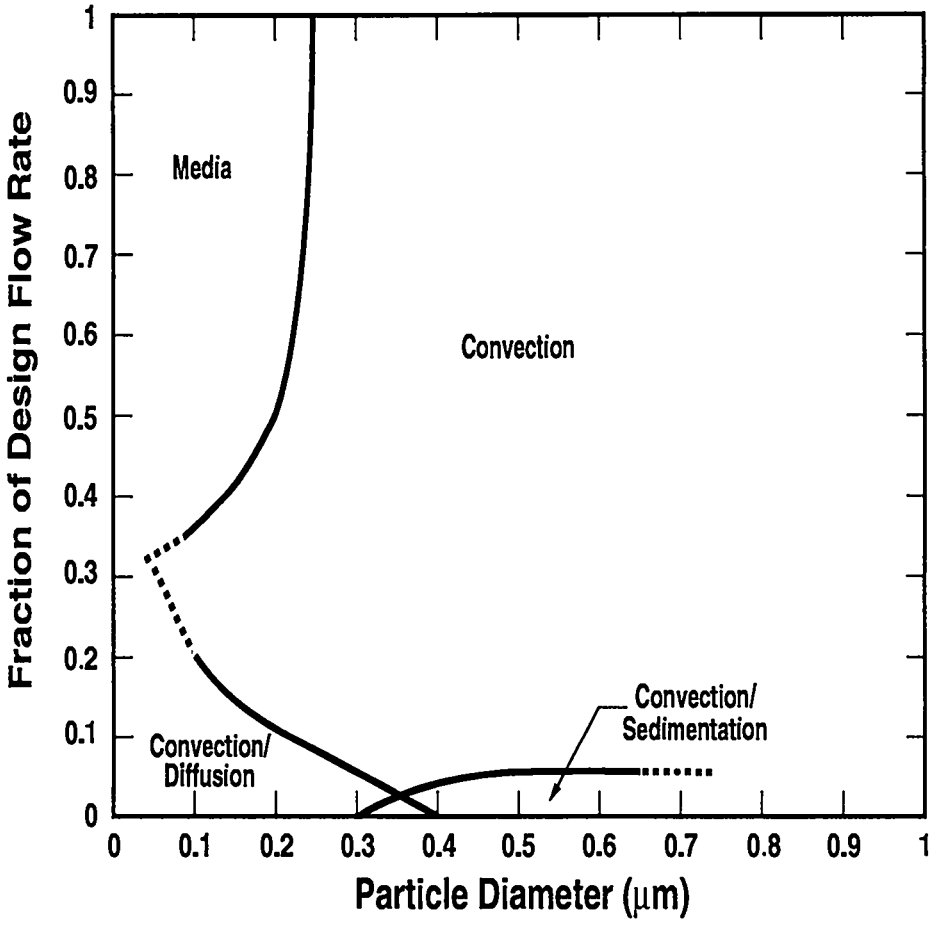

Figure V-10. Dominant penetration mechanisms mapped over the filter unit operating dimensions of flow rate and particle diameter.

V.F.1. Conclusions from Frame Evaluations

Frame leak flow rate was found to account for $\leq$10-4 of the whole filter flow rate. Methodical sealing of the filter frame indicated frame leak flow was directly through flat surfaces of the plywood frame and not through frame joints. Flow rate was found to be proportional to Δp. This finding suggests that frame leak flow is in the Poiseuille laminar flow region. The Δp dependence is the same that was found for the entire filter unit. Consequently, the frame leak flow rate fraction of the whole filter flow rate (f_{fr}) should be independent of Δp.

Only a small fraction of the leak flow rate was found to carry particles downstream of the filter unit. Frame penetration was found to be less than f_{fr} and contributed up to 20% of the overall filter unit leak penetration. A model that considered diffusional and gravitational sedimentation particle losses in leak flow paths was fit to the frame penetration data.

V.F.2. Conclusions from Media Pack Evaluations

Analysis of data on media pack performance indicates that many of the filter units had pre-existing media pack leaks. In this study these leaks were referred to as internal leaks. The leaks have leak rates as high 0.015% and dominate media pack performance outside the region of maximum media penetration defined by fibrous filtration theory. Internal leak flow, except in one instance, appears to be in the Poiseuille laminar flow region. A model that considered diffusional and gravitational sedimentation particle losses in leak flow paths was fit to the media pack penetration data.

V.F.3. Conclusions from Whole Filter Evaluations

Estimates of whole filter penetration made from frame and media pack penetration data show good agreement with whole filter penetration data. This finding suggests that frame and media pack penetration fully account for penetration through the entire filter unit. Leaks that affect whole filter performance were found to be largely in the Poiseuille laminar flow region. Consequently, the convection component of leak penetration

is independent of Δp. Variation of leak penetration with filter unit flow rate and particle size was explained in terms of diffusional and gravitational sedimentation particle loss in leak flow paths.

CHAPTER VI. IMPLICATIONS AND FOLLOW-ON STUDIES

Results from this study potentially have important implications for health and environmental protection issues associated with the use of nuclear grade HEPA filter air cleaning systems. In this chapter connections are made between study results and these issues. First, study results are interpreted in terms of effects on HEPA filter performance. Then the potential ramifications of the performance effects are described for specific components of aerosol emission control and monitoring programs. Finally, follow-on studies coming from questions raised during the investigation are described.

VI.A. Leak Effects on Filter Unit Performance

Even though leaks were found in every filter unit, in no case did the leaks compromise filter unit performance to the point they would fail the filter quality assurance tests (DOE90). Penetration measurements on unloaded units were all less than the penetration limit of 0.03%.

Leaks found in filter units were shown to affect how filter unit penetration depends on aerosol particle size, on flow rate, and on loading.

These aspects of HEPA filter unit penetration are not evaluated by current quality assurance tests. In this section, study results are used to illustrate these effects on penetration and highlight operating conditions under which these effects may affect health and environmental protection.

VI.A.1. Penetration Dependence on Particle size

The dependence of penetration on particle size predicted by filtration theory is shown by the solid line in Figure VI-1 for nuclear grade HEPA filter media operating at Q_{de}. Penetration is expected to decrease dramatically for particle sizes above the size of maximum penetration. For example, at a particle diameter of 1 μm predicted penetration is approximately 10^{-20}.

The predicted dependence of penetration on particle size has a profound effect on the expected aerosol size distribution penetrating filter media. In Figure VI-2, the expected count median diameter (CMD) of aerosol penetrating HEPA filter media is plotted against the CMD of a challenge aerosol with a log normal size distribution having a geometric standard deviation of 2. The CMD of the penetrating aerosol predicted by filtration theory increases slowly with challenge CMD. At a challenge CMD of 20 μm the penetrant CMD is less than 0.3 μm. The plot shows that

filtration theory predicts that very few large particles (e.g. particles with diameters > 1 μm) penetrate the filter media. It has generally been assumed that the performance of the entire filter unit is determined by filter media performance (Os92, Dy92, Ni92, and Mc93). Consequently, almost no large particles have been expected to penetrate HEPA filter units.

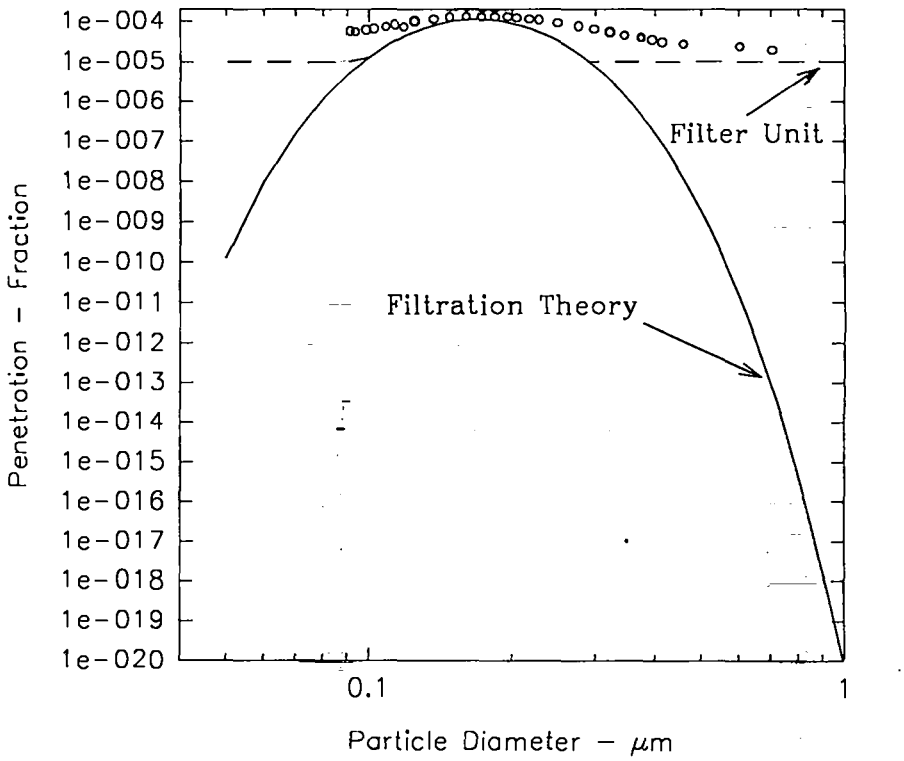

Figure VI-1. Plots of media penetration predicted from filtration theory, average filter unit penetration (open circles), and an approximation of filter unit penetration (dashed line).

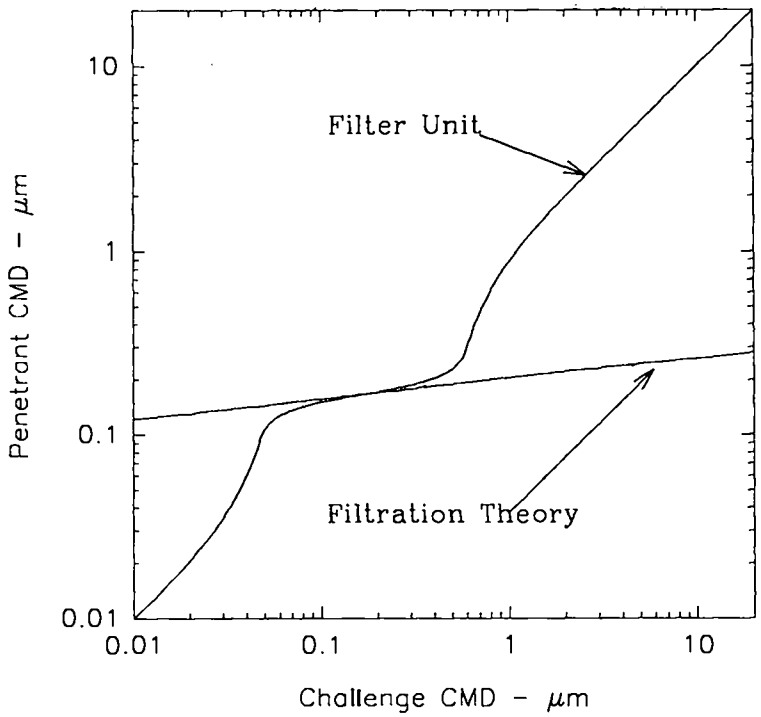

Figure VI-2. Predictions of penetrant aerosol count median diameter (CMD) from filtration theory and from idealized filter unit performance. Geometric standard deviation is 2.0.

Results of this investigation indicate performance of HEPA filter units are predicted by filtration theory in only a narrow range of operating conditions (See Figure V-10). Average values of penetration from whole filter tests performed in the formal study are plotted in Figure VI-1 for Q_{de}. These values match the predictions only in a small range of particle diameters near the size of maximum penetration. For particle diameters

above the size of maximum penetration, average penetration appears to approach a value of 10^{-5}.

An approximation of this averaged performance is shown in Figure VI-1. In the vicinity of the size of maximum penetration, filter unit penetration is given by the predicted filter media penetration. Outside this region, filter unit penetration is assumed to equal 10^{-5}. This idealized filter unit penetration either equals or is less than the average values shown in Figure VI-1. Outside the particle diameter range shown in Figure VI-1 filter unit penetration is expected to drop below 10^{-5} because of particle loss in external and internal leak paths (See Section II.D.).

The idealized HEPA filter unit leak performance was used to calculate CMD of aerosol penetrating a filter unit. Results of these calculations are shown in Figure VI-2 for a challenge aerosol with a log normal size distribution having a geometric standard deviation of 2. Penetrant CMD for the HEPA filter unit intersects that calculated from filtration theory only for an aerosol with a challenge CMD equal to the size of maximum penetration. At greater challenge CMDs the filter unit penetrant CMD exceeds that predicted from filtration theory. For challenge aerosols with smaller CMDs the filter unit penetrant CMD is below that predicted from filtration theory. Away from the region of maximum penetration, HEPA filter unit penetrant CMD approaches the

challenge CMD. This result suggests that the size distribution of aerosol penetrating HEPA filter units is primarily determined by the size distribution of the challenge aerosol and not by the media in the filter unit.

VI.A.2. Penetration Dependence on Flow Rate

The dependence of penetration on flow rate predicted by filtration theory is shown in Figure I-2 for nuclear grade HEPA filter media and in Figure I-3 for HEPA filter media. In contrast, measurements on HEPA filter units made in this study and other studies (Ko80, Sc86, Sc87b, Hi87a, Hi87b, and Bi88) show departures from this predicted dependence due to leaks in the filter units.. These departures have been described in Sections I.C.2.b and V.B.1.

Leak flow character determines the dependence of penetration on flow rate. All but one of the filter units evaluated in the formal study displayed Poiseuille laminar leak flow. Figure II-2 illustrates penetration dependence on filtration velocity for a filter unit with leaks operating in the Poiseuille region neglecting leak particle loss. An example of experimental results for a filter unit with leaks operating in this region is

shown in Figure IV-2. In both figures penetration is observed to decrease with flow rate.

Non-Poiseuille leak flow was observed in one of the filter units evaluated in the formal study. Expected performance of filter units with non-Poiseuille leaks is illustrated in Figure II-1. Penetration in these units is expected to increase as flow rate decreases over a specific range of flow rates. Such a penetration increase was observed in whole filter and media pack tests of filter unit 3597 (see Figure V-9). The media pack test results show penetration increasing from values below 5×10^{-5} to values just below 10^{-4} at flow rates $\leq$142 LPM. The increase in penetration is balanced against decreases in penetration because of particle loss in leak paths. Under the filter unit operating conditions and leak geometry evaluated here these losses are expected to increase as flow rate decreases.

The penetration increase characteristic of non-Poiseuille leaks is a mechanism by which filter unit penetration may potentially exceed quality assurance test limits. This will likely occur when flow rates are below Q_{de}.

VI.A.3. Penetration Dependence on Filter Unit Loading

Study results implicate filter unit leaks as a cause of an increase of penetration with loading (See Section V.D.2.b). Interpretation of the results suggests that the penetration increase could be proportional to the increase in differential pressure that a filter unit undergoes as it loads while operating at a constant flow rate. Commonly, differential pressure across banks of HEPA filter units is allowed to increase by approximately a factor of five before units are replaced. For unloaded units just meeting the penetration limit the differential pressure increase could translate into a filter unit penetration as high as 0.15%. The likelihood of all units in a bank having initial penetration at this limit is remote. Average filter unit leakage observed in this study was on the order of 10^{-5} (See Section VI.A.1). The penetration of such units could increase to approximately 5×10^{-5} under the above replacement criteria. Penetration above the quality assurance limit is potentially possible for loaded filter units with non-Poiseuille leaks operating below Q_{de}.

VI.B. Health and Environmental Protection Implications

A number of observations from this study support conventional wisdom regarding performance of HEPA filter units. For example peak penetration of unloaded filter units operating at Q_{de} was observed to coincide with the maximum penetration predicted by filtration theory. Conversely, certain conclusions from this study run counter to a number of conventions about the performance of HEPA filter units. HEPA filter units have been generally thought to prevent penetration of large aerosol particles. In this study the presence of large particles downstream of HEPA filter units was shown to be a result of filter unit leaks and was linked to challenge aerosol particle size. Penetration of HEPA filters is generally thought to decrease dramatically as flow rate is lowered. This study indicates conditions under which filter unit penetration can either decrease slowly, remain unchanged, or increase, when flow rate is lowered. HEPA filter penetration is generally thought to decrease with loading. In this study under certain conditions penetration was observed to increase with loading. This new understanding of HEPA filter unit performance may require that certain philosophies used in development of aerosol emissions control and monitoring programs be revisited. In this

section, the potential ramifications of this study are described in terms of these philosophies.

VI.B.1. Design, and Construction of HEPA Filter Units

To assure performance of nuclear grade HEPA filters in critical health and environmental protection applications strict requirements for their design and construction have been adopted (MS88 and DOE88). Filter unit models must pass specific destructive tests to be included in a list of products qualified for use in these crucial applications. Each individual unit undergoes quality assurance testing prior to being installed in an air cleaning system.

Filter units evaluated in this study were subject to the qualifications and quality assurance testing described above. Purchase orders for the filter units required that filter design and construction meet US DOE standards (DOE88). The filter units passed quality assurance tests performed at a US DOE Filter Test Facility. Consequently, leaks found in the filters and the effects the leaks had on filter performance were within the limits defined by these standards.

While current standards allow a certain degree of leakage, design and construction practices do exist that could reduce this leakage to levels below that observed in this study. Examples of such practices are those used to manufacture ultra low penetration air (ULPA) filters. These filters are routinely produced with penetration well below the levels observed in this study. ULPA filters are used in clean rooms where restrictions on particle emissions, on a particle count basis, can exceed those for nuclear facilities. While the ULPA filters have lower penetration ratings than the nuclear grade HEPA filters (IES86) they are not constructed to the same requirements for withstanding hostile environments. Consequently, the ULPA filters cannot be viewed as viable replacements for HEPA filters. What can be taken from the development of ULPA filters is an understanding of how leaks in filter units can be reduced.

Development of ULPA filters built on the technology for HEPA filter units. A major difference between the two types of filters is the media. ULPA media is composed of fibers with a smaller effective diameter than HEPA media. These finer fibers result in ULPA media having a lower penetration and higher pressure drop than HEPA media (Li85b).

The lower penetration advantage of ULPA media would be compromised if leakage in ULPA filter units was at levels observed in this study. Consequently, development of ULPA filter units required improved

construction materials and techniques that reduce filter unit leakage. Frame leakage was reduced by using seamless plastic frames. Media pack leakage was reduced by in a number of ways. Quality control on the media reduces defects in the media. One aspect of this media quality control was to control the uniformity of the fibrous glass used to make media. Some by-products of glass fiber production are called "shot". Shot are small glass beads produced during glass fiber production. The dimensions of these by-products can be much greater than the nominal fiber diameter. They can be incorporated into media during production where they cause inhomogenities. If they drop out of the media they can leave voids that locally reduce media thickness or even penetrate the media. The occurrence of these media defects can be minimized by controlling shot production.

Another means to reduce leakage in ULPA filter units is to locate and repair leaks as prescribed by the Institute of Environmental Sciences (IES86). This method can detect leaks in the media and in the seal between the media pack and frame. Two main sources of media leaks are: 1) defects in the media such as the shot problems described above, and 2) damage to the media during construction and handling. Standards for ULPA filters require scan testing of ULPA media packs for leaks and repair of leaks found during scanning (IES86). HEPA filters are not

required to be scanned and only seal leaks can be repaired. Repairs to HEPA media are thought to potentially weaken the media strength and consequently reduce filter unit ability to withstand certain off-normal conditions. Such repairs to HEPA filter media are specifically forbidden.

Leakage in nuclear grade HEPA filter units could potentially be reduced through changes in construction materials and fabrication procedures. Results of this study indicate frame leaks in wood frame filter units result from aerosol penetration through plywood. These leaks could be reduced by constructing frames from impervious materials. Plastic frames are used in ULPA filter construction. While this plastic may be less penetrable than wood, the ability of the plastic to withstand hostile environments, in which HEPA filters are sometimes used, needs evaluation.

Metal frames are allowed by current nuclear grade HEPA filter standards (DOE88, MS88). This material is also probably less penetrable than wood. However, the vast majority of HEPA filters used in US nuclear facilities are wood framed. The wood framed filters cost less than the metal framed filters. The popularity of the wood framed HEPA filters may be related to this cost differential.

Frame leakage may also be reduced by adopting procedures for eliminating leaks through frame joints. The greatest frame leak observed

in this study was found to be the result of a leak in a frame joint seal. This seal leakage can be reduced by scanning all frame joints and sealing any leaks that are found. Another approach for reducing this leakage is to use seamless frames such as those used in ULPA filters. These frames require different construction techniques than are used to assemble filter units with jointed frames.

Results from this study show that, at least for small nuclear grade HEPA filters, the major leak source are media pack leaks. These leaks include leaks in filter media and leaks in the seal between the media pack and frame (See Figure III-1). Three approaches used in ULPA filter construction to reduce these types of leaks are 1) media quality control, 2) extra-care taken to avoid handling damage, and 3) scan testing and leak repair. The first two of these approaches are probably already used to some degree in construction of nuclear grade HEPA filters. The third approach is probably not fully used in the manufacture of HEPA filters. Scan testing is not required by standards for HEPA filter construction. Limited scan testing is performed on HEPA filters to find and repair leaks in media pack seals. This testing and repair need only be done on nuclear grade HEPA filters whose penetration is at or above quality assurance limits. Extending this testing and repair to all filter units could reduce this type of leakage for the entire filter population.

Results of this study also indicate that filter unit air flow resistance is determined by the intact media while, over much of the filter operating domain, penetration is determined by filter unit leaks. Costs of filter unit operation depend on air flow resistance. The greater the resistance the greater the electrical utility costs for moving air through filters. In general resistance for a given type of filter is inversely related to media penetration. Low penetration media has a higher air flow resistance than media with high penetration.

Consequently, costs of operating the filters are determined by the media while performance is determined by filter unit leaks. At the same operating costs, filter units without leaks may have much better performance than filter units with leaks. Savings in operating costs without sacrificing performance may be possible by adjusting media formulation so that media penetration more closely matches that of the filter unit.

VI.B.2. Design of HEPA Filter Systems

Aerosol penetration through HEPA filter air cleaning systems can be separated into three regimes: 1) penetration dominated by intact filter media, 2) penetration dominated by filter unit leaks, and 3) penetration

dominated by leaks in system components other than filters. These system penetration regimes are distinguished by magnitude of penetration and the dependence of penetration on aerosol particle size. System penetration values are the lowest in the intact media regime. In this regime system penetration dependence on particle size is given by filtration theory (See Figure VI-1). System penetration in the filter leak regime is greater than system penetration in the intact media regime but is less than 0.03%. Size dependence in this regime is determined by particle loss in filter leak paths. The highest potential system penetration values are in the system leak regime. System leaks include for example leaks between filter gaskets and the system sealing plate; leaks at penetrations through the sealing plate; leaks around the periphery of the sealing plate where welding of the sealing plate to the filter housing may not be leak proof. Penetration in the system leak regime can be greater than 0.03%. Penetration dependence on aerosol size is determined by particle loss in system leaks.

Typically nuclear grade HEPA filter systems are designed assuming overall system penetration is in the system leak regime. The design is considered conservative for a number of reasons. First nuclear air cleaning systems are constructed to rigorous specifications such as ANSI/ASME N509 (ANSI76, ANSI80b, and ASME89a). These

specifications call for system designs and construction techniques that minimize leakage. Second, the systems are acceptance tested using procedures such as those in ANSI/ASME N510 (ANSI75, ANSI80a, and ASME89b). These tests assure that system leakage other than that associated with filter gaskets is within acceptable limits. Third, all HEPA filters used in the systems must pass quality assurance tests which assure that filter unit penetration is less than 0.03%. Fourth, continued system performance is assured with periodic in-place system tests. These tests assure that overall system penetration is less than some leakage limit which is typically on the order of 0.05%. Finally, the assumption of system penetration being in the system leak regime is thought to be conservative because filtration theory predicts very low penetration outside the aerosol size region of maximum penetration (See Figure VI-1).

Recent reviews of HEPA air cleaning systems at DOE facilities found several areas for improvement (Mo94). Many of the air cleaning systems were designed and built prior to the issuance of the ANSI/ASME standards. The majority of the systems were found to not meet requirements of these standards. However, many of the precautions described above and included in the standards have been incorporated into system design, construction and operation. System design and construction focused on minimizing leakage. Filters used in the systems

were quality assurance tested. In-place test were performed periodically. However, the degree of protection provided by these systems is uncertain. Few of the systems were acceptance tested. Acceptance testing establishes the validity of in-place tests and determines inherent system leakage. Without acceptance testing the accuracy of in-place tests is unknown.

Results from this study may also affect the degree to which designs of nuclear air cleaning systems are conservative. Filter unit penetration was found not to follow predictions of filtration theory. In aerosol size regions away from the penetration maximum, filter unit penetration was observed to drop to an average of approximately 10^{-5} (See Figure VI-1). This penetration is far greater than the penetration predicted by filtration theory in these regions. In addition the study indicates that filter unit penetration may increase as the unit loads. A five fold increase in filter unit air flow resistance may lead to same relative increase in filter unit leak penetration. From the results of this study, on average leak penetration could increase from 10^{-5} to 5×10^{-5}. For filter units operating at the quality assurance acceptance limit of 0.03% penetration, loaded filter penetration could be as high as 0.15%.

These factors all contribute to the uncertainty in the degree of protection afforded by nuclear air cleaning systems. In addition to these

uncertainties significant reductions in air emission limits have occurred over the past few decades. Over the lifetime of many DOE nuclear facilities these limits have decreased by a factor of 50. With the 1990 revisions the Clean Air Act current limits may be reduced by more 100 times in the near future. The uncertainties coupled with the reduced emission limits are narrowing the margin of safety traditionally attributed to nuclear air cleaning system designs.

VI.B.3. HEPA Filter Qualification and Quality Assurance Testing

As mentioned above nuclear grade HEPA filters undergo rigorous qualification and quality assurance testing. Filter unit models are qualified in a series of destructive tests that evaluate performance under various adverse conditions. For example, certain tests are conducted to assess effects of elevated temperatures and high differential pressures on filter unit penetration. These tests involve determining filter unit penetration before and after a specified adverse condition exposure.

Quality assurance tests are non-destructive tests performed on each filter unit prior to installation. These tests are conducted to determine such performance parameters as filter unit penetration and air

flow resistance. The penetration tests are the same as those used in qualification. The tests entail determination of penetration at a particle size in the range of the predicted media penetration maximum. Results from this study indicate that maximum filter unit penetration occurs in this region. The tests are performed at both Q_{de} and 20% of Q_{de}.

Results from quality assurance penetration tests provide an estimate of overall filter unit penetration. This penetration includes the combined effects of intact media penetration and penetration from external and internal filter unit leaks. The penetration estimate is conservative in that penetration over any other range of aerosol particle sizes should not exceed the estimate. However, these penetration tests do not provide independent assessment of media or leak penetration. Independent assessment of these penetrations may be important in predicting field performance of filter units in normal and off-normal conditions. Independent assessment of leak penetration in quality assurance tests could be used in limiting filter unit leakage. Such a leakage limit combined with a filter unit loading limit would determine an upper bound on penetration increase as a result of loading. For example, limiting leakage to 6×10^{-5} and loading to less than a five fold increase in differential pressure is expected to limit overall filter unit penetration to 0.03% or less. For this loading limit, higher leakage rates than 6×10^{-5} could result in

overall penetration of loaded filter units increasing to levels above the quality assurance acceptance limit.

Independent assessment of leak penetration could be used to determine flow character of filter unit leaks. When leak flow path particle loss is negligible, leak penetration is expected to be unaffected by filter unit flow rate for leaks in the Poiseuille laminar flow range. If leak path particle loss dominates, filter unit penetration is expected to decrease with flow rate. Penetration in filter units with non-Poiseuille leaks is expected to increase as filter unit flow rate decreases. Determining filter unit leak flow character is important in air cleaning systems designed to provide protection over a wide range of system flow rates.

Independent assessment of leak penetration in qualification tests could be used to determine the affects of exposure to elevated temperature and high air flow resistance on filter units leaks. Such exposures may have different effects on media penetration and leak penetration. Differentiating these effects is important in determining interaction of factors affecting filter unit performance. For example loading affects filter unit penetration in more than one way. Loading affects penetration by decreasing the ratio of leak air flow resistance to intact media air flow resistances described in Section V.D.2.b. Loading independently affects filter unit penetration by stressing weak areas of the

filter unit and deforming leak geometry in these areas. The interaction of these effects could result in a super-linear relation between filter unit penetration and loading.

One approach for assessing filter unit leak penetration is as follows. For penetration tests that use an aerosol spectrometer, the normal challenge aerosol would be augmented with a monodisperse aerosol having a particle diameter in the range where leaks dominate penetration. The monodisperse aerosol would be generated for example, from the nominal 1 μm diameter standard reference micro-sphere material available from NIST. Penetration of the monodisperse aerosol would be an independent assessment of filter unit leakage. With the augmented challenge, quality assurance tests at Q_{de} would be used to determine filter unit leakage. Results from tests at Q_{de} and 20% Q_{de} would be analyzed to determine flow character of filter unit leaks.

The augmented challenge could also be used to expand information available from qualification tests. Results from pre- and post-exposure tests using the augmented challenge may be analyzed to differentiate between exposure effects on media and exposure effects on leaks. Exposures that increase filter unit leakage may exacerbate loading effects on filter unit penetration. Consequently, loading limits based on

unexposed filter leakage may not be adequate to assure that the increase in penetration due to loading is within quality assurance acceptance limits.

VI.B.4. HEPA Filter System Operation

Operators of hazardous material air cleaning systems must understand limits of system design and conditions under which challenges to systems may exceed these limits. For HEPA systems these limits and conditions depend on the penetration regime in which the system is operating. The penetration regime determines how the size distribution of the challenge aerosol affects system performance, how system performance is affected by system flow rate, and how loading affects system performance.

VI.B.4.a. Aerosol Size Effects on System Operation

Performance of systems operating in the intact media regime is assumed to be predicted by filtration theory. For challenge size distributions with count median diameters above approximately 0.3 μm, penetrant size distributions are largely independent of the challenge size

distribution (See Figure VI-2). Penetration for these challenge aerosols drops rapidly with increasing particle size. Consequently, performance depends little on operation of facility processes upstream of the air cleaning system capable of producing these challenges.

Filtration theory may not predict performance of systems operating in the filter unit leak or system leak regimes. Performance in these regimes may differ from performance in the intact media regime in a number of ways. Size distribution of penetrant aerosol may be affected by upstream processes producing challenge aerosols with CMDs greater than 0.3 μm, increasing with increasing challenge size distribution.

Emission levels may be much more closely linked to the operation of these processes than they would be for air cleaning systems operating in the intact media regime. For example processes producing micrometer size aerosols may affect emission levels from air cleaning systems operating in the filter unit leak or system leak regimes. These effects may be greatly diminished for systems operating in the intact media regime because of the extremely low penetration expected from filtration theory for aerosol particles of this size. For the same reason emission levels may be much greater for systems operating in the leak regimes than those operating in the intact media regime when challenge aerosols are composed of the micrometer size particles.

When operating in the leak regimes, peaks in aerosol emission levels may be related to the aerosol output of processes and the operational status of the processes. For example increases in emissions levels might be expected with operation of processes that produce high aerosol concentrations of the large size particles. Levels would be expected to drop when operation of these processes ceases. For systems operating in the intact media regime, emission levels may be independent of changes in operation of processes that produce high concentrations of large particle aerosols.

Approaches for assuring control of air emissions depend on interaction between system operating regime, and the operational status and output of processes served by the air cleaning system. Assuring control for systems operating in leak regimes requires knowledge of both the processes served by the system and the system itself. Strategies such as limiting operation of processes that produce high concentrations of large particles may be appropriate for air cleaning systems operating in the leak regimes and not necessary for systems operating in the intact media regime.

Understanding process aerosol output under off-normal or upset conditions is important for assuring emission control under these conditions. As an example emissions control may be compromised when

off-normal process operation produces high aerosol concentrations of large particles. Assuring control may require anticipation of such occurrences, planning alternative control strategies, and maintaining excess air cleaning capacity. The amount of excess capacity will depend on challenge aerosol size and the penetration regime in which the air cleaning system is operating.

VI.B.4.b. Flow Rate Effects on System Operation

Just as filter unit performance depends on flow rate so does system performance. Flow rate effects on system performance depend on system operating regime. Performance of systems operating in the intact media regime is expected to improve as system flow rate is lowered. As flow rate is lowered, performance of systems operating in the leak regimes can improve, remain unchanged, or degrade depending leak flow character and leak path particle loss. Data collected in this study shows that when leak flow character matches that of the entire filter unit, filter unit performance can improve or remain unchanged as filter unit flow rate is reduced. Improved performance is expected when leak path particle loss dominates filter unit penetration. Performance independent of flow rate is

expected when the particle losses in leak flow paths are negligible. Degradation of performance with decreasing flow rate associated with non-Poiseuille leak flow. Similar flow rate effects on system performance are expected.

Variations in system flow rate are expected in a number of situations. Flow rates above nominal design may occur in existing systems when ventilation capacities are increased without commensurate increases in air cleaning capacities. Flow rates above or below design levels may occur when automatic damper systems malfunction.

Extremely low flow rates may occur under loss of power situations. One approach to deal with such situations in nuclear facilities involves maintenance of uninteruptable power supplies. These supplies assure that ventilation/air cleaning systems can operate to minimal standards even when electrical power to a facility is lost.

Another approach to deal with loss of power situations is safe shutdown procedures which allow facilities to breathe at free convection flow rates by opening system dampers. Under nuclear facility creditable accident scenarios ventilation/air cleaning systems are expected function under these conditions for extended periods.

An indication of the protection afforded by HEPA filter air cleaning systems at the extremely low flow rates may be obtained by extrapolating

results from this study for filter unit performance. The degree of protection afforded by HEPA systems depends on the system operating regime. The most likely regime when operating at the extremely low flow rates would be one of the leak regimes.

In these regimes system performance is expected to remain unchanged or improve with decreasing system flow rate for leak flow in the Poiseuille region. For non-Poiseuille leak flow, penetration may increase as system flow rate is decreased. In a worst case, leak flow is in the non-Poiseuille region and system penetration, P_S, would be proportional to $Q_S^{-1/2}$, where Q_S = the system flow rate (See Section II.A). System emission rate, E_S, can be written as:

$$E_S = C_c \bullet Q_S \bullet P_S \qquad \text{Equation VI-1}$$

where, C_c = the challenge aerosol concentration. For P_S proportional to $Q_S^{-1/2}$, E_S is proportional to $Q_S^{1/2}$. Consequently, protection is expected to improve because emission rates decrease as system flow rates drop.

VI.B.4.c. Loading Effects on System Operation

Extrapolation from the filter unit results of this study indicates HEPA air cleaning system performance may degrade with loading when system operation is in one of the leak regimes. Leak penetration of filter units was observed to increase with loading. The increase was linked to preferential loading of intact media flow paths relative to leak flow paths. The media paths are also expected to load preferential to system leak paths. Consequently, performance of systems operating in a leak regime will likely degrade with loading.

Systems operating in the intact media regime may be pushed toward operation in the leak regimes as filter units load. With loading, media penetration of filter units is expected to decrease at the same time that leak penetration is increasing. The resultant affect of these actions is to move filter performance to leak dominated penetration regimes. This performance change is also expected for systems operating in the intact media regime where media paths are loading preferentially to system leak flow paths. Consequently, loading is expected to push system operation in the direction of the leak regimes.

After sufficient loading, system operation could shift to one of the leak regimes. For systems operating in the intact media regime the shift

could affect system performance. This shift could change the effects that upstream process outputs have on the size distribution of emissions, and on emission levels. The shift could affect the dependence of system performance on flow rate.

VI.B.5. Aerosol Emissions Monitoring

Emissions from HEPA air cleaning systems are typically monitored prior to being released to the atmosphere. This monitoring can be used to detect unplanned emissions, to document routine emissions, and to demonstrate compliance with emissions standards (CFR91).

Challenges to the monitoring systems are an important variable in their design and operation. The range of challenge aerosol sizes affects specifications of aerosol sampling and transport hardware and may influence interpretation of monitoring results. For example particles with aerodynamic diameters over one micrometer may require isokinetic sampling to assure collection of representative samples.

The nature of the aerosol at the emission monitors is determined by air cleaning system challenges and the performance of the air cleaning system. For systems operating in the intact media regime, performance

can be predicted by filtration theory. The theory predicts negligible penetration of particles large enough to require isokinetic sampling (See Figure VI-2). Some operators of HEPA filter systems have used this prediction to justify relaxing isokinetic sampling requirements (Os92, Dy92, Ni92, Mc92).

Isokinetic sampling is required for systems operating outside the intact media regime. The size distribution of emissions from air cleaning systems operating in the leak regimes depends on the size distribution of the system challenge. Air cleaning system challenges containing particles large enough to require isokinetic sampling may result in emissions monitoring that also requires isokinetic sampling (Ni92). The large particles can account for a substantial portion of emissions. Underestimation of the large particle contribution can result in significant underestimation of total emissions.

VI.B.6. Aerosol Emissions Exposure Assessment

One component of the assessment of exposure to aerosol emissions is the evaluation of environmental source characteristics. These characteristics can affect emission transport as well as receptor

dose. For aerosol emissions, the source characteristics depend on the penetration regime in which the facility air cleaning system is operating. Assumptions made in the exposure assessment based on air cleaning operation in the intact media regime may have to be reevaluated if operation is found to be in either of the leak regimes.

Air cleaning system operating regime can affect a number of the source characteristics important to exposure assessment for aerosol emissions. Operating regime can affect the size distribution of aerosol emissions. The size distributions of emissions from systems operating in leak regimes can be larger than those from systems operating in the intact media regime. The larger size distributions can potentially affect estimates of receptor dose in two ways. First, the larger distributions can be associated with higher receptor exposure concentrations. For the same number concentration, aerosols composed of larger particles have a higher mass concentration than those composed of smaller particles. The mass concentration difference is a result of the geometric relation between particle size and particle mass. Aerosol particle mass varies with the cube of particle diameter. Consequently, a micrometer aerosol with a given number concentration contains 1000 times the mass of a tenth micrometer aerosol with the same number concentration. At the same time, the process energy required to produce a unit mass of the smaller aerosol is

much greater than that for the larger aerosol. The thrust of these relations is directed towards emission mass concentration increasing with emission size distribution. For example, this relation between concentration and size is observed in welding/cutting torch operations which produce low concentration sub-mircometer size aerosol emissions and grinding operations which can produce higher concentrations of micrometer size aerosols. Notwithstanding size dependent transport effects, the receptor exposure concentration for a larger size aerosol emission could reasonably be expected to be higher than that for the smaller size emission because toxic activity is frequently related to aerosol mass concentration.

The second potential receptor dose affect is related to the dependence of lung deposition factor on aerosol particle size. For particles above a half micrometer but less than 10 μm aerodynamic diameter the larger the particles the higher deposition factor in lung (Hi82). This means not only do the larger particles possibly result in a high exposure concentration at the receptor but per unit exposure the larger particles may result in a higher fraction of the exposure being deposited in lung. Independent of uptake effects related to aerosol size, the higher deposition factor can lead to a greater dose per unit of exposure.

Other source characteristics that can be affected by air cleaning system penetration regime are emission levels and emission rates. Emission levels may be linked to process output and operation, if the air cleaning system is operating in a leak regime. In the leak regimes, emissions may rise as the air cleaning system loads. Emission rates may not drop as fast as expected from filtration theory for systems operating in the leak regimes when system flow rate is reduced.

These examples of the potential effects that system penetration regime may have on exposure assessment illustrate the need to revisit assumptions made in exposure assessment in the light of the findings of this study. The particular effects that study results may have depend on a number of factors such as transport conditions and aerosol material toxicity. For example, the increase in receptor exposure concentration related to large particles could be mitigated if particle losses between source and receptor increase with particle size. If the site of toxic action is remote from lung, the dose effect of deposition factor could be compensated for by a decrease in in vivo transport efficiency of the toxic material with increased aerosol size. Thus, the specific effects the present study results may have on exposure assessment depend on the context in which the assessment is made.

VI.C. Follow-on Studies

During the course of this study a number of technical issues were raised that could not be addressed completely within the scope of the current work. Follow-on studies to address these issues are described in this section. For each study, the issue is outlined, the need to address the issue is described, and finally, potential approaches to study the issue are discussed.

VI.C.1. Performance of Multiple Non-Poiseuille Leaks

Review of ideal leak flow performance (See Section II.B.2.b) revealed that a pair of non-Poiseuille leaks could not be mimicked by the performance of single equivalent leak using the Kreith and Eisenstadt approach. The explanation of this result is unclear at this point. However, one potential explanation is that multiple non-Poiseuille leaks cannot be represented by a subset of equivalent leaks.

If this explanation is accurate then modeling non-Poiseuille leak flow may be difficult. The review of ideal leak performance indicated that multiple leaks operating in the Poiseuille laminar flow region could be

represented by a single equivalent leak. This property of the Poiseuille leaks simplifies modeling of flow through complex leak geometries. The flow behavior of such geometries can be predicted from a set of equivalent leaks with specific diameters and lengths. No information about actual leak geometries is needed. If no such equivalent set exists for non-Poiseuille leaks then predicting leak flow in these situations may require detailed leak geometry information. Obtaining such information is often not possible.

Understanding flow in non-Poiseuille leaks may be important in certain health protection scenarios. Hinds et al (Hi87a, Hi87b) first used the Kreith and Eisenstadt correlation to explain leak flow data from air purifying respirators. A computer simulation of respirator fit tests by Tillery (Ti92) determined that under many conditions non-Poiseuille leaks were an essential feature in predicting respirator performance. In this study, non-Poiseuille laminar leak flow was observed in one filter unit. Examination of potential filter unit performance showed that the likelihood of non-Poiseuille leak flow increased with filter unit size. The vast majority of filters used in nuclear facilities are larger than the units evaluated in this study. Consequently, non-Poiseuille leak flow may be important in understanding aerosol emission controls in these facilities.

The possibility that the non-Poiseuille leakage is associated with multiple leak flow paths cannot be ruled out. While the degree of leakage is minimized in devices such as air purifying respirators with face seals and HEPA filter units, the precise number of leak paths remains uncontrolled. The target leakage for such devices is probably not zero but rather some value within acceptable limits as defined by appropriate standards. The focus is on meeting leakage limits, not assuring leakage is from a single leak path. Consequently, the multiple path non-Poiseuille leakage is a potentially important component in predicting device performance.

Recently negative pressure decay methods for evaluating respirator face seal leakage have been proposed by a couple of groups (Ca88, Cr91). An assumption made in these tests is that leakage can be modeled as an equivalent single flow path leak. This assumption appears to be valid in the Poiseuille laminar flow region. However, Tillery (Mi92) found that respirator leak flow undergoes a transition the to the non-Poiseuille region soon after the start of inhalation and remains in the region for most of the inhalation portion of the breathing cycle. Therefore, the assumption of single flow path equivalence may not be valid unless there is some assurance that respirator face seal leaks are the result of single flow paths.

Certain numerical and experimental studies could be performed to develop procedures for predicting performance of multiple non-Poiseuille leaks. A sensitivity analysis could be performed to determine if the variation in leak geometry observed in this study (See Section II.B.2.b) was attributable to imprecision in fitting the Kreith and Eisenstadt data. Laboratory measurements of the flow performance of multiple leaks could be used to evaluate predictions from the Kreith and Eisenstadt correlation and other theoretical formulations.

VI.C.2. Particle Losses in Non-Poiseuille Laminar Flow

Prediction of leak flow path particle loss in this study assumed leak flow in the Poiseuille laminar flow region. Theoretical formulations of particle loss mechanisms operating in this flow region were used to predict losses. Experimental observations of filter unit leakage in this study showed that almost all filter unit leakage was in Poiseuille region. Prediction of filter unit leak flow character suggests (See Section II.C) that leak flow in larger filters could commonly be in the non-Poiseuille region. Consequently, particle loss predictions in non-Poiseuille leak flow paths may be important in understanding performance of the larger filters.

Formulations for predicting losses in non-Poiseuille leaks currently do not exist. The absence of these formulations is a potential obstacle in characterizing performance of large filter units. The derivation of the non-Poiseuille formulations may be more difficult than the derivations for the Poiseuille flow case. A potential complicating factor is that in the non-Poiseuille case velocity profile changes with position along the leak flow path. The reason that non-Poiseuille flow differs from Poiseuille flow is that the entrance effect in the non-Poiseuille case is sufficiently large to modify the flow performance of the entire leak. The entrance effect resides over the initial portion of the flow path where the viscous flow boundary layer develops. The layer thickness increases in this region, growing inward from interior surface of the flow path. A certain distance along the flow path from the entrance, called the entrance length, the layer thickness has grown to occupy the entire flow path breadth. This is the first point along the flow path that the velocity profile characteristic of Poiseuille flow is established. This profile is maintained for the remainder of the path length.

The velocity profile upstream of this point varies with position along the flow path. Potential flow exists at the leak entrance, having a flat velocity profile. A shrinking potential flow core persists over the entire entrance length. The core vanishes at a position an entrance length from

the leak entrance. The core is surrounded by the developing viscous boundary layer. The core and developing boundary layer forms the varying flow profile for which particle losses in non-Poiseuille leaks must be evaluated. Formulations for the individual loss mechanisms must be developed that allow for the integration of the varying flow profile effects over the entrance length portion of the leak flow path. These formulations must also couple with the Poiseuille flow formulations that predict losses in the remainder of the leak flow path.

VI.C.3. Performance of Static Mixing Units for Micrometer and Larger Aerosols

Static mixing units designed for mixing gases were evaluated in this study for the mixing of sub-micrometer aerosols. Performance of the units in mixing the small particle size aerosols did not differ from their gas mixing performance. However, general use of these mixing units may not be restricted to aerosols composed of these particle sizes. Potential aerosol mixing applications for these units may involve particles larger than the particles evaluated in this study. Transport properties of these larger particles may affect mixer performance. The properties could affect

the degree of mixing provided by the mixers and particle losses in the mixers.

Both of these potential effects must be evaluated prior to the use of the static mixing units for the mixing of large particle aerosols. Theoretical and experimental evaluations similar to those performed in this study are appropriate for examination of these issues.

VI.C.4. Leak Performance of Large HEPA Filters

Review of HEPA filter specifications in Section II.C revealed that filter unit size can have an affect on parameters that determine the filter unit leak performance. Maximum filter unit leak flow rate was found to increase with filter unit size. The dependence of potential leak path length, the leak flow parameter, X, and leak diameter on filter size were developed in Section II.C.

A conclusion from the review was that leak performance of HEPA filter units depends on filter unit size. Larger filter units were more likely to display non-Poiseuille leak behavior than smaller units. These findings agree with experimental results of this study and others (Ko80, Sc86). In this study almost all leak flow was found in the Poiseuille laminar flow

region. Data on size 2 HEPA filter units (Ko80) showed crossing of penetration plots at a penetration of approximately 10^{-5}. The crossing is an indication of non-Poiseuille leak flow. Crossing was observed in penetration measurements on size 5 HEPA filter units at penetrations above 10^{-4} (Sc86). Crossing at higher penetrations suggests leak performance at lower values of X than does crossing at lower penetrations. This relation between X and filter size agrees with the trend between X and Q_{de} shown in Figure II-7.

As mentioned above filter units larger than the those evaluated in this study make-up the bulk of HEPA filters used in nuclear facilities. Consequently, the performance of these sizes of filters is most germane to assuring control aerosol emissions. The potential affects of filter unit size on leak performance limits simple extrapolation of experimental results from this study to the expected performance of larger filters.

The potential filter size effects suggests that additional studies on the larger filters are needed to accurately understand the performance of the larger filters. Experimental studies similar to those performed in this study should be carried out to assess performance of the larger filters. Interpretation of data from these studies will likely require information from the investigations of multiple non-Poiseuille leaks described above.

VI.C.5. Loading Effects on Fibrous Filter Unit Penetration

Filter unit penetration in this study was observed to increase with loading under two conditions. First, penetration increases in the region of maximum penetration were linked to loading with liquid aerosol particles. Second, penetration increases in regions where leaks dominate performance were associated with preferential loading effects on intact media air flow resistance (See Section V.D.2.b).

Understanding such loading effects is likely to be important in defining conditions where filter unit performance may not meet specifications required for assuring protection. An example of such conditions might be fire suppression situations where HEPA filters might become loaded with water spray.

VI.C.6. Field Studies on HEPA Filtration Systems

Translation of the findings of this study to the expected performance of HEPA filtration systems is uncertain. Follow-on field studies of existing systems are needed to evaluated the implications of findings from the current study on system performance. The field studies are needed to

determine whether effects observed in this study are manifested in terms of affects on system performance. For example, this study indicates that large particle penetration in HEPA filter units should be orders of magnitude greater than predictions of filtration theory indicate. However, HEPA filters are generally thought to prevent penetration of these large particles (Os92, Dy92, Mc92). Investigation of the presence of large particles downstream of HEPA filter banks would resolve this contradiction. Resolution of such issues is important because of the potential health and environmental protection implications of the results of the current study.

A variety of HEPA filter system studies are required. Studies similar to that reported by Nininger and Osborne (Ni92) are needed to determine large particle penetration in these systems. A potential improvement of the Nininger study would be the use of test aerosols. The Nininger study used field aerosols present in the air cleaning system at the time of the study. Although particles larger than 10 μm diameter were observed downstream of the HEPA filters, Nininger reported difficulty in interpreting the data because of low count rates of large diameter particles both upstream and downstream of the filtration bank. Use of test aerosols could increase these count rates.

Studies are needed to determine the penetration regime in which HEPA filter systems operate. These regime studies will require assessing dependence of system penetration on aerosol particle size and system flow rate. Results from these studies will enable prediction of system performance over a range of operating conditions.

Predictions of effects from system loading and system operation at low flow rates should be confirmed through additional studies. Observational loading studies could be performed on existing systems by repeating penetration measurements on a system as it progresses through a normal loading cycle. Low flow rate evaluation of system performance should be performed on systems prior to commissioning to limit the potential of release.

APPENDICES

Appendix A - Listing of Computer Codes

A number of computer codes were written in this course of this study. These codes are listed in this Appendix. All but one of the codes were written in BASIC using the Microsoft QuickBASIC Programming System Version 4.5. The BASIC codes run on IBM compatible personal computers.

The remaining code was written in HP BASIC. This is a programming language for Hewlett-Packard microcomputers. The code was written on a Model HP-85 microcomputer.

A.1. Code for Estimating Diffusion Losses in Leak Flow paths

The following code was written to estimate diffusion particle losses in leak flow paths. Algorithms used in the code and estimates determined with the code are discussed in Section II.D.1. This code was written in

BASIC using the Microsoft QuickBASIC Programming System Version 4.5 and runs on an IBM-compatible personal computer.

```
CLS
OPEN "777875d.dat" FOR OUTPUT AS 1
REM INPUT "I = ", I
I = 7.77875
p50 = .5
di = 10: REM mm
q = .0000043#: REM cm^3/sec
DO UNTIL di < .001
REM calculate D
k = 1.38E-16: REM dyn*cm/K
t = 293: REM K
la = .0857: REM mm
cc = 1 + (la / di) * (2.514 + .8 * EXP(-.55 * di / la))
pi = 3.14159
n = .000181: REM g/(cm*sec)
d = k * t * cc / (3 * pi * n * di * .0001): REM cm^2/sec
REM start Q do loop
diff = 1
```

```
DO UNTIL diff < .00001
mu = d * l / q
IF mu < .007 THEN p = 1 - 5.5 * mu ^ (2 / 3) + 3.77 * mu
IF mu > .007 THEN p = .819 * EXP(-11.5 * mu) + .0975 * EXP(-70.1 * mu)
+ .0325 * EXP(-179 * mu)
diff = ABS(p - p50)
q = q * 1.00001: REM cm^3/sec
LOOP
WRITE #1, di, d, q
x = l * pi * n / (4 * q * (.0012 * 585 / 760))
IF di > 10 THEN
di = di - .2: REM mm
ELSEIF di > 1 THEN
di = di - .1
ELSEIF di > .1 THEN
di = di - .05
ELSE di = di - .01
END IF
LOOP
CLOSE 1
```

A.2. Code for Estimating Interception Losses in Leaks

The following code was written to estimate interception particle losses in leak flow paths. Algorithms used in the code and estimates determined with the code are discussed in Section II.D.2. This code was written in BASIC using the Microsoft QuickBASIC Programming System Version 4.5 and runs on an IBM-compatible personal computer.

```
CLS
OPEN "ntrcep.dat" FOR OUTPUT AS 1
p50 = .5
dp = 1: REM µm
DO UNTIL dp > 20.1
d = dp: REM µm
diff = 1
DO UNTIL diff < .001
p = 1-((2 * d * dp - dp ^ 2) / d ^ 2)
diff = ABS(p - p50)
d = d * 1.001: REM µm
LOOP
d = d / 1.001
```

```
REM Calculate QL
REM Calculate XY^-1/2
l = 1.905: REM cm
n = .000181: REM g/(cm*sec)
pi = 3.14159
rhof = .001205 * 585 / 760: REM g/cm^3
difp = 1.3 * 1010000! / 408: REM dyn/cm^2
c = .4342944819#
xy12 = l * n * SQR(2 / (rhof * difp)) / (2 * ((d * .0001) ^ 2))
IF xy12 < .083431358914602# THEN
  x = 10 ^ (1.906687943581# + 2.332670369065# * c * LOG(xy12) +
.22204228140805# * ((c * LOG(xy12)) ^ 2))
  ql = l * n * pi / (rhof * x * 4)
ELSE
ql = pi * difp * ((d * .0001) ^ 4) / (128 * n * l)
x = l * n * pi / (rhof * ql * 4)
xxy = 64 * xy12 ^ 2
END IF
qlqde = ql / (25 * ((12 * 2.54) ^ 3) / 60)
dcm = d * .0001
WRITE #1, dp, dcm, ql
```

```
IF dp > 10 THEN
dp = dp + .2: REM μm
ELSE
dp = dp + .1
END IF
LOOP
CLOSE 1
```

A.3. Code for Estimating Gravitational Sedimentation Losses in Leaks

The following code was written to estimate gravitational sedimentation particle losses in leak flow paths. Algorithms used in the code and estimates determined with the code are discussed in Section II.D.3. This code was written in BASIC using the Microsoft QuickBASIC Programming System Version 4.5 and runs on an IBM-compatible personal computer.

```
CLS
OPEN "7787gs.dat" FOR OUTPUT AS 1
p50 = .5
```

```
dp = .1: REM µm
d = 250 * dp
DO UNTIL dp > 20.1
l = 7.77875: REM cm
rhop = 1: REM g/cm^3
g = 981: REM cm/sec^2
lam = .0857: REM µm
cc = 1 + (lam / dp) * (2.514 + .8 * EXP(-.55 * dp / lam))
n = .000181: REM g/(cm*sec)
pi = 3.14159
rhof = .001205 * 585 / 760: REM g/cm^3
vts = rhop * (dp * .0001) ^ 2 * g * cc / (18 * n): REM cm/sec
difp = 1.3 * 1010000! / 408: REM dyn/cm^2
c = .4342944819#
diff = 1
DO UNTIL diff < .001
REM Calculate QL
REM Calculate XY^-1/2
xy12 = l * n * SQR(2 / (rhof * difp)) / (2 * (d * .0001) ^ 2)
IF xy12 < .083431358914602# THEN
```

```
x = 10 ^ (1.9066687943581# + 2.332670369065# * c * LOG(xy12) +
.22204228140805# * ((c * LOG(xy12)) ^ 2))
ql = l * n * pi / (rhof * x * 4): REM cm^3/sec
ELSE
ql = pi * difp * ((d * .0001) ^ 4) / (128 * n * l): REM cm^3/se
x = l * n * pi / (rhof * ql * 4)
END IF
re = rhof * ql * 4 / (pi * d * .0001 * n)
e = .75 * (l * (d * .0001) * vts * pi / (4 * ql))
arg = ((e ^ (1 / 3)) / (SQR(1 - e ^ (2 / 3))))
asn = ATN((e ^ (1 / 3)) / (SQR(1 - e ^ (2 / 3))))
p = 1 - (2 / pi) * ((2 * e * SQR(1 - e ^ (2 / 3))) - (e ^ (1 / 3) * SQR(1 - e ^ (2 /
3))) + (asn))
diff = ABS(p - p50)
d = d + .001
LOOP
qlqde = ql / (25 * ((12 * 2.54) ^ 3) / 60)
dcm = d * .0001
PRINT dp, dcm, ql, xy12
WRITE #1, dp, d, ql
IF dp > 10 THEN
```

```
dp = dp + .2: REM μm
ELSEIF dp > 1 THEN
dp = dp + .1
ELSE
dp = dp + .05
END IF
LOOP
CLOSE 1
```

A.4. Code for Approximating Leak Performance of Filter Unit

The following code was written to approximate the leak performance of filter units with specified leak geometries. Algorithms used in the code and estimates determined with the code are discussed in Section II.D.5. This code was written in BASIC using the Microsoft QuickBASIC Programming System Version 4.5 and runs on an IBM-compatible personal computer.

```
CLS
OPEN "PEN10.dat" FOR OUTPUT AS 1
```

```
OPEN "PEN5.dat" FOR OUTPUT AS 2
OPEN "PEN2.dat" FOR OUTPUT AS 3
OPEN "PEN1.dat" FOR OUTPUT AS 4
OPEN "PEN05.dat" FOR OUTPUT AS 5
OPEN "PEN02.dat" FOR OUTPUT AS 6
OPEN "PEN01.dat" FOR OUTPUT AS 7
DIM dlp(200), Q(10), QL(10), Qel(10), Qil(10)
QDE = 25 * ((12 * 2.54) ^ 3) / 60: REM cm^3/sec
Nel = 10
Nil = 1
delp0 = 1 * 2490.82: REM dyn/cm^2
dlp(1) = delp0
dlp(2) = delp0 * .5
dlp(3) = delp0 * .2
dlp(4) = delp0 * .1
dlp(5) = delp0 * .05
dlp(6) = delp0 * .02
dlp(7) = delp0 * .01
P0 = .00001
l = 1.905: REM cm
l = 1
```

```
DO UNTIL I = 8

Q(I) = dlp(I) * QDE / delp0

QL(I) = Q(I) * P0

Qel(I) = QL(I) * .2 / Nel

Qil(I) = QL(I) * .8 / Nil

dp = .05: REM µm

DO UNTIL dp >= 1.01

REM calculate D

k = 1.38E-16: REM dyn*cm/K

t = 293: REM K

la = .0857: REM µm

cc = 1 + (la / dp) * (2.514 + .8 * EXP(-.55 * dp / la))

pi = 3.14159

n = .000181: REM g/(cm*sec)

diffu = k * t * cc / (3 * pi * n * dp * .0001): REM cm^2/sec

muel = diffu * I / Qel(I)

IF muel < .007 THEN Peld = 1 - 5.5 * muel ^ (2 / 3) + 3.77 * muel

IF muel > .007 THEN Peld = .819 * EXP(-11.5 * muel) + .0975 * EXP(-70.1

* muel) + .0325 * EXP(-179 * muel)

muil = diffu * I / Qil(I)

IF muil < .007 THEN Pild = 1 - 5.5 * muil ^ (2 / 3) + 3.77 * muil
```

```
IF muil > .007 THEN Pild = .819 * EXP(-11.5 * muil) + .0975 * EXP(-70.1 *
muil) + .0325 * EXP(-179 * muil)
rhop = 1: REM g/cm^3
g = 981: REM cm/sec^2
rhof = .001205 * 585 / 760: REM g/cm^3
vts = rhop * (dp * .0001) ^ 2 * g * cc / (18 * n): REM cm/sec
c = .4342944819#
xel = l * pi * n / (4 * rhof * Qel(1))
IF xel < .45082990128# THEN
yel = 10 ^ (1.8310496159345# + 1.1071308650233# * c * LOG(xel) +
.14510722167522# * ((c * LOG(xel)) ^ 2))
d = (8 * rhof * Qel(1) ^ 2 * yel / (dlp(l) * pi ^ 2)) ^ .25: REM cm
ELSE
d = (128 * n * l * Qel(1) / (pi * dlp(l))) ^ .25: REM cm
END IF
re = rhof * Qel(l) * 4 / (pi * d * n)
e = .75 * (l * d * vts * pi / (4 * Qel(l)))
IF e >= 1 THEN
Pels = 0
GOTO 100
END IF
```

```
arg = ((e ^ (1 / 3)) / (SQR(1 - e ^ (2 / 3))))
asn = ATN((e ^ (1 / 3)) / (SQR(1 - e ^ (2 / 3))))
Pels = 1 - (2 / pi) * ((2 * e * SQR(1 - e ^ (2 / 3))) - (e ^ (1 / 3) * SQR(1 - e ^
(2 / 3))) + (asn))
100 xil = l * pi * n / (4 * rhof * Qil(1))
IF xil < .45082990128# THEN
yil = 10 ^ (1.8310496159345# + 1.1071308650233# * c * LOG(xil) +
.14510722167522# * ((c * LOG(xil)) ^ 2))
d = (8 * rhof * Qil(1) ^ 2 * yil / (dlp(l) * pi ^ 2)) ^ .25: REM cm
ELSE
d = (128 * n * l * Qil(1) / (pi * dlp(l))) ^ .25: REM cm
END IF
re = rhof * Qil(l) * 4 / (pi * d * n)
e = .75 * (l * d * vts * pi / (4 * Qil(l)))
IF e >= 1 THEN
Pils = 0
GOTO 200
END IF
arg = ((e ^ (1 / 3)) / (SQR(1 - e ^ (2 / 3))))
asn = ATN((e ^ (1 / 3)) / (SQR(1 - e ^ (2 / 3))))
```

```
Pils = 1 - (2 / pi) * ((2 * e * SQR(1 - e ^ (2 / 3))) - (e ^ (1 / 3) * SQR(1 - e ^
(2 / 3))) + (asn))
200
Pel = Peld * Pels * Qel(l) * Nel / Q(l)
Pil = Pild * Pils * Qil(l) * Nil / Q(l)
P = Pel + Pil
IF l = 1 THEN
PRINT "1", dp, P, Pel, Pil
WRITE #1, dp, P, Pel, Pil
ELSEIF l = 2 THEN
PRINT "2", dp, P, Pel, Pil
WRITE #2, dp, P, Pel, Pil
ELSEIF l = 3 THEN
PRINT "3", dp, P, Pel, Pil
WRITE #3, dp, P, Pel, Pil
ELSEIF l = 4 THEN
PRINT "4", dp, P, Pel, Pil
WRITE #4, dp, P, Pel, Pil
ELSEIF l = 5 THEN
PRINT "5", dp, P, Pel, Pil
WRITE #5, dp, P, Pel, Pil
```

```
ELSEIF I = 6 THEN
PRINT "6", dp, P, Pel, Pil
WRITE #6, dp, P, Pel, Pil
ELSE
PRINT "7", dp, P, Pel, Pil
WRITE #7, dp, P, Pel, Pil
END IF
dp = dp + .01
LOOP
I = I + 1
LOOP
CLOSE 1
CLOSE 2
CLOSE 3
CLOSE 4
CLOSE 5
CLOSE 6
CLOSE 7
```

A.5. Code for Computing Particle Diameter From Particle Electrical Mobility

The following code was written to compute particle diameter from particle electrical mobility. Algorithms used in the code and estimates determined with the code are discussed in Section III.C.4.b. This code was written in HP BASIC on a Model HP-85 microcomputer.

```
1000        !*EC/TSI 3071 CALIBRATION*
1010        !BY RONALD C. SCRIPSICK
1020        CLEAR @ CLEAR
1030        D4 = .000000037 @ M=4 .809894907E-23 @ N=6
            .022169E23 @ R=83100000
1040        K1=1.38E-16 @ K2=6 .44157433 9E-11
1050        !ITERATIVE CALCULATION OF PARTICLE SIZE
1060        D2=.000000001
1070        DISP "ENTER ATMOSPHERIC PRESSURE IN TORR"
1080        INPUT P
1090        P=P * .1/.0000750062
1100        DISP "ENTER CALIBRATION TEMPERATURE IN
DEGREES C"
```

```
1110        INPUT T
1120        T=T+273
1130        L=R * T/(SQR(2) * PI * N * P * D4^2)
1140        U=.0001723304+.000000481233 * (T-273)
1150        DISP "ENTER EC FLOW IN LPM"
1160        INPUT Q
1170        Q=Q * 1000/60
1180        DISP "ENTER VOLTAGE READING IN VOLTS"
1190        INPUT V
1200        C=1 @ D0=1
1210        D1=C * V * K2/(U * Q)
1220        D3=D1-D0 @ D3=ABS(D3)
1230        IF D3<D2 THEN 1280
1240        D0=D1
1250        L1=L/D1
1260        C=1+L1 * (2.514+.8 * EXP( - (.55/L1)))
1270        GOTO 1210
1280        D1=D1 * 10000
1290        PRINT "Dp=";D1;" UM"
1300        PRINT "THIS IS FOR A VOLTAGE OF ";V;" VOLTS"
1310        PRINT "L=";L;" C=";C;" Q=";Q;" P=";P;" T=";T;" U=";U
```

```
1320        GOTO 1180
1330        END
```

Appendix B - Compilation of Experimental Data by Filter Unit

In this appendix experimental data are presented for each filter unit evaluated in this study. Data from the pilot study precede those from the formal study. Pilot study data include physical inspection data, and typically data from whole filter and media pack tests. Test data include a plot of the flow rate/differential pressure data and a plot of the penetration data. Formal study data include the above plus data from frame tests.

B.1. Pilot Study Data

B.1.a. Filter Unit 5-2C

Data from the physical inspection of filter unit 5-2C are shown in Table B-I.

No whole filter tests were performed on this filter unit. Media pack test flow rates were limited to 460 Lpm and below because of the test system flow rate capacity at the time of the tests. Improvements in the system subsequent to these tests allowed testing at flow rates in excess of

920 Lpm. Data from media pack flow rate evaluations are shown in Figure B-1. These data represent the initial flow rate measurements. No final measurements were made. Data from media pack penetration determinations are shown in Figure B-2.

Table B-I

Physical Description of Filter 5-2C

Design Volume Flow Rate (Lpm): 460 Manufacturer: Donaldson Identification Number: 5-2C Lab Book: S 20042 Page: 41	Media Area Height (cm): 14.80 Width (cm): 16.00 Depth of Pleats (cm): 6.350 Number of Pleats Upstream: 16 Downstream: 17 Effective Area (cm^2): 3007.36
Gaskets Upstream: Yes Downstream: Yes	Media/Frame Sealant Type: Epoxy Position Upstream: Top & Bottom (Horizontal) Downstream: Top & Bottom (Horizontal)
Outside Dimensions Height (cm): 20.320 Width (cm): 20.320 Depth (cm): 7.620 Board Thickness (cm): 1.90	Face Guards: No Separators: Yes
Frame Joints Fasteners: Nails & Staples Sealed: No	Inspection: No Large Cracks

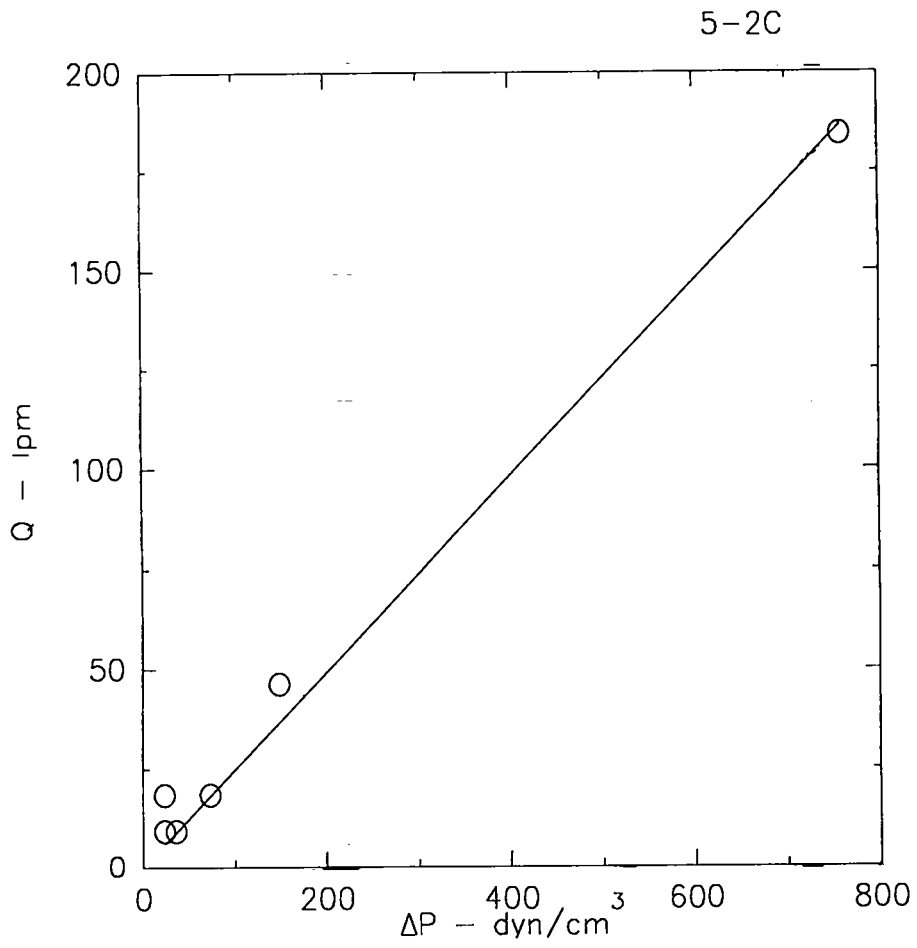

Figure B-1. Media pack flow rate evaluation data for filter 5-2C.

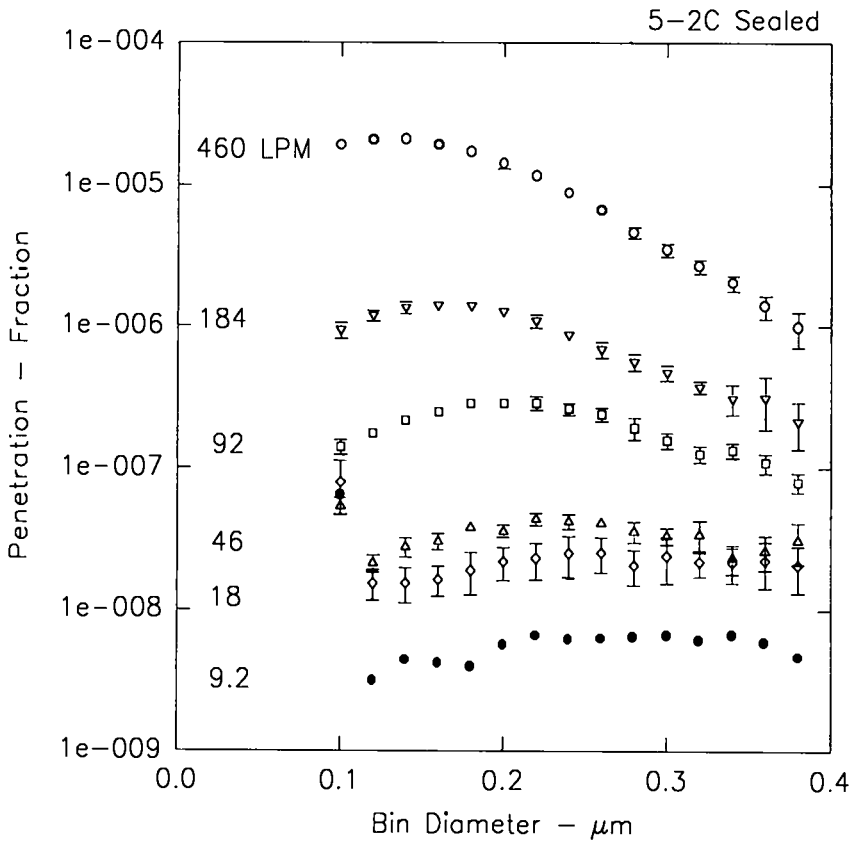

Figure B-2. Media pack penetration data for filter 5-2C.

B.1.b. Filter Unit 7-2C

Data from the physical inspection of filter unit 7-2C are shown in Table B-II

Whole filter flow rate evaluation data are shown in Figure B-3. No final flow rate measurements were made. Data from whole filter penetration determinations are shown in Figure B-4.

Data from media pack flow rate evaluations are shown in Figure B-5. These data represent the initial flow rate measurements. No final measurements were made. Data from media pack penetration determinations are shown in Figure B-6.

Table B-II

Physical Description of Filter 7-2C

Design Volume Flow Rate (Lpm): 920 Manufacturer: Donaldson Identification Number: 7-2C Lab Book: S 20042 Page: 49	Media Area Height (cm): 14.90 Width (cm): 16.00 Depth of Pleats (cm): 6.350 Number of Pleats Upstream: 16 Downstream: 17 Effective Area (cm^2): 3027.68
Gaskets Upstream: Yes Downstream: Yes	Media/Frame Sealant Type: Epoxy Position Upstream: Top & Bottom (Horizontal) Downstream: Top & Bottom (Horizontal)
Outside Dimensions Height (cm): 20.320 Width (cm): 20.320 Depth (cm): 7.620 Board Thickness (cm): 1.90	Face Guards: No Separators: Yes
Frame Joints Fasteners: Nails & Staples Sealed: No	Inspection: No Large Cracks

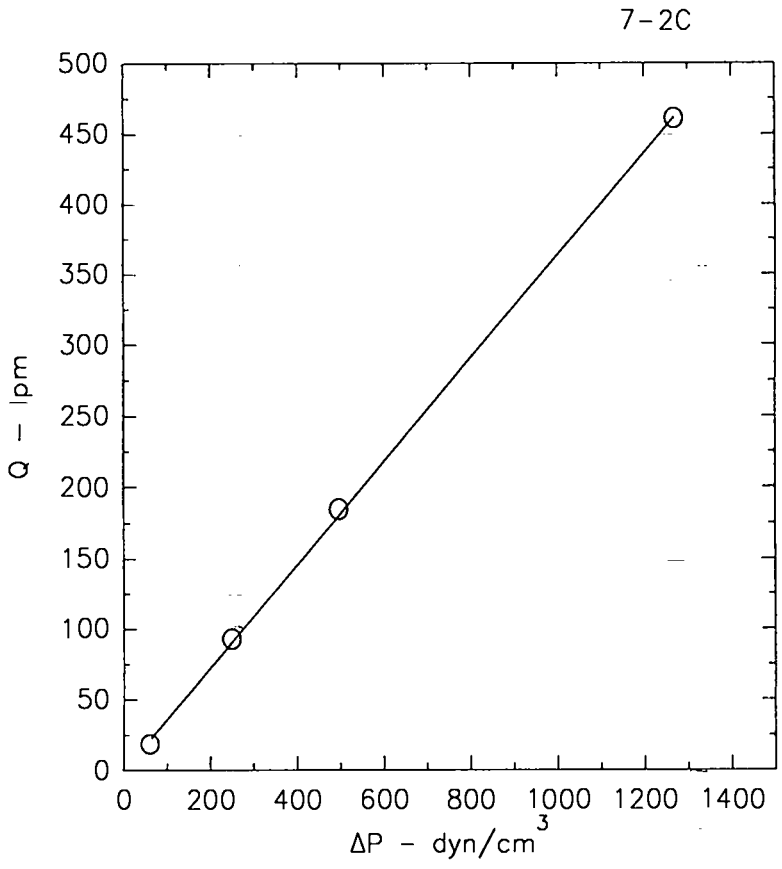

Figure B-3. Whole filter flow rate evaluation data for filter 7-2C.

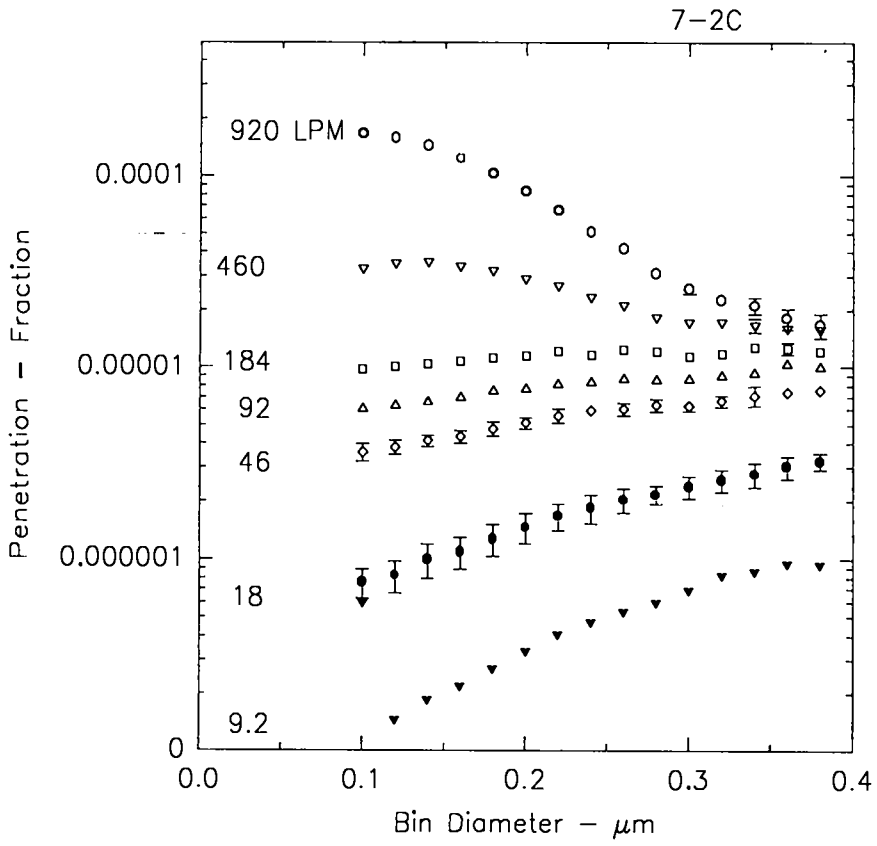

Figure B-4. Whole filter penetration data for filter 7-2C.

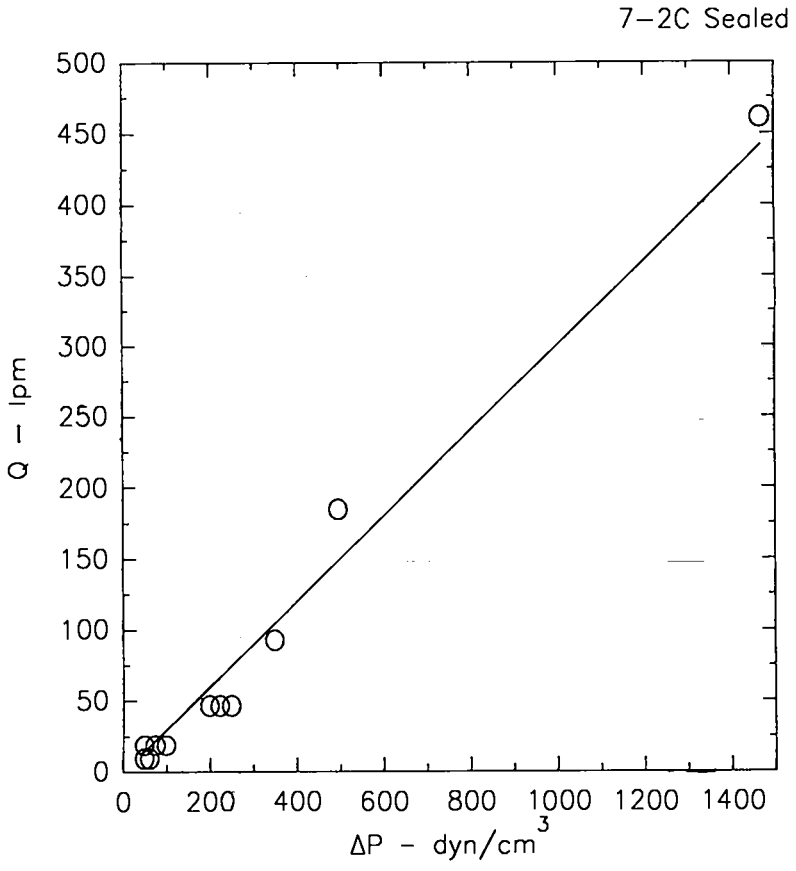

Figure B-5. Media pack flow rate evaluation data for filter 7-2C.

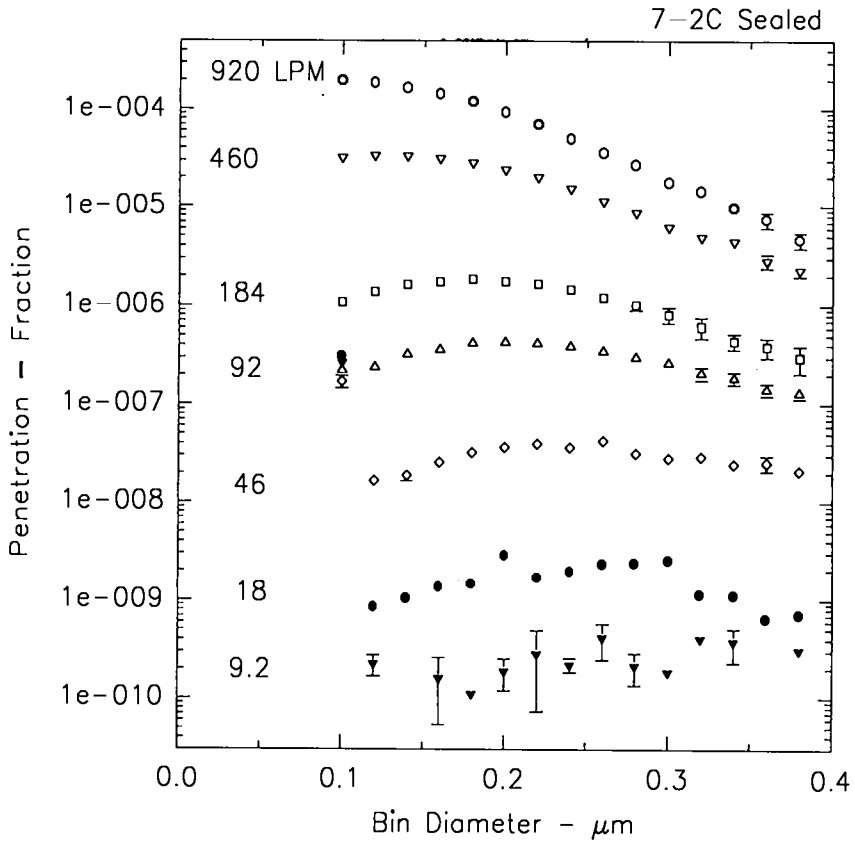

Figure B-6. Media pack penetration data for filter 7-2C.

B.1.c. Filter Unit 2-2C

Data from the physical inspection of filter unit 2-2C are shown in Table B-III.

Whole filter flow rate evaluation data are shown in Figure B-7. Data from whole filter penetration determinations are shown in Figure B-8.

No media pack tests were conducted on 2-2C because of excessive loading during the whole filter tests.

Table B-III

Physical Description of Filter 2-2C

Design Volume Flow Rate (Lpm): 920 Manufacturer: Donaldson Identification Number: 2-2C Lab Book: S 20042 Page: 70	Media Area Height (cm): 14.80 Width (cm): 16.00 Depth of Pleats (cm): 6.350 Number of Pleats Upstream: 16 Downstream: 17 Effective Area (cm^2): 3007.36
Gaskets Upstream: Yes Downstream: Yes	Media/Frame Sealant Type: Epoxy Position Upstream: Top & Bottom (Horizontal) Downstream: Top & Bottom (Horizontal)
Outside Dimensions Height (cm): 20.320 Width (cm): 20.320 Depth (cm): 7.620 Board Thickness (cm): 1.90	Face Guards: No Separators: Yes
Frame Joints Fasteners: Nails & Staples Sealed: No	Inspection: No Large Cracks

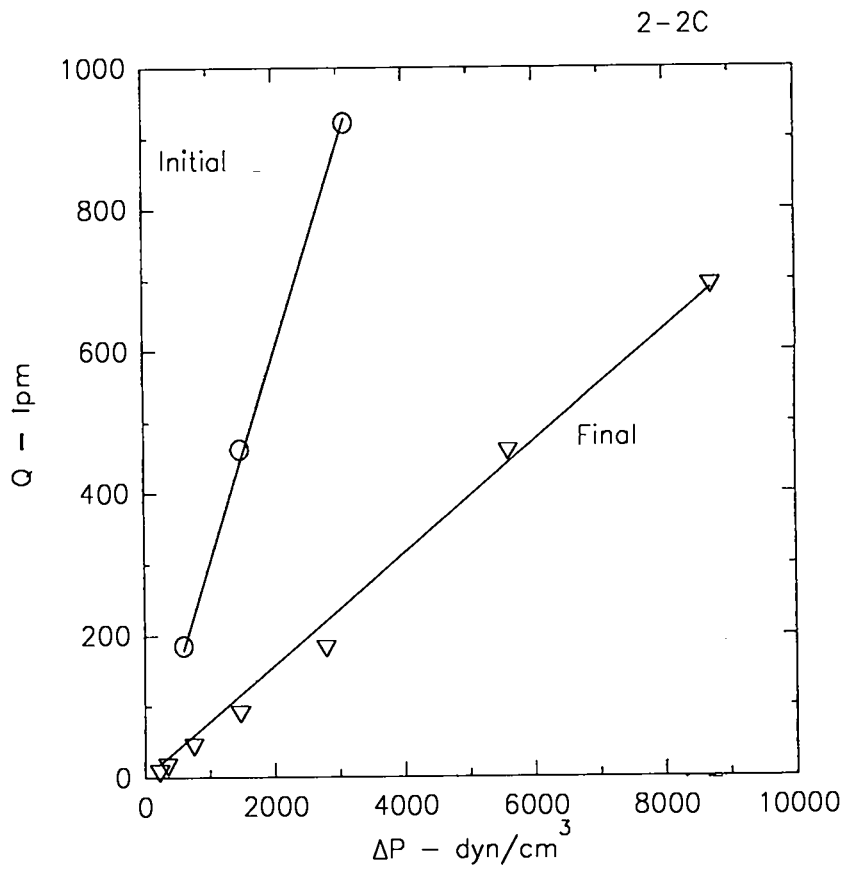

Figure B-7. Whole filter flow rate evaluation data for filter 2-2C.

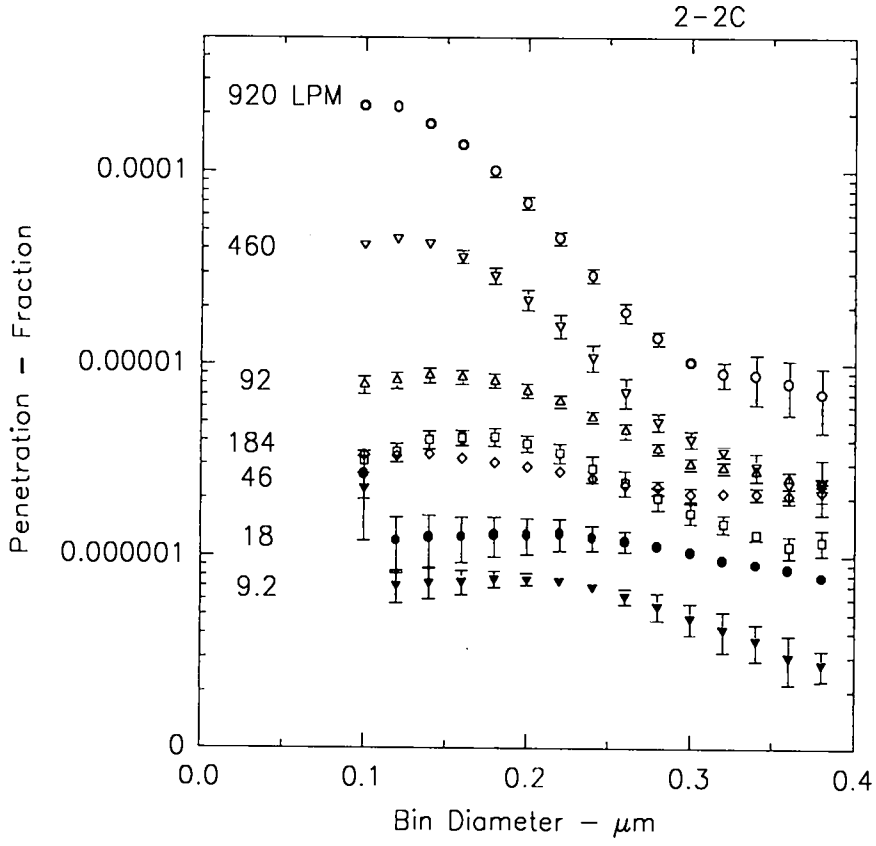

Figure B-8. Whole filer penetration data for filter 2-2C.

B.1.d. Filter Unit 4-2C

Data from the physical inspection of filter unit 4-2C are shown in Table B-IV.

Whole filter flow rate evaluation data are shown in Figure B-9. Data from whole filter penetration determinations are shown in Figure B-10.

Data from media pack flow rate evaluations are shown in Figure B-11. Data from media pack penetration determinations are shown in Figure B-12.

Table B-IV

Physical Description of Filter 4-2C

Design Volume Flow Rate (Lpm): 920 Manufacturer: Donaldson Identification Number: 4-2C Lab Book: S 20042 Page: 84	Media Area Height (cm): 14.80 Width (cm): 15.80 Depth of Pleats (cm): 6.350 Number of Pleats Upstream: 16 Downstream: 17 Effective Area (cm^2): 3007.36
Gaskets Upstream: Yes Downstream: Yes	Media/Frame Sealant Type: Epoxy Position Upstream: Top & Bottom (Horizontal) Downstream: Top & Bottom (Horizontal)
Outside Dimensions Height (cm): 20.3200 Width (cm): 20.3200 Depth (cm): 7.6200 Board Thickness (cm): 1.90	Face Guards: No Separators:
Frame Joints Fasteners: Nails & Staples Sealed: No	Inspection: No Large Cracks

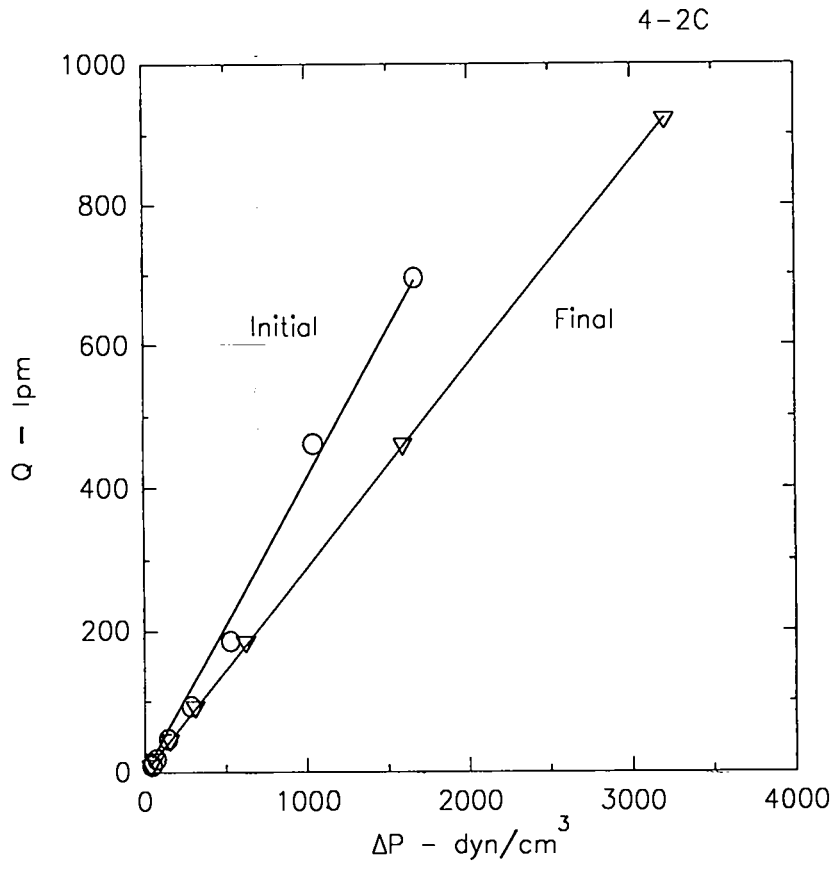

Figure B-9. Whole filter flow rate evaluation data for filter 4-2C.

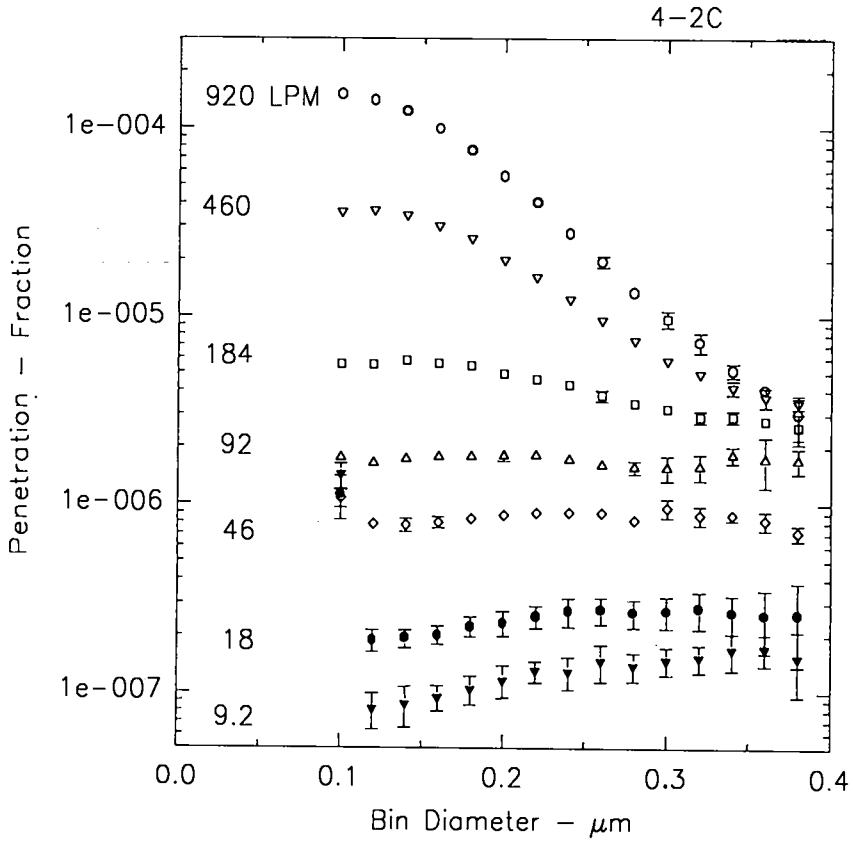

Figure B-10. Whole filter penetration data for filter 4-2C.

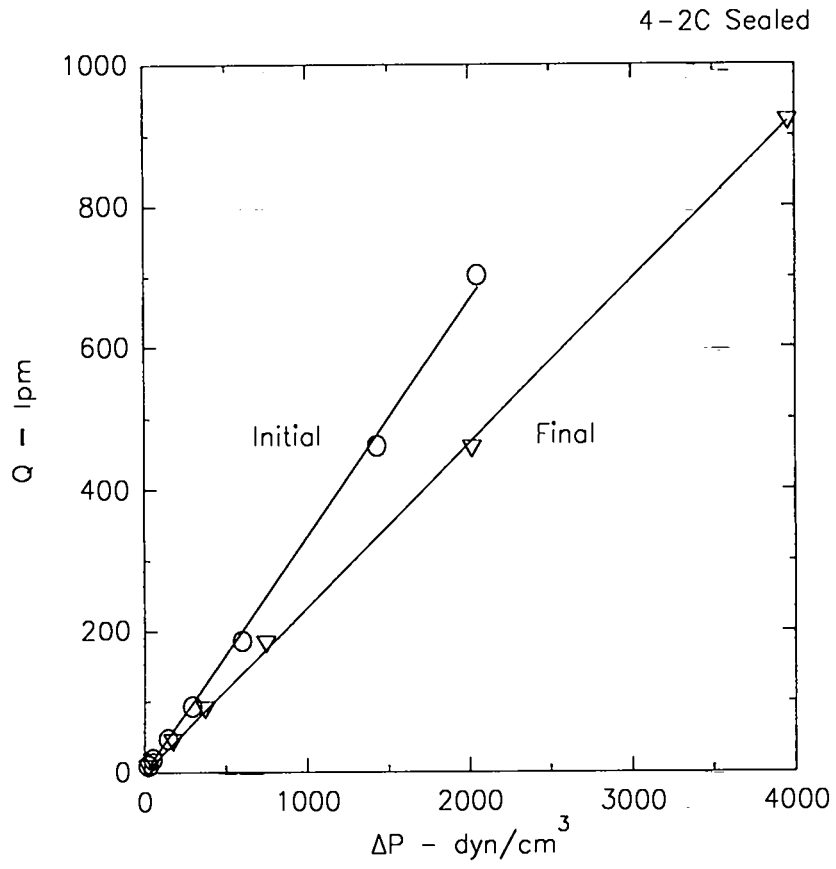

Figure B-11. Media pack flow rate evaluation data for filter 4-2C.

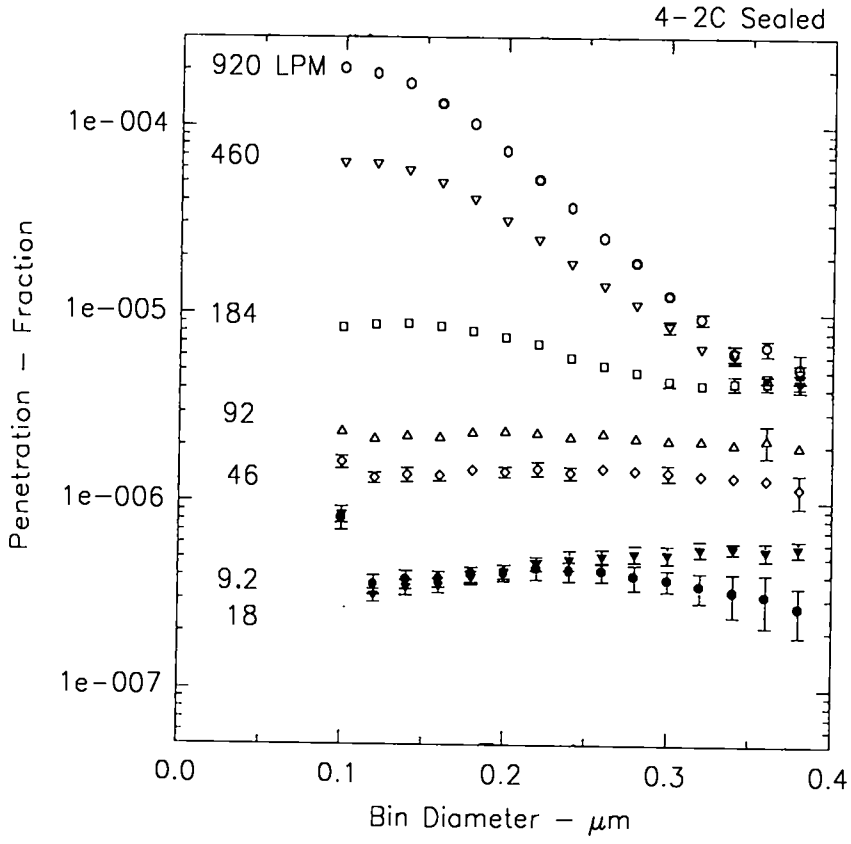

Figure B-12. Media pack penetration data for filter 4-2C.

B.1.e. Filter Unit 8-2C

Data from the physical inspection of filter unit 8-2C are shown in Table B-V. Whole filter flow rate evaluation data are shown in Figure B-13. Data from whole filter penetration determinations are shown in Figure B-14.

Data from media pack flow rate evaluations are shown in Figure B-15. Data from media pack penetration determinations are shown in Figure B-16.

Table B-V

Physical Description of Filter 8-2C

Design Volume Flow Rate (Lpm): 920 Manufacturer: Donaldson Identification Number: 8-2C Lab Book: S 20042 Page: 109	Media Area Height (cm): 14.80 Width (cm): 15.80 Depth of Pleats (cm): 6.350 Number of Pleats Upstream: 16 Downstream: 17 Effective Area (cm^2): 3007.36
Gaskets Upstream: Yes Downstream: Yes	Media/Frame Sealant Type: Epoxy Position Upstream: Top & Bottom (Horizontal) Downstream: Top & Bottom (Horizontal)
Outside Dimensions Height (cm): 20.3200 Width (cm): 20.3200 Depth (cm): 7.6200 Board Thickness (cm): 1.90	Face Guards: No Separators:
Frame Joints Fasteners: Nails & Staples Sealed: No	Inspection: No Large Cracks

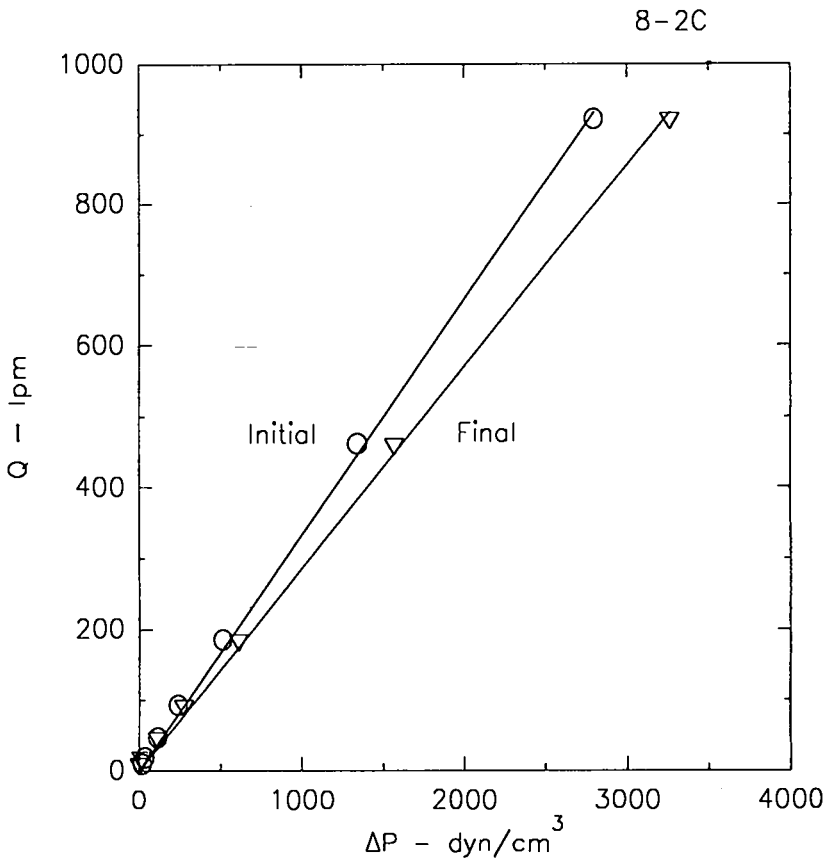

Figure B-13. Whole filter flow rate evaluation data for filter 8-2C.

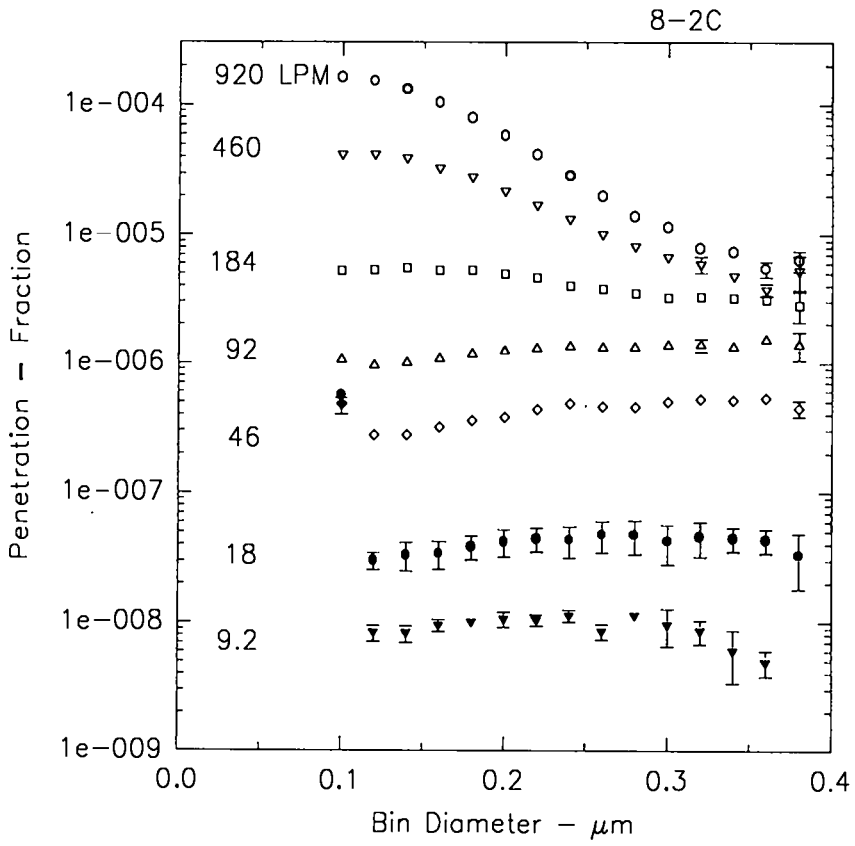

Figure B-14. Whole filter penetration data for filter 8-2C.

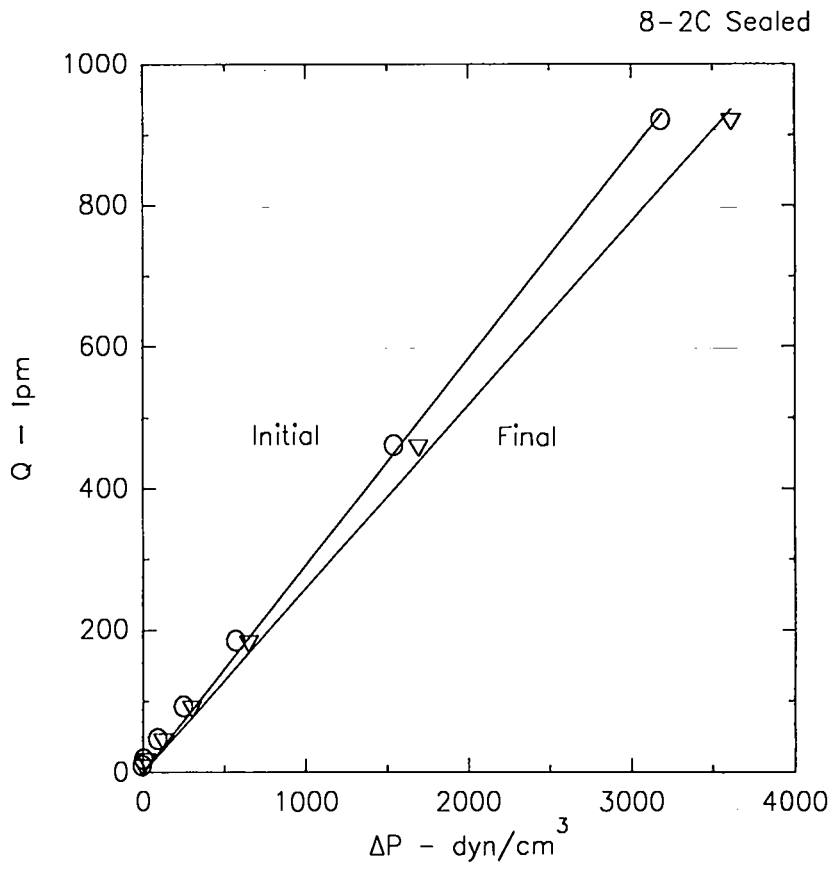

Figure B-15. Media pack flow rate evaluation data for filter 8-2C.

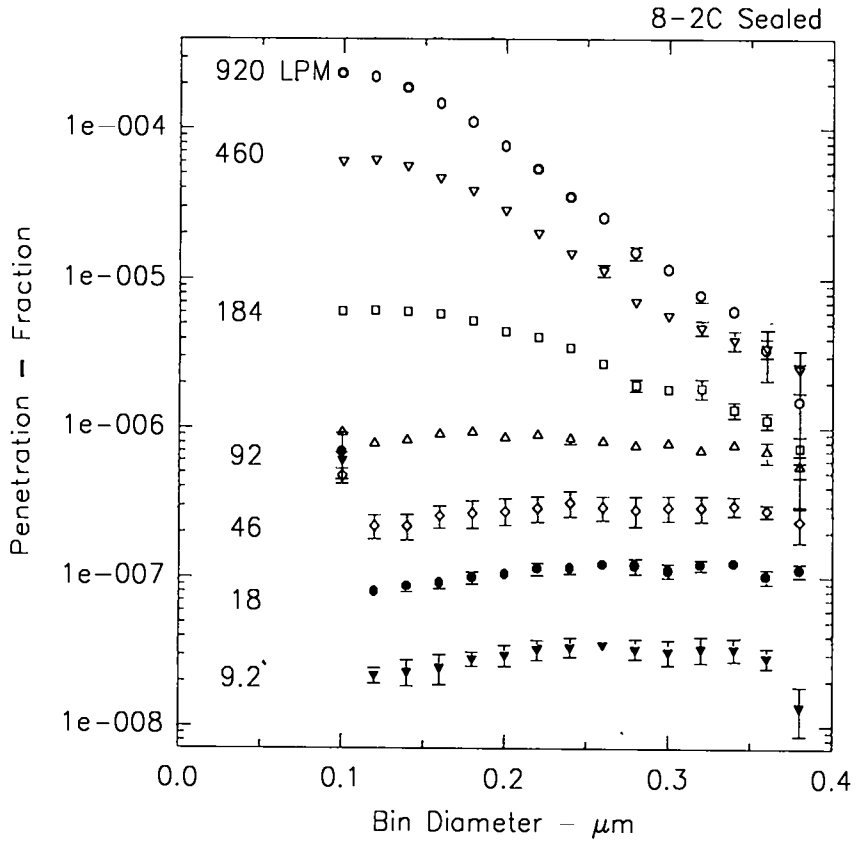

Figure B-16. Media pack penetration data for filter 8-2C.

B.2. Formal Study Data

B.2.a. Filter Unit 9351

Data from the physical inspection of filter unit 9351 are shown in Table B-VI. Whole filter flow rate evaluation data are shown in Figure B-17. Data from whole filter penetration determinations are shown in Figure B-18.

Data from frame leak flow rate evaluations are shown in Figure B-19. Data from frame penetration determinations are shown in Figure B-20.

Data from media pack flow rate evaluations are shown in Figure B-21. Data from media pack determinations are shown in Figure B-22.

Table B-VI

Physical Description of Filter 9351

Design Volume Flow Rate (m^3/min): 7.6200 Manufacturer: Flanders Identification Number: N 219351 Lab Book: S 20042 Page: 142	Media Area Height (cm): 15.000 Width (cm): 15.200 Depth of Pleats (cm): 5.0800 Number of Pleats Upstream: 51 Downstream: 54 Effective Area (cm^2): 7772.4
Gaskets Upstream: Yes Downstream: Yes	Media/Frame Sealant Type: Silicone Rubber Position Upstream: Four sides Downstream: Top & Bottom Sides(Horizontal)
Outside Dimensions Height (cm): 20.3200 Width (cm): 20.3200 Depth (cm): 7.6200 Board Thickness (cm): 1.9050	Face Guards: No Separators: No
Frame Joints Fasteners: Nails Sealed: Yes	Inspection:

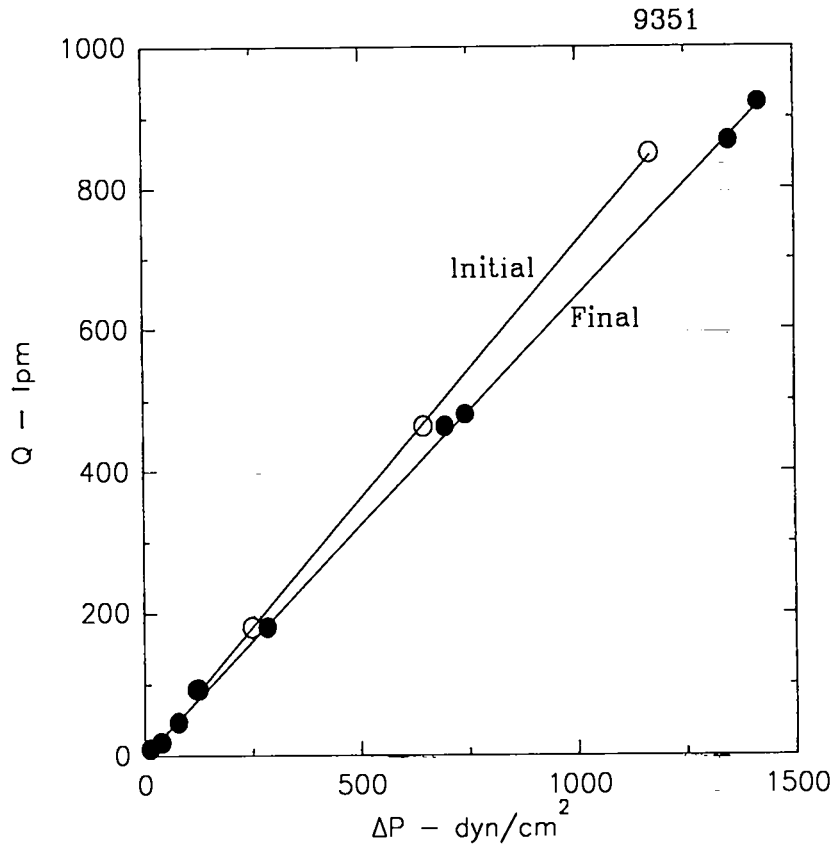

Figure B-17. Whole filter flow rate evaluation data for filter 9351.

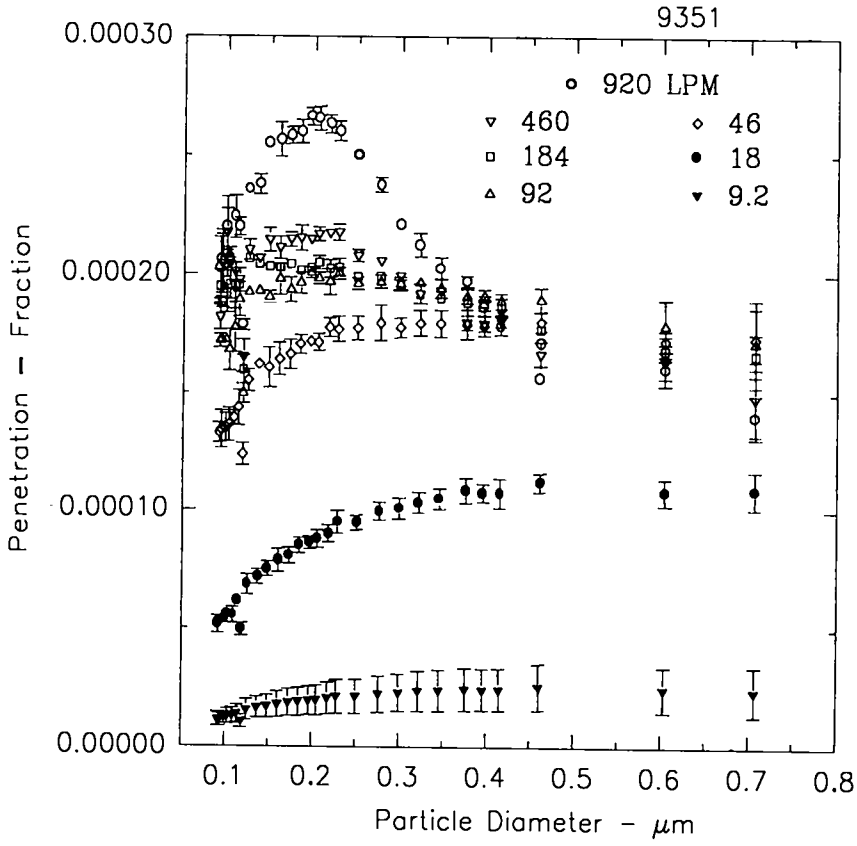

Figure B-18. Whole filter penetration data for filter 9351.

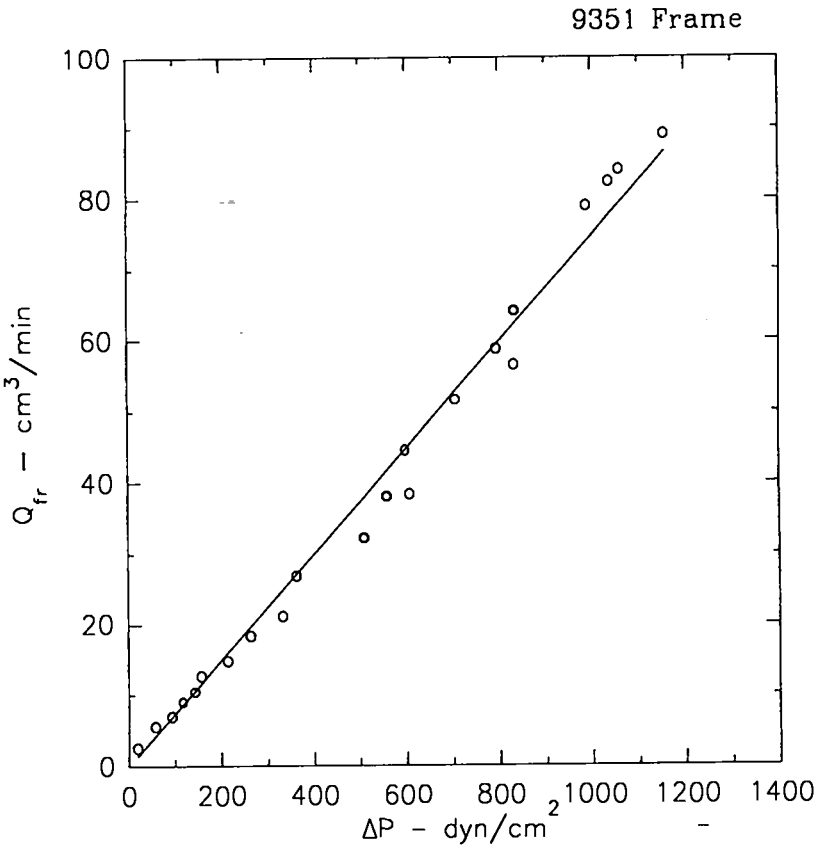

Figure B-19. Frame leak flow rate evaluation data for filter 9351.

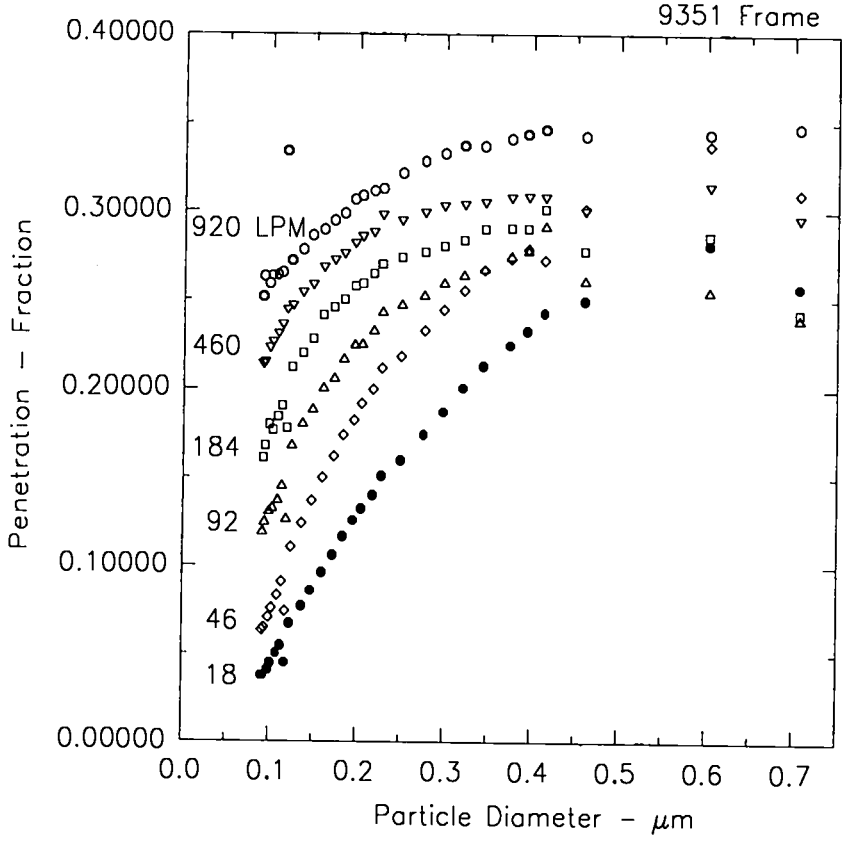

Figure B-20. Frame penetration data for filter 9351.

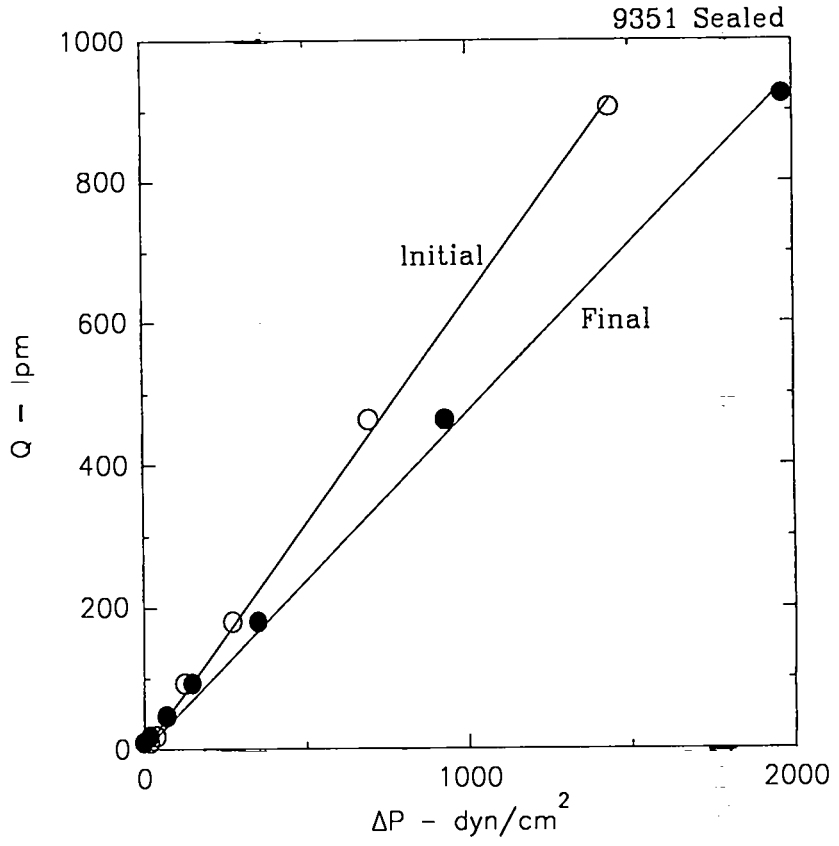

Figure B-21. Media pack flow rate evaluation data for filter 9351.

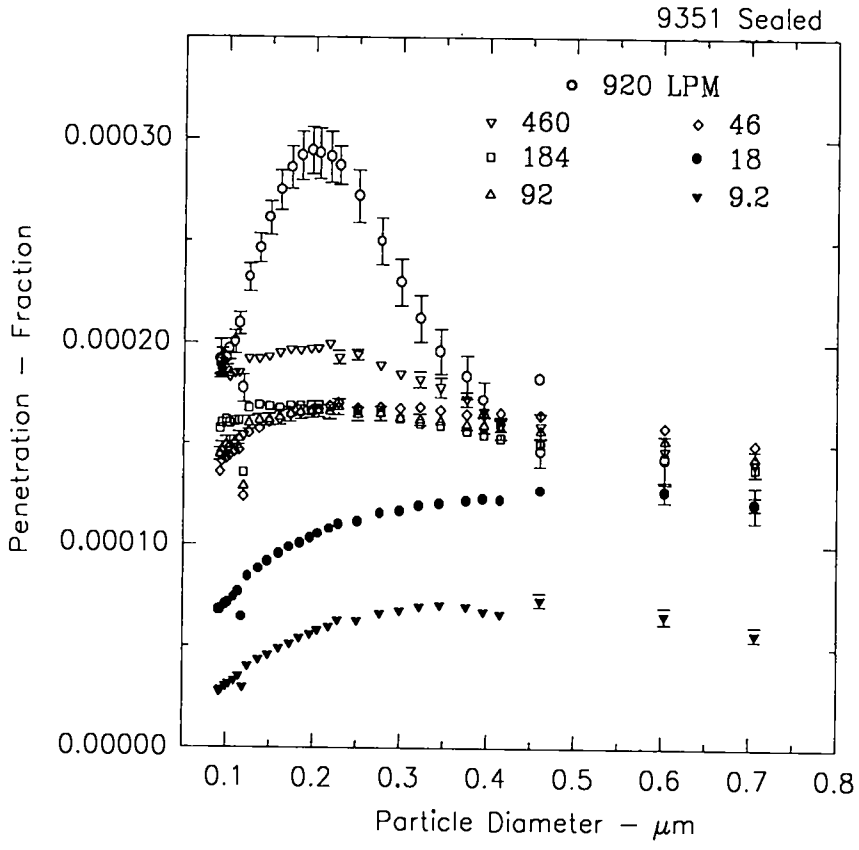

Figure B-22. Media pack penetration data for filter 9351.

B.2.b. Filter Unit 9346

Data from the physical inspection of filter unit 9346 are shown in Table B-VII. Whole filter flow rate evaluation data are shown in Figure B-23. Data from whole filter penetration determinations are shown in Figure B-24.

Data from frame leak flow rate evaluations are shown in Figure B-25. Data from frame penetration determinations are shown in Figure B-26.

Data from media pack flow rate evaluations are shown in Figure B-27. Data from media pack determinations are shown in Figure B-28.

Table B-VII

Physical Description of Filter 9346

Design Volume Flow Rate (Lpm): 920 Manufacturer: Flanders Identification Number: N 219346 Lab Book: S 024872 Page: 44	Media Area Height (cm): 15.00 Width (cm): 15.200 Depth of Pleats (cm): 5.0800 Number of Pleats Upstream: 50 Downstream: 54 Effective Area (cm^2): 7620
Gaskets Upstream: Yes Downstream: Yes	Media/Frame Sealant Type: Silicone Rubber Position Upstream: Four Sides Downstream: Top & Bottom(Horizontal Sides)
Outside Dimensions Height (cm): 20.3200 Width (cm): 20.3200 Depth (cm): 7.6200 Board Thickness (cm): 1.9050	Face Guards: No Separators: No
Frame Joints Fasteners: Nails Sealed: Yes	Inspection:

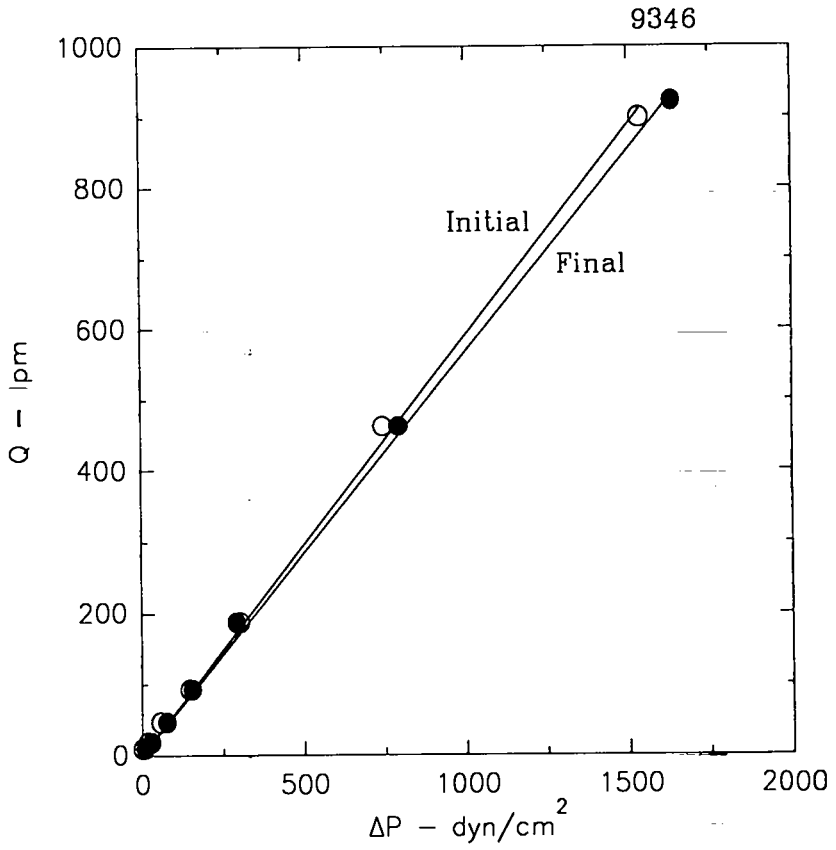

Figure B-23. Whole filter flow rate evaluation data for filter 9346.

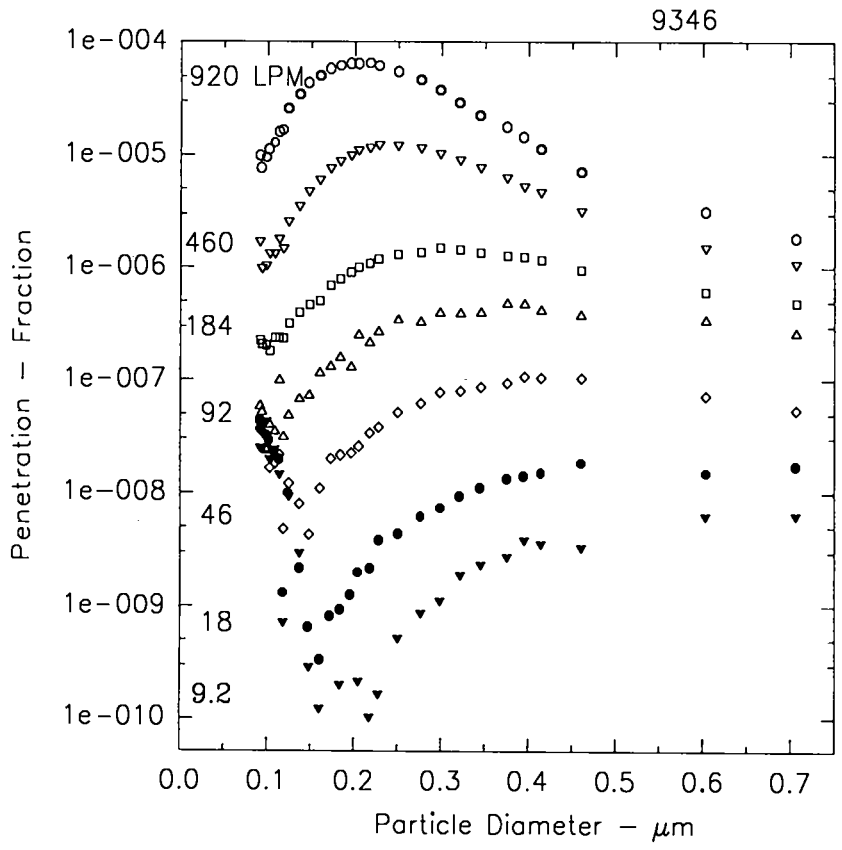

Figure B-24. Whole filter penetration data for filter 9346.

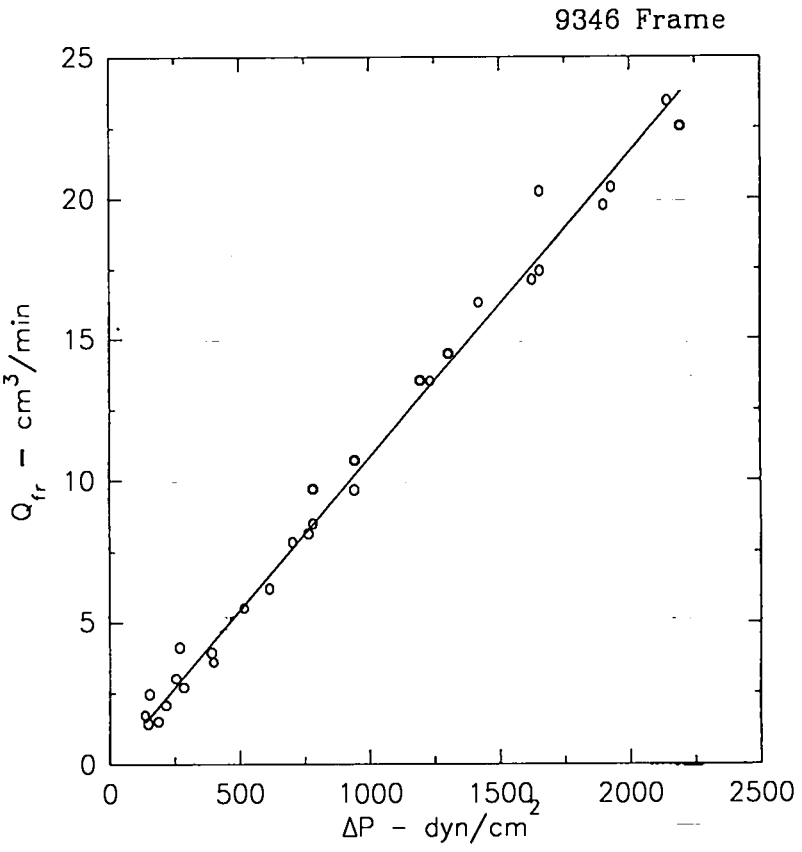

Figure B-25. Frame leak flow rate evaluation data for filter 9346.

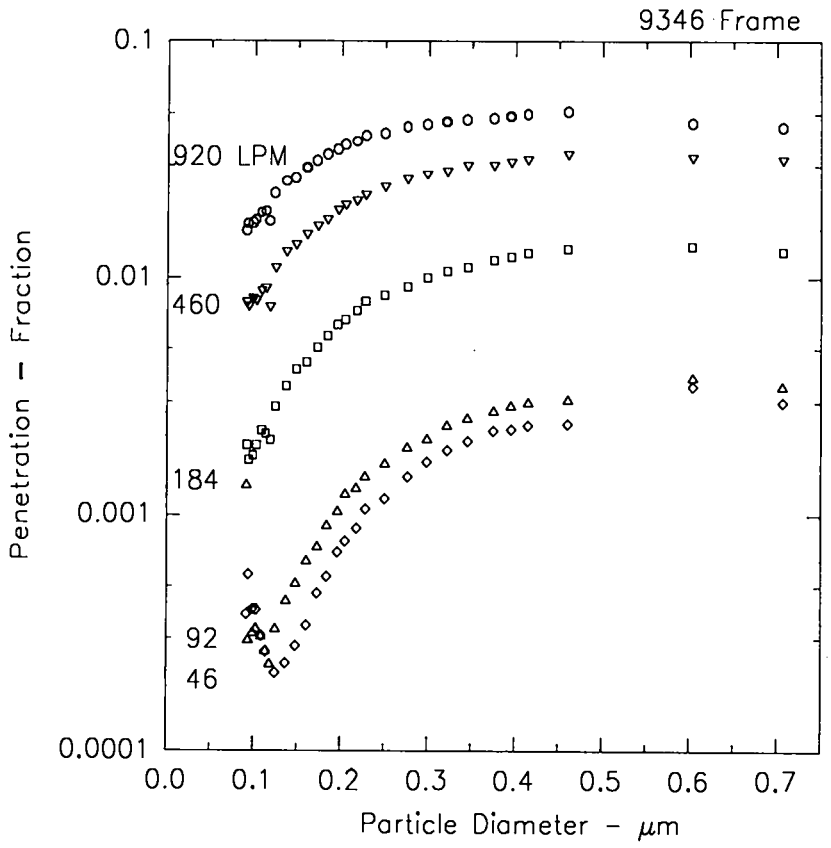

Figure B-26. Frame penetration data for filter 9346.

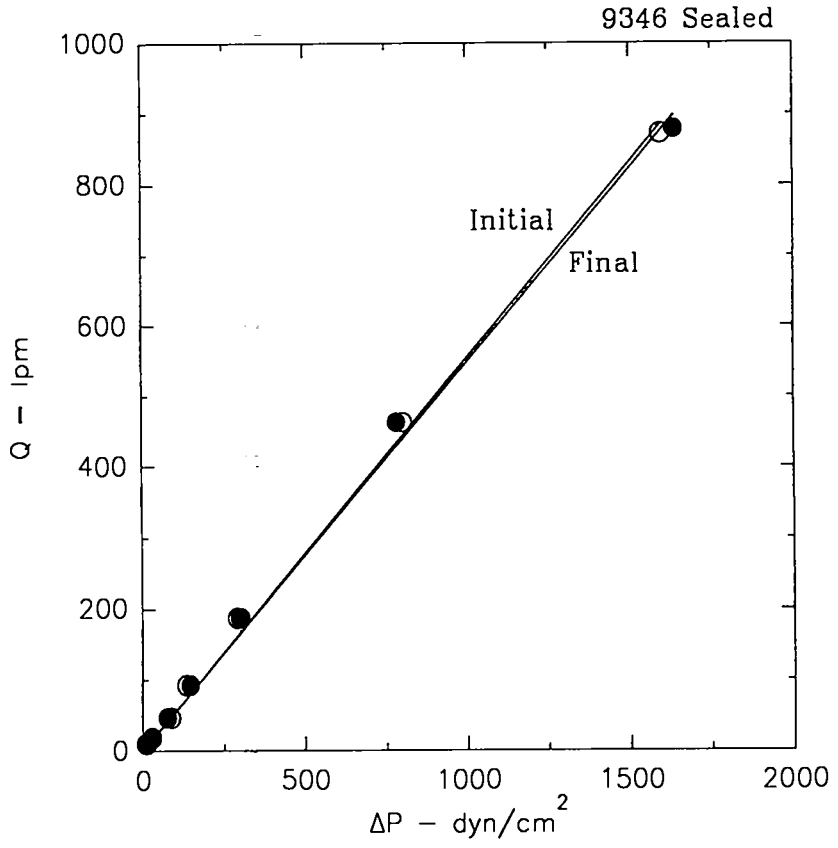

Figure B-27. Media pack flow rate evaluation data for filter 9346.

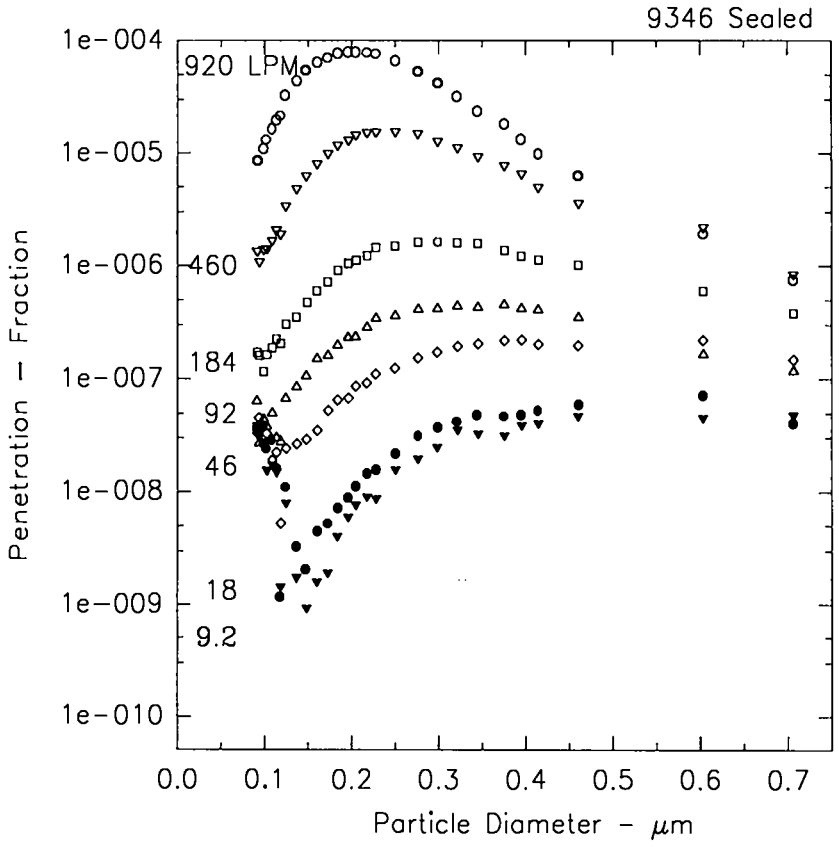

Figure B-28. Media pack penetration data for filter 9346.

B.2.c. Filter Unit 9343

Data from the physical inspection of filter unit 9343 are shown in Table B- Whole filter flow rate evaluation data are shown in Figure B-29. Data from whole filter penetration determinations are shown in Figure B-30.

Data from frame leak flow rate evaluations are shown in Figure B-31. Data from frame penetration determinations are shown in Figure B-32.

Data from media pack flow rate evaluations are shown in Figure B-33. Data from media pack determinations are shown in Figure B-34.

Table B-VIII

Physical Description of Filter 9343

Design Volume Flow Rate (Lpm): 920 Manufacturer: Flanders Identification Number: N 219343 Lab Book: S 024872 Page: 90	Media Area Height (cm): 15.10 Width (cm): 15.50 Depth of Pleats (cm): 5.0800 Number of Pleats Upstream: 53 Downstream: 51 Effective Area (cm^2): 7824.22
Gaskets Upstream: Yes Downstream: Yes	Media/Frame Sealant Type: Silicone Rubber Position Upstream: Potted Top & Bottom(Horizontal Sides) Downstream: Potted on All Four Sides
Outside Dimensions Height (cm): 20.3200 Width (cm): 20.3200 Depth (cm): 7.6200 Board Thickness (cm): 1.9050	Face Guards: No Separators: No
Frame Joints Fasteners: Nails Sealed: Yes	Inspection:

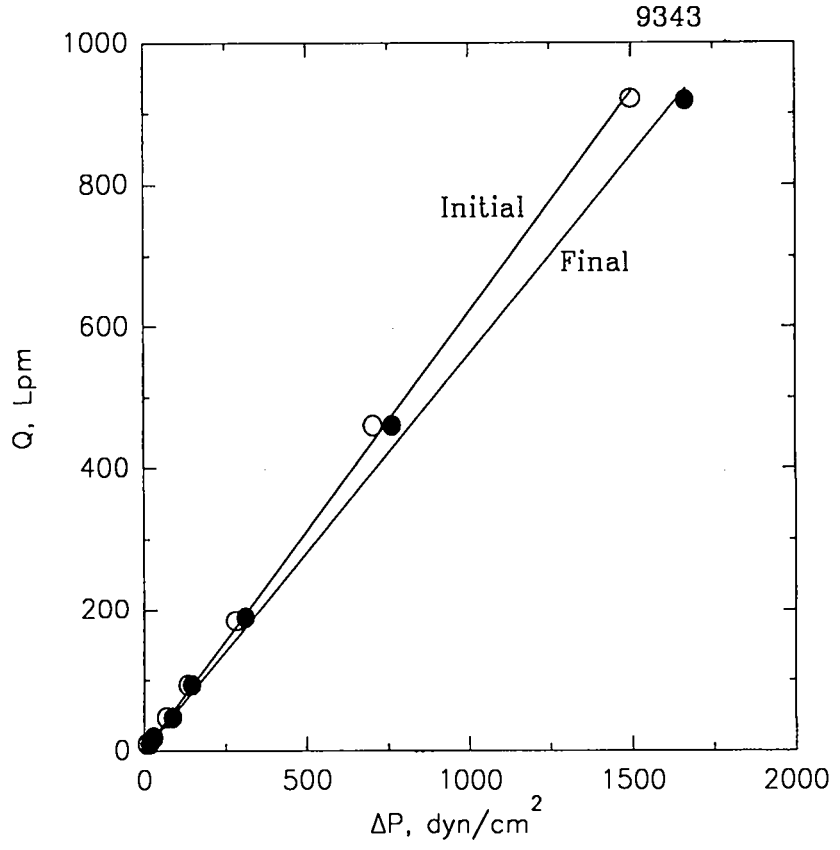

Figure B-29. Whole filter flow rate evaluation data for filter 9343.

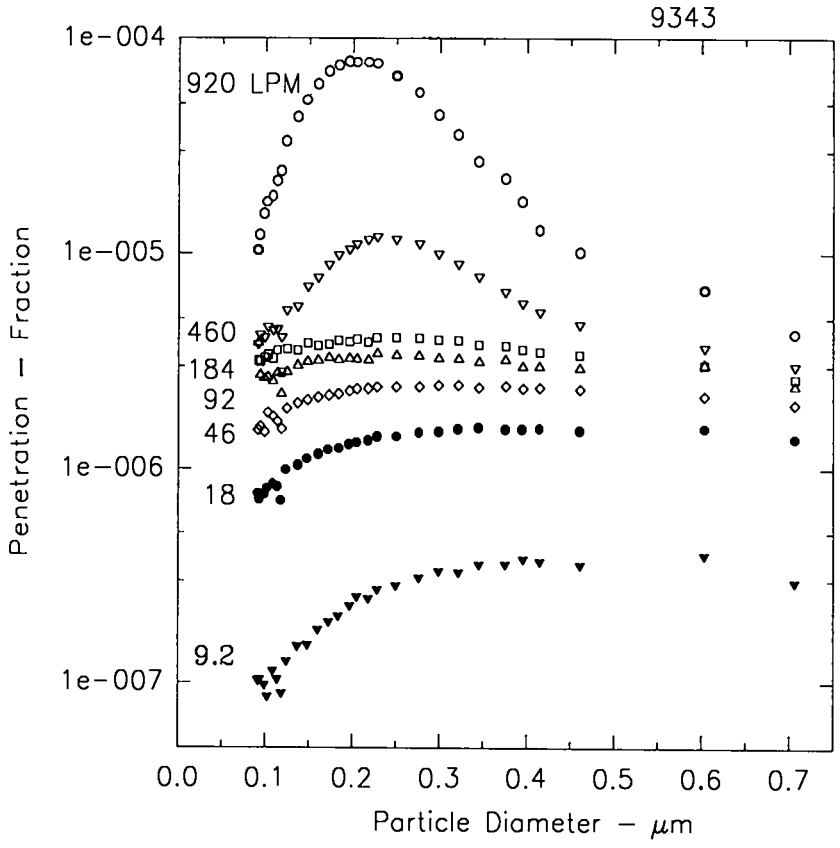

Figure B-30. Whole filter penetration data for filter 9343.

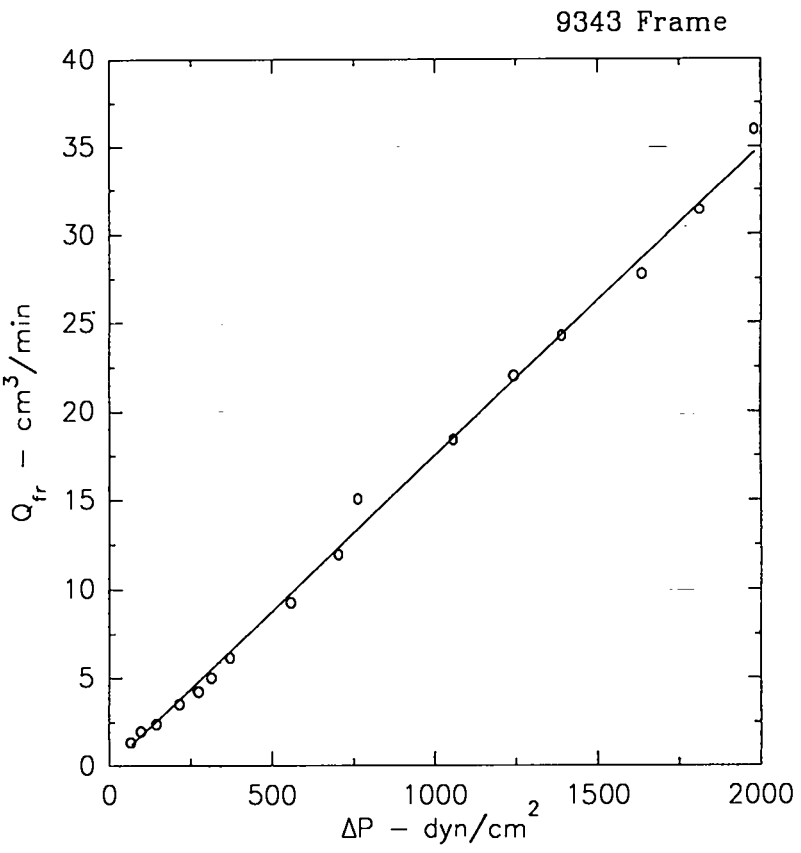

Figure B-31. Frame leak flow rate evaluation data for filter 9343.

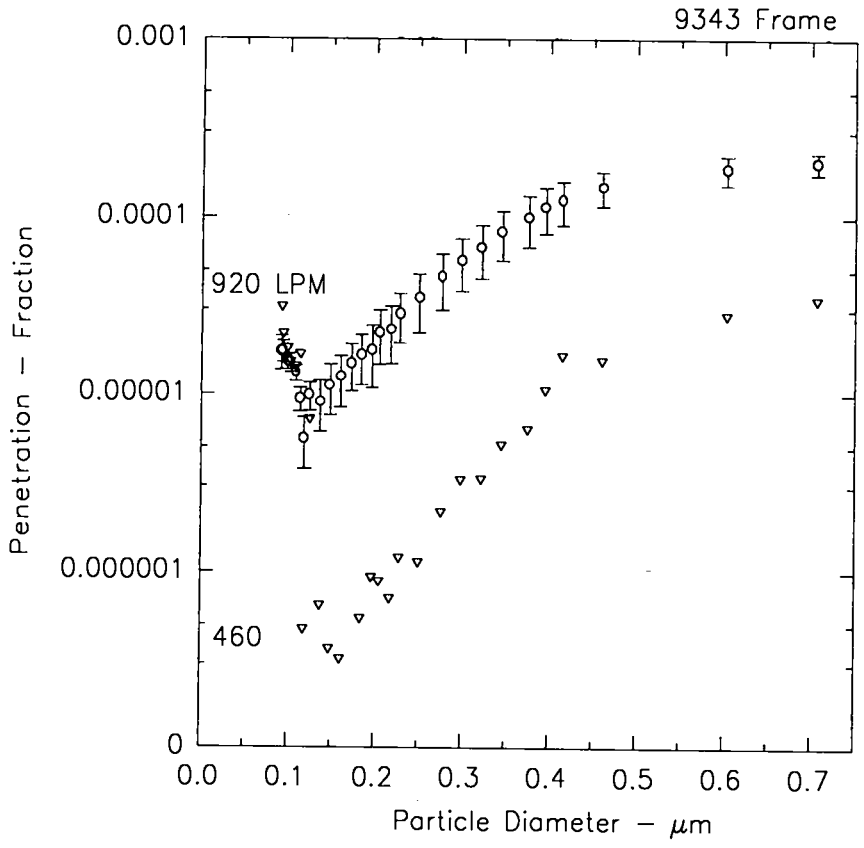

Figure B-32. Frame penetration data for filter 9343.

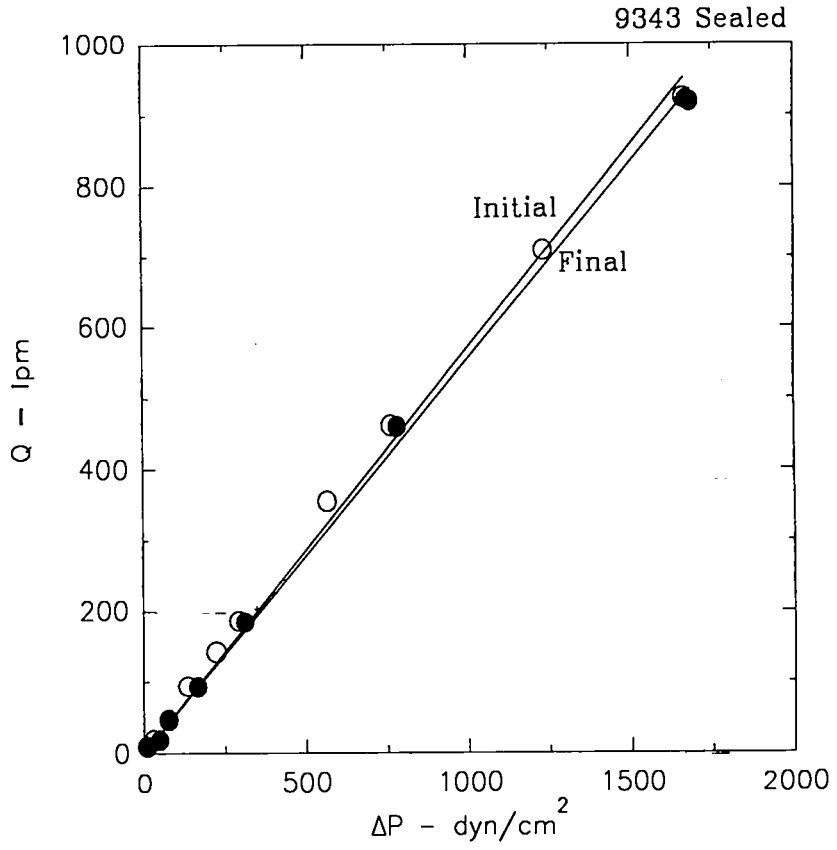

Figure B-33. Media pack flow rate evaluation data for filter 9343.

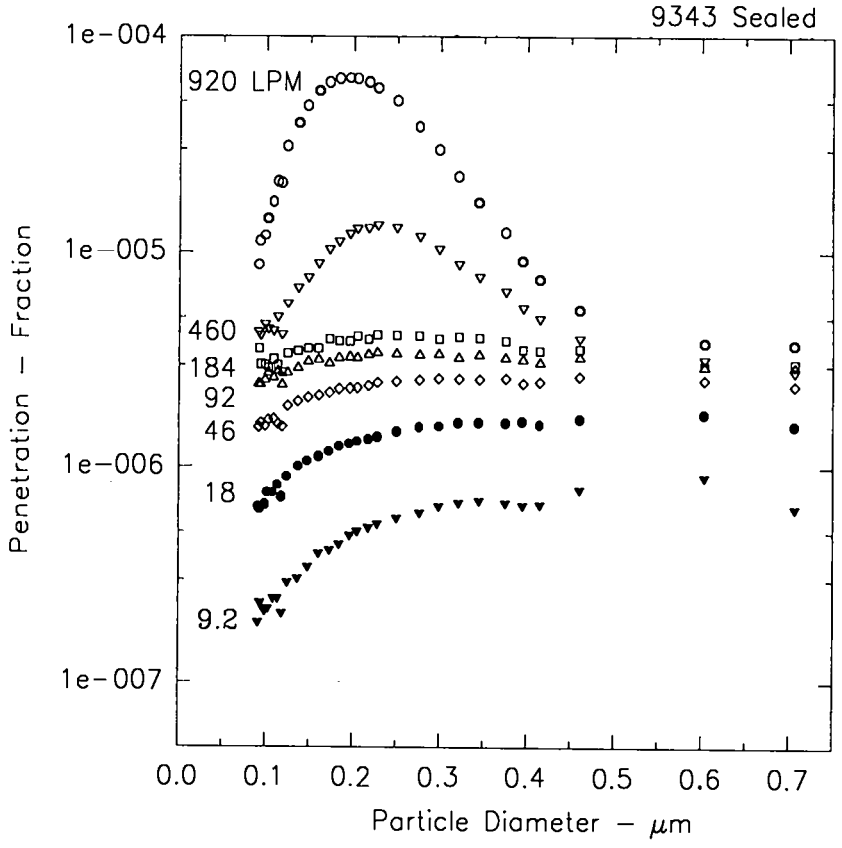

Figure B-34. Media pack penetration data for filter 9343.

B.2.d. Filter Unit 3037

Data from the physical inspection of filter unit 3037 are shown in Table B-IX. Whole filter flow rate evaluation data are shown in Figure B-35. Data from whole filter penetration determinations are shown in Figure B-36.

Data from frame leak flow rate evaluations are shown in Figure B-37. Data from frame penetration determinations are shown in Figure B-38.

Data from media pack flow rate evaluations are shown in Figure B-39. Data from media pack determinations are shown in Figure B-40.

Table B-IX

Physical Description of Filter 3037

Design Volume Flow Rate (Lpm): 708 Manufacturer: American Air Filter Identification Number: 41403037 Lab Book: 24872 Page: 146	Media Area Height (cm): 14.50 Width (cm): 14.60 Depth of Pleats (cm): 5.239 Number of Pleats Upstream: 24 Downstream: 25 Effective Area (cm^2): 3646.3
Gaskets Upstream: Yes Downstream: Yes	Media/Frame Sealant Type: Epoxy Position Upstream: Four sides Downstream: Four sides
Outside Dimensions Height (cm): 20.320 Width (cm): 20.320 Depth (cm): 7.620 Board Thickness (cm): 1.905	Face Guards: Yes (Upstream & Downstream) Separators: Yes
Frame Joints Fasteners: Nails Sealed: No	Inspection:

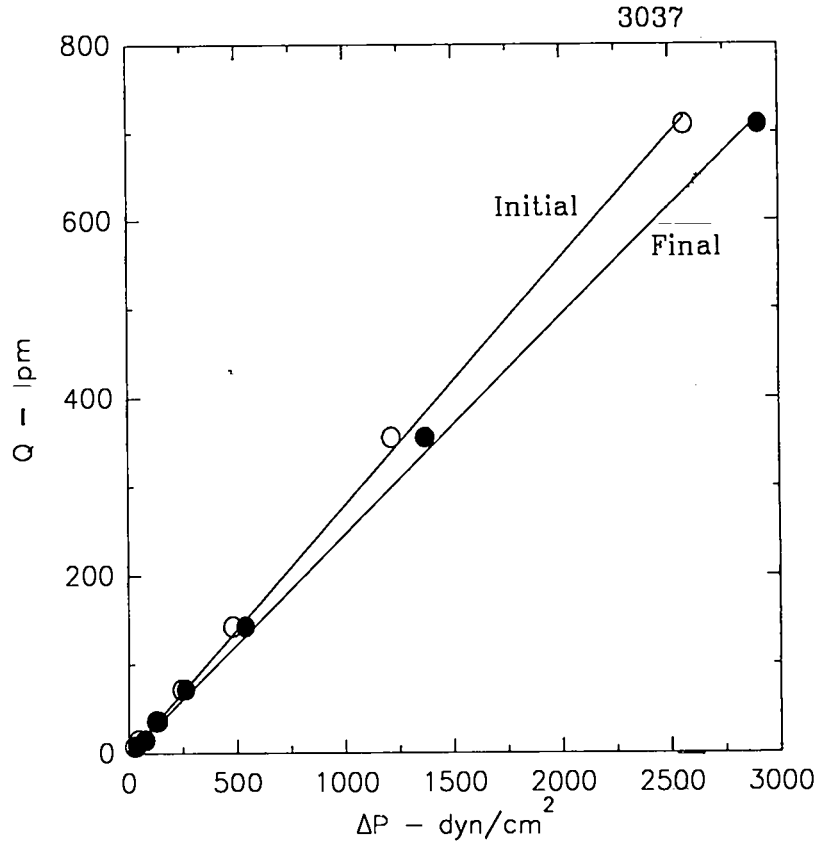

Figure B-35. Whole filter flow rate evaluation data for filter 3037.

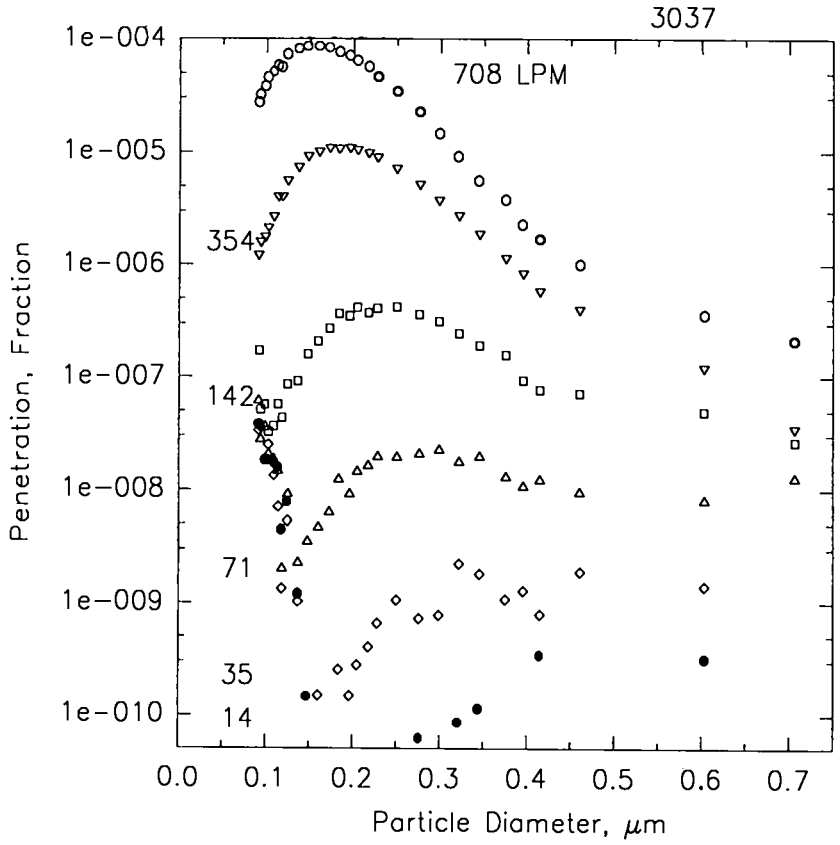

Figure B-36. Whole filter penetration data for filter 3037.

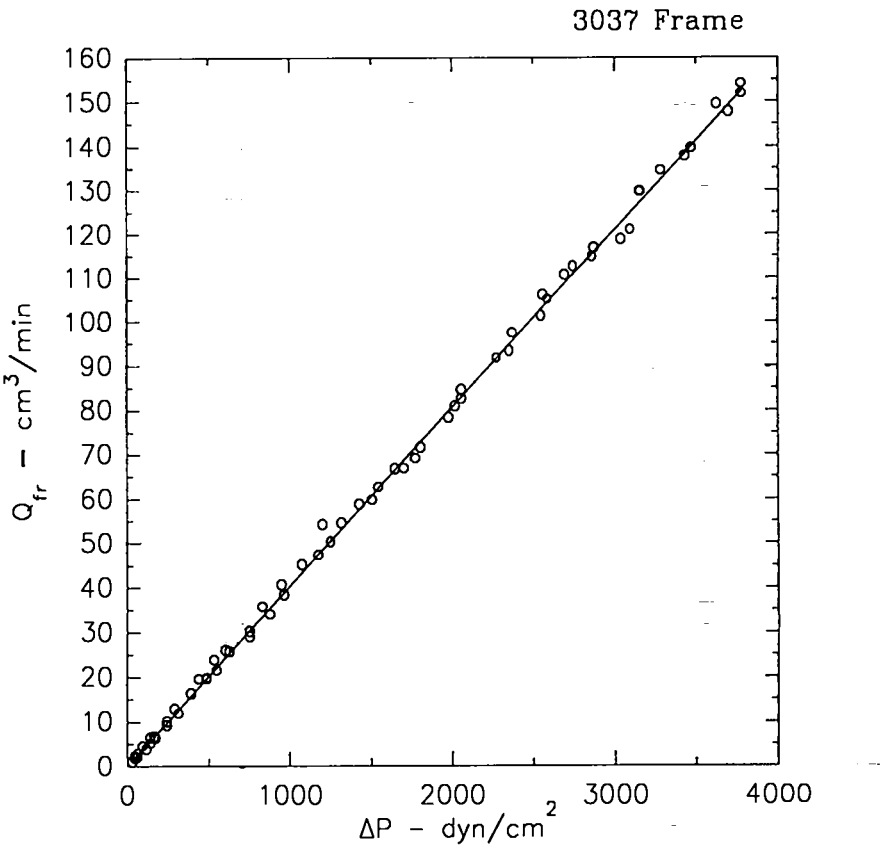

Figure B-37. Frame leak flow rate evaluation data for filter 3037.

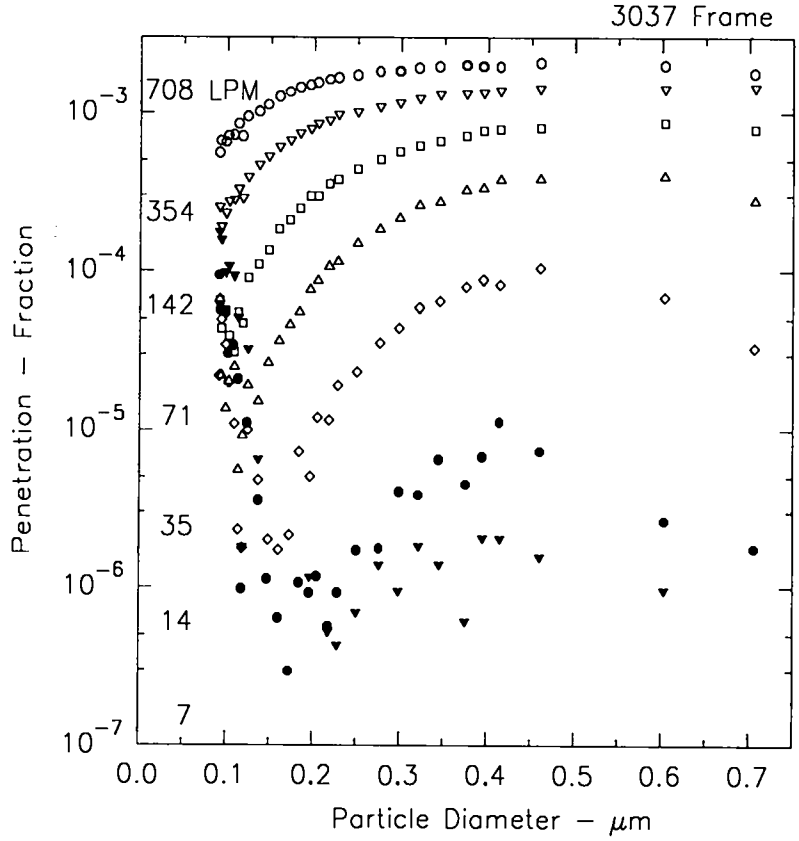

Figure B-38. Frame penetration data for filter 3037.

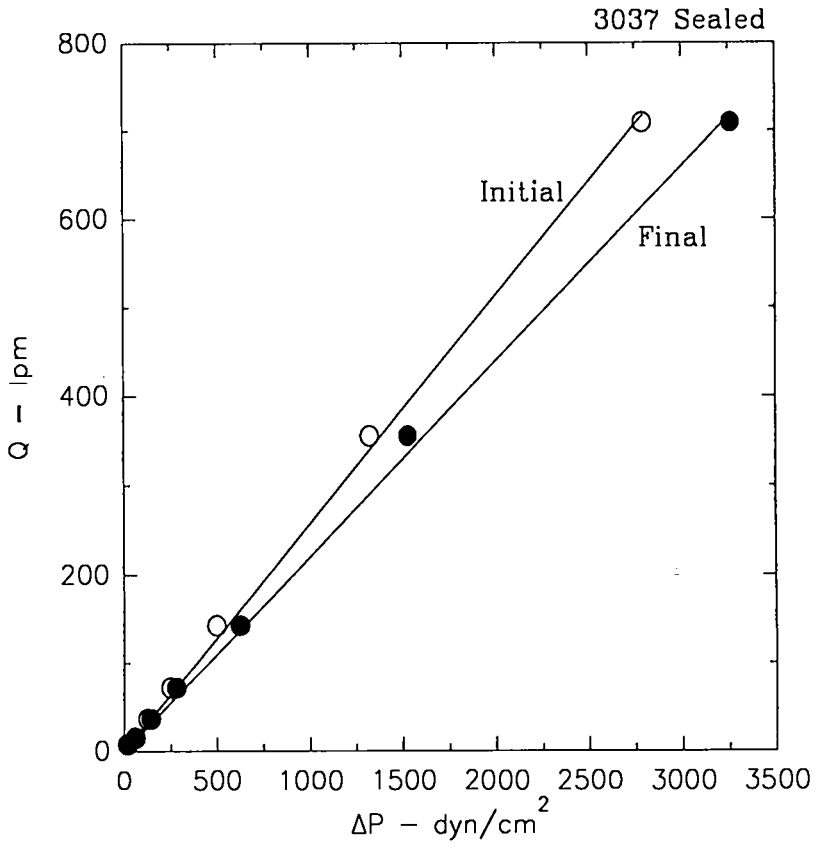

Figure B-39. Media pack flow rate evaluation data for filter 3037.

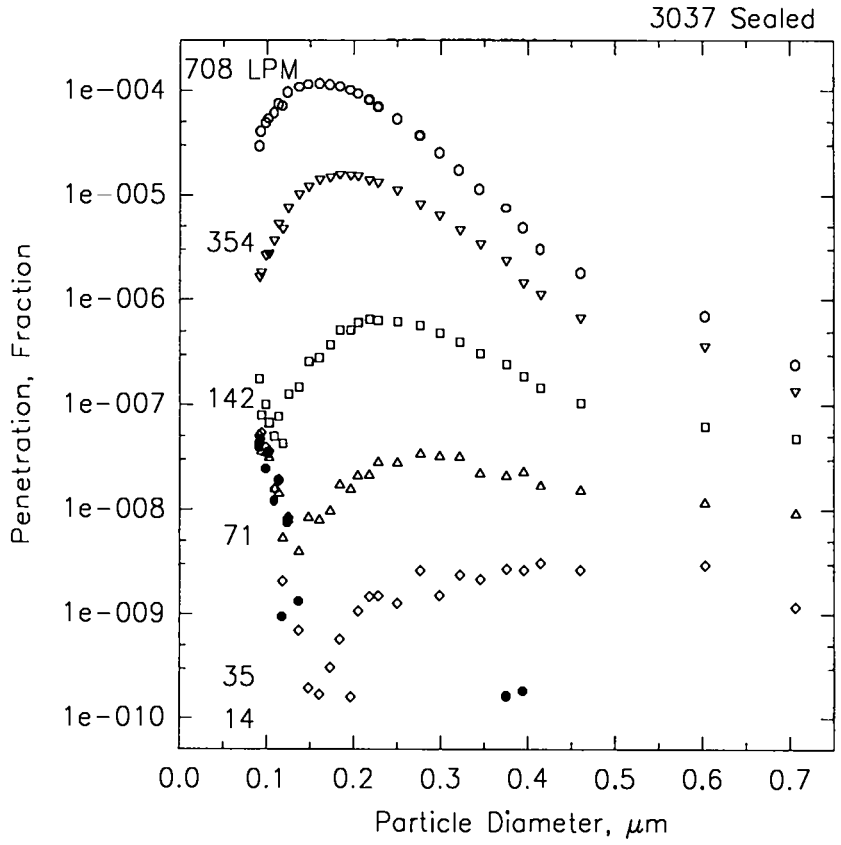

Figure B-40. Media pack penetration data for filter 3037.

B.2.e. Filter Unit 3045

Data from the physical inspection of filter unit 3045 are shown in Table B-X. Whole filter flow rate evaluation data are shown in Figure B-41. Data from whole filter penetration determinations are shown in Figure B-42.

Data from frame leak flow rate evaluations are shown in Figure B-43. Data from frame penetration determinations are shown in Figure B-44.

Data from media pack flow rate evaluations are shown in Figure B-45. Data from media pack determinations are shown in Figure B-46.

Table B-X

Physical Description of Filter 3045

Design Volume Flow Rate (Lpm): 708 Manufacturer: American Air Filter Identification Number: 41403045 Lab Book: 25610 Page: 34	Media Area Height (cm): 14.50 Width (cm): 14.70 Depth of Pleats (cm): 5.239 Number of Pleats Upstream: 24 Downstream: 25 Effective Area (cm^2): 3646.17
Gaskets Upstream: Yes Downstream: Yes	Media/Frame Sealant Type: Epoxy Position Upstream: Four Sides Downstream: Four Sides
Outside Dimensions Height (cm): 20.320 Width (cm): 20.320 Depth (cm): 7.620 Board Thickness (cm): 1.9050	Face Guards: Yes (Upstream & Downstream) Separators: Yes
Frame Joints Fasteners: Nails Sealed: No	Inspection:

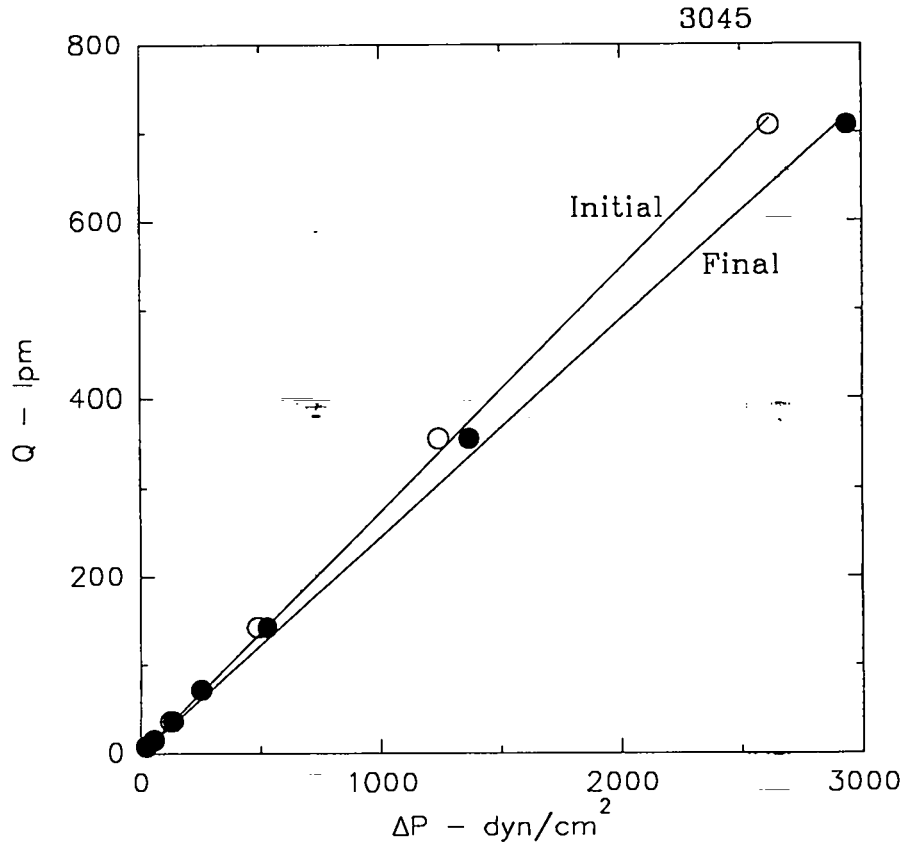

Figure B-41. Whole filter flow rate evaluation data for filter 3045.

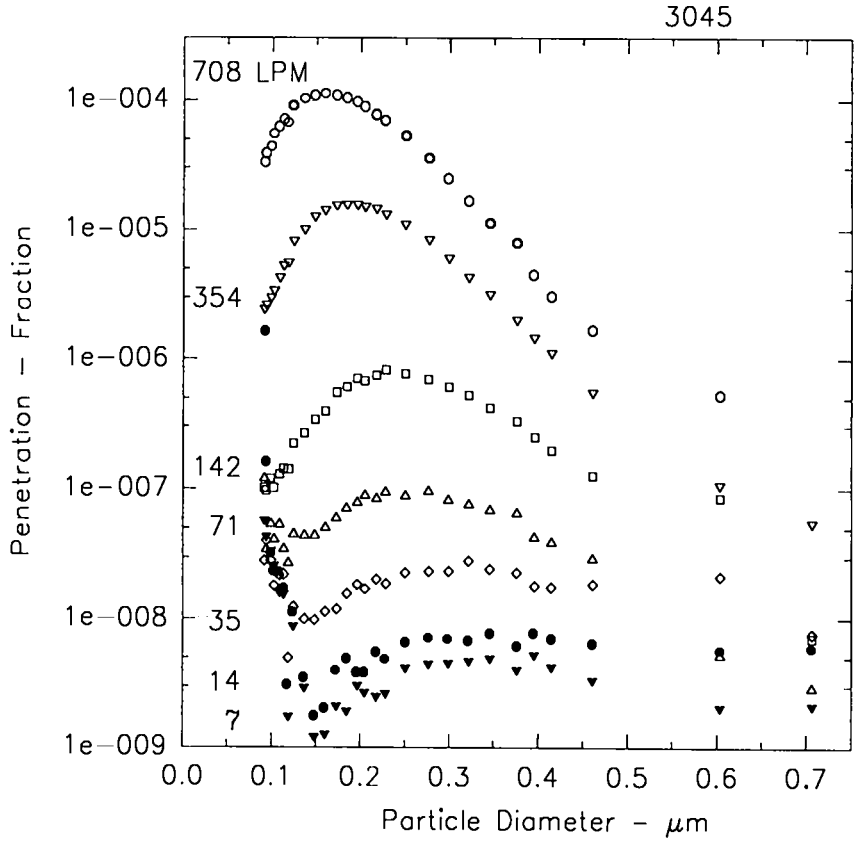

Figure B-42. Whole filter penetration data for filter 3045.

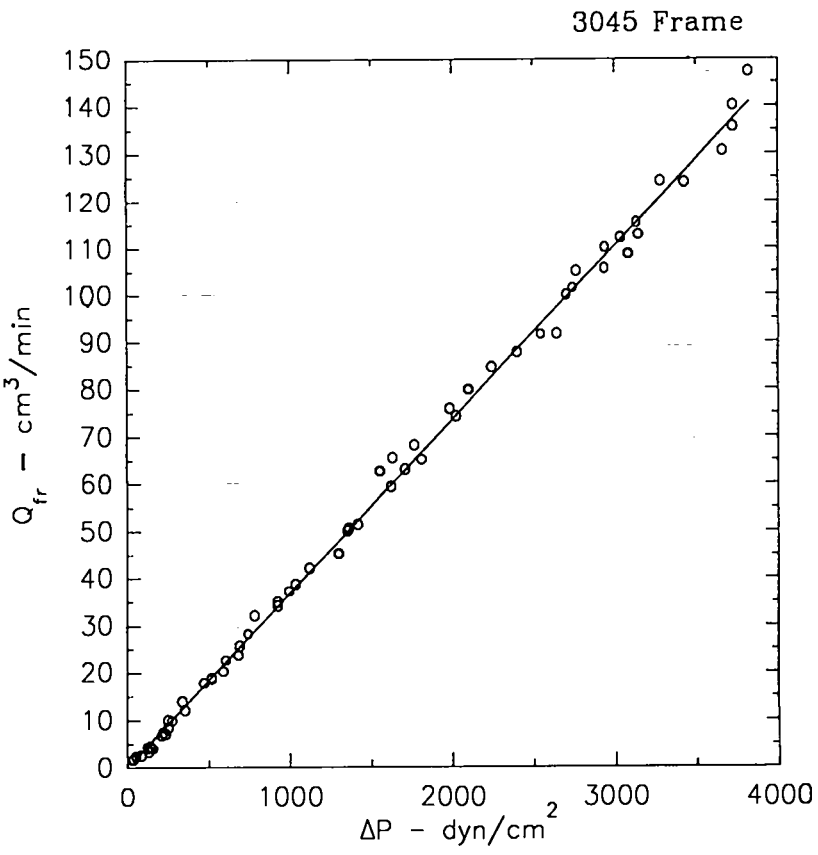

Figure B-43. Frame leak flow rate evaluation data for filter 3045.

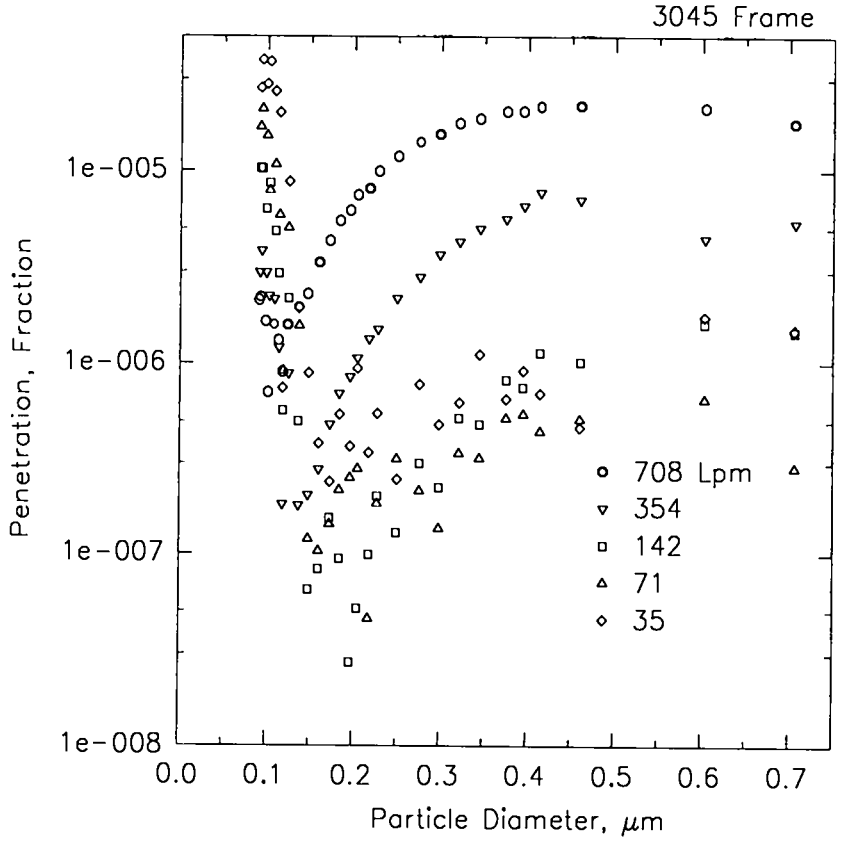

Figure B-44. Frame penetration data for filter 3045.

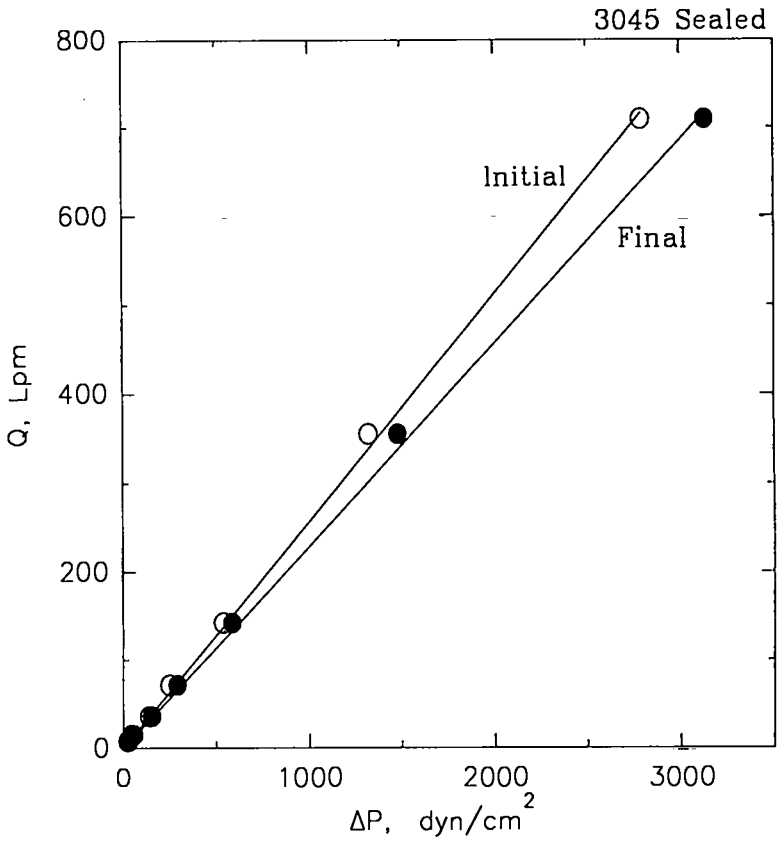

Figure B-45. Media pack flow rate evaluation data for filter 3045.

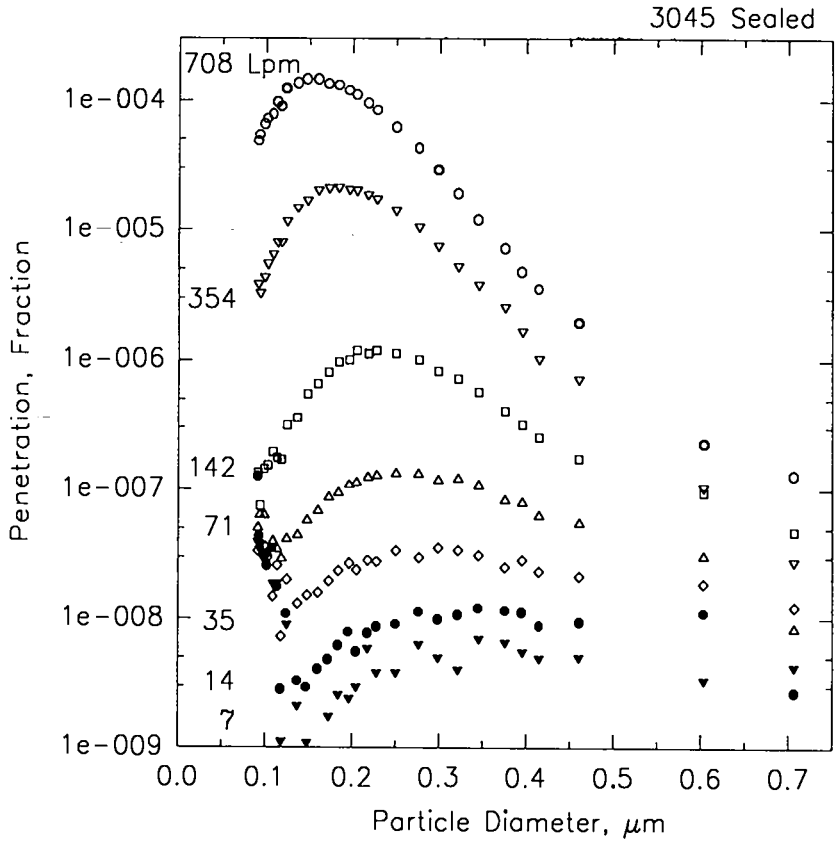

Figure B-46. Media pack penetration data for filter 3045.

B.2.f. Filter Unit 3041

Data from the physical inspection of filter unit 3041 are shown in Table B-XI. Whole filter flow rate evaluation data are shown in Figure B-47. Data from whole filter penetration determinations are shown in Figure B-48.

Data from frame leak flow rate evaluations are shown in Figure B-49. Data from frame penetration determinations are shown in Figure B-50.

Data from media pack flow rate evaluations are shown in Figure B-51. Data from media pack determinations are shown in Figure B-52.

Table B-XI

Physical Description of Filter 3041

Design Volume Flow Rate (Lpm): 708 Manufacturer: American Air Filter Identification Number: 41403041 Lab Book: 25610 Page: 75	Media Area Height (cm): 14.50 Width (cm): 14.75 Depth of Pleats (cm): 5.239 Number of Pleats Upstream: 24 Downstream: 25 Effective Area (cm^2): 3646.17
Gaskets Upstream: Yes Downstream: Yes	Media/Frame Sealant Type: Epoxy Position Upstream: Four Sides Downstream: Four Sides
Outside Dimensions Height (cm): 20.320 Width (cm): 20.320 Depth (cm): 7.620 Board Thickness (cm): 1.9050	Face Guards: Yes (Upstream & Downstream) Separators: Yes
Frame Joints Fasteners: Nails Sealed: No	Inspection:

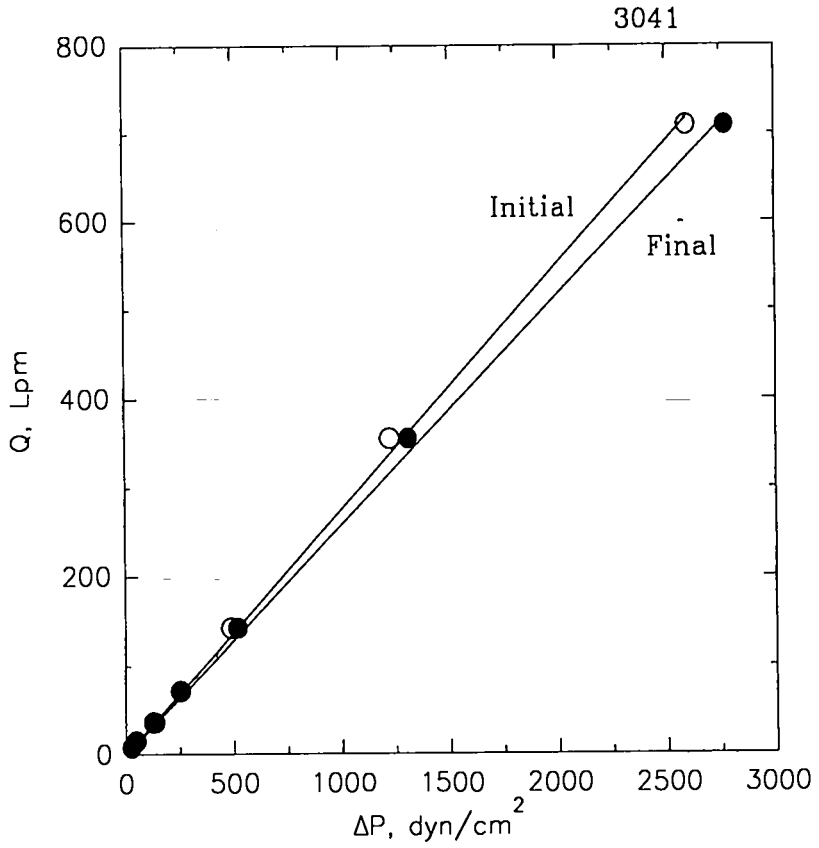

Figure B-47. Whole filter flow rate evaluation data for filter 3041.

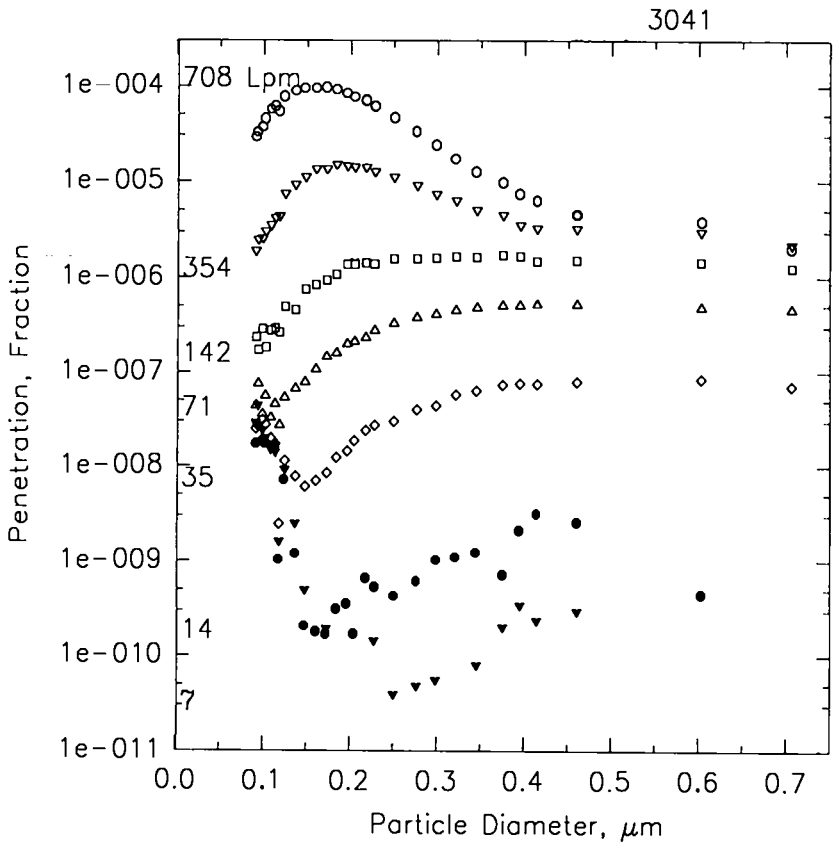

Figure B-48. Whole filter penetration data for filter 3041.

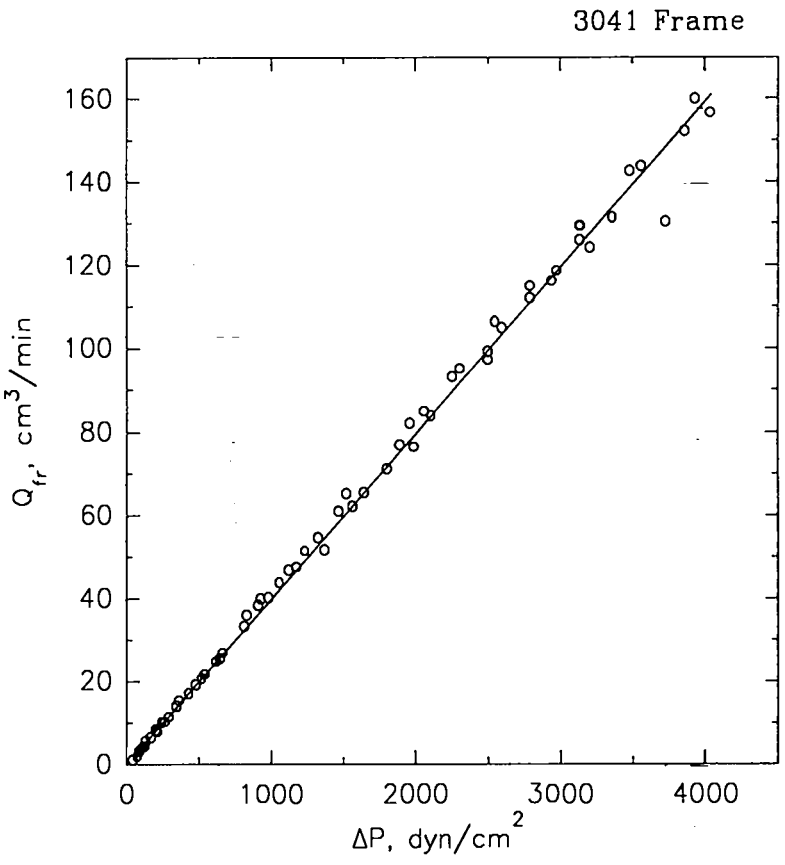

Figure B-49. Frame leak flow rate evaluation data for filter 3041.

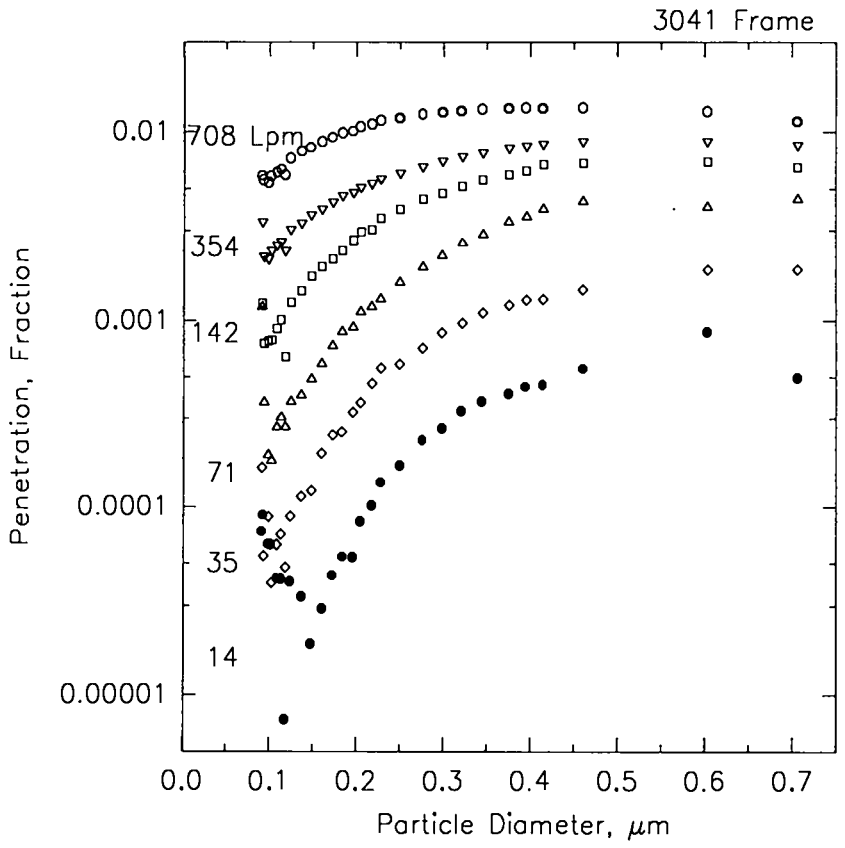

Figure B-50. Frame penetration data for filter 3041.

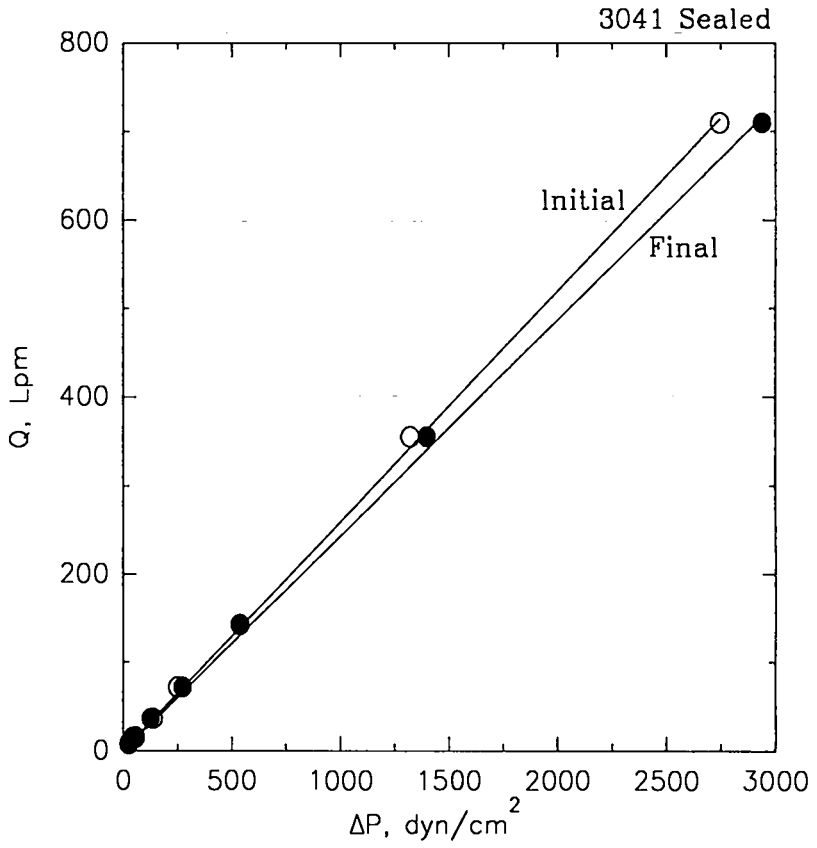

Figure B-51. Media pack flow rate evaluation data for filter 3041.

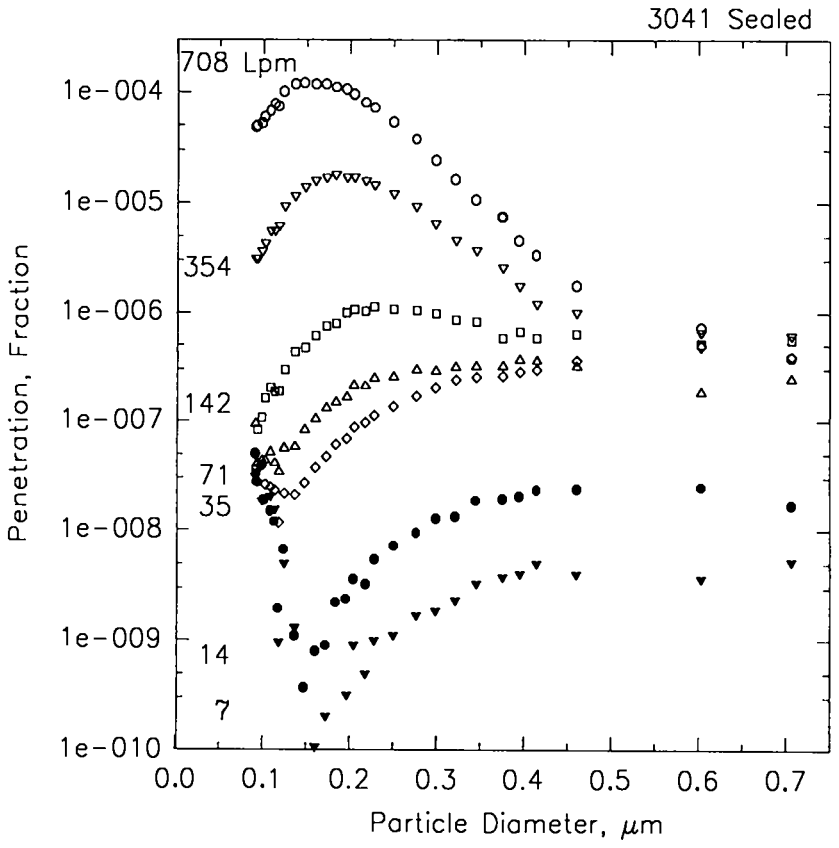

Figure B-52. Media pack penetration data for filter 3041.

B.2.g. Filter Unit 3597

Data from the physical inspection of filter unit 3597 are shown in Table B-XII. Whole filter flow rate evaluation data are shown in Figure B-53. Data from whole filter penetration determinations are shown in Figure B-54.

Data from frame leak flow rate evaluations are shown in Figure B-55. Data from frame penetration determinations are shown in Figure B-56.

Data from media pack flow rate evaluations are shown in Figure B-57. Data from media pack determinations are shown in Figure B-58.

Table B-XII

Physical Description of Filter 3597

Design Volume Flow Rate (m^3/min): 7.620 Manufacturer: Cambridge (Farr) Identification Number: 8113597 Lab Book: 25610 Page: 117	Media Area Height (cm): 14.75 Width (cm): 15.75 Depth of Pleats (cm): 5.3975 Number of Pleats Upstream: 22 Downstream: 22 Effective Area (cm^2): 3502.97
Gaskets Upstream: Yes Downstream: Yes	Media/Frame Sealant Type: Silicone rubber Position Upstream: Top & Bottom Sides Downstream: All Four Sides
Outside Dimensions Height (cm): 20.5 Width (cm): 20.5 Depth (cm): 8.0 Board Thickness (cm): 1.90	Face Guards: No Separators: Yes
Frame Joints Fasteners: Nails Sealed: No	Inspection:

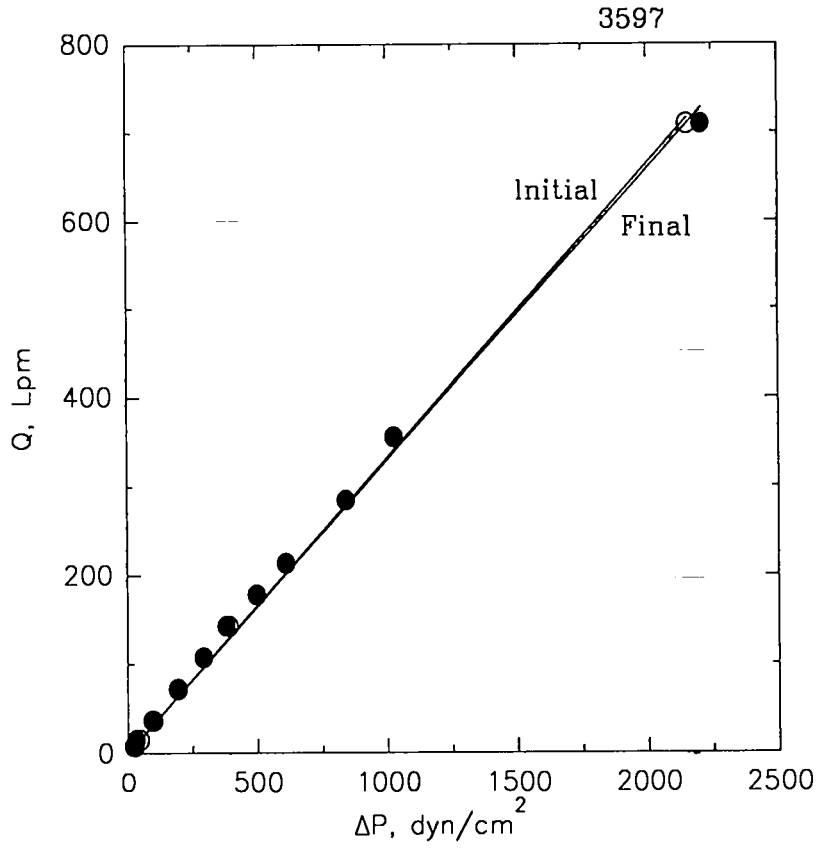

Figure B-53. Whole filter flow rate evaluation data for filter 3597.

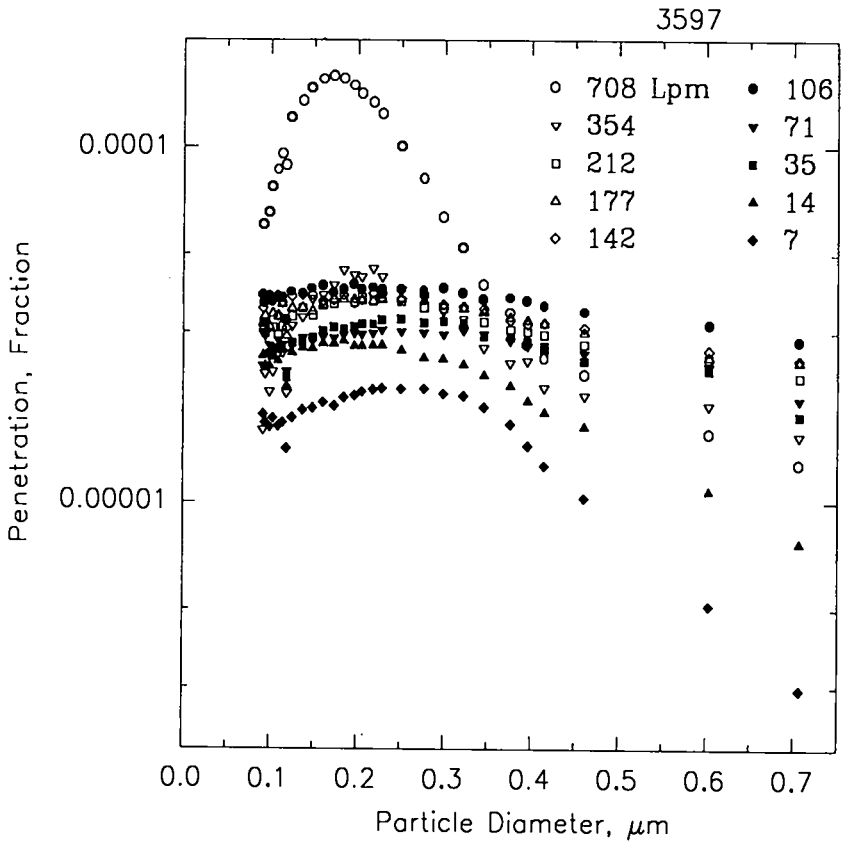

Figure B-54. Whole filter penetration data for filter 3597.

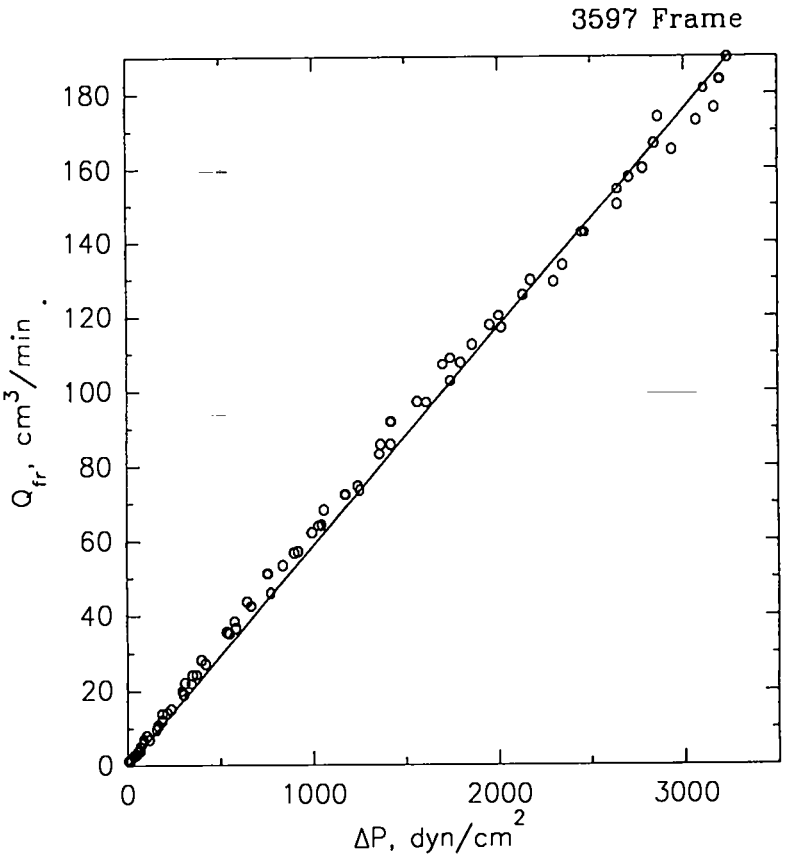

Figure B-55. Frame leak flow rate evaluation data for filter 3597.

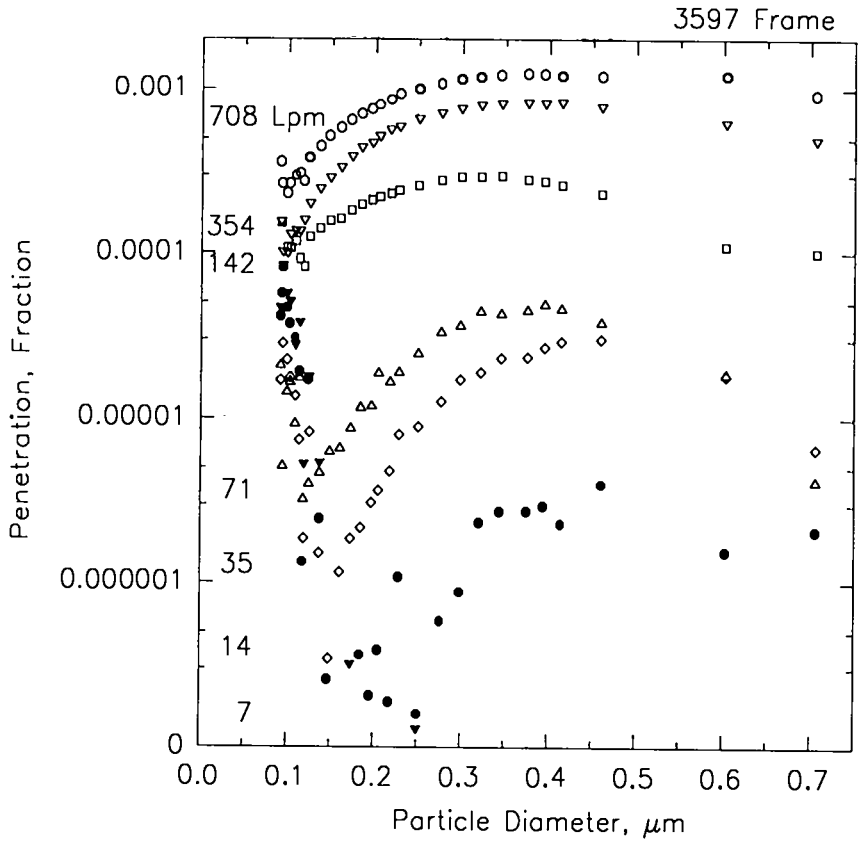

Figure B-56. Frame penetration data for filter 3597.

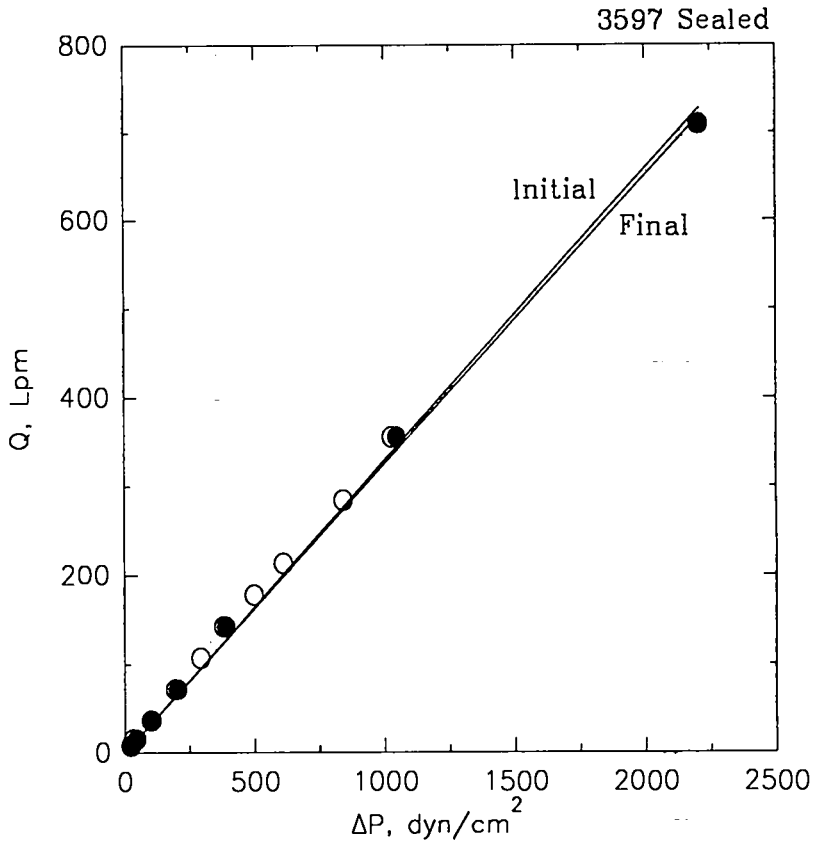

Figure B-57. Media pack flow rate evaluation data for filter 3597.

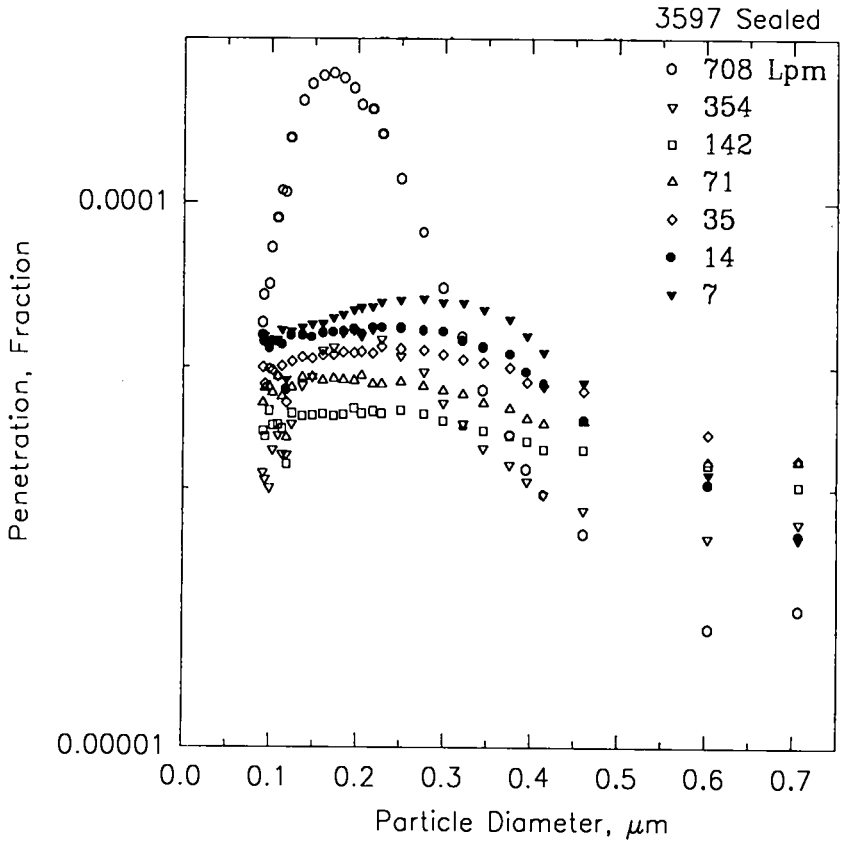

Figure B-58. Media pack penetration data for filter 3597.

B.2.h. Filter Unit 3598

Data from the physical inspection of filter unit 3598 are shown in Table B-XIII. Whole filter flow rate evaluation data are shown in Figure B-59. Data from whole filter penetration determinations are shown in Figure B-60.

Data from frame leak flow rate evaluations are shown in Figure B-61. Data from frame penetration determinations are shown in Figure B-62.

Data from media pack flow rate evaluations are shown in Figure B-63. Data from media pack determinations are shown in Figure B-64.

Table B-XIII

Physical Description of Filter 3598

Design Volume Flow Rate (Lpm): 708 Manufacturer: Cambridge (Farr) Identification Number: 8113598 Lab Book: 25946 Page: 12	Media Area Height (cm): 14.75 Width (cm): 15.75 Depth of Pleats (cm): 5.3975 Number of Pleats Upstream: 23 Downstream: 23 Effective Area (cm^2): 3662.20
Gaskets Upstream: Yes Downstream: Yes	Media/Frame Sealant Type: Silicone Rubber Position Upstream: Top & Bottom Downstream: All Four Sides
Outside Dimensions Height (cm): 20.5 Width (cm): 20.5 Depth (cm): 8.0 Board Thickness (cm): 1.90	Face Guards: No Separators: Yes
Frame Joints Fasteners: Nails Sealed: No	Inspection:

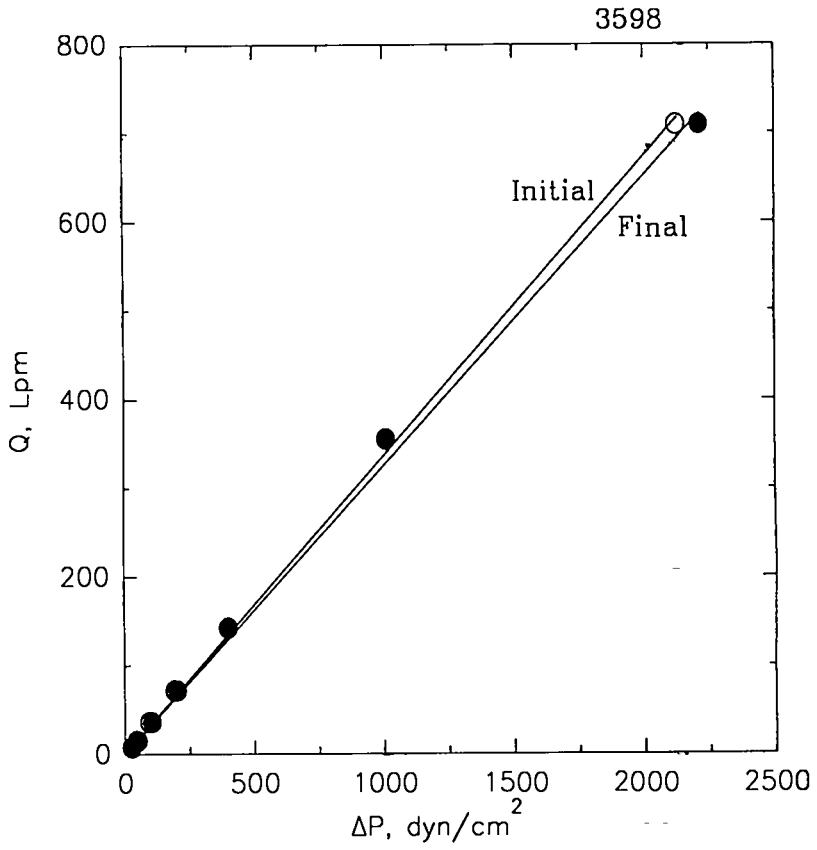

Figure B-59. Whole filter flow rate evaluation data for filter 3598.

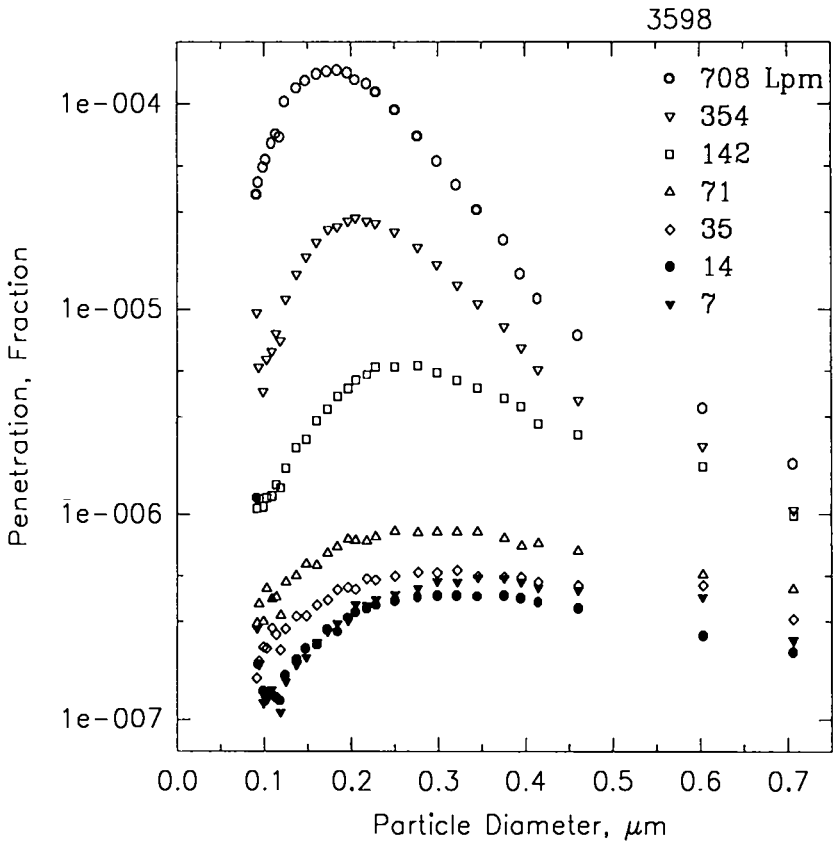

Figure B-60. Whole filter penetration data for filter 3598.

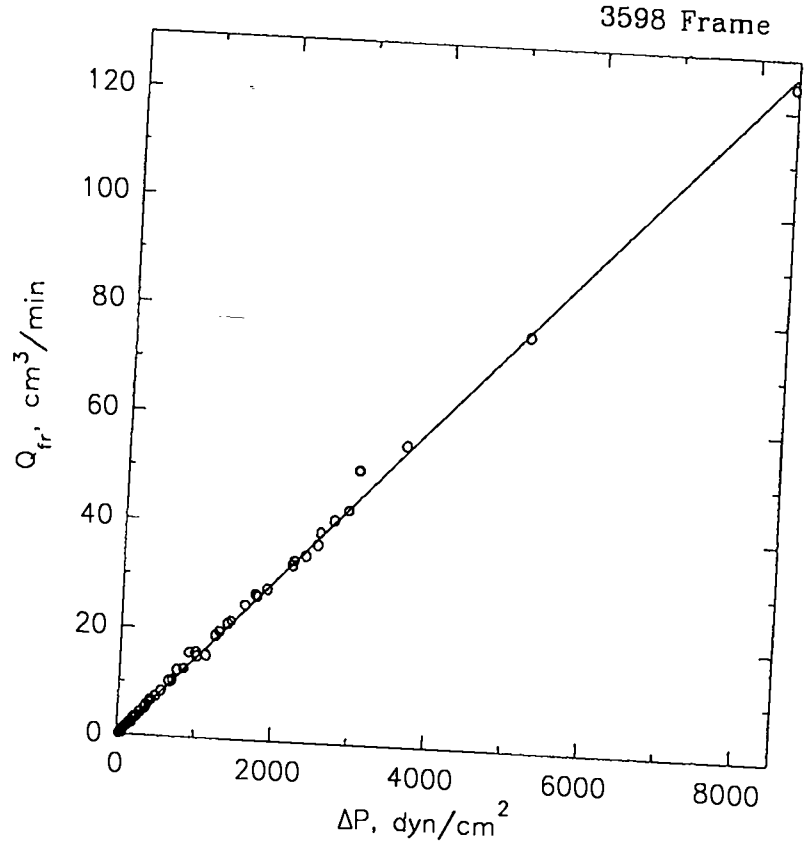

Figure B-61. Frame leak flow rate evaluation data for filter 3598.

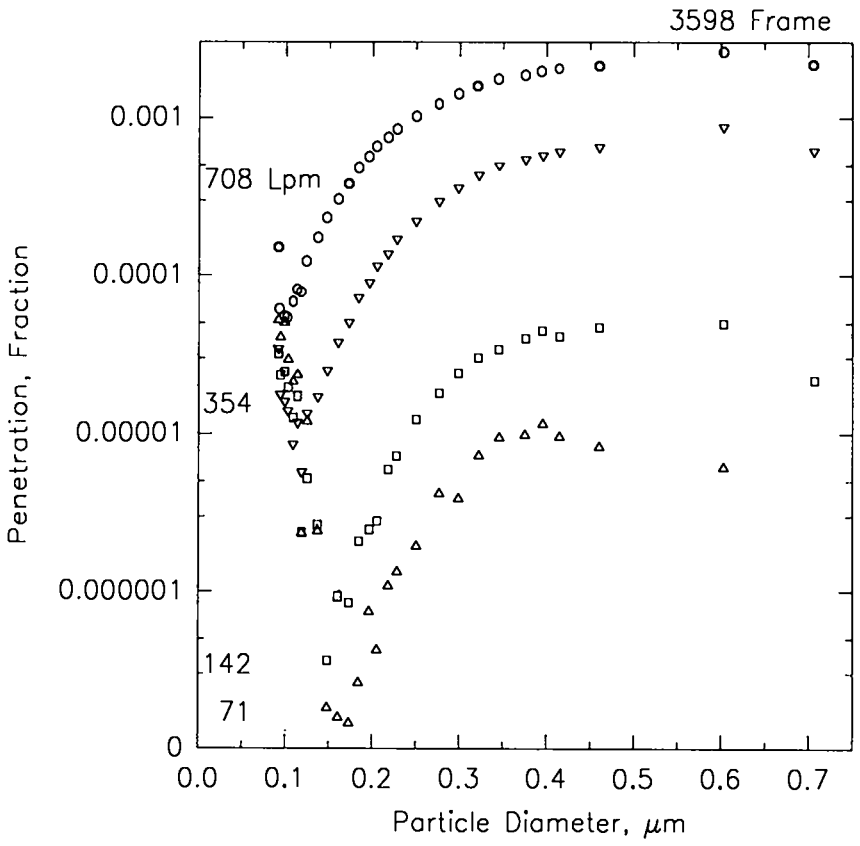

Figure B-62. Frame penetration data for filter 3598.

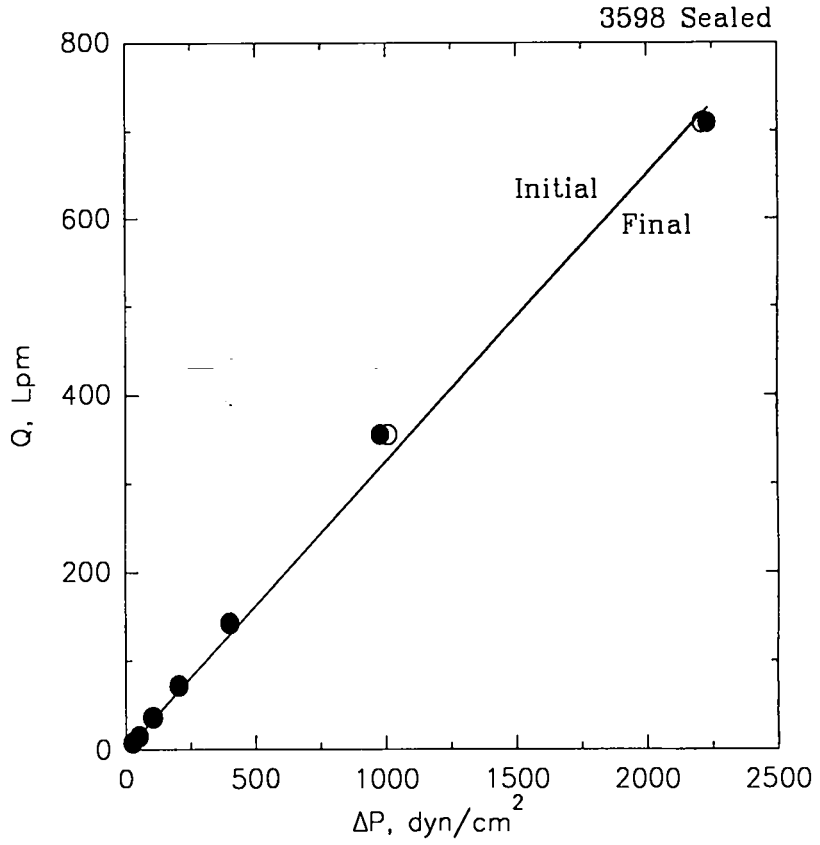

Figure B-63. Media pack flow rate evaluation data for filter 3598.

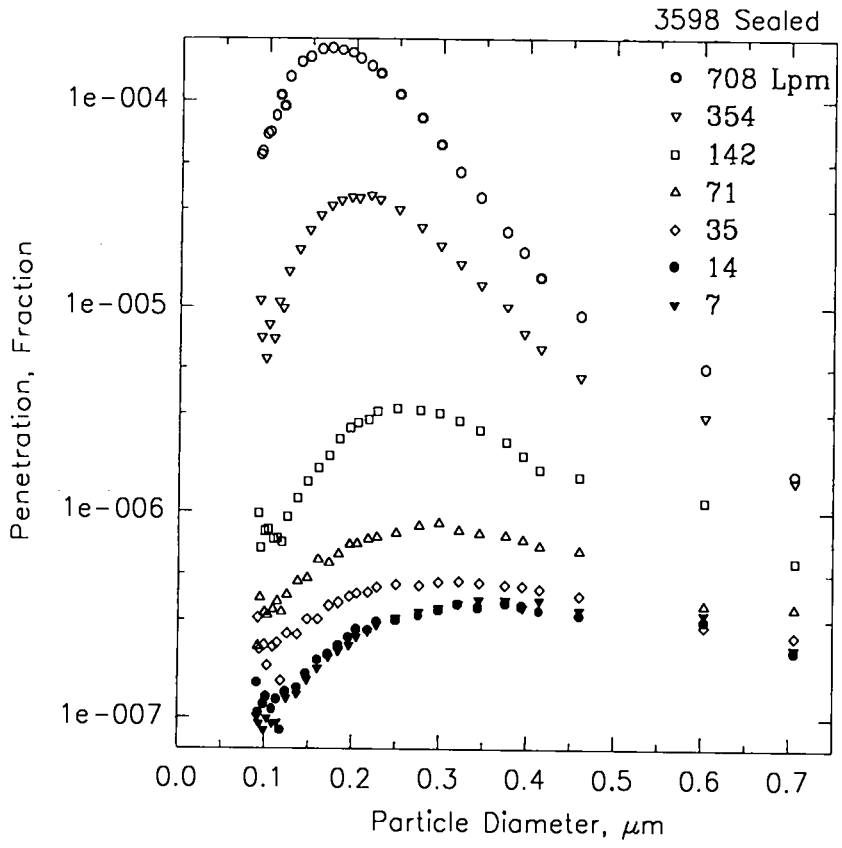

Figure B-64. Media pack penetration data for filter 3598.

B.2.i. Filter Unit 3591

Data from the physical inspection of filter unit 3591 are shown in Table B-XIV. Whole filter flow rate evaluation data are shown in Figure B-65. Data from whole filter penetration determinations are shown in Figure B-66.

Data from frame leak flow rate evaluations are shown in Figure B-67. Data from frame penetration determinations are shown in Figure B-68.

Data from media pack flow rate evaluations are shown in Figure B-69. Data from media pack determinations are shown in Figure B-70.

Table B-XIV

Physical Description of Filter 3591

Design Volume Flow Rate (Lpm): 708 Manufacturer: Cambridge (Farr) Identification Number: 8113591 Lab Book: 25946 Page: 47	Media Area Height (cm): 14.75 Width (cm): 15.75 Depth of Pleats (cm): 5.3975 Number of Pleats Upstream: 22 Downstream: 22 Effective Area (cm^2): 3502.97
Gaskets Upstream: Yes Downstream: Yes	Media/Frame Sealant Type: Silicone Rubber Position Upstream: Top & Bottom Downstream: All Four Sides
Outside Dimensions Height (cm): 20.5 Width (cm): 20.5 Depth (cm): 8.0 Board Thickness (cm): 1.90	Face Guards: No Separators: Yes
Frame Joints Fasteners: Nails Sealed: No	Inspection:

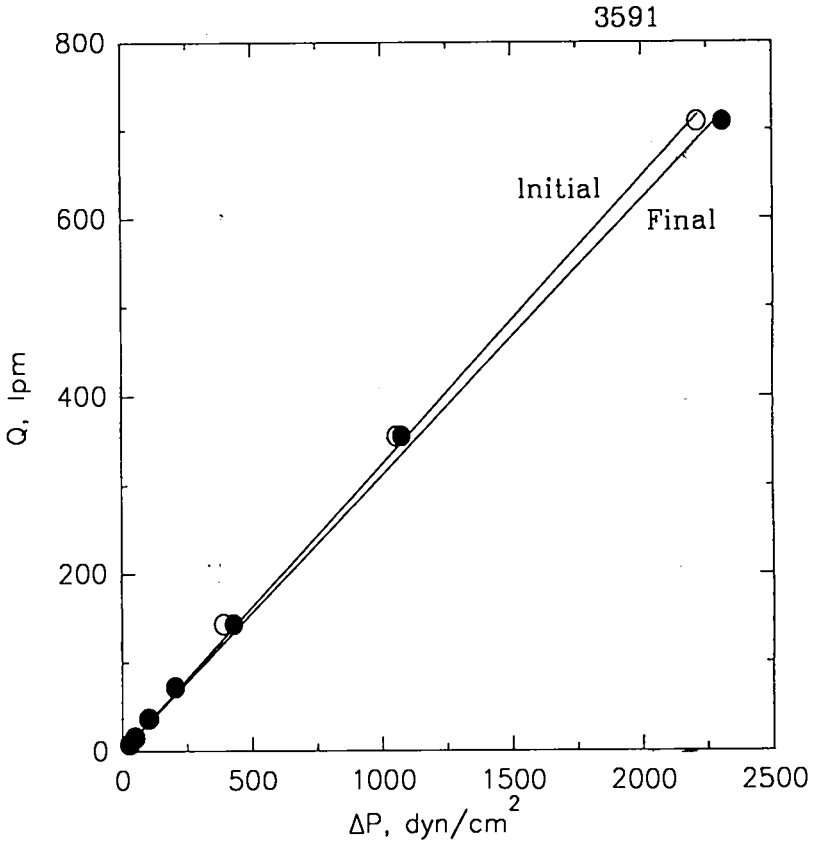

Figure B-65. Whole filter flow rate evaluation data for filter 3591.

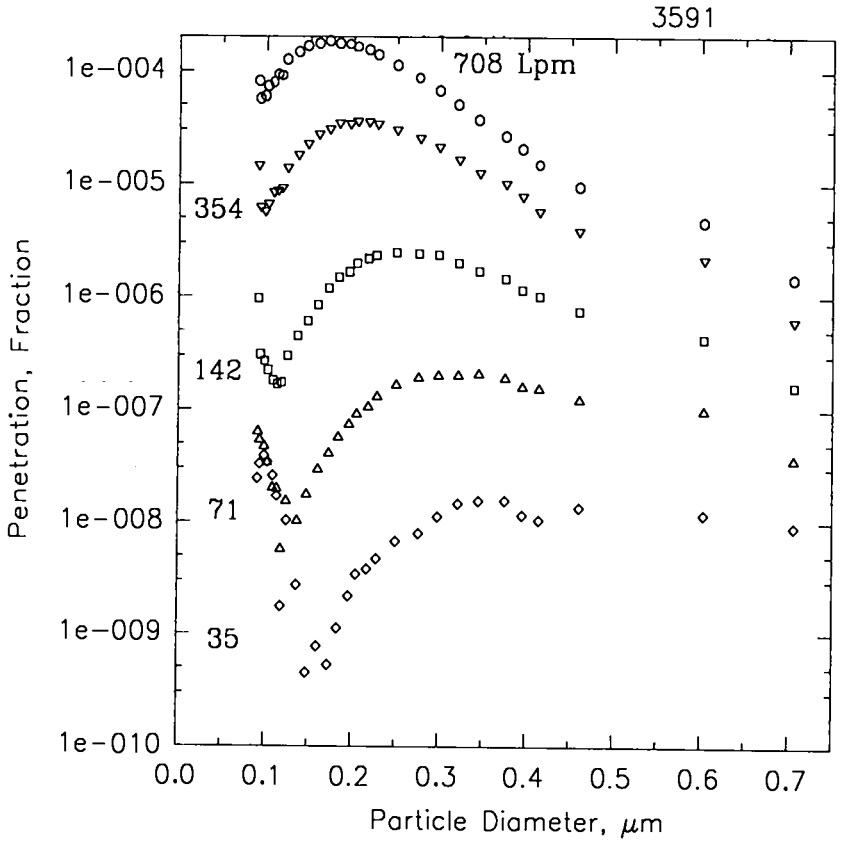

Figure B-66. Whole filter penetration data for filter 3591.

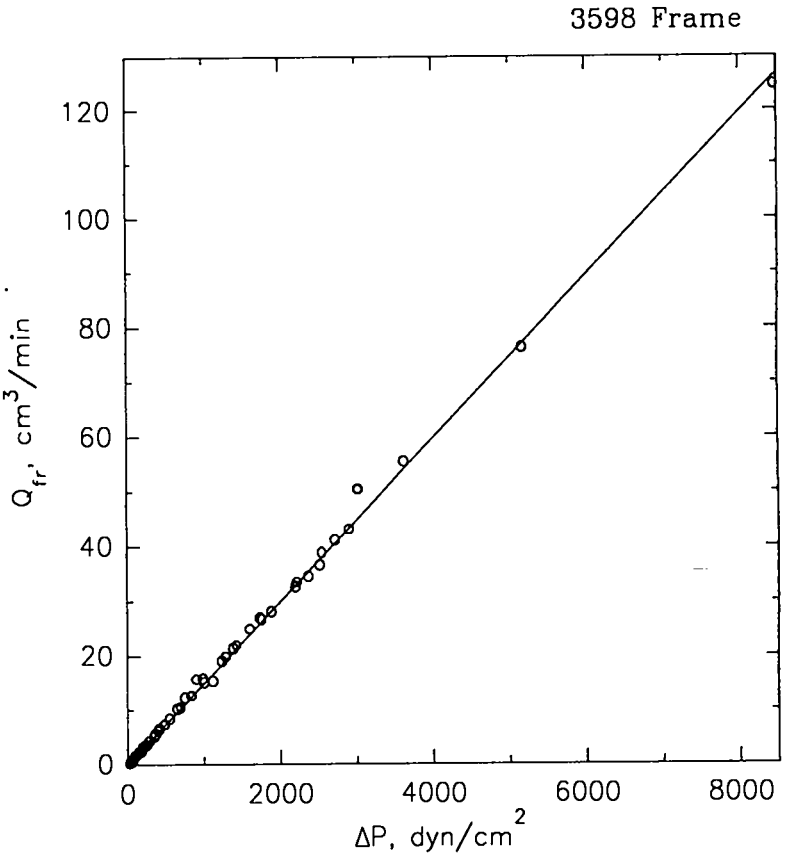

Figure B-67. Frame leak flow rate evaluation data for filter 3591.

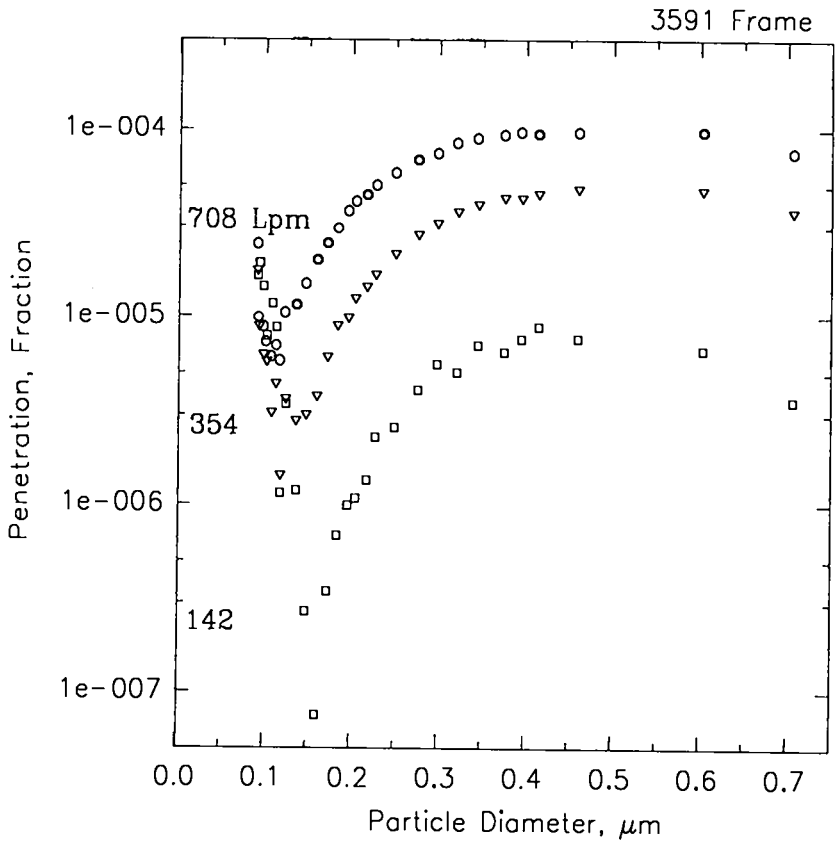

Figure B-68. Frame penetration data for filter 3591.

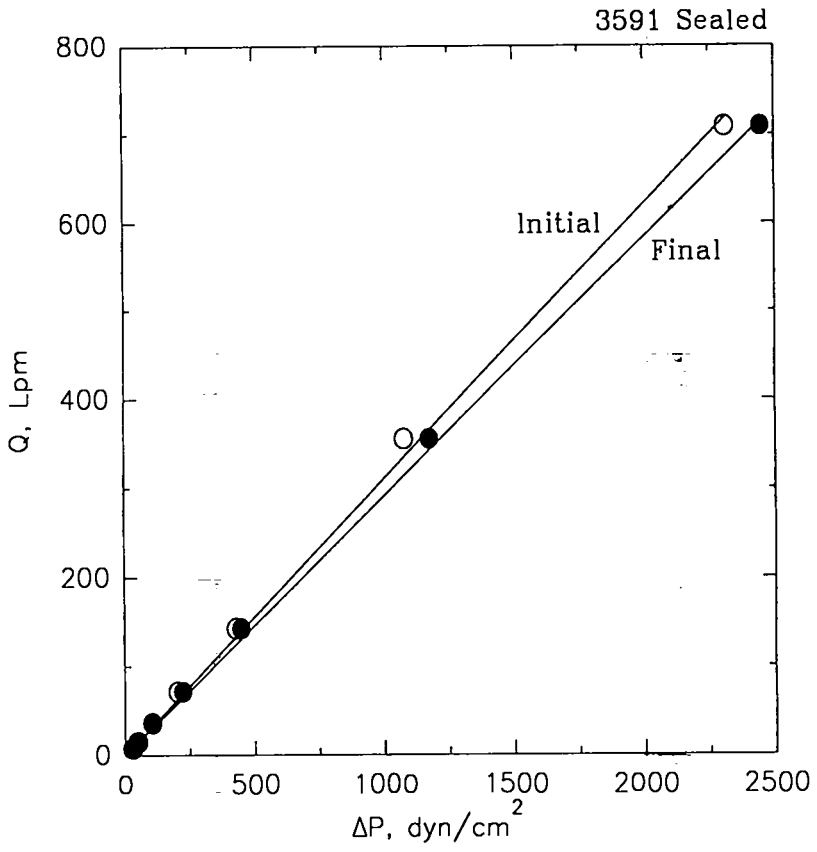

Figure B-69. Media pack flow rate evaluation data for filter 3591.

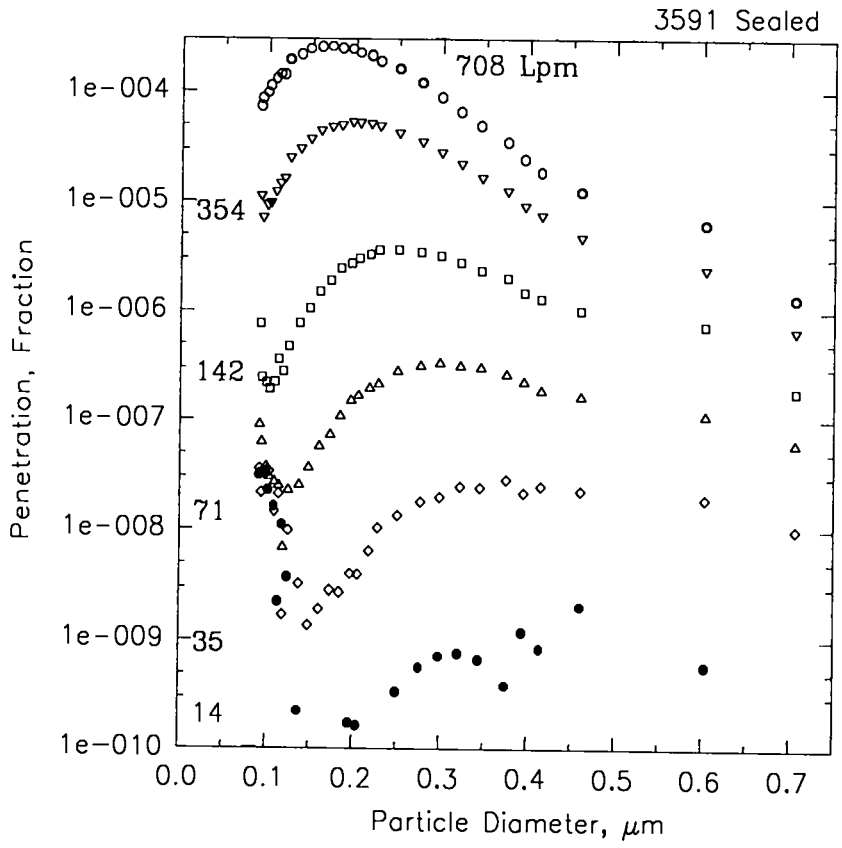

Figure B-70. Media pack penetration data for filter 3591.

REFERENCES

ACGIH91 **American Conference of Governmental Industrial Hygienists:** Di-sec-Octyl Phthalate. in *Documentation of the Threshold Limit Values and Biological Exposure Indices, Vol. 1.* 6th ed. Cincinnati, Ohio: American Conference of Governmental Industrial Hygienists, 1991. pp. 528-531.

Al31 **Albrecht, F.:** Theoretische Untersuchungen uber die ablegerung von Staub und Luft und ihre Anwendung auf die Theorie der Staubfilter. *Physik, Zeits. 32:*48 (1931).

ANSI75 **The American Society of Mechanical Engineers:** *An American National Standard, Reactor Plants and Their Maintenance: Testing of Nuclear Air-Cleaning Systems* (ANSI/ASME N510-1975). New York: The American Society of Mechanical Engineers, 1975.

ANSI76 **The American Society of Mechanical Engineers:** *An American National Standard: Nuclear Power Plant Air Cleaning Units and Components* (ANSI/ASME N509-1976). New York: The American Society of Mechanical Engineers, 1976.

ANSI80a **The American Society of Mechanical Engineers:** *An American National Standard: Testing of Nuclear Air-Cleaning*

Systems (ANSI/ASME N510-1980). New York: The American Society of Mechanical Engineers, 1980.

ANSI80b **The American Society of Mechanical Engineers:** *An American National Standard: Nuclear Power Plant Air Cleaning Units and Components* (ANSI/ASME N509-1980). New York: The American Society of Mechanical Engineers, 1980.

ASME89a **The American Society of Mechanical Engineers:** *Nuclear Power Plant Air-Cleaning Units and Components: An American National Standard* (ASME N509-1989). New York: The American Society of Mechanical Engineers, 1989.

ASME89b **The American Society of Mechanical Engineers:** *Testing of Nuclear Air Treatment Systems: An American National Standard* (ASME N510-1989). New York: The American Society of Mechanical Engineers, 1989.

Be83 **BEILSTEIN:** Physical Properties of Di(2-ethylhexyl) Phthalate (BRN-1890696). In *BEILSTEIN Database*. Columbus, Ohio: STN International/Chemical Abstract Service. [Database].

Bi60 **Bird, R.B., W.E. Stewart, and E.N. Lightfoot:** *Transport Phenomena*. New York: John Wiley and Sons, 1960.

Bi88 **Biermann, A.H. and W. Bergman:** Filter Penetration Measurements Using a Condensation Nuclei Counter and Aerosol Photometer. *J. Aerosol Sci. 19*:471–483 (1988).

Bo90 **Los Alamos National Laboratory:** *Los Alamos Climatology* by B.M. Bowen (LA-11735-MS). Los Alamos, New Mexico: Los Alamos National Laboratory, 1990.

Br89 **Brown, R.C.:** Modern Concepts of Air Filtration Applied to Dust Respirators. *Ann. Occup. Hyg. 33(4)*:615–644 (1989).

Ca88 **Carpenter, D.R. and K. Willeke:** Noninvasive, Quantitative Respirator Fit Testing through Dynamic Pressure Measurement. *Am. Ind. Hyg. Assoc. J. 49(10)*:485–491 (1988).

CFR91 "National Emission Standards for Emissions of Radionuclides Other Than Radon From Department of Energy Facilities," *Code of Federal Regulations* Title 40, Part 61, Subpart H. 1991. pp. 49-53.

Cr91 **Crutchfield, C.D., M.P. Eroh, and M.D. Van Ert:** A Feasibility Study of Quantitative Respirator Fit Testing by Controlled Negative Pressure. *Am. Ind. Hyg. Assoc. J. 52*:172–176 (1991).

CRC70 **Weast, R.C.:** *Handbook of Chemistry and Physics: A Ready-Reference Book of Chemical and Physical Data.* 51st ed. Cleveland, Ohio: The Chemical Rubber Co., 1970. p. F-43.

Da69 **Dawson, S.V.:** "Theory of collection of airborne particles by fibrous filters." Ph.D. diss., The Harvard School of Public Health, Boston, Mass., 1969.

Da73 **Davies, C.N.:** *Air Filtration.* London: Academic Press, 1973.

Di57 **Dixon, W.J. and F.J. Massey:** *Introduction to Statistical Analysis.* New York: McGraw-Hill, 1957. pp. 121–124.

DOE88 **U.S. Department of Energy:** *Specifications for HEPA Filters Used by DOE Contractors* (Nuclear Standard NE F 3-45T). Washington, D.C.: U.S. Department of Energy/ Nuclear Energy Programs, 1988.

DOE90 **U.S. Department of Energy:** *Quality Assurance Testing of HEPA Filters,*" (Nuclear Standard NE-F-3-43). Washington, D.C.: U.S. Department of Energy/ Nuclear Energy Programs, 1990.

Dy69 **Atomic Weapons Research Establishment:** *The Penetration of Glass Fibre Media by Aerosols as a Function of Particle Size and*

Gas Velocity. Part 1: Non-Radioactive Aerosols by J. Dyment (AWRE-05/69). Aldamaston, UK: United Kingdom Atomic Energy Authority, 1969.

Dy70 **Dyment, J.:** Use of Goetz Aerosol Spectrometer for Measuring the Penetration of Aerosols Through Filters as a Function of Particle Size. *J. Aerosol Sci. 1*:53–67, (1970).

Dy92 **Dykes, D.M.:** "Draft Review - Test Standard." August 14, 1992. [Letter to Julie MacIntyre]. Westinghouse Savannah River Company; Aiken, SC 29802.

Ec63 **U.S. Naval Research Laboratory:** *Studies of Portable Air-Operated Aerosol Generators* by W. Echols, and J. Young (NRL-5929). Washington, D.C.: U.S. Naval Research Laboratory, 1963.

Ei05 **Einstein, A.:** On the movement of small particles suspended in a stationary liquid demanded by the molecular-kinetic theory of heat. *Ann. Phys. 17*:549 (1905).

Fa70 **Fahrbach, J.:** The Effect of Leaks on Total Penetration—Velocity and Concentration Measurement at Perforated Filters. *Staub-Reinhalt. Luft 30*:45–52 (1970).

Fa86 **Fain, D.E.:** Standards for Pressure Drop Testing of Filters as Applied to HEPA Filters. In *Fluid Filtration: Gas, Vol. 1* (ASTM STP 975). Philadelphia, Penn.: American Society for Testing and Materials, 1986. pp. 364-382.

Fa88 **Fardi, B.:** "A Fundamental Study of Air Filtration for Respiratory Protection." Ph.D. diss., University of Minnesota, Minneapolis, Minn., 1988.

Fi56 **Fitzgerald, J.J., and C.G. Detwiler:** Collection Efficiency of Air Cleaning and Air Sampling Filter Media in The Particle Size Range of 0.005 to 0.1 Micron. In *Fourth Atomic Energy Commission Air Cleaning Conference Held at Argonne National Laboratory, November 1955* (TID-7513, Pt. 1). Washington, D.C.: U.S. Atomic Energy Commission, 1956. pp. 76-106.

Fl93 **Fluka Chemical:** *Chemical Specifications.* [Product Catalog]. Ronkonkoma, New York: Fluka Chemical Corporation, 1993.

Fr26 **Freundlich, H.:** *Colloid and Capillary Chemistry.* Translated by H. S. Hatfield, London: Methuen, 1926. pg. 785.

Fr57 **Friedlander, S.K.:** Mass and Heat Transfer to Single Spheres and Cylinders at Low Reynolds Numbers. *A.I.Ch.E. Journal 3(1):*43-48 (1957).

Fr58 **Friedlander, S.K.:** Theory of Aerosol Filtration. *Ind. Eng. Chem.*, *50(8)*:1161–1164 (1958).

Fr70 **Frostling, H.:** Vapour Pressure Determinations of Phthalic Esters by Analysis of a Static Aerosol with The Aid of A Flame Ionization Instrument. *J. Aerosol Science 1*:341–356, (1970).

Fr77 **Friedlander, S.K.:** *Smoke, Dust, and Haze; Fundamentals of Aerosol Behavior.* New York: John Wiley and Sons, 1977.

Fu89 **Fuchs, N. A.:** *The Mechanics of Aerosols.* New York: Dover Publications, 1989.

Ge86 **Gebhart, J., and C. Roth:** Background Noise and Counting Efficiency of Single Optical Particle Counters. In *AEROSOLS: Formation and Reactivity.* Oxford: Pergamon Press, 1986. pp. 607-611.

Gi60 **Gilbert, H., and G. Hurwitz:** Filter Rating and Testing Program. In *6th AEC Air Cleaning Conference* (TID-7593). Washington, D.C.: U.S. Atomic Energy Commission, 1960. pp. 161-181.

Go87 **Gogins, M., B. McDonald, R. Nicholson, and R. Cardinal:** Design and Operation of Optimized High Efficiency Filter Element Test

Systems. In *Proceedings of the 33rd Annual Technical Meeting.* Mount Prospect, Illinois: Institute of Environmental Sciences, 1987.

Ha59 **Happel, J.:** Viscous flow relative to arrays of cylinders. *Am. Inst. Chem. Eng. J. 5:*174–177 (1959).

Ha86 **Hampl, V., R. Niemela, S. Shulman, and D.L. Bartely:** Use of Tracer Gas Technique for Industrial Exhaust Hood Efficiency Evaluation—Where to Sample? *Am. Ind. Hyg. Assoc. J. 47(5):* 281–287 (1986).

He90 **Heidenreich, E., A. Neuber, H. Fissan, and W. Schmitz:** Performance of High Efficiency Air Filters. In *International Committee of Contamination Control Societies (ICCCS), 10th International Symposium on Contamination Control* (ICCCS 90) held in Zurich, Switzerland, September 10–14, 1990.

Hi82 **Hinds, W.C.:** *Aerosol Technology: Properties, Behavior, and Measurement of Airborne Particles.* New York: John Wiley and Sons, 1982.

Hi83 **Hinds, W.C., J.M. Macher, and M.W. First:** Size Distribution of Aerosols Produced by the Laskin Aerosol Generator Using Substitute Materials for DOP. *Am. Ind. Hyg. Assoc. J. 44(7):* 495–500 (1983).

Hi84 **Hinds, W.C., and G. Kraske:** Performance of PMS Model LAS-X Optical Particle Counter. In *Aerosols: Science, Technology, and Industrial Applications of Airborne Particles.* New York: Elsevier Science Publishing, 1984. pp. 31-34.

Hi86 **Hinds, W.C. and G. Kraske:** Performance of PMS Model LAS-X Optical Particle Counter. *J. Aerosol Sci. 17(1):* 67–72 (1986).

Hi87a **Hinds, W.C. and G. Kraske:** Performance of Dust Respirators with Facial Seal Leaks: I. Experimental. *Am. Ind. Hyg. Assoc. J. 48(10)*:836–841 (1987).

Hi87b **Hinds, W.C. and P. Bellin:** Performance of Dust Respirators with Facial Seal Leaks: II. Predictive Model. *Am. Ind. Hyg. Assoc. J. 48(10):* 842–847 (1987).

IES86 **Institute of Environmental Sciences:** *IES Recommended Practice: HEPA* Filters (IES-PP-CC-001-86). Mount Prospect, Illinois: Institute of Environmental Sciences, 1986.

Is91 **Isom, S.:** "Specifications and Performance of Koch Static Mixing Units," 1991. [Private Conversation]. Koch Engineering Company, Inc.; P.O. Box 8127; Wichita, KA 67208.

Je54 **Jeans, J.H.:** *The Dynamical Theory of Gases.* New York: Dover Publications, 1954. pp. 288.

Ko91 **Koponen, H.:** Air Permeability Coefficients of Birch, Pine, Spruce and Birch Plywood. In *Drying 91, 7th International Drying Symposium.* Amsterdam: Elsevier Science Publishers, 1991. pp. 518-528.

Ki70 **Klein, M.V.:** *Optics.* New York: John Wiley and Sons, 1970. pp. 629-639.

Ki75 **Kirsch, A.A., I.B. Stechkina, and N.A. Fuchs:** Efficiency of Aerosol Filters Made of Ultrafine Polydisperse Fibres. *J. Aerosol Sci. 6:*119–124 (1975).

Kn45 **U.S. Naval Research Laboratory:** *Development of Smoke Penetration Meters* by H.W. Knudson, and L. White (NRL-P-2642). Washington, D.C.: U.S. Naval Research Laboratory, 1945. pp. 6-8.

Kn79 **Knollenberg, R.G.:** Single Particle Light Scattering Spectrometers. In *Aerosol Measurement.* Gainesville, Florida: University Presses of Florida 1979. pp. 271-293.

Ko80 **Kozuka, M., S. Mikami, and Y. Ikezawa:** Penetrations of high efficiency air filters for submicron DOP aerosol using a laser particle spectrometer. *VDI-Berichte NR. 386*: 23–26 (1980).

Kr57 **Kreith, F., and R. Eisenstadt:** Pressure Drop and Flow Characteristics of Short Capillary Tubes at Low Reynolds Numbers. *Trans. ASME 79:*1070-1078 (1957).

Ku59 **Kuwabara, S.:** The forces experienced by randomly distributed parallel circular cylinders or spheres in viscous flow at small Reynolds numbers. *J. Phys. Soc. Japan, 14 (4:*527–532 (1959).

La42 **U.S. Atomic Energy Commission:** *Report on Smokes and Filters* by I. Langmuir (OSRD-865, Part IV). Washington, D.C.: U.S. Atomic Energy Commission, Office of Scientific Research and Development, 1942.

La43 **U.S. Atomic Energy Commission:** *Progress Report on "A Portable Optical Instrument for the Measurement of Particle Size in Smokes, the "Owl"; and an improved Homogeneous Aerosol Generator"* by V.K. LaMer, , and D. Sinclair (OSRD-1668). Washington, D.C.: U.S. Atomic Energy Commission, Office of Scientific Research and Development, 1943.

La61 **Langmuir, I.:** Report on Smokes and Filters. In *The Collected Works of Irving Langmuir, Vol. 10.* Oxford: Pergamon Press, 1961.

Le82a **Lee, K.W., and B.Y.H. Liu:** Experimental Study of Aerosol Filtration by Fibrous Filters. *Aerosol Sci. Tech, 1*:35–36 (1982).

Le82b **Lee, K.W., and B.Y.H. Liu:** Theoretical Study of Aerosol Filtration by Fibrous Filters. *Aerosol Sci Tech. 1*:147–161 (1982).

Le89 **Letourneau, P., Ph. Mulcey, and J. Vendel:** Prediction of HEPA Filter Pressure Drop and Removal Efficiency During Dust Loading. In *Proceedings of the 20th DOE/NRC Nuclear Air Cleaning Conference.* Washington, D.C.: U.S. Department of Energy, 1989. pp. 984–993.

Li74 **Liu, B.Y.H., and D.Y.H. Pui:** A Submicron Standard and the Primary Absolute Calibration of the Condensation Nuclei Counter. *J. Colloid Interface Sci. 47*: 155–171 (1974).

Li78 **Lippmann, M.:** Filter Media for Air Sampling. In *Air Sampling Instruments for Evaluation of Atmospheric Contaminants, 5th ed.* Cincinnati, Ohio: American Conference of Governmental Industrial Hygienist, 1978. pp. N-1 - N-22.

Li85a **Liu, B.Y.H.:** Air Filtration. November 1985. [Tutorial Handout]. Particle Technology Laboratory, Mechanical Engineering Department, University of Minnesota, Minneapolis, Minn. 55455.

Li85b **Liu, B.Y.H., K.L. Rubow, and D.Y.H. Pui:** Performance of HEPA and ULPA Filters. In *Proceedings of the 31st Annual Technical Meeting.* Mount Prospect, Illinois: Institute of Environmental Sciences, 1985.

Li86 **Liu, B.Y.H., and W.W. Szymanski:** On Sizing Accuracy, Counting Efficiency and Noise Level of Optical Particle Counters. In *AEROSOLS: Formation and Reactivity.* Oxford: Pergamon Press, 1986. pp. 603-606.

Lo81 **U.S. Army Dugway Proving Ground:** *Some Considerations for Choosing Decontamination Simulants* by D. Long and V. Wallance (DPG-T-180-A). Dugway, Utah: U.S. Army Dugway Proving Ground, 1981.

Mc92 **Aerosol Technology Laboratory:** *Use of Shrouded Probes for Sampling Stacks and Ducts* by A.R. McFarland and J.C. Rodgers (ATL-6796/01/11/92/ARM). College Station, TX: Aerosol Technology Laboratory, Texas A&M University, 1992.

MS56 **U.S. Department of Defense:** *Military Standard-Filter Units, Protective Clothing, Gas-Mask Components and Related Products: Performance Test Methods* (MIL-STD-282). Washington, D.C.: U.S. Department of Defense, 1956.

MS88 **U.S. Department of Defense:** *Military Specification-Filter, Medium, Fire-Resistant, High-Efficiency* (MIL-F-51079D). Washington, D.C.: U.S. Department of Defense, 1988.

Mo94 **Los Alamos National Laboratory:** *High Efficiency Filter Systems-General Observations, 1992-1993* by B.V. Mokler and R.C. Scripsick (LA-12763-SR). Los Alamos, New Mexico: Los Alamos National Laboratory, 1994.

Na57 **Natanson, G.L.** *Proc. Acad. Sci. USSR. Phys. Chem. Sec., 112:*21, (1957).

Ni92 **EG&G Rocky Flats, Inc.:** *Determination of Particle Size Distribution and Composition of the Effluent Air Emissions from Building 559* by R. Nininger and W. Osborne. Golden, Colorado: EG&G Rocky Flats, 1992.

No92 **Novick, V.J., P.R. Monson, and P.E. Ellison:** The Effect of Solid Particle Mass Loading on the Pressure Drop of HEPA Filters. *J. Aerosol Sci. 23(6):* 657–665 (1992).

NTP82 **U.S. National Toxicology Program:** *Carcinogenesis Bioassay of Di(2-Ethylhexyl)Phthalate (Cas No. 117-81-7) in F344 Rats and B6C3F1 Mice (Feed Study),*" (No. 217). Washington, D.C.: U.S. National Toxicology Program, 1982.

Os92 **EG&G Rocky Flats, Inc.:** *Test Plan for the Determination of Particle Size Distribution and Composition of the Effluent Air Emissions from Building* by W.E. Osborne, G. Langer, and R. Nininger. Golden, Colorado: EG&G Rocky Flats, 1992.

Pa60 **Pasceri, R.E. and S.K. Friedlander:** The Efficiency of Fibrous Aerosol Filters: Deposition by Diffusion of Particles of Finite Diameter. *Can. J. Che. Eng.:* 212–213 (1960).

Pa63 **Oak Ridge National Laboratory:** Tests of High-Efficiency Filters and Filter Installations at Oak Ridge National Laboratory by E.C. Parrish, and R.W. Schneider (ORNL-3442). Oak Ridge, Tenn.: Oak Ridge National Laboratory, 1963.

Pa92 **Payet, S., D. Boulaud, G. Madelaine, A. Renoux:** Penetration and Pressure Drop of a HEPA Filter During Loading with Submicron Liquid Particles. *J. Aerosol Sci. 23(7):*723–735 (1992).

Pi79 **Pinnick, R.G. and H.J. Auvermann:** Response Characteristics of Knollenberg Light-Scattering Aerosol Counters. *J. Aerosol Sci. 10*:55–74 (1979).

Pe50 **Perry, J.H.(Ed.):** *Chemical Engineers' Handbook*. 3rd ed. New York: McGraw-Hill Book Co., 1950. pp. 388-389.

PMSHSLAS **Particle Measuring Systems:** *High Sensitivity Laser Aerosol Spectrometer Probe PMS Model HS-LAS 32 CH Operating and Servicing Manual.* [Product Operating and Servicing Manual]. Boulder, Colorado: Particle Measuring Systems, 1990.

PMSLAS-X **Particle Measuring Systems:** *Laser Aerosol Spectrometer Special with Single Dynamic Range PMS Model LAS-X-M.* [Product Operating and Servicing Manual]. Boulder, Colorado: Particle Measuring Systems, 1987.

Ra51 **Ramskill, E. A. and W.L. Anderson:** The inertial mechanism in the mechanical filtration of aerosols. *J. Colloid Sci. 6*:416–428 (1951).

Ru86 **Rubow, K. L., and B. Y. H. Liu:** Characteristics of Membrane Filters for Particle Collection. In *Fluid Filtration: Gas, Vol. 1* (ASTM STP 975). Philadelphia, Penn.: American Society for Testing and Materials, 1986. pp. 74-94.

Sc72 **Schuster, B.G. and R. Knollenberg:** Detection and Sizing of Small Particles in an Open Cavity Gas Laser. *Applied Optics 11(7)*:1515–1520 (July 1972).

Sc76 **Los Alamos National Laboratory:** *Multiple HEPA Filter Test Methods* by B.G. Schuster, and D.J. Osetek (LA-6443-PR). Los Alamos, New Mexico: Los Alamos National Laboratory, 1975.

Sc77 **Schuster, B.G., and D.J. Osetek:** The Use of A Single Particle Intra-cavity Laser Particle Spectrometer for Measurements of HEPA Filters and Filter Systems. In *Proceedings of the 14th ERDA Air Cleaning Conference*. Washington, D.C.: U.S. Department of Energy, 1976. pp. 528-540.

Sc84 **Scripsick, R.C., S.C. Soderholm, and M.I. Tillery:** Evaluation of Aerosol Spectrometers for Quality Assurance Filter Penetration Measurements. In *Aerosols: Science, Technology and Industrial Application of Airborne Particles*. New York: Elsevier Science Publishing Co. 1984. pp. 547-550.

Sc86 **Scripsick, R.C:** New Filter Efficiency Tests Being Developed for the DOE. In *Fluid Filtration: Gas, Vol. 1* (ASTM STP 975). Philadelphia, Penn.: American Society for Testing and Materials, 1986. pp. 345-363.

Sc87a **Los Alamos National Laboratory:** *Final Report: Evaluation of Methods, Instrumentation and Materials Pertinent to Quality Assurance Filter Penetration Testing* by R.C. Scripsick, and S.C. Soderholm (LA-10748). Los Alamos, New Mexico: Los Alamos National Laboratory, 1987.

Sc87b **Scripsick, R.C., R.L. Smitherman, and S.A. McNabb:** Operational Evaluation of the High Flow Alternative Filter Test System. In *Proceedings of the 19th DOE/NRC Air Cleaning Conference.* Washington, D.C.: U.S. Department of Energy, 1987. pp. 863-889.

Se31 **Sell, W.:** Staubausscheidung an einfachern Kopern und in Luftfiltern. *V.D.I. Forschung, Heft 1*:347 (1931).

Si71 **Silverman, L., C.E. Billings, and M.W. First:** *Particle Size Analysis in Industrial Hygiene.* New York: Academic Press, 1976. p. 280.

Sm91 **Smith, P. R., I.H. Leslie, E.C, Hensel, T.M. Schultheis, J.R. Walls, and W.S. Gregory:** Investigation of Salt Loaded HEPA Filters. In *Proceedings of the 21st DOE/NRC Air Cleaning Conference.* Washington, D.C.: U.S. Department of Energy, 1987. pp. 366-375.

So84 **Soderholm, S.C., and G.C. Salzmann:** Laser Spectrometer: Theory and Practice. In *Aerosols: Science, Technology and*

Industrial Application of Airborne Particles. New York: Elsevier Science Publishing Co. 1984. pp. 11-14.

Sp68 **Spielman, L., and S.L. Goren.** *Environ. Sci. Technol. 2(4):*279. (1968).

St69 **Stechkina, I.B., A.A. Kirsh, and N.A. Fuchs:** Investigations of Fibrous Filters for Aerosols Calculation of Aerosol Deposition in Model Filters in the Region of Maximum Particle Breakthrough. *Colloid J. USSR (English translation) 31:*97-101 (1969).

Ta79 **Tasucher, W.A., and F.A. Streiff:** Static Mixing of Gases. *Chemical Engineering Progress, April 1979:*61-65 (1979).

Th63 **Thomas, J.W., and G.D. Crane:** Aerosol penetration through 9 mil HV-70 filter paper with and without pinholes. In *Eighth AEC Air Cleaning Conference*. Washington, D.C.: U.S. Atomic Energy Commission, 1963. pp. 189-207

Ti90 **Tillery, M.I.:** "Values of Air Viscosity at Various Temperatures," 1990. [Unpublished Information]. University of California, Los Alamos National Laboratory; P. O. Box 1663, K486; Los Alamos, NM 87545.

Ti92 **Tillery, M.I.:** "A Computer Simulation of Respirator Fit Tests." Ph.D. diss., Environmental Health Department, Colorado State University, Fort Collins, Colorado, 1992.

We86 **Wen, H.Y., and G. Kasper:** Counting Efficiencies of Six Commercial Particle Counters. *J. Aerosol Sci. 17(6)*:947–961 (1986).

Ye74 **Yeh, H.C. and B.Y.H. Liu:** Aerosol Filtration by Fibrous Filters-I. Theoretical. *J. Aerosol Sci. 5*:191–204 (1974).

*U.S. GOVERNMENT PRINTING OFFICE 1994-0-573-024/7018

Los Alamos
NATIONAL LABORATORY
Los Alamos, New Mexico 87545